TAXONOMY, DISTRIBUTION AND TOXICITY OF DINOFLAGELLATE SPECIES IN THE SOUTHERN BENGUELA CURRENT, SOUTH AFRICA.

Lizeth Botes

Submitted in fulfillment of the requirements for the degree of Doctor of Philosophy in the Faculty of Science (Department of Zoology), University of Cape Town

Supervisors: Associate Prof. Terry A. J. Hedderson

Associate Prof. Peter A. Cook

Dr. Grant C. Pitcher

April 2003

This thesis is dedicated to a very special

friend who has been my "supporting beam"

on more levels than one.

Thank you Lilian !

"Thus saith the Lord, in this thou shalt know that I am the Lord: behold, I will smite with the rod that is in mine hand upon the waters which are in the river, and they shall be turned to blood. And the fish that is in the river shall die, and the river shall stink; and the Egyptians shall lothe to drink of the water of the river."

Exodus 7: 17 - 18

"The sea in many places here is cover'd with a kind of brown scum . . ."

Captain James Cook, 28 August, 1770

TABLE OF CONTENTS

SECTION 2

(Distribution of bloom forming dinoflagellate species in False Bay and Walker Bay)

SECTION 3

(Potential threat of bloom forming dinoflagellates species to the developing abalone mariculture industry)

DECLARATION

This thesis reports the results of original research that I conducted at Marine and Coastal Management (M & CM) and the University of Cape Town (UCT). The ideas and work presented in this thesis are largely my own, although I am not first author on all chapters included here. The third chapter was a joint effort between Mitsonori Iwataki (first author), T. Sawaguchi, K. Sekiguchi, Y. Fukuyo and me, with myself as 2nd author. Although not all data that I contributed (light and electron micrographs as well as pigment data) to this chapter were used within the final publication, these data contributed toward describing the new species *Heterocapsa orientalis* Iwataki, Botes & Fukuyo sp. nov. and the emendation of the genus *Heterocapsa*. I also assisted with writing this chapter. The fifth chapter was a joint effort between Miguel de Salas (first author), C.J.S. Bolch, G. Nash, G. M. Hallegraaf and me, with myself as 3rd author. Here I contributed data (light and electron micrographs, pigment data and LSU rDNA data) toward describing the new species, *Takayama helix* de Salas, Bolch, Botes *et* Hallegraeff sp. nov. I contributed to discussions on erecting and delimiting the new genus, *Takayama* de Salas, Bolch, Botes *et* Hallegraeff *gen. nov.*, and assisted with writing this chapter. For chapters on which I am first author, I generated all the data except for chapter 7 where Mrs. D. Calder (M & CM) counted the phytoplankton samples from Gordon's Bay between 1992 – 1996 (prior to this thesis) and in chapter 8 where Dr. A.J. Smit (UCT) assisted with statistical analyses.

This work has not been submitted for a degree at any other university and any assistance I received is fully acknowledged.

Signature removed

Lizeth Botes

ACKNOWLEDGEMENTS

This thesis was undertaken at Marine and Coastal Management (M & CM) and I would like to thank the director, Dr. Johann Augustyn, for putting the facilities at my disposal. My sincere appreciation is extended to my previous supervisor Dr. Danie Brink (University of Stellenbosch) for his unfailing support, encouragement and assistance with furthering my studies, and Dr. Anthony Richardson (Sir Alister Hardy Foundation for Ocean Science, UK) for encouraging me to upgrade this project from a Masters to a Ph.D. I am especially indebted to Associate Professor Terry A.J. Hedderson (University of Cape Town) and Dr. Grant C. Pitcher (M & CM) for insightful comments, valuable discussions and the innumerable rewrites that have, with their attention to detail, greatly improved my thesis. Many a time we had "Pub sessions" where even then they contributed to the knowledge I portray within this thesis. The financial assistance provided by the National Research Foundation (NRF) and M & CM which was arranged through my supervisors Dr. Peter Cook (Centre of Excellence in Natural Resources Management, Australia) and Dr. Grant C. Pitcher, and their efforts with that, is greatly appreciated. The Abalone Farmers Association (AFASA) provided funding to attend my first international conference on Harmful Algal Blooms (HABs) as well as financial assistance during my last two years; this, together with their continuous support, are warmly appreciated.

As part of this multidisciplinary project, I collaborated with many people and have made use of various facilities. I would like to thank Prof. Richard N. Pienaar, Dr. Stuart D. Sym and Mr. Claudio Marangoni for the use of their facilities at the University of the Witwatersrand and their always willing assistance. To the personnel at Irvin & Johnson (Ltd.) Abalone Culture Division, Gansbaai, thank you for always receiving me with such warmth, for providing accommodation and synchronizing the availability of larvae and spat to my needs.

To the M &CM inspectorate at Kalk Bay and Gordon's Bay, the personnel of Aquafarms at Hermanus, and I & J at Gansbaai, thank you for your unfailing cooperation with daily sampling within False Bay and Walker Bay. Many hours were spent at the Electron Microscope Unit, University of Cape Town and the assistance and advice received from Prof. Trevor Sewell, Mrs. Miranda Waldron, Dr. Brendon Price and Mr. Mohammed Jaffer are greatly appreciated. I would like to thank Dr. Colleen O' Ryan for the use of her laboratory facilities and would like to express my sincere gratitude to Miss Geeta Eick and Miss Paula Hedley for their assistance during the early days of my molecular work. I am especially indebted to Dr. John Tyrell (Biolab Biosciences, New Zealand) for his input, help, encouragement and advice on sequencing and troubleshooting. Mr. Miguel de Salas (University of Tasmania, Australia) kindly provided sequences that without which, essential phylogenetic comparisons would not have been possible.

I would like to thank Dr. Ray Barlow and Mrs. Heather Session (M & CM) for running HPLC samples, Miss. Diane Gianakouros (M & CM) for running nutrient samples, Mr. Ashley Johnsen and Miss. Christene Illert (M & CM) for providing wind data, Mrs. Scala J. Weeks and Mr. Christo P. Whittle (Ocean Space, University of Cape Town) for providing satellite imagery, Mr. Andre du Randt, Mrs. Desiree Calder, Mr. Deon Horstman and Mr. Mike Berryman (M & CM) for their technical support during the time spent at M & CM. Advice from Dr. Betty Mitchell-Innes, Dr. Larry Hutchings, Dr. Hans Verheye and Dr. Trevor Probyn, on various issues, was much appreciated.

To the following people: My Family, **Mrs. Lilian Viviers**, Mr. Nick Loubser, Dr. Albertus J. Smit, Mr. Hugo Marais, Mr. Alan Kemp, Miss Charmaine Ailwood, Associate Professor Terry A.J. Hedderson, Dr. Betty Mitchell-Innes, Dr. Jeanie Bailey and Mr. Jacques

van Heerden many thanks for your encouragement and moral support that has recently pulled me through a very difficult time!

To the family and friends that not so long ago wanted to file a "missing persons report"... I'm alive!

Lastly I would like to thank my fiancé, Jacques Swart, for always being cool, calm and collected yet, warm, supportive and loving. " Jy is my sonskyn, my suurstof, my hartklop, my bottel rooiwyn, my asmapompie, my daggastompie, my boksie matchies, my nikotien patchies, die 'gel' in my 'hair-do', die 'g' in my 'string', die draad in my bra, ... Jy sal altyd my 'alles' bly."

ABSTRACT

The threat of harmful algal blooms with their attendant problems, exists throughout the Benguela region. In the southern Benguela upwelling system, water discolorations, referred to as 'red tides', are common and usually attributed to dinoflagellate species. The first aim of the thesis was to investigate the taxonomy of gymnodinioid species in the southern Benguela current. In order to investigate the morphology of the southern Benguela isolates, a simple and rapid scanning electron microscope preparative technique was developed. In the course of these studies, a new genus and new species were identified and described. Nine isolates from the Benguela current were phylogenetically compared to similar and related species from elsewhere in the world based on morphological, pigment and DNA sequence data. A well resolved and robust tree was obtained during these analyses and was used to investigate the diagnostic value of morphological characters at genus and species level by assessing the evolution of morphological characters on this well resolved tree. The second aim was to investigate the distribution of bloom-forming dinoflagellate species in False Bay and Walker Bay, where several land based abalone farms are situated. Monitoring data over an eight year period revealed the presence of 26 dinoflagellate species, seven of which are bloom formers. Interannual and seasonal variations are discussed as well as their longshore distribution. The final aim of the thesis was to investigate which of the bloom forming species pose a threat to the abalone mariculture industry. The growth phase potentially most threatening to abalone was investigated as well as possible mitigation methods. *Artemia* larvae, abalone larvae and abalone spat was used to established that four dinoflagellate species were potentially threatening, that the exponential growth phase for *K. brevis* is the most toxic and that ozone could serve as an effective mitigation agent on abalone farms. Of the four dinoflagellate species established as potentially toxic to the abalone industry, two species (*K. cristata and A. sanguinea*) were isolated locally and two (*K. mikimotoi and K. brevis*) were isolated overseas.

GENERAL INTRODUCTION

Harmful algal blooms (HABs) are common world wide and pose a serious problem to the aquaculture and fishing industries as well as human health (Hallegraeff 1995). While HABs are a natural phenomena, there has been a general argument that HAB events have increased in frequency, intensity and geographic distribution (Hallegraeff 1995). This increase has been attributed to increased utilisation of coastal waters for aquaculture, eutrophication and (or) unusual climatological conditions and transport of dinoflagellate resting cysts either in ships' ballast water or during translocation of shellfish stocks (Hallegraeff 1995).

The threat of HABs and their consequences exist throughout the Benguela region. The Benguela is one of the four major eastern boundary current regions and is divided into the northern and southern Benguela upwelling systems (Shannon 1985). In the southern Benguela upwelling system, water discolorations, referred to as 'red tides', are common and usually attributed to dinoflagellates (Horstman 1981). The massive mortalities of abalone in 1988 and 1989 due to blooms of a toxic species referred to as *Gymnodinium* sp. (Horstman *et al.* 1991, Pitcher & Matthews 1996) or *Gymnodinium* cf. *mikimotoi* (Pitcher & Calder 2000, Horstman *et al.* 1991) greatly increased awareness of the effects of HABs in the southern Benguela upwelling system. In 1989, a monitoring programme was implemented which included the daily collection of water samples at Elands Bay, situated approximately 180 km north of Cape Point on the West Coast, and at Gordon's Bay, approximately 45 km east of Cape Point on the South Coast (Figure 1).

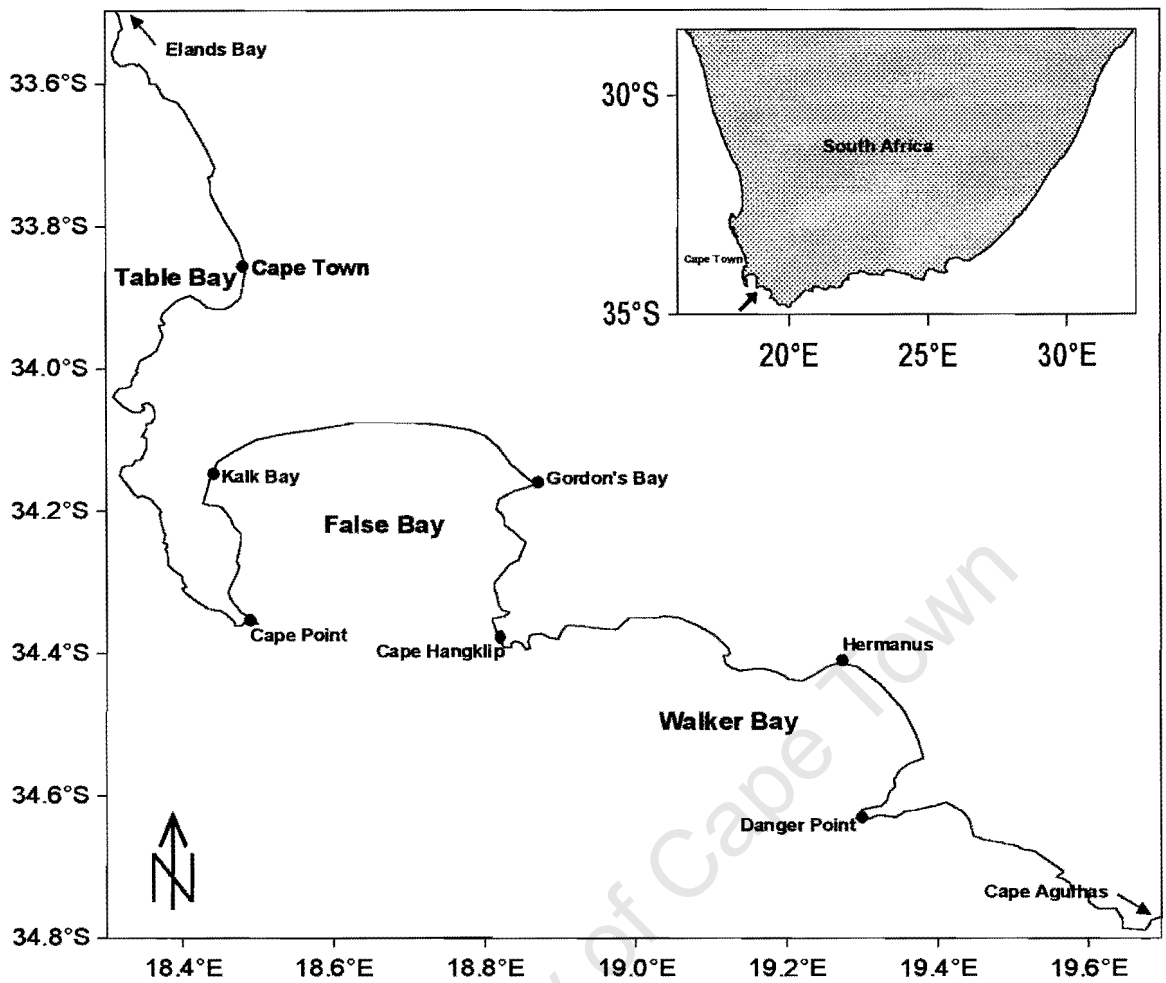

Figure 1. Map of the southern Benguela current study area.

Subsequent blooms of the same species in 1995-96 prompted the initiation in 1997 of the research described in this thesis; to investigate the species' identity, distribution and ecology. Attempts to isolate the *Gymnodinium* sp. revealed the presence of several morphologically similar and potentially harmful gymnodinioid species, several of which resembled *Gymnodinium mikimotoi sensu lato*. The scope of the project was therefore broadened to investigate the taxonomy of the gymnodinioid species in the southern Benguela current, to investigate the distribution of bloom forming dinoflagellate species in False Bay and Walker Bay where several land based abalone farms are situated, and to assess which of these bloom formers pose a threat to the developing abalone mariculture industry. The growth

phase of the overseas *K. brevis* isolate (similar aerosol toxin to *K. cristata* which is local but difficult to maintain in culture) most threatening to abalone was investigated as well as possible toxin mitigation methods.

Considerable confusion existed world wide with regard to the identity of many species belonging to the unarmoured genus *Gymnodinium sensu lato* and as a result many species were lumped into the so-called "*mikimotoi* species complex" (Gentien 1989). Species in genera such as *Gymnodinium sensu lato* and *Gyrodinium sensu lato* were previously erected based on mostly on light microscope (LM) observations (Larsen 994, 1996). However, at this level of resolution morphological features such as apical grooves, ventral pores, thin thecal plates and scales are often difficult to observe and can result in the misidentification of dinoflagellates, thereby necessitating the use of scanning electron microscopy (SEM) (Steidinger *et al.* 1996, Hansen 1995). Unfortunately, delicate dinoflagellate species lack thick cellulosic plates within their thecal vesicles, which render them highly susceptible to distortion during standard SEM techniques which involve centrifugation, filtration, fixation, dehydration and critical point drying (CPD) (Truby 1997). Chapter 1 of the thesis deals with development of a simple and inexpensive SEM preparative technique for delicate dinoflagellates, that overcomes cell distortion such as shrinking and collapsing that result from centrifugation, filtering and CPD. The combination of poly-L-lysine and hexamethyldisilazane (HMDS) not only yields good results but requires limited expertise and equipment, is inexpensive and less time consuming than traditional SEM techniques that incorporate centrifugation, filtration and CPD. Steidinger *et al.* (1996) reiterated the importance and value of SEM for identification purposes, particularly in cases where small gymnodinioid species contain thin thecal plates that are difficult to observe with LM. One such example is discussed in Chapter 2. Here, a species initially thought to be *Gymnodinium*

pyrenoidosum Horiguchi et Chihara, is described as *Heterocapsa orientalis* Iwataki, Botes et Fukuyo. This assignment is based on its very thin and delicate thecal plates and the details of its triangular body scales that are characteristic of *Heterocapsa* (Iwataki *et al.* in press). Recent publications (Chang 1999, Daugbjerg *et al.* 2000, Yang *et al.* 2000, Yang et al. 2001) have clarified some of the confusion existing around the "*mikimotoi* species complex" when species such as *Karenia brevisulcata* (Chang) G.Hansen et Moestrup, *Karenia digitata* Yang, Takayama, Matsuoka et Hodgkiss and *Karenia longicanalis* Yang, Hodgkiss et Hansen were described. The revision by Daugbjerg and his colleagues Dauggjerg *et al.* 2000) of the taxonomy of unarmoured dinoflagellates, based on ultrastructure, pigment content and rDNA sequence data, split the genus *Gymnodinium sensu lato* into four genera namely *Karenia, Karlodinium, Akashiwo* and *Gymnodinium sensu stricto*. This has contributed to further delineation of the morphologically similar species previously lumped into the "*mikimotoi* species complex". Over the last decade, phylogenetic studies based on molecular data have become common practice and the revised taxonomic system prompted renewed interest world wide. A further two *Karenia* species from South African waters were described, as part of this study, based on morphological, pigment and DNA sequence data and descriptions of these two species namely *Karenia cristata* Botes, Sym et Pitcher and *Karenia bicuneiformis* Botes, Sym et Pitcher are detailed in Chapter 3. Chapter 4 focuses on the phylogenetic relationships among 33 species, including 9 South African isolates, which were compared in analyses of morphological, pigment and DNA sequence data. The addition of the South African isolates provides improved resolution between all species and resolves several groups in the current taxonomic system. Morphological character evolution is explored by examining character state optimisations. These support the erection of several new genera. Chapter 5 deals with the erection of a new genus, *Takayama* de Salas, Bolch, Botes et Hallegraeff gen nov. and

includes the description of two new species, one of which, a South African isolate also found in Australia namely *T. helix* de Salas, Bolch, Botes et Hallegraeff sp. nov.

Knowledge of the geographic distribution of harmful species and long-term fluctuations in species composition are essential for distinguishing novel and recurrent HAB events, and for evaluating the global spreading hypothesis (Anderson 1989, Smayda 1990, Hallegraeff 1993). Comprehensive inventories and the diversity of harmful species off the South African coast are poorly established. The few phytoplankton studies that have been undertaken between Cape Point and Danger Point, South Africa (Chapter 6, Figure 1), mostly described red tide events (Grindley & Taylor 1964, Grindley & Taylor 1970, Brown *et al.* 1979, Horstman 1981, Horstman *et al.* 1991, Pitcher & Matthews 1996). As part of the monitoring programme that was implemented in 1989, daily sampling at Gordon's Bay was extended, for the period 1997 – 2000, to include Kalk Bay. It was further extended, for the same period, to include Hermanus and Danger Point where abalone mariculture facilities are based. An 18 nautical mile transect from Gordon's Bay, consisting of 12 stations, was sampled monthly from December 1996 – December 1999. Chapter 6 thus investigated the dinoflagellate species composition within False Bay and Walker Bay, the seasonal and interannual variation of dinoflagellate species in Gordon's Bay and their longshore variation within the two bays.

The effects of HABs on shellfish such as oysters, mussels, surf clams and scallops (Matsuyama *et al.* 1998b, Matsuyama 1999, Nagai *et al.* 1996, Shumway *et al.* 1990, Shumway and Cambella 1993, Shumway 1995, Shumway *et al.* 1994, Smolowitz & Shumway 1997) have developed into a world wide concern. Consuming molluscan shellfish, crabs and fish that have accumulated algal toxins via the food chain can result in human illness and even death (Cembella *et al.* 1994, Shumway *et al.* 1995). An additional concern is

that onshore transport of NSP toxins in aerosols has been linked to respiratory problems in humans and to allergy-like reaction such as skin irritations (Baden 1983). The abalone *Halitotis midae* Linnaeus forms one of the oldest fisheries on the South African coast, with present-day operations including recreational, subsistence and commercial activities (Pitcher *et al.* 2001). Other than the reported toxic effect of *Heterocapsa circularisquama* Horiguchi, and *Karenia mikimotoi* (Miyake et Kominami ex Oda) G. Hansen et Moestrup, on the abalone *Haliotis discus* Reeve (Matsuyama *et al.* 1998a), and the cases of paralytic shellfish poisoning (PSP) toxicity in *Haliotis tuberculata* Linnaeus from north-west Spain (Bravo *et al.* 1996, Bravo *et al.* 1999, Martinez *et al.* 1993, Nagashima *et al.* 1995) and *Haliotis midae* Linnaeus from South Africa (Pitcher *et al.* 2001), no published information is available on the effect of HABs on abalone. Chapter 8 discusses the effect of various dinoflagellate species on abalone larvae and abalone spat (3mm individuals) and assesses whether these species pose a threat to the mariculture industry, particularly in South Africa. The growth phase of algal cultures most toxic to abalone, as well as the possibility of using ozone as an effective mitigation agent were also investigated.

SECTION 1

Taxonomy of the gymnodinioid species in the southern Benguella current

CHAPTER 1

A SIMPLE AND RAPID SCANNING ELECTRON MICROSCOPE PREPARATIVE TECHNIQUE FOR DELICATE "GYMNODINIOID" DINOFLAGELLATES.

ABSTRACT

Light microscopy (LM) is routinely used to investigate delicate (unarmoured and lightly armoured) "gymnodinioid" dinoflagellate species but at this level of resolution, morphological features such as apical grooves, apical pores, thin thecal plates and scales are often difficult to observe, thereby necessitating the use of scanning electron microscopy (SEM). Good results were obtained when harvested cells were fixed with osmium tetroxide (OsO_4) as the primary fixative, adhered with poly-L-lysine to round glass coverslips, dehydrated in an ethanol series and dried with hexamethyldisilazane (HMDS). Poly-L-lysine has in the past effectively been used to adhere biological material such as human red blood cells, mouse leukemic cells and marine dinoflagellates to glass coverslips. HMDS has been used to substitute critical point drying (CPD) to dry soft insect tissues, rat hepatic endothelial cells and the cilia of rat trachea. By combining and fine-tuning these two protocols in SEM studies of delicate "gymnodinioid" dinoflagellates, it is possible to overcome cell distortion such as shrinking and collapsing that result from centrifuging, filtering and CPD. The combination of poly-L-lysine and HMDS not only produces good results but also requires limited expertise and equipment, is inexpensive and less time consuming.

INTRODUCTION

Considerable confusion exists with regard to the identity of many delicate (unarmoured and lightly armoured) "gymnodinioid" dinoflagellate species. Genera such as *Gymnodinium, Gyrodinium, Amphidinium* and *Katodinium* were erected during the late 1800's and early

1900's and were based on light microscope observations (Daugbjerg *et al.* 2000). However, at this level of resolution morphological features such as apical grooves, apical pores, thin thecal plates and scales are often difficult to observe and can result in the misidentification of dinoflagellates, thereby necessitating the use of scanning electron microscopy (SEM) (Steidinger *et al.* 1996, Hansen 1995). Attention has recently been focused on constructing a more satisfactory taxonomic system for unarmoured species by combining results obtained from light microscopy, electron microscopy as well as pigment and phylogenetic analysis (Daugbjerg *et al.* 2000, Hansen *et al.* 2000a). Unfortunately, unlike their armoured counterparts, delicate dinoflagellate species lack thick cellulosic plates within their thecal vesicles, which render them highly susceptible to distortion during standard SEM techniques which involve centrifugation, filtration, fixation, dehydration and critical point drying (CPD) (Truby 1997). By using poly-L-lysine in combination with hexamethyldisilazane (HMDS), we have managed to overcome cell distortion thereby obtaining results in which morphological features such as the apical grooves and cingulum displacement are clearly visible. Poly-L-lysine has in the past effectively been used to adhere biological material such as human red blood cells, mouse leukemic cells as well as dinoflagellates to glass coverslips (Takayama 1985, Tsutsui & Kumon 1976). The adhesion of biological material to the surface of poly-L-lysine coated coverslips is a consequence of the attraction between the polyanionic surface of the biological material and the polycationic surface of the coverslip. HMDS, which has a reduced surface tension when evaporating, has effectively been used to dry soft insect tissues, rat hepatic endothelial cells and the cilia of rat trachea (Braet *et al.* 1997, Bray *et al.* 1993, Nation 1983).

The objective of this paper, therefore, was to develop a technique for obtaining scanning electron micrographs of delicate "gymnodinioid" dinoflagellate species that will minimise cell

distortion, require limited expertise and equipment, and that is inexpensive and less time consuming.

MATERIALS AND METHODS

Cultures of various delicate "gymnodinioid" dinoflagellate species present on the south and west coasts of South Africa were grown at 18°C in F_2 medium (Guillard & Ryther, 1962) under a 12h light: 12h dark cycle. To avoid centrifugation, cells of the various cultures were harvested just before the light phase when swarming at the bottom of the culture flask.

Harvested cells in culture medium were fixed 1:1 (for 1 hour at room temperature) with 2% osmium tetroxide (OsO_4) which was made up with filtered seawater. While cells were being fixed, glass coverslips (10mm in diameter) were washed with acetone, placed on a heating block and coated with 0.1 % poly-L-lysine (Molecular Weight 70, 000 – 150, 000). To ensure that the coverslips were well coated, poly-L-lysine was applied repeatedly. Once the coverslips had cooled, they were mounted onto SEM stubs with silver paint. The 1% solution of fixed cells and OsO_4 was applied to the coverslips and left for ~ 30 minutes to allow the now negatively charged cells to adhere to the now positively charged coverslips. Cells were washed by submerging the stubs for 10 minutes in a 1:1 solution of distilled water and filtered seawater, followed by a second wash in distilled water for 10 minutes. The stubs were then taken through a graded ethanol series (30%, 50%, 70%, 80%, 90%, 95% and 3X in 100% - 10 minutes at each step). Following removal from the 100% ethanol, a few drops of HMDS were immediately dispensed onto the coverslips. If necessary, once the HMDS had evaporated (5min), more HMDS could be added to ensure a well-dried sample. The stubs were sputter coated with gold-palladium (60:40) and viewed with a LEO S440 SEM. This procedure was completed in ~ 3hours and 30 minutes.

RESULTS

Four delicate "gymnodinioid" dinoflagellate species were investigated using the technique described above (Fig. 1). Cells were well preserved with very little morphological distortion and features such as the apical groove, cingulum-sulcus juncture as well as the transverse and longitudinal flagella were clearly visible. An apical groove (Figs 1 a, b) encircling the apex of *Akashiwo sanguinea* (Hirasaka) G. Hansen et Moestrup, was clearly visible. The species, *Gymnodinium pulchellum* J. Larsen displayed a sigmoid apical groove on the ventral side (Fig. 1c) extending on to the dorsal side (Fig. 1d) of the cell. A horseshoe-shaped apical groove (Fig. 1e) and square-shaped scales (Fig. 1f) were clearly visible on the cell surface of *Lepidodinium viride* Watanabe, Suda, Inouye, Sawaguchi et Chihara. Thin thecal plates (Fig. 1g) and triangular-shaped scales (Fig. 1h), obscured by a membrane-like structure and not visible with LM, were present on the "gymnodinioid" species, *Heterocapsa* sp.

EXPLANATION OF PLATE

Figure 1. Scanning electron micrographs of delicate "gymnodinioid" dinoflagellate species. (a, b) *Akashiwo sanguinea* (Hirasaka) G. Hansen et Moestrup with apical groove encircling the apex (c, d) *Gymnodinium pulchellum* J. Larsen with a sigmoid apical groove (e, f) *Lepidodinium viride* Watanabe, Suda, Inouye, Sawaguchi et Chihara with a horseshoe-shaped apical groove and square-shaped scales covering the cell surface (g, h) *Heterocapsa* sp. with thin thecal plates and triangular-shaped scales underneath a membrane-like structure.
a: apex, aa: antapex, ag: apical groove, c: cingulum, cd: cingulum displacement, lf: longitudinal flagellum, tf: transverse flagellum, s: sulcus, sc: scales, tp: thecal plate, m: membrane-like structure.

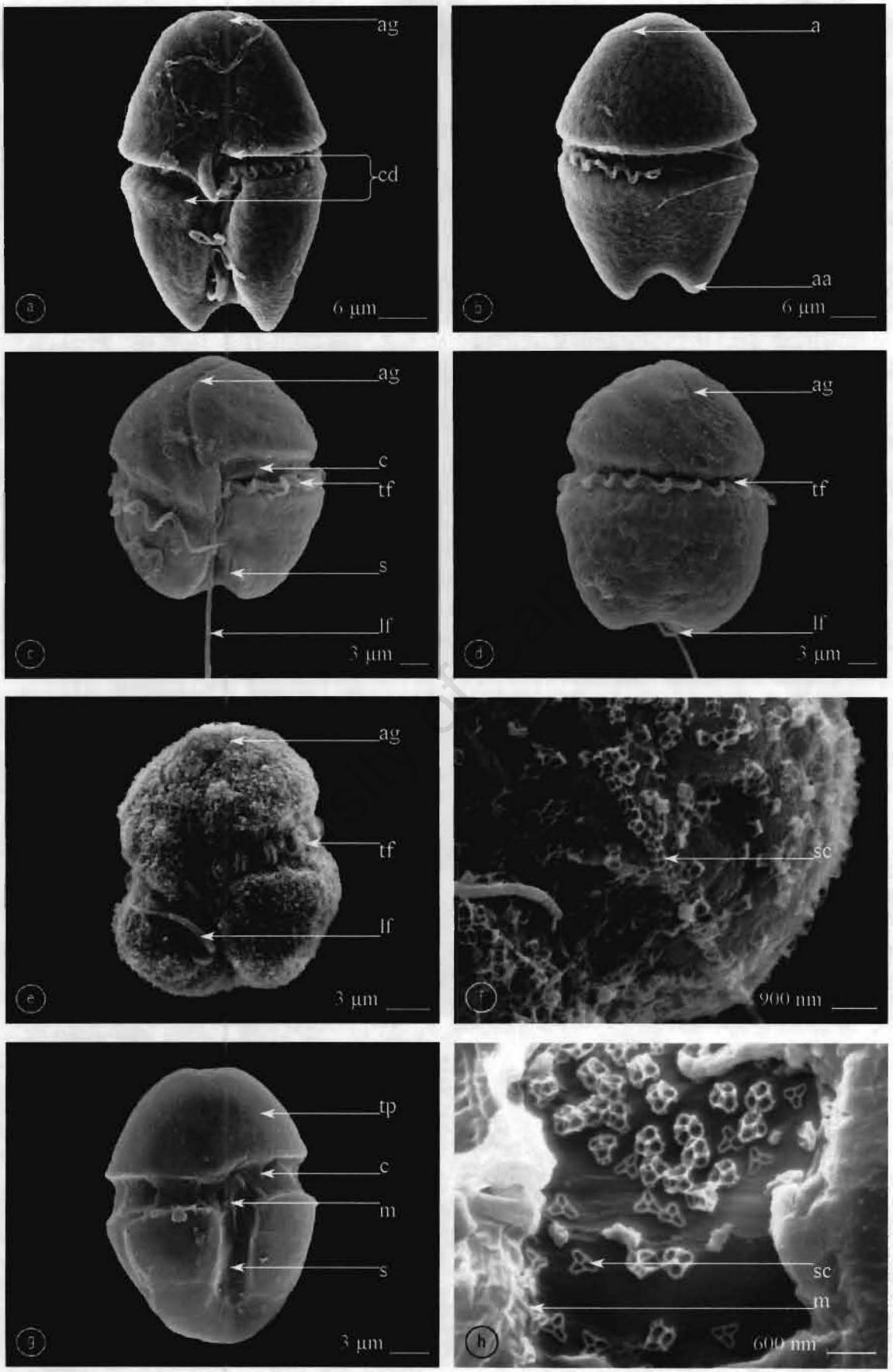
ag
cd
6 µm
a
aa
6 µm
ag
c
tf
s
lf
3 µm
ag
tf
lf
3 µm
ag
tf
lf
3 µm
sc
900 nm
tp
c
m
s
3 µm
sc
m
600 nm

DISCUSSION

Standard SEM techniques involve gentle centrifuging, filtering, fixing, dehydrating and CPD. Apart from the negative effect of centrifugation and filtration on delicate dinoflagellate species and apart from the little information available in the literature on the CPD parameters, and the negative effect of the vigorous solvent exchanges on the cells, as well as temperature and pressure changes during CPD, we found the standard SEM techniques to be very time consuming. With minimisation of cell distortion as the main objective, we obtained good scanning electron micrographs of various delicate dinoflagellate species present on the south and west coasts of South Africa in a quick and simple manner by using a poly-L-lysine in combination with HMDS. Features such as apical grooves, cingulum-sulcus juncture, thin thecal plates and scales were clearly visible. Limited expertise and equipment is needed and the technique is inexpensive and less time consuming.

CHAPTER 2

CELLULAR AND BODY SCALE STRUCTURE OF *HETEROCAPSA OVATA* SP. NOV. AND *HETEROCAPSA ORIENTALIS* SP. NOV. (PERIDINIALES, DINOPHYCEAE)

ABSTRACT

Armoured dinoflagellate species, *Heterocapsa ovata* Iwataki et Fukuyo sp. nov. and *Heterocapsa orientalis* Iwataki, Botes et Fukuyo sp. nov., are described with cellular and body scale morphology using light, fluorescence, scanning electron and transmission electron microscopy. These species possess thecal plate arrangement typical to that of the genus *Heterocapsa*, Po, cp, 5', 3a, 7", 6c, 5s, 5"', 2"", and triradiate three-dimensional body scales consisting of a reticulated basal plate, spine-like uprights, bars etc. The cell shape of *H. ovata* and *H. orientalis* are not similar to other described *Heterocapsa* species due to their ovoid cell configuration. In addition, the body scale of *H. ovata* is relatively simple and that of *H. orientalis* is complicated, and the ultrastructures of both scale types have never been reported for other *Heterocapsa* species.

INTRODUCTION

The genus *Heterocapsa* is a group of armored dinoflagellates, which was originally described as an assemblage of armored dinoflagellates possessing a sutured epitheca and an unsutured hypotheca (Stein 1883). The criteria of the genus, however, have changed over time (e.g. Kofoid 1907, Campbell 1973, Morrill & Loeblich 1981, Hansen 1995, Horiguchi 1995, Iwataki *et al.* 2002a). Since the discovery of body scales on the species *H. triquetra* (Pennick & Clarke 1977), *Heterocapsa* species have been infallibly identified and described by the use of this

character. This resulted in the transfer of *H. niei* and *H. illdefina* from the genus *Cachonina* (Morrill & Loeblich 1981), and *H. rotundata* from the genus *Katodinium* (Hansen 1995) to the genus *Heterocapsa*. In addition, new species were described based on mainly thecal plate arrangement and body scale structure (Loeblich *et al.* 1981, Horiguchi 1995, Horiguchi 1997, Iwataki *et al.* 2002a), i.e. *H. pygmaea*, *H. circularisquama*, *H. arctica*, *H. lanceolata* and *H. horiguchii*. Almost all species ascribed to the genus *Heterocapsa* described before the discovery of body scales, are no longer treated as members of the genus *Heterocapsa*, namely *H. umbilicata* Stein, *H. quadridentata* Stein, *H. quinquecuspidata* Massart, *H. kollmeriana* Swift & McLaughlin and *H. chattonii* (Biecheler) Campbell (Stein 1883, Massart 1920, Swift & McLaughlin 1970, Campbell 1973). Eleven species, including two species without body scale descriptions, i.e. *H. pacifica* (Kofoid 1907) and *H. minima* (Pomroy 1989), are currently still referred to as members of the genus *Heterocapsa* (Iwataki *et al.* 2002a).

Diagnostic morpho-characters at genus and species level have gradually been clarified and it is on the basis of these morpho-characters that we describe two new *Heterocapsa* species *H. ovata* Iwataki et Fukuyo sp. nov. and *H. orientalis* Iwataki, Botes et Fukuyo sp. nov. In addition we propose an emendation of the genus *Heterocapsa* Stein 1883.

MATERIAL AND METHODS

Clonal cultures of *Heterocapsa ovata* were established from the coastal waters Kashiwazaki, Niigata collected in August 1986 and May 2000. The culture isolated in 1986 is maintained in Natural Institute of Environmental Studies as NIES472 strain (Watanabe *et al.* 1997). *Heterocapsa orientalis* was collected in Miyako Bay, Iwate in November 2000. Cell

morphology and thecal plate arrangements were observed using a light microscope with Nomarski differential interference contrast and a fluorescence excitation (Olympus BX-60). For thecal plate observation, samples were pre-stained with fluorescence brightener 28 (Sigma F-3543) for 1 hour (Fritz & Triemer 1985). For observations of intracellular and body scale ultrastructure, thin sections and whole mounts of the cells were prepared. Cells of whole mounts were stained by uranyl acetate for 1.5 min. Thin sections and whole mounts were observed using a transmission electron microscope model JEOL JEM 1010 operated at an accelerating voltage of 80 kV. For scanning electron microscopy, specimens were fixed with 4% OsO_4, dehydrated through and dried in a critical point dryer (Hitachi HCP-2). Observations were made by using a scanning electron microscope (Hitachi S-430) operated at an accelerating voltage of 15kV. All preparations for LM and EM observations were done according to Iwataki *et al.* (2002a).

RESULTS

Heterocapsa ovata Iwataki et Fukuyo sp. nov.

Figs 1-16, 29-33

Cellula ovoidea, epitheca aequilonga hypotheca; 23.6-33.2 μm longa, 18.4-28.0 μm lata; tabulatio thecalis Po, cp, 5', 3a, 7", 6c, 5s, 5"', 2""; chloroplastus lutei-brunneus, parietalis; pyrenoides sphaerica, per vaginam amylorum tenuis obtecta, vulgo cavea cytoplasmatis tubularis plena, in parte sub nucleum sita; sine stigmate; nucleus sphaericus, in parte media epiconi situs; squama plus minusve triangularis, columna rigida.

Holotype: Figure 13.

Type locality: Kashiwazaki, Sea of Japan.

Etymology: ovata = ovate, from its cell shape.

Cells of *Heterocapsa ovata* are ovoid (Fig. 1). The epitheca is slightly smaller than the hypotheca (Fig. 2) or similar in size (Fig. 3). The upper part of the hypotheca is the widest part of the cell (Fig. 2). Cells are 23.6-33.2 μm (mean 26.9 μm, n = 30) in length and 18.4-28.0 μm (mean 21.4 μm, n = 30) in width. The cingulum is median and displaced is approximately 1/2 –1x its own width (Figs 1, 4). The proximal end of the sulcus is narrow and shallow and flares out toward the antapex (Figs 1, 4). The peripheral chloroplasts are irregularly shaped (Fig. 1). No eyespot was observed. The pyrenoid is located in the upper part of the hypotheca and surrounded by starch grains (Fig. 2). A spherical nucleus is situated in middle of the epitheca.

Thecal plates are very thin and almost impossible to observe with light microscopy (Fig. 1, 2). On the contrary, fluorescence microscopy of cells which are stained with Fluoresence Brightner, revealed the thecal plate arrangements (Figs 4-12). The typical plate arrangement is Po, cp, 5', 3a, 7", 6c, 5s, 5"', 2"", and diagrammatic illustrations is given in Fig 13. An apical pore plate (Po) is situated at the apex with the minute canal plate (cp) bordered by Po and 1' and 5' (Fig. 4). The apical, anterior intercalary and precingular series consists of five, three and seven plates, respectively. The large 5' plate is sometimes split into several platelets when the plates deployed (Figs 10, 12). However, fusion of plates 4" and 5" were occasionally observed among the precingulars (Fig. 11). The variation of the plate 2a reported in most *Heterocapsa* species, was also observed in *H. ovata*, i.e. the plate 2a is usually seven-sided (Fig. 6), and sometimes changes to six-sided (Fig. 7). The precingulars consist of seven plates (2a in Fig. 10 however, occasionally they were observed to have six (2a in Fig. 12) or five sides (2a in Fig. 11).

In cells where plate 2a was six-sided, it bordered with plate 3" and 4" and the number of precingular plates can be six (Fig. 7). The cingular series consists of six plates and the 1c plate bordered by the anterior sulcal plate (Figs 4, 5). The sulcal series consisted of five plates (Figs 5, 8), i.e. the anterior sulcal (as), the right sulcal (rs), the left anterior sulcal (las), the left posterior sulcal (lps) and the posterior sulcal (ps) plate, according to the terminology of Loeblich *et al.* (1981). The as plate deeply extends far into the epitheca to border with apical plate 1' (Fig. 4) or apical plates 1' and 5' (Fig. 5). The postcingular and antapical series consist of five and two, respectively.

Transmission electron microscopy revealed that the species contains organelles typical to that of dinoflagellates (Fig. 14). A dinokaryotic nucleus is located in the epitheca. Chloroplasts are peripheral and include three appressed thylakoid lamellae (Fig. 15). The chloroplast connects with a pyrenoid, which is perforated by many membranous tubes (Fig. 16). The pyrenoid is located in the hypotheca, and surrounded by starch sheaths.

A considerable amount of body scales are present on the cell surface (Figs 29, 30). The scale consists of a triradiate basal plate and spine-like uprights. The outline of the reticulated basal plate is that of a rounded triangle, and measures approx. 220 nm in diameter. Its schematic drawing is given in Fig. 13e. The uprights of the scale are relatively thick and consist of a central upright and six vertically peripheral uprights (Figs 31, 32). Six radial ridges on the basal plate reach to the proximal part of each peripheral upright (Fig. 33). The scale ultrastructure was consistent within this species (Fig. 33).

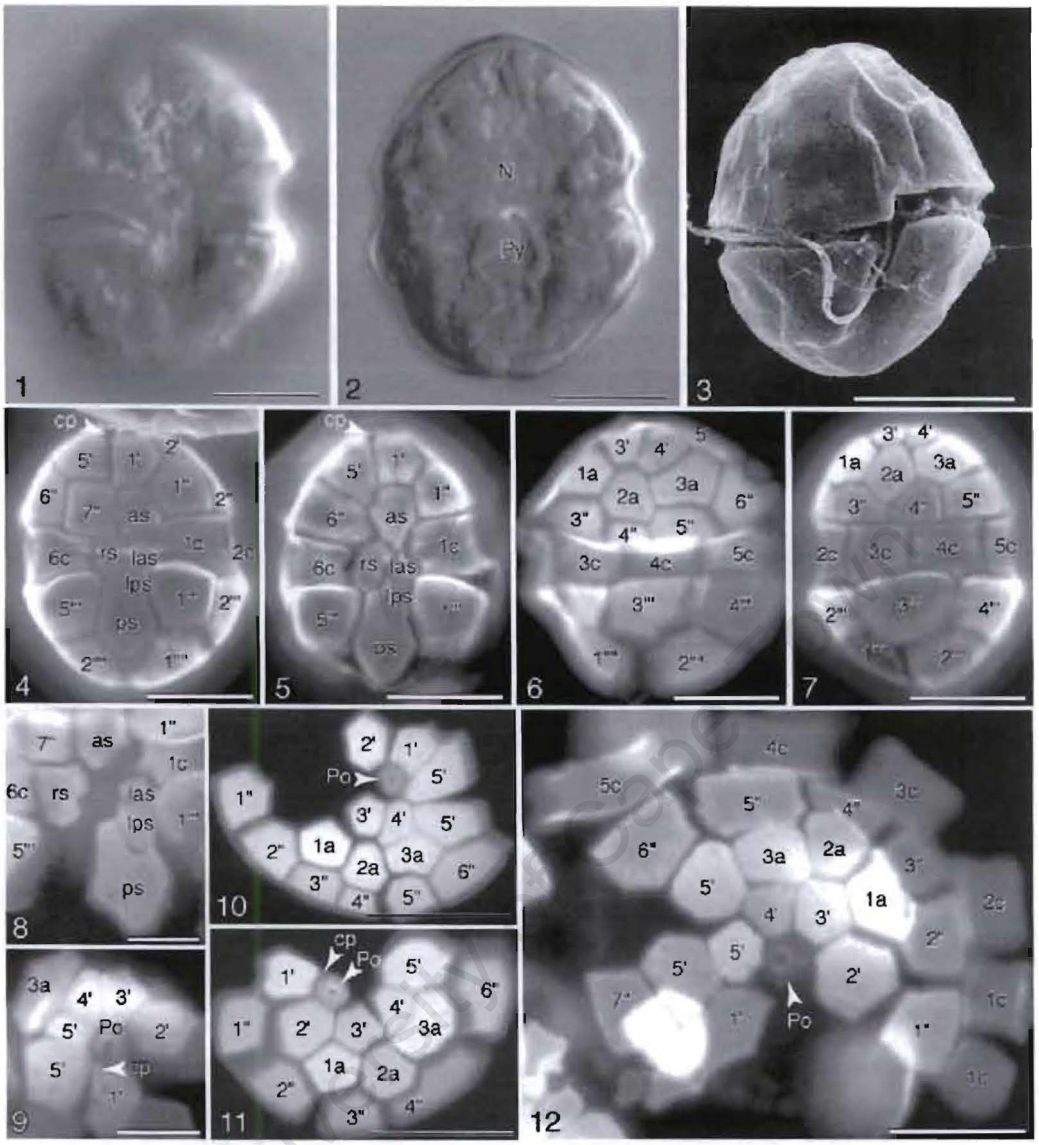

Figures 1 – 12. *Heterocapsa ovata* sp. nov. Scale bars = 10µm. Figs 1 – 2 Light microscopy, optical sections of cell in ventral view. N, nucleus; Py, pyrenoid. Fig. 3 Scanning electron microscopy, ventral view. Figs 4 – 12 Fluorescence microscopy, showing thecal plate arrangements. Po, pore plate; cp, canal plate; 1'-5', apical plates; 1a-3a, anterior intercalary plates; 1"-7", precingular plates; lps, left posterior sulcal plate; rs, right sulcal plate; ps, posterior sulcal plate; 1'''-5''', postcingular plates; 1''''-2'''', antapical plates.

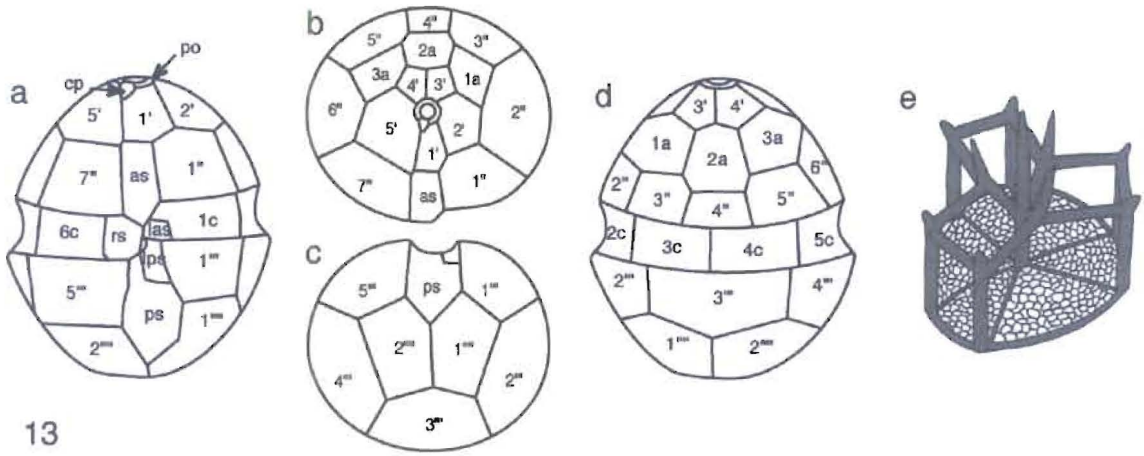

Figure 13. *Heterocapsa ovata* sp. nov. Line drawings of thecal plate arrangement and body scale (holotype), a, ventral view; b, apical view; c, antapical view; d, dorsal view; e, body scale.

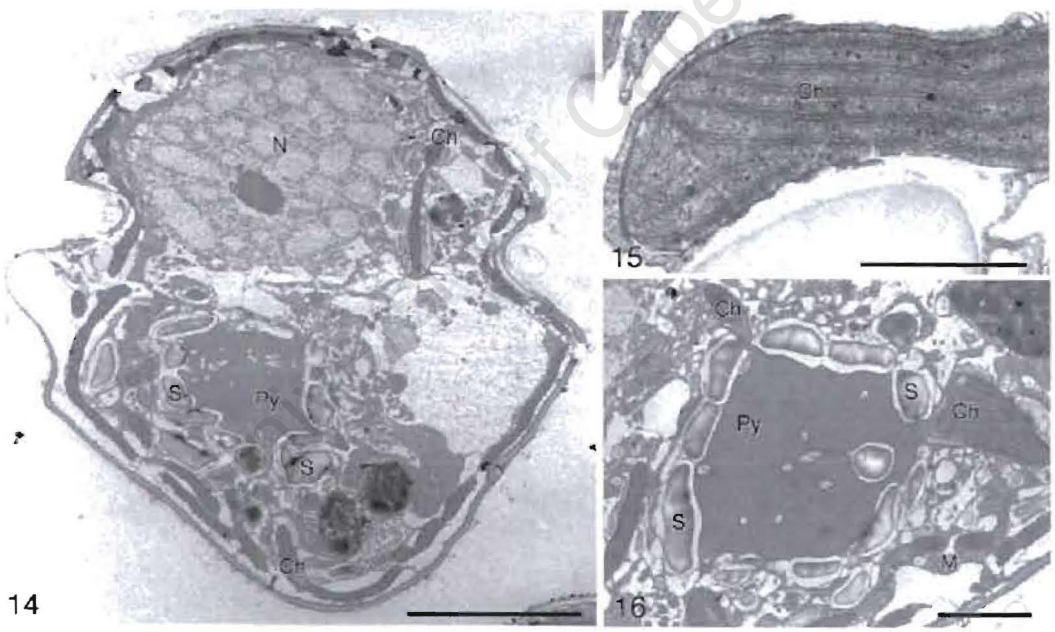

Figures 14 – 16. *Heterocapsa ovata* sp. nov. Fig. 14 Transmission electron microscopy showing longitudinal section. Ch, chloroplast; M, mitochondrion; Py, pyrenoid; S, starch grain; T, trichocyst, scale bar = 5 μm. Fig. 15 Section of a chloroplast showing three appressed thylakoids, scale bar = 500 nm. Fig. 16 Pyrenoid showing many sections of tubular cytoplasmic invagination in the matrix, scale bars = 2 μm.

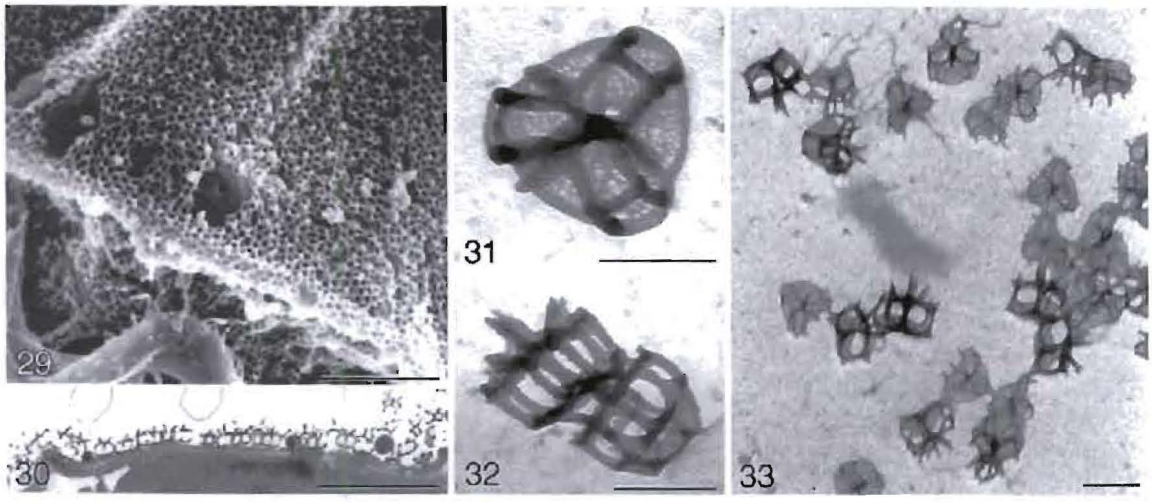

Figures 29 –33. *Heterocapsa ovata* sp. nov., body scales. Scale bars = 200 nm. Fig. 29 SEM of cell surface showing small body scales surrounding the cell body. Fig. 30 Thick section. Figs 31 –33 Whole mount preparations.

***Heterocapsa orientalis* Iwataki, Botes et Fukuyo sp. nov.**

Figs 17-28, 34-42

Cellula ovoidea, cum hypotheca aequilonga vel leviter glandi quam epitheca; 18.4-34.4 µm longa, 16.0-24.0 µm lata; tabulatio thecalis Po, cp, 5', 3a, 7", 6c, 5s, 5"', 2""; chloroplastus lutei-brunneus, in peripheria sito; pyrenoides sphaerica, per vaginam amylorum tenuis obtecta, vulgo cavea cytoplasmatis tubularis plena, in parte supra nucleum sita; sine stigmate; nucleus dinokaryoticus, sphaericus vel ovoideus, grandi, in centro hypoconi occupans; squama plus minusve triangularis, manifeste complexa, inter fila tenuius supra apices columnaribus contiens.

Holotype: Figure 28.

Type locality: Miyako Bay, Iwate Prefecture, Japan.

Etymology: orientalis = oriental, from its type locality.

Cells of *Heterocapsa orientalis* are ovoid and have a hemispherical epitheca and hypotheca (Figs 17, 18). The epi- and hypotheca are almost equal in size, at times the hypotheca can be slightly larger. The cell size is 18.4-34.4 µm (mean 25.7 µm, n = 30) in length and 16.0-24.0 µm (mean 19.6 µm, n = 30) in width. The cingulum is wide and displaced by almost 1/2 its own width (Figs 17, 19). The chloroplast is distributed peripherally in the cell and superficially appears granular. It contains a pyrenoid, which is situated in the epitheca and sometimes surrounded by starch sheaths. An ellipsoidal amd rather large nucleus occupies the bulk of the hypotheca (Fig. 18).

Thecal plates of this species are rather thin. The thecal plate arrangement, Po, cp, 5', 3a, 7", 6c, 5s, 5"', 2"", were determined using a fluorescence microscopy (Figs 19-26). Variation of plate 2a shape was observed in that it has either six sides (Fig 21) or seven sides (Figs 22).

Transmission electron microscopy revealed that *H. orientalis* has organelles typical to that of dinoflagellates (Fig. 27). The chloroplast is situated peripherally in the cell and connects with a spherical pyrenoid. The pyrenoid is located in the lower part of the epitheca and is surrounded by relatively thin starch sheaths. Many tubular cytoplasmic invaginations are present in the pyrenoid matrix. Trichocysts typical to that of dinoflagellates are present (Fig. 27).

Body scales were observed on the cell surface (Figs 27, 37, 38). The scale consists of a reticulated basal plate and spine-like uprights similar to other *Heterocapsa* species, but the three-dimensional structure is relatively complicated (Figs 34-42). Its three-dimensional structure was reconstructed from the thick vertical sections (Figs 37, 38) and thin transverse serial sections (Figs 39-42), and a diagrammatic illustration is given in Fig. 28e. The basal plate has a fine fibrous texture, approx. 300 nm in diameter and a triangular outline (Fig 34, 39). A long vertical upright rises at the center of the basal plate (Fig. 38), and nine peripheral uprights rise nearby each triangular corner (Figs 34, 40). Six radiating ridges reach the base of the six peripheral uprights, which do not stand on the corner of triangle (Fig. 39). Each peripheral upright is connected to each other at the distal part by horizontal peripheral bars (Fig. 40). The two outer most peripheral uprights are connected to three radiating bars which in turn are connected to a central upright (Fig. 40).

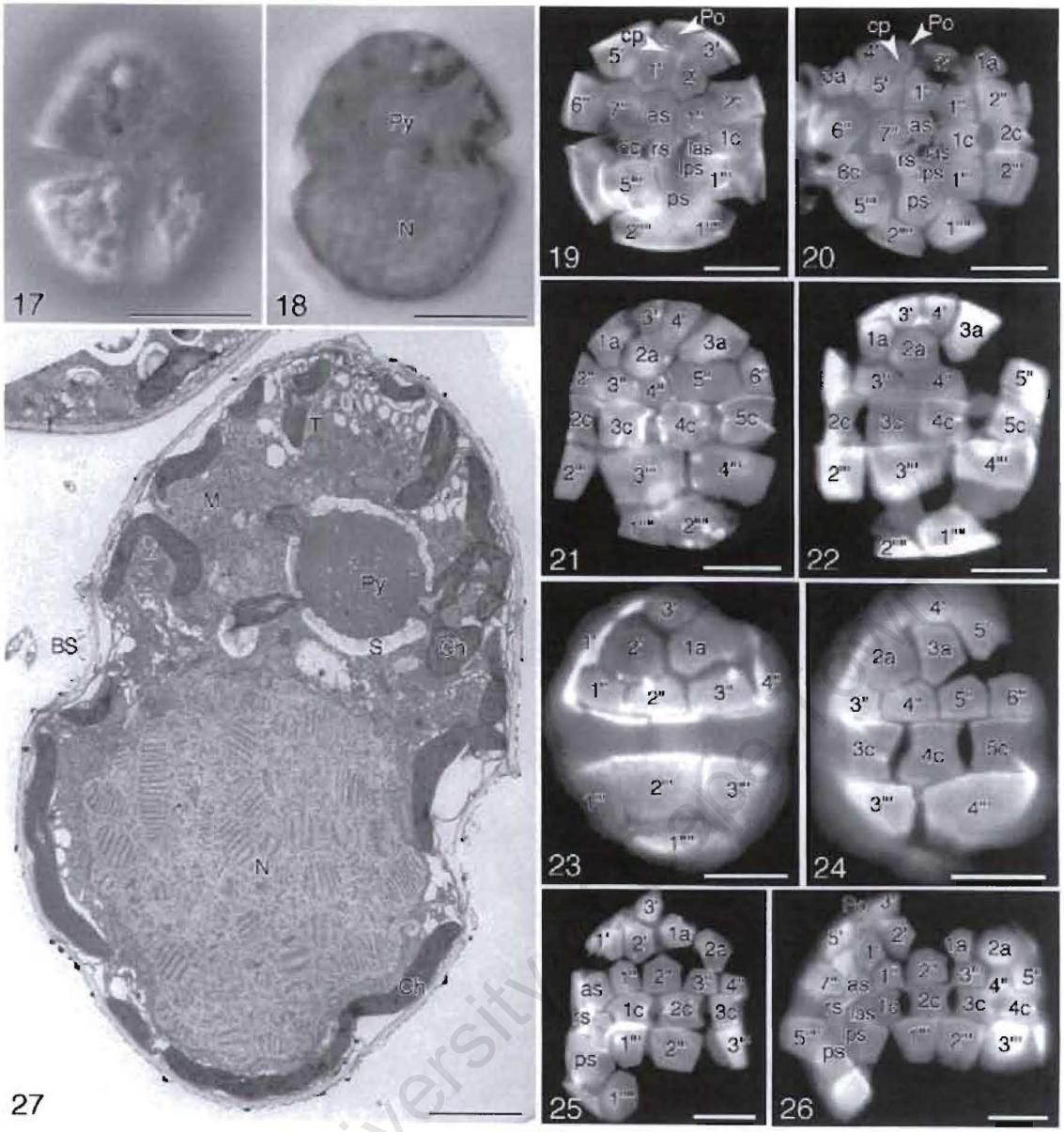

Figures 17 – 27. *Heterocapsa orientalis* sp. nov. (see figs. 1 – 16 for abbreviations). Scale bar of fig. 23 = 2 μm, others = 5 μm. Figs 17, 18. Light microscopy, optical sections of cell in ventral view. The pyrenoid (Py) is visible in the epitheca. The nucleus (N) is located in the hypotheca. Figs 19 – 26 Fluoresence microscopy showing thecal plate arrangements. Fig. 27. TEM of thin section, showing a pyrenoid including many tubular cytoplasmic invaginations.

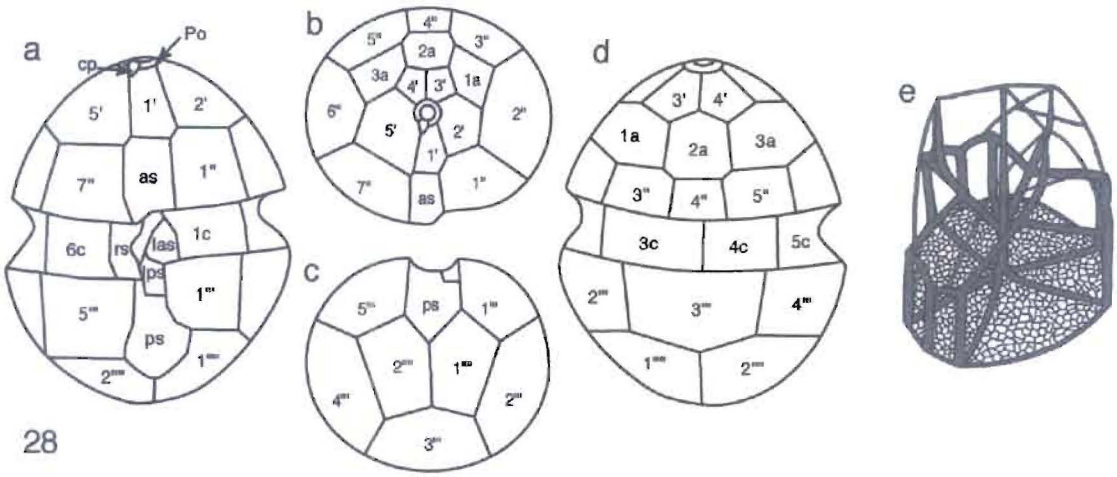

Figure 28. *Heterocapsa orientalis* sp. nov. Line drawings of thecal plate arrangement and body scale (holotype), a, ventral view; b, apical view; antapical view; d, dorsal view; e, body scale.

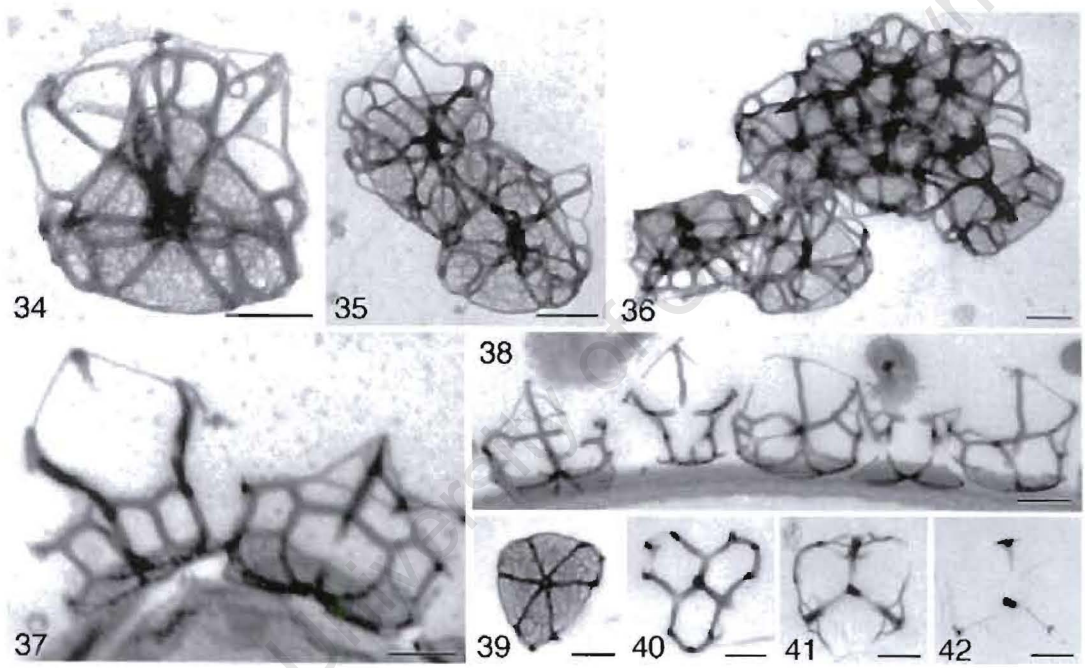

Figures 34 – 42. *Heterocapsa orientalis* sp. nov., body scales. TEM of body scales. Scale bars = 200 nm. Figs 34 – 36 Whole mount preparations. Figs 37, 38 Thick sections, showing thin thread connections at the top of the scale. Figs 39 - 42 Serial sections of a body scale.

All these scale structures are largely similar to those of *H. triquetra*, however, the scale of *H. orientalis* also contains thin threads at the tip of radiate bars (Figs 34, 35) that connect the distal part of the radiate bars and a central spine (Figs 37, 38, 42). Contrary to *H. ovata* (Fig. 13e), *H.*

orientalis don't have short spines on the peripheral uprights. All these structures are consistent within the specimen (Figs 35, 36).

DISCUSSION

Heterocapsa ovata and *H. orientalis* are relatively small thecate dinoflagellates. Their thecal plate arrangements correspond to that of the genus *Heterocapsa*, Po, cp, 5', 3a, 7", 6c, 5s, 5"", 2"". A sheathed pyrenoid and three-dimensional triradiate body scales are present in both species. These morphological characters strongly support their affinity to the genus *Heterocapsa*.

Cells of *H. ovata* possess a nucleus in the epitheca and a pyrenoid below the nucleus, this positioning of organelles is identical to *H. triquetra*. However, its ovoid cell shape is not similar to *H. triquetra* and other described species. In addition to the cell shape, the body scale ultrastructure of this species is relatively simple in comparison to other *Heterocapsa* species. This scale is composed of a triangular basal plate and a three-dimensional structure with six peripheral uprights. In other *Heterocapsa* species such as *H. circularisquama* and *H. horiguchii*, the scales also possess six peripheral uprights (spines) on the rim of basal plates, but the outline of those basal plates are somewhat circular rather than triangular, and the peripheral spines do not have horizontal bars at the distal part (Horiguchi 1995, Iwataki *et al.* 2002b). We thus conclude that the species is a new *Heterocapsa* species, *H. ovata*.

Cell of *H. orientalis* has a nucleus situated in the hypotheca with a pyrenoid located above it. Other *Heterocapsa* species known to have this orientation are *H. niei*, *H. pygmaea* and *H.*

minima (Loeblich III 1968, Loeblich III *et al.* 1981, Pomroy 1989). The cell size of *H. orientalis* is, however, larger than these species. The body scale of *H. orientalis* possesses nine peripheral uprights, with the distal parts connected to each other by bars. Although this structure resembles that of *H. triquetra* (Pennick & Clarke 1977), the scale possesses additional thin threads at the top of the uprights instead of short spines, contributing to a more complicated structure, and in fact, more complicated than any other scale structure of the genus *Heterocapsa*. The distinctive structure of the cell and body scale therefore renders this species a new species, *H. orientalis*.

The former *Heterocapsa* species, *H. ovata,* was first collected in 1986 and again in 2000 at the same location in the Sea of Japan, and it has not been found anywhere else thus far. The latter species, *H. orientalis,* has been found in Ofunato Bay in 1997 and 2000, in Miyako Bay in 2000, and it was also found on the south coast of South Africa in 1998 (Botes *et al.* 2002).

A *Glenodinium* sp. reported from Nagasaki Harbor (Uchida 1975) has resemblance to *Heterocapsa* species due to its thin thecal plates and cell shape, as noted by Loeblich *et al.* (1981). The cell shape of is rather similar to *H. orientalis* and *H. ovata,* but the identity of this species could not be verified due to the unavailability of samples of this species (Uchida, pers. comm.).

The genus *Heterocapsa* was described in 1883 by Stein and recently eleven species have been assigned to the genus (Iwataki *et al.* 2002a). As a result, several morphological characters have revealed itself as synapomorphies which are important at the generic level, i.e. thecal plate

arrangement and the triradiate three-dimensional body scales (Hansen 1989, Hansen 1995, Horiguchi 1995, Horiguchi 1997, Iwataki *et al.* 2002a). These synapomorphies seem specific *Heterocaps*, and molecular phylogeny e.g. partial SSU rDNA (Saunders *et al.* 1997) and partial LSU rDNA (Daugbjerg *et al.* 2000) have supported *Heterocapsa* as a monophyletic group.

Although all *Heterocapsa* species share the characters mentioned above, each species can be distinguished by comparing characters and its character states on species level such as (1) cell size and shape (e.g. large epitheca, antapical horn), (2) tubular invaginations in pyrenoid matrix, (3) position of nucleus and pyrenoid, and (4) structure of body scales: (1) Cell size and shape are similar and often overlapping, however, several morphological characters specific to certain species, such as large epitheca and antapical horn, could be recognized as species criteria. For example, *H. arctica*, *H. lanceolata*, *H. rotundata* and *H. triquetra* could be distinguished by their cell shape (Horiguchi 1997, Hansen 1995, Iwataki *et al.* 2002a, Stein 1883). A small species *H. minima* also possesses a relatively large epitheca (Pomroy 1989) and *H. pacifica* has a large epitheca and an enigmatic antapical horn (Kofoid 1907), but other decisive specific characters of these species are still not confirmed. (2) Tubular invaginations in the pyrenoid matrix have been found in *H. arctica*, *H. illdefina*, *H. triquetra*, *H. orientalis* and *H. ovata* (Horiguchi 1997, Herman & Sweeny 1976, Dodge & Crawford 1971, this paper). The function of this character is unclear, but it has been observed as a consistent structure in these species. In fact, *H. illdefina* and *H. circularisquama* are distinguished from one another by the presence/absence of this structure (Horiguchi 1995). The invaginations appear to exist in *Heterocapsa* species of very large size. (3) Two shapes of nuclei, ellipsoidal and spherical, have been observed in *Heterocapsa* species. In the case of a spherical nucleus, it can be located either

in the epitheca or the hypotheca, and then pyrenoid can either be below or above the nucleus. *H. triquetra*, *H. horiguchii* and *H. ovata* contain a nucleus in its epitheca with the pyrenoid below it (Stein 1883, Iwataki *et al.* 2002a, this paper). On the other hand, *H. niei*, *H. pygmaea* and *H. orientalis* have these organelles in inversed positions. Loeblich (1977) mentioned that the spherical nucleus of *H. niei* is located in the hypotheca and moves to the center during mitosis, this was also observed in *H. pygmaea* (Loeblich *et al.* 1981). However, the nucleus never penetrates into the other hemitheca and the basic position of nucleus and pyrenoid can therefore be used as a diagnostic character. Many other *Heterocapsa* species, e.g. *H. circularisquama* and *H. lanceolata*, have ellipsoidal nuclei and it is therefore difficult to differentiate in the positioning. (4) The body scale ultrastructure is the most useful character for distinction at species level (Morrill & Loeblich 1983, Hansen 1989, Horiguchi 1995, Iwataki *et al.* 2002a). Almost all species could be distinguished by using the ultrastructural characteristics of the body scale such as the shape of basal plate, number of uprights, bars, spines, and threads. For example, the number of peripheral uprights in *H. orientalis* is nine, the basal plate is triangular and no short spines are present. In *H. ovata*, the number of peripheral uprights is six, the basal plate is a circular triangle and short spines are present.

Since these four diagnostic characters exhibit different states at species level and subdivide the genus into several monphyletic groups, they could be expected to serve as a key-character for solving phylogenetic relationships between species withinin the genus *Heterocapsa*. The overlap between species indicate the phylogenetic relationships between species within the genus and that some characters evolved several times in the evolution of these species. Additional molecular information may further resolve these relationships.

The genus *Heterocapsa* was originally established as a taxon of dinoflagellates commonly possessing a sutured epitheca and an unsutured hypotheca (Stein 1883). As it stands, however, this generic criterion has lost its diagnostic value. Consequently, we need to revise the current status of the genus proposed by Stein (1883). We consider the presence of thecal plates and their arrangements as well the presence of three-dimensional triradiate body scales as important generic criteria, and propose the revision of the genus *Heterocapsa* as described below.

The genus *Heterocapsa* Stein emend Iwataki et Fukuyo

Unicellular, thecate, photosynthetic dinoflagellates. Typical thecal plate arrangement: Po, cp, 5', 3a, 7", 6c, 5s, 5"', 2"''. Chloroplast parietal, containing peridinin as major carotenoid, with pyrenoid. Eyespot lacking. Three-dimensional triradiate body scales present.

Type species: *Heterocapsa triquetra* (Ehrenberg) Stein 1883

Synonym: *Cachonina* Loeblich III 1969

CHAPTER 3

KARENIA CRISTATA SP. NOV. AND *KARENIA BICUNEIFORMIS* SP. NOV. (GYMNODINIALES, DINOPHYCEAE): TWO NEW *KARENIA* SPECIES FROM THE SOUTH AFRICAN COAST

ABSTRACT

In 1988 and 1989, an undescribed gymnodinioid dinoflagellate species turned the waters of the largest bay in South Africa, False Bay, to a dirty olive-green colour. The bloom was accompanied with extensive abalone (*Haliotis midae* Linnaeus) mortalities and noxious gases causing eye, nose, skin and throat irritations in humans. In 1995, another undescribed gymnodinioid species bloomed in the same bay but with no adverse effects to marine fauna and humans. These two species both form an established component of the phytoplankton assemblage on the south coast of South Africa. They are here described as *Karenia cristata* Botes, Sym et Pitcher and *Karenia bicuneiformis* Botes, Sym et Pitcher. *K. cristata* has a straight apical groove which is elevated into an apical crest and extends down immediately to the right of the sulcal extension on the ventral side. The hypocone is asymmetrical with the right lobe larger and more rounded than the left, and the nucleus is central with the bulk of the nucleus situated in the hypocone. Its pigment content is similar to that of *K. mikimotoi* and *K. brevis*. Other than *K. brevis*, *K. bicuneiformis* is significantly larger than the other *Karenia* species and is distinctly dorso-ventrally flattened. The hypocone is w-shaped and the epicone is conical, giving the cell a distinctly angular outline. Pairwise distance comparisons of partial large subunit (28S) rDNA sequences indicate that these two species are clearly different to other species within the genus.

INTRODUCTION

Until recently considerable confusion existed world-wide with regard to the identity of many closely related species resembling *Gymnodinium mikimotoi* Miyake et Komani ex Oda *sensu lato* (Steidinger *et al.* 1998). Recent publications (Chang 1999, Daubjerg *et al.* 2000, Hansen *et al.* 2000, Yang *et al.* 2000, Yang *et al.* 2001) have partially clarified this confusion by revising the genus *Gymnodinium sensu lato* (which resulted in the genus being split into four genera: *Gymnodinium sensu stricto, Karenia, Karlodinium* and *Akashiwo*) and by describing species such as *K. brevisulcata* (Chang) G. Hansen et Moestrup, *K. digitata* Yang, Takayama, Matuoka et Hodgkiss and *K. longicanalis* Yang, Hodgkiss et Hansen.

As part of a larger study, several gymnodinioid species present on the south coast of South Africa were studied with respect to light microscopy (LM), scanning electron microscopy, pigment content and partial large subunit (28S) rDNA sequences. During the course of this study (he results thereof are published separately) it became evident that two of these species are markedly different than their counterparts and should therefore be described as two new *Karenia* species, here named *K. cristata* Botes, Sym et Pitcher sp. nov. and *K. bicuneiformis* Botes, Sym et Pitcher sp. nov.. The former is known in the literature as *Gymnodinium* sp. (Horstman *et al.* 1991, Matthews & Pitcher 1996, Pitcher & Matthews 1996) or *Gymnodinium* cf. *mikimotoi* (Pitcher & Calder 2000) and bloomed at the H.F. Verwoerd Nature Reserve, South Africa (Fig. 1) during April in 1988 and again during March in 1989 (Horstman *et al.* 1991). It subsequently bloomed again at Gordon's Bay in 1995-6 (Pitcher & Matthews 1996) and was responsible for eye, nose, throat and skin irritations as well as extensive mortalities of sub- and intertidal fauna. Blooms of *K. cristata* were associated with calm periods and sea surface temperatures exceeding 17°C followed by an onshore wind necessary to concentrate the blooms inshore (Horstman *et al.* 1991). In 1995, *K.*

bicuneiformis bloomed in Gordon's Bay, South Africa (Fig. 1) and thereafter again in 1997. No adverse effects were attributed to this species. Both species form an established component of the phytoplankton on the south coast of South Africa and are typically present in False Bay and Walker Bay, South Africa. The type localities of *K. cristata* and *K. bicuneiformis* are H.F. Verwoerd Nature reserve and Gordon's Bay respectively (Fig. 1).

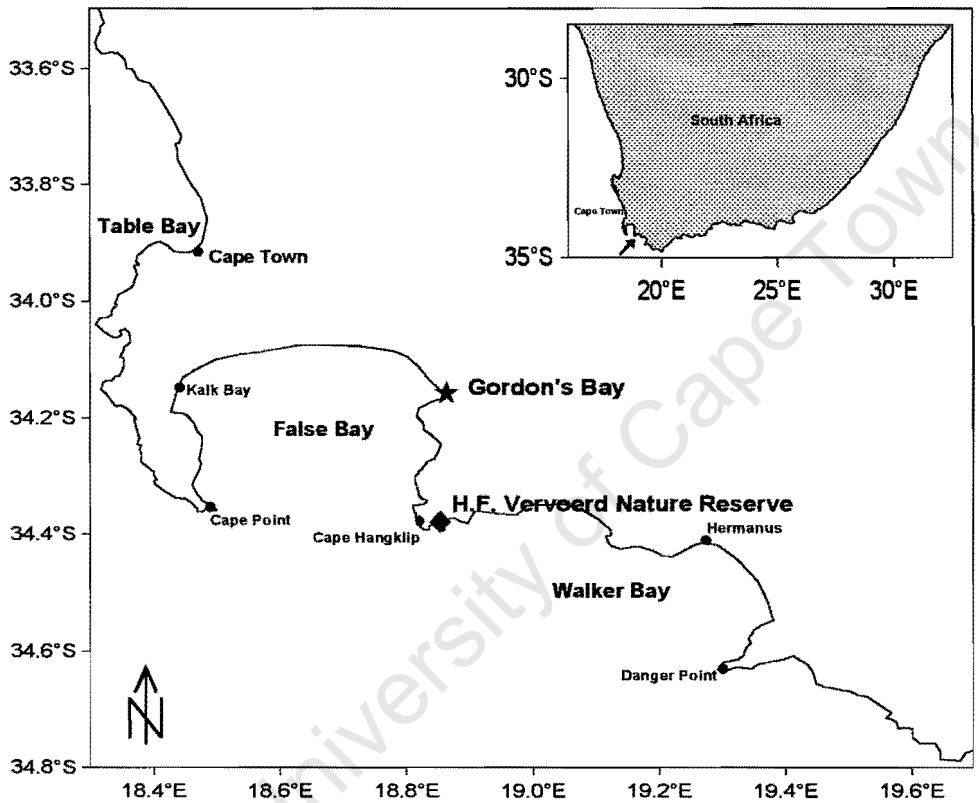

Figure 1. Sites within False Bay and Walker Bay, South Africa, where *K. cristata* and *K. bicuneiformis* have been recorded. The type locality of *K. cristata* (♦) and *K. bicuneiformis* (★) are indicated by the respective symbols.

MATERIALS AND METHODS

Samples and sampling

Field samples were collected at Gordon's Bay (Fig. 1) and preserved with 5% formaldelyde (buffered with $CaCO_3$ AR grade, pH ≥ 7). For live observation, pigment extraction and light microscopy, samples were collected with a 20µm net and concentrated by means of a 10µm mesh.

Light microscopy

Specimens of both species were observed, measured and photographed with either an Olympus B201 light microscope equipped with an Olympus DP10 digital camera or a Zeiss Axiophot photomicroscope with a photographic set-up that included the production of videoprints, video recording and micrographs.

Scanning electron microscopy

Scanning electron micrographs were obtained according to the technique developed by Botes *et al.* (2002), except that cells of *K. cristata* and *K. bicuneiformis* were preserved with buffered 5% formaldehyde, instead of osmium tetroxide (OsO_4).

Pigment composition

Cells of *K. cristata* were filtered through 4.7 cm GF/F (Whatman) microfiber filter paper. Pigments were extracted in 2 ml 90 % acetone using ultrasonication and centrifugation and were analysed by HPLC according to Barlow *et al.* (1997) at a flow rate of 1 $mlmin^{-1}$ on a C-8 column using a binary linear gradient. Solvent A consisted of 70:30 (v/v) methanol: 1 M ammonium acetate and solvent B was 100% methanol. Pigments were detected by absorbance at 440 nm using a Thermo Separations UV 6000 diode array detector. Pigments were

identified by retention time and appropriate diode array spectra (Jeffrey *et al.* 1997). Chlorophyll *a* and *b*, and α- and β- carotene standards were obtained from Sigma Chemical Co. and the Water Quality Institute (VKI) Hørsholm, Denmark.

DNA extraction, amplifications and determination of partial large subunit (28S) rDNA sequences (D1-D3).

For *K. cristata*, isolation and preparation of individual live cells and PCR protocols of Bolch (2001) were followed to amplify ~ 850 base pairs of LSU rDNA, using terminal primers D1R (Scholin *et al.* 1994) and D3Ca (Lenaers *et al.* 1989) (Table 1). The protocol for polymerase chain reaction (PCR) amplification and thermal cycling of Hansen *et al.* (2000) were followed but with a reaction volume of 25µl, 3mM $MgCl_2$ and Bioline Taq polymerase (Whitehead Scientific, Cape Town, South Africa). DNA fragments were checked on 1% agarose gels containing ethidium bromide (EtBr), cut out with a sterile surgical blade and purified using the QIAquick Gel Extraction Kit (Qiagen, Southern Cross Biotechnology, Cape Town, South Africa). Both strands of PCR product were sequenced by using the ABI PRISM BigDye terminator Cycle-Sequencing Ready Reaction Kit (v. 2) (PE Biosystems, Johannesburg, South Africa). The sequence reactions were run on an ABI PRISM 3100 Genetic Analyser, following the recommendations of the manufacturer.

Table 1 Oligonucleotide primer sequences used to amplify the partial large subunit (28S) rDNA sequences

Primer name	Primer sequence (5' - 3')
D1R	5' ACCCGCTGAATTTAAGCATA 3' (forward)
D3Ca	5' ACGAACGATTTGCACGTCAG 3' (reverse)

Pairwise distance comparisons

Pairwise distance comparisons between isolates within the same species and, species within the same genus were calculated based on the partial LSU rDNA sequences (Table 2). Sequences used for parsimony comparisons were between 543 and 962 base pairs in length. The Tamura-Nei Model (Tamura & Nei 1993) was used to calculate the distances using PAUP*4.0b8 (Swofford 1998) (Table 4). Note that the pairwise distances for K. bicuneiformis were based on the New Zealand species (U92251).

Table 2. Specimens included in pairwise distance comparisons. Two *Akashiwo sanguinea* isolates and two *Karenia mikimotoi* isolates were used to calculate pairwise distances for isolates within species and the various *Karenia* species were used to calculate pairwise distances for species within the same genus.

Species name (Names in brackets are as it appears in Genbank)	Origin	Isolated by	Accession number (GenBank)
Akashiwo sanguinea	False Bay, RSA	L. Botes	AY518424
Akashiwo sanguinea (*Gymnodinium sanguineum*)	Marlborough Sounds, NZ	L. Rhodes	U92253
Karenia brevis	Florida, USA	W.B. Wilson	AF200677
Karenia brevisulcata	Wellington Harbour, NZ	L. Mackenzie	AY243032
Karenia cristata	False Bay, RSA	L. Botes	AY525907
Karenia mikimotoi	Seto Island Sea, JAPAN	T. Ikeda & S. Mutsuno	AF200681
Karenia mikimotoi	Plymouth, UK	D. Harbor	AF200678
Karenia bicuneiformis (*Gymnodinium* sp.)	Hawke's Bay, NZ	A. Haywood	U92251
Karenia sp. (*Gymnodinium* sp.)	CHILE	-	AF200677

OBSERVATIONS & RESULTS

Karenia cristata Botes, Sym et Pitcher sp. nov.

Figs 2 – 9

DIAGNOSIS

Cellulae dorsiventraliter complanatae (25.7µm ± 1.65µm [n=15] longae, 24.29µm ± 2.50µm [n=15] lataeque circum, 10µm [n=1] altaeque). Hypoconus asymmetricus excentricus lobo dextero maiore rotundatioreque quam lobo sinistro. Canalis apicalis rectus et in crista apicali elevatus et ad juncturam cinguli sulcique in superficie ventrali et tantum distantia brevi in superficie dorsali extensus. Nucleus in hypocono centralis sed aliquantum in epicono extensus. Sulcus in epicono extensus et in hypocono versus antapicem dilatatus. Cingulum loco motum 2 plo latitudine suo. Chloroplasti numerosi chlorinique et in forma variabiles.

Cells dorso-ventrally flattened (25.70 ± 1.65µm [n=15] long, 24.29 ± 2.50µm [n=15] wide, 10µm [n=1] deep). Hypocone asymmetric, with larger and more-rounded right lobe. Apical groove straight and elevated into an apical crest, extending to the cingulum-sulcal junction on ventral side of cell and only a short distance on dorsal side of cell. Nucleus central in hypocone, but extending somewhat into epicone. Sulcus extends onto the epicone and flares out to antapex. Cingulum displaced twice its own width. Chloroplasts numerous, yellow-green and variable in shape.

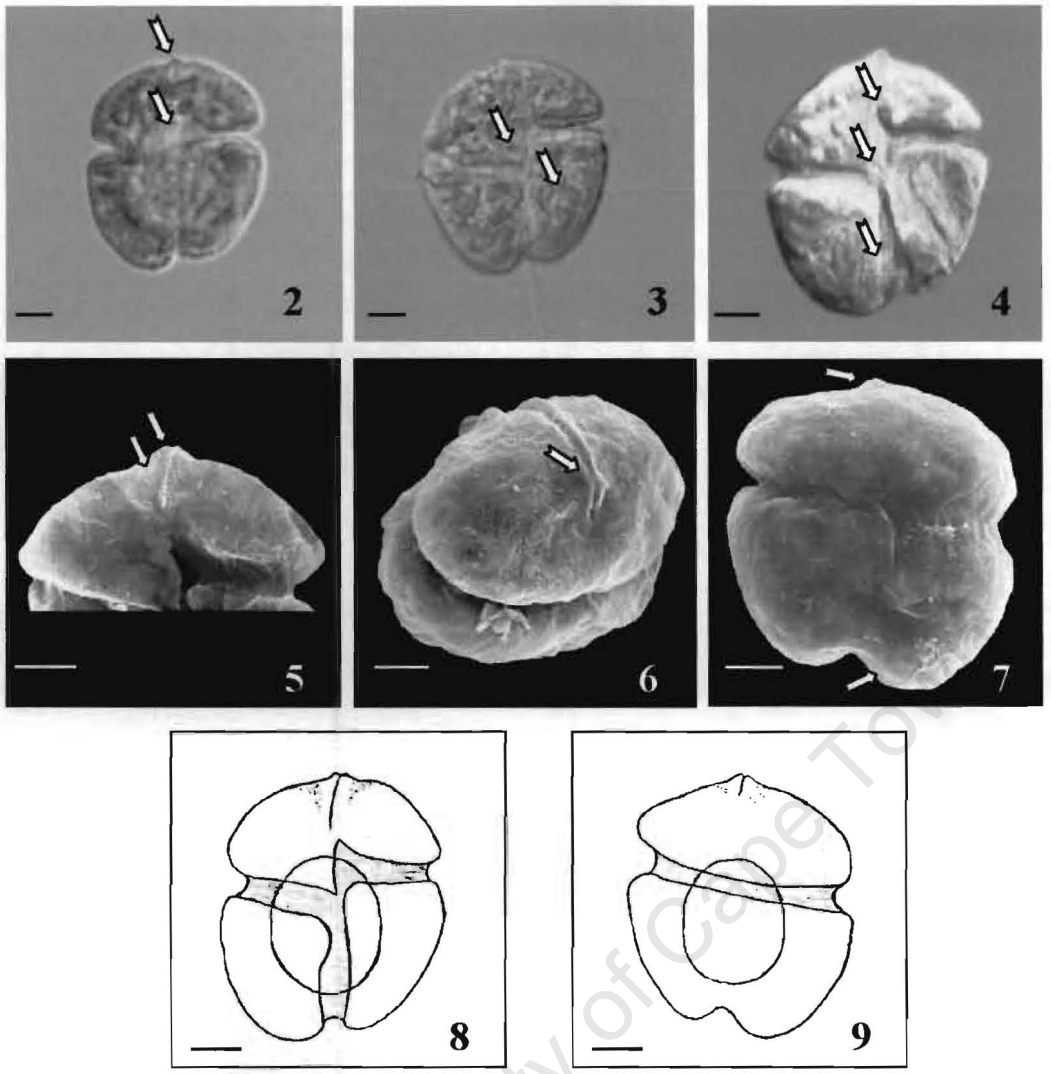

Figures 2 – 9. *K. cristata* sp.nov. Scale bar = 5μm. Figs. 2 – 6 Light micrographs of live cells. Fig. 2 Typical cell shape in ventral view showing the asymmetric hypocone, nucleus position (bottom arrow) and the apical crest with the apical groove (top arrow). Fig. 3 Ventral view of the cell showing the cingular displacement (top arrow) and the chloroplasts (bottom arrow) which are variable in shape. Fig. 4 Ventral view showing the cingular displacement (middle arrow) and the sulcus which extends anteriorly onto the epicone (top arrow) and posteriorly flares out to antapex (bottom arrow). Figs 5 - 7 Scanning electron micrographs of formalin preserved cells. Fig. 5 Ventral view of the apical crest (bottom arrow) with the apical groove (top arrow). Fig. 6 Anterior view of the apical groove (arrow) extending from the ventral side across to the dorsal side. Fig. 7 Dorsal view of the apical crest (top arrow) and asymmetric hypocone (bottom arrow). Figs 8, 9 Line drawings of the ventral and dorsal surfaces respectively.

HOLOTYPE: Fig. 2

ISOTYPE: SEM stub containing specimens of *K. cristata* (Accession number J 100091) were submitted to the Moss Herbarium, School of Animal, Plant and Environmental Sciences, University of the Witwatersrand, Johannesburg, South Africa

ETYMOLOGY: Latin *cristata*, crest

TYPE LOCALITY: H.F. Verwoerd Nature Reserve, South Africa (Fig.1)

DISTRIBUTION: False Bay and Walker Bay, South Africa (Fig. 1)

DESCRIPTION: Motile cells of *K. cristata* are dorso-ventrally flattened (25.70 ± 1.65µm long [n = 15], 24.29 ± 2.50µm [n = 15] wide and ~ 10µm deep [n = 1 (Fig. 6)]). The hypocone is asymmetric with a larger and more rounded right lobe (Figs 2, 3, 4, 7). The cingulum is median to premedian (Fig. 3) with a displacement of twice its own width (Fig. 4). The sulcus extends onto the epicone and widens toward the antapex on the hypocone (Fig. 4). The apical groove is straight (Figs 2, 5, 6) and elevated to form a crest on the apex (Figs 2, 4, 5). On the ventral surface the apical groove starts immediately to the right of the sulcal extension (Fig. 5) and extends for a short distance onto the dorsal surface (Fig. 6). The nucleus is round to oval and situated in the centre of the cell, with the bulk of the nucleus situated in the hypocone (Fig. 2). Several yellow-green chloroplasts which are variable in shape, are present (Fig. 3).

REMARKS: The swimming behaviour is similar to the "falling leaf" motion of *K. mikimotoi* (Matsuoka *et al.* 1989), however it seems to be affected by the large right lobe. Whilst rotating around its own axis during forward propulsion, the asymmetric nature of the hypocone makes it appear that the right lobe labours "uphill" but falls "downhill" effortlessly.

The main carotenoid of *K. cristata* is fucoxanthin and, like *K. mikimotoi* and *K. brevis*, this species contains the accessory pigment gyroxanthin-diester (Table 3).

Pairwise distance values obtained from comparison of partial LSU rDNA sequences confirm the status of *K. cristata* as a new species with values falling within the range calculated for species within the same genus and not within the range calculated for isolates within the same species (Table 4).

K. cristata, like *K. brevis* and *K. brevisulcata* (Table 3), contains an aerosol toxin which causes coughing, burning of nasal passages, difficulty in breathing, stinging of the eyes and irritation to the skin (Chang 1999, Hemmert 1975, Steidinger & Baden 1984) . A sea-urchin bioassay indicated that a cell concentration of ~ 0.5 x 10^6 cells.l^{-1} of *K. cristata* inhibits normal development of sea urchin embryos (Horstman *et al.* 1991). This species also has adverse effects on abalone (*Haliotis midae*) larvae (2 days old) and spat (3mm animals) with a LC10 value of 1,143184 ± 57,678 cells.l^{-1} for abalone larvae and a LC10 value of 2,526,651 ± 73,814 cells.l^{-1} for abalone spat (Botes *et al.* 2003 a). Cell concentrations in excess of 10^6 cells.l^{-1} were reported when 40 tons of adult abalone washed ashore during the 1989 bloom (Horstman *et al.* 1991).

Table 3. Comparison of features for differentiating related *Karenia* species

Parameters	*K. cristata* sp. nov.	*K. bicuneiformis* sp. nov.	*K. mikimotoi* Takayama & Adachi (1984) *Hansen *et al*. (2000a)	*K. brevis* Takayama (1990) *Millie *et al*. (1995)	*K. brevisulcata* Chang (1999)	*K. longicanalis* Yang *et al*. (2001)	*K. digitata* Yang *et al*. (2000)
Cell length (μm)	25.70 ± 1.65, n=15	36.25 ± 2.37, n=15	25 - 35	18 - 40	19-25 (big) 13-17 (small)	25.9± 5.5, n=50	21.46± 2.96, n=50
Cell width (μm)	24.29 ± 2.50, n=15	33.83 ± 2.53, n=15	23 - 33	15 - 70	18-22 (big) 10-17 (small)	21.1± 4.3, n=50	18.25± 2.54, n=50
Dorso-ventrally flattened	~ 10 μm in side view	~ 5 μm in side view	no data	no data	no data	no data	no data
Hypocone shape	eccentric	W-shaped	bilobed	bilobed	circular outline	hemispherical	rounded to hemisperical
Sulcus extension	present	present	present	present	present	absent	present
Apical groove - ventral - dorsal	long short	long short	long short	long short	short short	long long	long short
Apical crest	present	absent	absent	absent	absent	absent	absent
Carina	absent	absent	absent	present	absent	absent	absent
Nucleus	round to oval, central	oval, left in hypocone	reniform, left in hypocone	round, left in hypocone	round to horisontally elongated, left to central in hypocone	round, central	round, subcentral
Chloroplasts	variable in shape	variable, diso-shaped upon fixation	shapeless	peripheral	elongated	round	shapeless
Aerosol Toxin	present	absent	absent	present	present	absent	absent
Pigment content:	Chlorophyll c_2, c_3, a But-Fucoxanthin Fucoxanthin Hex-fucoxanthin Diadinoxanthin Gyroxanthin-diester β-Carotene	no data	* Chlorophyll c ½c_2, c_3, a But-Fucoxanthin Fucoxanthin Hex-fucoxanthin Diadinoxanthin Gyroxanthin-diester β-Carotene	* Chlorophyll c ½c_2, c_3, a But-Fucoxanthin Fucoxanthin Hex-fucoxanthin Diadinoxanthin Gyroxanthin-diester β-Carotene	no data	no data	no data

Table 4. Pairwise distance values, obtained from comparison of LSU rDNA sequences, calculated for species within the same genus and isolates within the same species.Note that the pairwise differences for *K. bicuneiformis* were based on the sequence of *Karenia* sp. (*Gymnodinium* sp. U92251).

Pairwise distance comparison (Taimura-Nei Model):		Actual value of comparison between individuals	Mean	Range
Isolates within the same species:			0.000372004	0.00000000 - 0.0008178
examples ~	*K. mikimotoi* (UK) - *K. mikimotoi* (Japan)	0.00012345	-	
	A. sanguinea (Dk) - A. sanguinea (NZ)	0.00064774	-	
Species within the same genus:			0.024450356	0.01335893 - 0.03854208
examples ~	*K. cristata* (RSA.) - *K. brevisulcata* (NZ)	0.01426310	-	-
	K. cristata (RSA.) - *Karenia* sp. (Chile)	0.01189127	-	-
	K. cristata (RSA) - *K. mikimotoi* (Japan)	0.02132520	-	-
	K. cristata (RSA) - *K. brevis* (USA)	0.01927742	-	-
	K. brevisulcata (NZ) - *Karenia* sp. (Chile)	0.01389328	-	-
	K. mikimotoi (Japan) - *K. brevis* (USA)	0.01335893	-	-
	K. bicuneiformis (NZ) - *K. cristata* (RSA.)	0.02615790	-	-
	K. bicuneiformis (NZ) - *K. brevisulcata* (NZ)	0.03757461	-	-
	K. bicuneiformis (NZ) - *K. mikimotoi* (Japan)	0.03854208	-	-
	K. bicuneiformis (NZ) - *K. brevis* (USA)	0.03474694	-	-

Karenia bicuneiformis Botes, Sym et Pitcher sp. nov.

Figs 10 –19

DIAGNOSIS

Cellulae dorsiventraliter complanatae (36.25 ± 2.37µm [n=15] longae, 33.83 ± 2.53µm [n=15] lataeque circum, ~ 5µm [n=1] altaeque). Hypoconus bicuneiformis et epiconus acute conicus igitur cellula quinquangularis. Lobus uterque hypoconi fortasse indentatus. Canalis apicalis rectus ad juncturam cinguli sulcique in superficie ventrali et tantum distantia brevi in superficie dorsali extensus. Nucleus ovalis et in hypocono in late sinistro situs. Extensio sulci in epicono praesens. Cingulum loco motum 1 plo latitudine suo. Chloroplasti numerosi chlorinique et in forma variabiles. Chloroplasti fixi conservatique globosi.

Cells dorso-ventrally flattened (36.25 ± 2.37µm [n=15] long, 33.83 ± 2.53µm [n=15] wide and ~ 5µm [n=1] deep). Hypocone w-shaped and epicone sharply conical, giving the cell a markedly angular outline. Each lobe of hypocone can be indented at times. Apical groove is straight, extending down to the cingulum-sulcus junction on ventral side of cell and only a short distance on dorsal side of cell. Nucleus oval and on the left side of the hypocone. Sulcus extension present on the epicone. Cingulum displaced by one cingulum width. Chloroplasts numerous, yellow-green and variable in shape. Preserved chloroplasts round up.

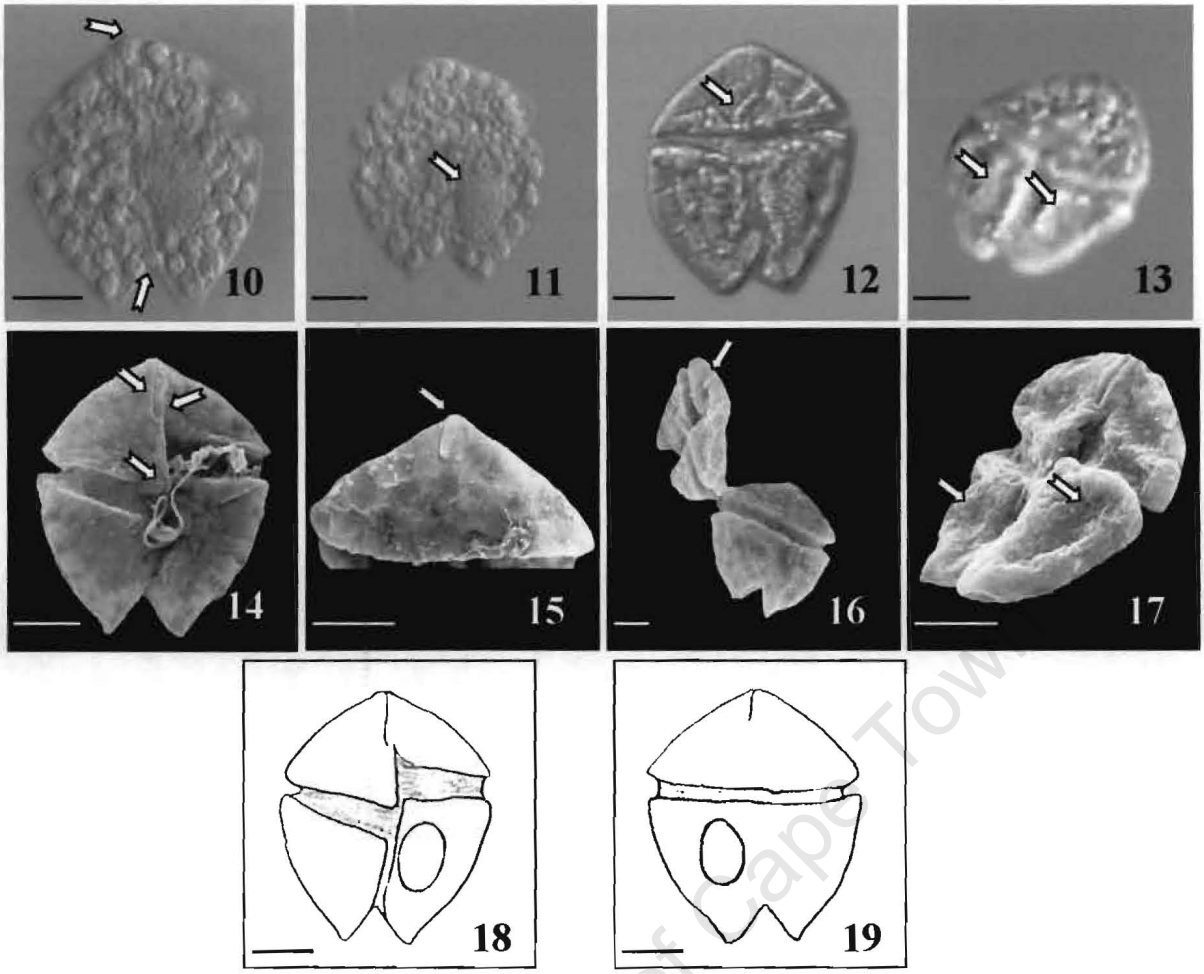

Figures 10 – 19. *K. bicuneiformis* sp.nov. Scale bar = 10μm. Figs 10 – 13 Light micrographs. Fig. 10 Typical cell shape (formalin preserved) in ventral view showing the w-shaped hypocone (bottom arrow) and the apical groove (top arrow). Fig. 11 Ventral view of the cell (formalin preserved) showing the oval shaped nucleus (arrow) on the left-hand side of the cell. Fig. 12 Ventral view of a live cell showing the variably shaped chloroplasts (arrow). Fig. 13 Dorsal view of a live cell showing the indentations in the right and left lobes of the hypocone (arrows). Figs 14 - 17 Scanning electron micrographs of formalin preserved cells. Fig. 14 Typical cell shape in ventral view showing straight apical groove (top arrow), sulcal extension (middle arrow) and the cingulum displacement (bottom arrow). Fig. 15 Apical groove on the dorsal side of the cell. Fig. 16 Dorsal view of one cell and the anterior view of the ventral side of another showing clearly the degree of dorso-ventral flattening. Fig. 17 Ventral view of the indentations in the left and right lobes of hypocone (arrows). Figs 18, 19 Line drawing of the ventral and dorsal surfaces respectively.

HOLOTYPE: Fig. 14

ISOTYPE: SEM stub containing specimens of *K. bicuneiformis* (Accession number J 100090) were submitted to the Moss Herbarium, School of Animal, Plant and Environmental Sciences, University of the Witwatersrand, Johannesburg, South Africa

ETYMOLOGY: Latin *bi*, two and *cuneiformis*, wedge shaped

TYPE LOCALITY: Gordon's Bay, South Africa (Fig. 1)

DISTRIBUTION: False Bay and Walker Bay, South Africa (Fig. 1)

DESCRIPTION: Motile cells of *K. bicuneiformis* are dorso-ventrally flattened, (36.25 ± 2.37µm [n=15] long, 33.83 ± 2.53µm [n=15] wide and 5 µm deep [n=1 (Fig. 16)]). The hypocone is w-shaped and the epicone is conical, giving the cell a markedly angular outline (Figs 10, 14). The hypocone may occasionally possess indentations on its dorsal and ventral surfaces (Figs 13, 17). The cingulum is median to premedian and is displaced with one cingulum width (Fig. 14). The sulcus extends onto the epicone and does not flare in the hypocone. The apical groove is straight (Figs 10, 17). On the ventral side the apical groove starts immediately to the right of the sulcal extension (Fig. 14) and extends for a short distance onto the dorsal side (Fig. 15). The nucleus is oval and situated on the left side of the hypocone (Fig. 11). Several variably-shaped, yellow-green chloroplasts are present (Fig. 12) and, upon fixation, they form round discs (Fig. 11).

REMARKS: The swimming behaviour of *K. bicuneiformis* sp. nov. is smooth and slow and similar to the "falling leaf" motion described by Matsuoka *et al.* (1989).

Pigment data is unavailable for this species, however based on its affiliation to the genus *Karenia* and the colour of the species when observed under the light microscope, this species most likely contain fucoxanthin and not peridinin.

This species has not been associated with any harmful events.

Pairwise distance values obtained from comparison of partial LSU rDNA sequences confirm the status of *K. bicuneiformis* as a new species with values falling within the range calculated for species within the same genus and not within the range calculated for isolates within the same species (Table 4).

DISCUSSION

The genus *Gymnodinium sensu lato* has recently been divided into four genera (Daugbjerg *et al.* 2000). One of these, *Karenia* G. Hansen & Moestrup, is characterised as having a straight apical groove and fucoxanthin as its major carotenoid. It is readily distinguished from the genus *Karlodinium* J. Larsen gen. nov. by the absence of a ventral pore. *K. cristata* and *K. bicuneiformis* are placed within the genus *Karenia* because both species contain a straight apical groove, lack a ventral pore and contain fucoxanthin as the major carotenoid, rather than the more characteristic peridinin of most dinoflagellate species e.g. *Akashiwo sanguinea* (Hirasaka) G. Hansen & Moestrup (Daugbjerg *et al.* 2000).

K. cristata differs from other *Karenia* species (Table 3) by having an asymmetric hypocone with a larger and more rounded right lobe and a straight apical groove that is elevated to form an apical crest. These two features are considered as the diagnostic features for *K. cristata*. The apical crest present in *K. cristata* is however not similar to the much more pronounced carina found in *K. brevis*. The nucleus does not share the dual position and shape of the nucleus of *K. brevisulcata* (Chang 1999) but is large, round to oval and situated in the centre of the cell with the bulk of the nucleus in the hypocone. Although *K. cristata* is of a similar size to other *Karenia* species it does not share the circular cell shape of *K.*

brevisulcata (Chang 1999) and *K. digitata* (Yang *et al.* 2000). *K. cristata* has an apical groove that is long on the ventral side and short on the dorsal side similar to *K. mikimotoi* (Takayama & Adachi 1984), *K. brevis* (Taylor *et al.* 1995) and *K. digitata* (Yang *et al.* 2000). It does not contain an apical groove that is short on the ventral and dorsal side like *K. brevisulcata* (Chang 1999) or long on the ventral and dorsal side like *K. longicanalis* (Yang *et al.* 2001). Similarly to *K. mikimotoi* and *K. digitata*, the chloroplast shape of *K. cristata* is variable. Water discolouration during a bloom of *K. crisitata* was reported as olive-green (Pitcher & Matthews 1996), whereas a coffee-like colour has been reported for *K. mikimotoi* and a yellow-brown colour for *K. brevisulcata* (Chang 1999). As in all *Karenia* species, except *Karenia longicanalis* (Yang *et al.* 2001), *K. cristata* has a sulcal extension. It shares the same pigments as *K. mikimotoi* (Hansen *et al.* 2000) and *K. brevis* (Millie *et al* 1995) namely chlorophyll c_2 and c_3, 19'-butanoyloxy fucoxanthin, fucoxanthin, 19'-hexanoyloxy fucoxanthin, diadinoxanthin, gyroxanthin-diester, chlorophyll *a* and β-carotene and it also produces an aerosol toxin with harmful properties similar to that of *K. brevisulcata* (Chang 1999) and *K. brevis* (Hemmert 1975, Steidinger & Baden 1984).

New Zealand has the same species, but they have not yet been formally identified. The New Zealand equivalent of *K. cristata* has been referred to as *Gymnodinium* sp. and *Gymnodinium* sp. nov. (cf. *breve*) (Chang 1995, Chang *et al.* 1995), and the equivalent of *K. bicuneiformis* as *Gymnodinium* sp. (Haywood *et al.* 1996). The New Zealand equivalent of *K. cristata* has a crest, a nucleus that situated centrally, cell width and length that is almost equal in size and by being dorso-ventrally flattened (<10μm) (Mackenzie *et al.* 1995). Pairwise distance values obtained from comparison of partial LSU rDNA sequences provide additional evidence for describing *K. cristata* as a new *Karenia* species.

The overall cell size and shape of *K. bicuneiformis* are notably different to that of other *Karenia* species (Table 3). The large, angular and significantly dorso-ventrally flattened cell with a conical epicone and w-shaped hypocone are considered diagnostic features. As in *K. brevis* (Takayama 1990) and *K. mikimotoi* (Takayama & Adachi 1984) the nucleus of *K. bicuneiformis* is restricted to the left side of the cell. It is however, distinguished from the nucleus of *K. mikimotoi* in that it is not reniform and does not extend across the epi-and hypocone (Takayama & Adachi 1984), and it is not round as in *K. brevis* (Takayama 1990). The apical groove of *K. bicuneiformis* is long on the ventral side and short on the dorsal side and is distinguished from *K. brevisulcata* which has an apical groove that is short on the ventral and dorsal side (Chang 1999). It is also distinguished from *K. longicanalis* which has an apical groove that is long on the ventral and dorsal side (Yang *et al.* 2001). *K. bicuneiformis* does not contain an apical crest like *K. cristata* (Chang 1999), nor a very pronounced carina like *K. brevis* (Takayama & Adachi 1984). It has a sulcal extension similar to most *Karenia* species, except *Karenia longicanalis* (Yang *et al.* 2001). Its chloroplasts are variable in shape similar to those of *K. cristata, K. mikimotoi* (Takayama & Adachi 1984) and *K. digitata* (Yang *et al.* 2000). Unlike *K. brevisulcata, K. mikimotoi* and *K. brevis,* no toxic effects have been reported for this species. The *Karenia* sp. present in New Zealand waters which was referred to as *Gymnodinium* sp. is similar to *K. bicuneiformis* in that it is very large, has a w-shaped hypocone, a nucleus that is situated in the left of the hypocone and is dorso-ventrally flattened by about 10μm (Haywood *et al.* 1996). Pairwise distance values obtained from comparison of partial LSU rDNA sequences provide additional evidence for describing *K. bicuneiformis* as a new *Karenia* species.

The phylogenetic relationships and character evolution of these two new *Karenia* species and other gymnodinioid species (from the South African coast) within different genera were compared to related species occurring elsewhere in the world and are published separately.

CHAPTER 4

PHYLOGENY AND CHARACTER EVOLUTION OF DELICATE DINOFLAGELLATE SPECIES BASED ON MORPHOLOGICAL, PIGMENT AND DNA SEQUENCE DATA

ABSTRACT

Considerable confusion exists world-wide with regard to the identity of many species belonging to the unarmoured genera *Gymnodinium sensu lato* and *Gyrodinium sensu lato* as a result of their remarkable morphological diversity and because of the difficulty of working with unarmoured species. Daugbjerg and his co-workers (Daugbjerg *et al.* 2000) recently constructed a more satisfactory taxonomic system for the unarmoured dinoflagellate species, which resulted in the genus *Gymnodinium sensu lato* being split into four genera namely *Karenia, Karlodinium, Akashiwo* and *Gymnodinium sensu stricto*. Species level relationships within some of these genera remained unresolved. Phylogenetic relationships among 37 strains, including 9 isolates from the South African coast, were evaluated in simultaneous analyses of morphological and pigment data as well as large subunit (LSU) rDNA partial sequences (domain D1 – D3). Addition of the South African species including the newly described *Karenia* species, *K. cristata* Botes, Sym et Pitcher and *K. bicuneiformis* Botes, Sym et Pitcher, provides improved resolution between all species and resolves several groups in the current taxonomic system. Morphological character evolution is explored by examining character state optimisations which support the erection of new genera as monophyletic groups. The taxonomic status of one well supported group containing *Gymnodinium simplex*, *Gyrodinium* cf. *zeta* and *Gymnodinium corii* still remains uncertain.

INTRODUCTION

Considerable confusion exists world-wide with regard to the identity of many species belonging to the unarmoured genera *Gymnodinium sensu lato* and *Gyrodinium*. Light microscopy (LM) and electron microscopy (EM) have been used recently to describe species such as *K. brevisulcata* (Chang) G. Hansen et Moestrup (Chang 1999), *K. digitata* Yang, Takayama, Matuoka et Hodgkiss (Yang et *al.* 2000) and *K. longicanalis* Yang, Hodgkiss et Hansen (Yang *et al.* 2001). This has contributed to successful delineation of the morphologically similar species previously lumped into the so-called "*mikimotoi* species complex".

Over the last decade phylogenetic analyses of molecular data have become common practice and recently, Daugbjerg *et al.* (2000) constructed a taxonomic system for the unarmoured dinoflagellate species based on ultrastructure and partial rDNA sequence data. In this new classification the genus *Gymnodinium sensu lato* was split into four genera namely *Gymnodinium sensu stricto, Akashiwo, Karlodinium* and *Karenia*. The revised taxonomic system prompted renewed interest world-wide and a further two *Karenia* species, *K. cristata* and *K. bicuneiformis*, (Botes *et al.*, 2003b) were recently described based on morphology, pigment content and molecular data.

In 1988, *Karenia cristata* was responsible for extensive mortalities of sub- and intertidal fauna on the South African coast (Horstman *et al.* 1991, Pitcher & Matthews 1996) and attempts to isolate and culture this species revealed the presence of several morphologically similar "gymnodinioid" species. LM, SEM, pigment analyses and partial large subunit (LSU) ribosomal RNA gene sequencing were performed on these isolates in order to place them

within the revised taxonomic system of Daugbjerg and his co-workers (Daugbjerg *et al.* 2000).

Whilst reconstruction of phylogenetic relationships of dinoflagellates has been common practice over the last decade, formal discussion of character state evolution as inferred from character optimisations on phylogenetic trees is entirely lacking. This paper therefore investigates the phylogenetic relationships among 37 dinoflagellate strains (listed in Table 1) and the evolution of characters on a robust and well resolved tree retrieved from a combined data set which includes morphological, pigment and DNA sequence data. Characters chosen for optimisation included those used by Daugbjerg et *al.* (2000) to erect their new taxonomy (e.g. apical groove shape, pigment content, absence/presence of a ventral pore), characters of perceived 'importance' (e.g. hypocone shape, absence/presence of a peduncle- like structure, absence/presence of a apical crest) and characters that historically were thought to be taxonomically important (such as nucleus shape and position, presence/absence of scales and thecal plates or material). The LSU region (28S) from domain D1 – D3 was preferred over the small subunit (SSU, 18S) because of insufficient variation at species level within the SSU which decreases the effective use of this region in discriminating among *Karenia* species (Sako *et al.* 1998). LSU rDNA sequences have highly variable regions interspersed with very conservative areas, rendering it more appropriate for phylogeny reconstruction at different systematic levels (Daugbjerg *et al.* 2000). Domains D1 – D3 were preferred because D1 and D2 are very variable and contain one of the fastest evolving segments whereas a very conservative region is situated upstream of D3 (Daugbjerg *et al.* 2000).

The LSU rDNA sequences of the South African isolates were compared to sequences of similar and related species occurring elsewhere in the world in an attempt to further resolve specific groups within the current taxonomic system. The results indicate that within the

current taxonomic system problems of generic delimitation remain. The erection of new genera to resolve this problem are discussed.

Table 1. Specimens included in the study.

Species number	Species name (Listed as appearing in Genbank)	Origin	Isolated by	Accession number (GenBank)
1	*Akashiwo sanguinea*	False Bay, RSA	L. Botes	AY518424
2	*Cachonina hallii*	NZ		AF033867
3	*Gymnodinium aureolum*	Table Bay, RSA	L. Botes	AY464687
4	*Gymnodinium aureolum*	Niva Bugt, DK	G. Hansen	AF200671
5	*Gymnodinium breve*	Hawke's Bay, NZ	A. Haywood	U92252
6	*Gymnodinium catenatum*	Vigo, SPAIN		AF200672
7	*Gymnodinium chlorophorum*	Sylt, GERMANY	M. Elbrächter	AF200669
8	*Gymnodinium corii*	FRANCE	L. Boni	AF318226
9	*Gymnodinium* cf. *mikimotoi*	Waimangu Point, NZ	A. Haywood	U92249
10	*Gymnodinium* cf. *mikimotoi*	Foveaux, NZ	L. Mackenzie	U92250
11	*Gymnodinium* cf. *pulchellum* (*Takayama* cf. *pulchella*)	Kawau Island, NZ	L. Mackenzie	U92254
12	*Gymnodinium fuscum*	La Trobe, AUS	D.R.A. Hill	AF200676
13	*Gymnodinium galatheanum*	Oslo Fjord, NORWAY	K. Tangen	AF200675
14	*Gymnodinium impudicum*	Naples, ITALY	M. Montresor	AF200674
15	*Gymnodinium nolleri*	AUS		AY036079
16	*Gymnodinium pallustre*			AF260382
17	*Gymnodinium sanguineum*	Marlborough Sounds, NZ	L. Rhodes	U92253
18	*Gymnodinium simplex*	Gulf of Tehuantepec, USA	A. Dodson	AF060901
19	*Gymnodinium* sp.	Coromandel, NZ	A. Haywood	U92255
20	*Gymnodinium* sp.	Whangakoko, NZ	A. Haywood	U92257
21	*Gymnodinium* sp.	CHILE		AF318247
22	*Gymnodinium* sp.	SPAIN		L38640
23	*Gymnodinium* sp.	KOREA		AF067862
24	*Gymnodinium* sp. (*Karenia bicuneiformis*)	Hawke's Bay, NZ	A. Haywood	U92251
25	*Gymnodinium* sp. Corsica	Corsica, FRANCE		AF318249
26	*Gyrodinium* cf. *corsicum*	False Bay, RSA	L. Botes	-
27	*Gyrodinium* cf. *zeta*	Lambert's Bay, RSA	D. Calder	AY464688
28	*Heterocapsa orientalis*	False Bay, RSA	L. Botes	AY464690
29	*Heterocapsa* sp.	Woodshole,USA	G. Hansen	AF260399
30	*Heterocapsa triquetra*	DK		AF260401
31	*Karenia brevis*	Florida, USA	W.B. Wilson	AF200677
32	*Karenia brevisulcata*	Wellington Harbour, NZ	L. Mackenzie	AY243032
33	*Karenia cristata*	False Bay, RSA	L. Botes	AY525907
34	*Karenia mikimotoi*	Øresund, DK	G. Hansen	AF200682
35	*Karenia mikimotoi*	Seto Island Sea, JAPAN	T. Ikeda & S. Mu	AF200681
36	*Lepidodinium viride*	False Bay, RSA	L. Botes	AY464689
37	*Takayama helix*	False Bay, RSA	L. Botes	AY464691
38	* *Tetrahymena thermophila*			X54512
39	* *Plasmodium falciparum*			U21939

* Outgroup species

MATERIALS AND METHODS

SAMPLING AND ESTABLISHMENT OF CULTURES

Specimens were collected in the field with a 20µm net and concentrated through a 10µm mesh. Specimens were isolated by means of a micropipette and maintained in F/2 (Guillard & Ryther 1962) or Keller medium (Keller & Guillard 1985), at 18°C and under 12h light 12h dark cycle (ca. 200 $\mu Em^{-2}s^{-1}$). Specimens of species that proved difficult to culture were isolated directly into PCR tubes and frozen.

MORPHOLOGICAL AND PIGMENT DATA

Microscopy techniques

Specimens were observed, measured and photographed with either an Olympus B201 light microscope equipped with an Olympus DP10 digital camera or with a Zeiss Axiophot photomicroscope equipped with a photographic set-up that included the production of video prints, video recording and micrographs.

Scanning electron micrographs were obtained according to the technique developed by Botes *et al.* (2002). However, SEM's of *K. cristata* and *K. bicuneiformis* were obtained from routine water samples that were preserved in 5% formaldehyde (buffered with $CaCO_3$ AR grade, pH= ≥ 7).

Scale morphology was investigated with transmission electron microscopy. Copper grids were coated with formvar as described by Sym (1992). A drop of concentrated culture was dispensed onto the grid with a needled syringe followed by a drop of gluteraldehyde. Cells were allowed to settle onto the formvar coated grid for about 5 minutes. Excess culture medium was drawn off with Whatman no. 1 filter paper. The remaining medium was then

allowed to air dry. After drying, the grids were washed with distilled water and viewed under the light microscope to determine whether any cells had been captured. The grids were then stained with an aqueous 2% uranyl acetate solution for 30 mins, washed with distilled water and allowed to air dry. Grids were viewed with a JEM-100S transmission electron microscope.

Pigment composition

Cultures were filtered through 4.7 cm GF/F (Whatman) microfiber filter paper. Pigments were extracted in 2 ml 90 % acetone using ultrasonication and centrifugation. Pigment extracts were analysed by HPLC according to procedures of Barlow *et al.* (1997) at a flow rate of 1 $ml.min^{-1}$ on a C-8 column using a binary linear gradient. Solvent A consisted of 70:30 (v/v) methanol : 1 M ammonium acetate and solvent B was 100% methanol. Pigments were detected by absorbance at 440 nm using a Thermo Separations UV 6000 diode array detector. Pigments were identified by retention time and appropriate diode array spectra (Jeffrey *et al.* 1997). Chlorophyll *a* and *b*, and α- and β- carotene standards were obtained from Sigma Chemical Co. and the Water Quality Institute (VKI) Hørsholm, Denmark.

Morphological and pigment characters

Morphological and pigment characters used in the phylogenetic analyses are listed in Table 2. The nine South African isolates were scored according to results obtained during the study, while species from outside of South Africa were scored according to information available in the literature. Most features were scored as binary (i.e. presence/absence) characters, but characters 10, 11, 18, 20 and 21 have multiple states.

Table 2. List of morphological characters used in analyses

Number of Characters	Character States
1	Perdinin: absent (0), present(1)
2	Chlorophyll c_2: absent (0), present (1)
3	Fucoxanthin: absent (0), present (1)
4	Chlorophyll c_3: absent (0), present (1)
5	Gyroxanthin-diester: absent (0), Present (1)
6	Chlorophyll *b* : absent (0), present (1)
7	Violaxanthin: absent (0), present (1)
8	Lutein: absent (0), present (1)
9	Apical groove: absent (0), present (1)
10	Apical groove shape: encircling apex (0), horseshoe (1), straight (2), Sigmoid (3)
11	Straight apical groove shape: short front/short back (0), long front/short back (1)
12	Aerosol toxin: absent (0), present (1)
13	Scales: absent (0), present (1)
14	Scale shape: square (0), triangular (1)
15	Thecal plates: absent (0), present (1)
16	Thecal vesicles with thecal plates: absent (0), present (1)
17	Prymnesiophyte endosymbiont: absent (0), present (1)
18	Prasinohyte endosymbiont: absent (0), present (1)
19	Peduncle-like structure: absent (0), present (1)
20	Nucleus shape: round (0), ellipsoidal (1), round or ellipsoidal (2)
21	Ellipsoidal nucleus: horisontal (0), vertical (1)
22	Nucleus position: central (0), left (1)
23	Nucleus i.t.o.epicone: in epicone (0), in hypocone (1), across epicone and hypocone (2)
24	Apical crest: absent (0), present (1)
25	Ventral pore: absent (0), present (1)
26	Hypocone w-shaped: absent (0), present (1)
27	Hypocone eccentric: absent (0), present (1)

MOLECULAR DATA

DNA extraction, amplifications and determination of partial LSU rDNA sequences (D1-D3).

DNA extraction of species 3, 27, 28 and 37 (Table 1):

Genomic DNA was extracted from pellets, which were obtained by centrifuging (J2-21 centrifuge, 6000 rpm) approximately 50 ml of nonaxenic, exponentially growing cultures for 8 to 10 min at room temperature. The extraction protocol of Bolch *et al.* (1999) was followed but with the following exceptions:

- After STE buffer was added to the pellet, 50 µl of proteinase K (10mg/ml) was added. The mixture was incubated overnight at 56°C and then vortexed.
- The PEG precipitation step was left out.
- The precipitated pellet was resuspended in Tris (10mM, pH 8.5) and not in distilled water.

The extracted genomic DNAs were used as templates to amplify ~ 850 base pairs of LSU rDNA, using primers D1R (5' ACCCGCTGAATTTAAGCATA 3' (forward)) (Scholin *et al.* 1994) and D3Ca (5' ACGAACGATTTGCACGTCAG 3' (reverse)) (Lenaers *et al.* 1989). Polymerase chain reaction (PCR) amplification was carried out as in Hansen *et al.* (2000 a) with a reaction volume of 25µl, 3mM $MgCl_2$ and Bioline Taq polymerase. For taxa that were difficult to amplify, a second PCR reaction (15 - 20 cycles of denaturation, annealing and extension) was performed as above, using 1- 2µl of the product from the first set of reactions as template. Success of amplification was determined by running reactions in 1% agarose gels containing ethidium bromide (EtBr) and visualized by ultraviolet illumination. PCR products were purified using the QIAquick PCR Purification Kit (Qiagen). Both strands of PCR product were sequenced by using the ABI PRISM BigDye terminator Cycle-Sequencing Ready Reaction Kit (v. 2). The sequence reactions were run on an ABI PRISM 3100 Genetic Analyser, following the recommendations of the manufacturer.

DNA extraction of species 1, 33 and 36 (Table 1):

Individual live cells were isolated directly into PCR tubes containing the remaining reaction ingredients. The protocol of Bolch (2001) was followed but with primers specified in Table 3. DNA fragments were checked on 1% agarose gels containing EtBr, cut out with a sterile

surgical blade and purified using the QIAquick Gel Extraction Kit (Qiagen). PCR product was sequenced as described above.

DATA ANALYSIS

All sequence chromatograms were edited using BioEdit v5.0.9. Assembled sequences were aligned using the Clustal method in MegAlign v.4.0 and finally refined by eye (Appendix 1). Comparative studies using ultrastructural characters and phylogenetic reconstructions based on molecular data have indicated that ciliates and apicomplexons form sister groups to the dinoflagellates (Daugbjerg *et al.* 2000). We have therefore used *Tetrahymena thermophila* as a ciliate representative and *Plasmodium falciparum* as an apicomplexan representative, to polarise the ingroup.

The following phylogenetic analyses were performed using PAUP*4.0b 10 (Swofford 2003):

Unweighted Parsimony Analysis

Unweighted parsimony analysis was performed on the molecular, morphological and combined datasets. An initial heuristic search was conducted using 1 000 replicates of random taxon addition. All characters were given equal weight and states were unordered. Gaps were treated as missing data since none was potentially parsimony informative. At each replicate, a maximum of two trees were saved. The trees saved in this initial sweep of the tree space were used as starting trees in a second round of tree searching using the heuristic search option with stepwise addition of sequences (1000 replicates) and the tree bisection-reconnection (TBR) branch-swapping algorithm. All most parsimonious trees were saved up to a maximum of 500.

Weighted Parsimony Analysis

The three data sets were analysed as above after reweighting characters (base weight= 1000) by their maximum RCI. The process was repeated until there was no change in tree length over two successive rounds.

Maximum likelihood analysis

The General Time Reversible model (Yang 1993, Yang 1994), incorporating rate variation among sites and with a fraction set as invariant (GTR + G), was used during the unweighted heuristic search (stepwise addition of sequences = 250 replicates, TBR branch-swapping algorithm). Rate variation was incorporated by use of a discrete approximation (with four categories) to a gamma distribution with shape parameter γ. Each category was characterised by its median. Parameters of the likelihood model were estimated from the MPT recovered under successively approximated weights. The tree provided the following estimates for the GTR + G model: PINVAR = 0.000, γ = 0.59758, rmatrix = 0.689, 2.303, 0.937, 0.642, 5.629, 1.000 (A-C, A-G, A-T, C-G, C-T, G-T substitution rates, with G-T arbitrarily set to 1).

For the parsimony (molecular data set and the combined data set) and likelihood (molecular data set) analyses, node support was evaluated by the jackknife as implemented in PAUP 4.0 v.10. For parsimony analyses, 1 heuristic replicate, stepwise addition of sequences and the tree bisection-reconnection (TBR) branch-swapping algorithm were performed with 1000 jackknife replicates, while under the likelihood criterion, no branch swapping was performed and only 150 replicates were completed because of time constraints . At each replicate 36.79% of character were deleted and the "emulate Jac resampling" option was implemented. Only nodes occurring in > 55% of the replicates were retained in the jackknife consensus tree.

Pairwise distance comparisons

Pairwise distance comparisons among individuals within the same species, species within the same genus and species among genera were calculated based on their LSU rDNA sequences (D1-D3) using the Tamura-Nei Model (Tamura & Nei, 1993).

Morphology and pigment character scoring

Morphological features and pigment content of the various species concerned were scored as indicated in Table 2.

The following analyses were performed using MacClade v. 4 (Madison & Madison 2000):

Character optimisation

Morphological and pigment characters were optimised onto the tree topology retrieved from the molecular dataset which contain 38 strains. Character states were optimised to show all most parsimonious states at each node, and were treated as equivocal when they differed under accelerated (ACCTRAN) and delayed (DELTRAN) transformation.

RESULTS

MORPHOLOGICAL AND PIGMENT DATA

Morphological observations (see also, Appendix 2)

Light and electron microscopy revealed that *Akashwiwo sanguinea* (Hirasaka) G. Hansen et Moestrup has a large vertically ellipsoidal nucleus situated in the centre of the cell (Fig. 1), and an apical groove that encircles the apex in a clockwise manner (Fig. 2).

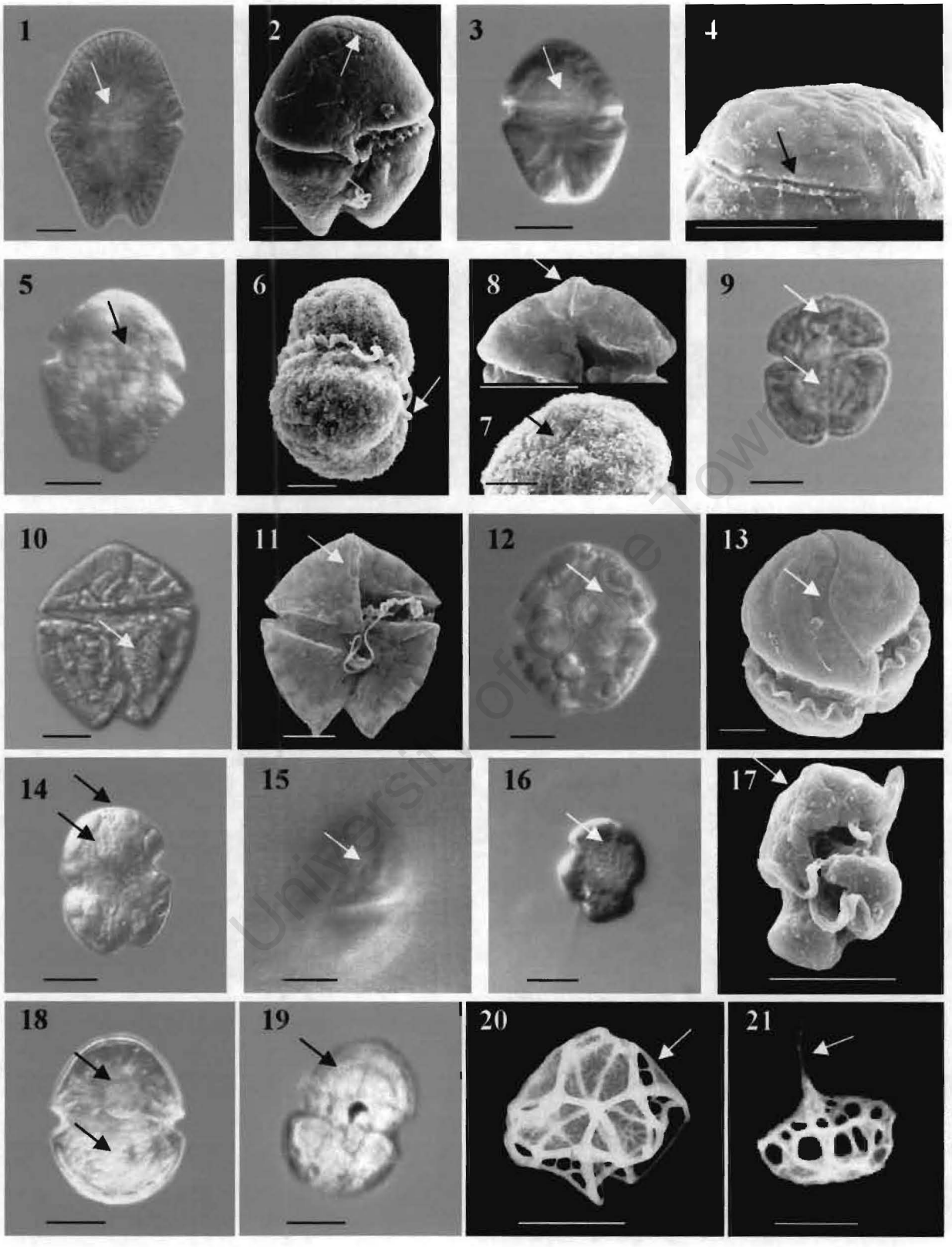

Figures 1 - 21. Light and electron micrographs of "gymnodinioid" species (Scale bar in all figs = 10μm, except fig. 16 = 5μm and figs 20-21 = 0.5μm).

Figs 1, 2. Typical cell shape of *Akashiwo sanguinea* with the vertically ellipsoidal nucleus visible in fig.1 and the apical groove that encircles the apex in a clockwise manner in fig. 2.
Figs 3, 4. Ventral view of *Gymnodinium aureolum* showing the horizontally ellipsoidal nucleus (fig. 3) and the horseshoe shaped apical groove (fig. 4).
Figs 5, 6 and 7. Cell surface of *Lepidodinium viride* is covered in basket shaped body scales (figs 6, 7) and has a centrally situated nucleus (fig. 5), a peduncle-like structure (fig. 6) and a horseshoe shaped apical groove (fig. 7).
Figs 8, 9. Ventral view of the epicone of *Karenia cristata* showing the straight apical groove (fig. 8), the apical crest (figs 8, 9) and the centrally situated nucleus (fig. 9).
Figs 10, 11. *Karenia bicuneiformis* contains an ellipsoidal nucleus that is vertically situated in the left side of the hypocone (fig. 10), a very distinct w-shaped hypocone (figs 10, 11) and a straight apical groove (fig. 11).
Figs 12, 13. *Takayama helix* contains an ellipsoidal nucleus that is vertically situated on the left side of the hypocone (fig. 12) and a sigmoid apical groove (fig. 13).
Figs 14, 15. Ventral view of *Gyrodinium* cf. *corsicum* with a straight apical groove (fig. 14), centrally situated nucleus (fig. 14) and a ventral pore on the epicone (fig 15).
Figs 16, 17. *Gyrodinium* cf. *zeta* has a nucleus that occupies most of the cell (fig. 16), a straight apical groove (fig. 17) and a z-shaped cingulum-sulcus juncture (fig. 17).
Figs 18, 19. Light micrographs of *Heterocapsa orientalis* showing the centrally situated nucleus (fig. 18), pyrenoid immediately above the nucleus (fig. 18) and thecal plates (fig. 19).
Figs 20, 21. Transmission electron micrographs of *H. orientalis* showing the triangular shaped scales (fig. 20) with a central spine and no short spines (fig. 21).

The nucleus of *Gymnodinium aureolum* (Hulburt) G. Hansen et Moestrup is horizontally ellipsoidal and situated across the epi- and hypocone but with the bulk of the nucleus in the epicone (Fig. 3) and the apical groove is horseshoe shaped (Fig. 4).

The nucleus of *Lepidodinium viride* Watanabe, Suda, Inouye, Sawaguchi et Chihara is similar to that of *A. sanguinea* (Fig. 5). The cell surface of *L. viride* is covered with square-shaped scales and contains a peduncle-like structure near the cingulum-sulcus juncture (Fig. 6). Its apical groove is similar to that of *G. aureolum* (Fig. 7).

The apical groove of *Karenia cristata* Botes, Sym et Pitcher (Botes *et al.* 2003) is straight and elevated into an apical crest (Fig. 8). The nucleus is situated centrally across the epi- and hypocone, but with the bulk of the nucleus in the hypocone (Fig. 9).

Karenia bicuneiformis Botes, Sym et Pitcher (Botes *et al.* 2003) contains an ellipsoidal nucleus that is vertically situated in the left side of the hypocone (Fig. 10). It has a very distinct w-shaped hypocone and a straight apical groove (Fig. 11).

Takayama helix de Salas, Bolch, Botes et Halegraeff Larsen has an ellipsoidal nucleus that is vertically situated on the left side of the cell, across the epi- and hypocone but with the bulk of the nucleus in the epicone (Fig. 12). The apical groove is sigmoid (Figure 13).

Gyrodinium cf. *corsicum* Paulmier, Berland, Billard et Nezan has a round to oval nucleus that is centrally situated with the bulk in the epicone and a straight apical groove (Figure 14). A ventral pore is present to the left of the apical groove (Fig. 15).

Gyrodinium cf. *zeta* J. Larsen is a tiny species with a straight apical groove (Fig. 17) and its nucleus centrally placed and occupying most of the cell (Fig. 16).

Heterocapsa orientalis Iwataki, Botes et Fukuyo (Iwataki *et al.* in press) which can easily be confused with *Gymnodinium pyrenoidosum* Horiguchi et Chihara has its nucleus in the hypocone with a pyrenoid located above it in the epicone (Fig. 18). The cell has a theca

with thecal plates (Fig. 19) and the triangular scales that are associated with the cell surface have a central spine and no short spines (Figs 20, 21).

Pigment composition

Four primary pigment profiles were observed for the South African isolates:

Pigment profile 1 (Fig. 22).

A. sanguinea, *G. aureolum*, *G.* cf. *zeta* and the *Heterocapsa orientalis* had pigment profiles typical of that of dinophytes namely chlorophyll c_2, peridinin, *cis*-peridinin, diadinoxanthin, chlorophyll *a* and β-carotene. The pigment content of these species therefore deviated very little from that of the dinoflagellate reference culture, *Amphidinium carterae,* provided by Jeffrey *et al.* (1997).

Pigment profile 2 (Fig. 23).

K. cristata had the following pigments: chlorophyll c_3, chlorophyll c_2, 19'-butanoyloxyfucoxanthin, fucoxanthin, 19'-hexanoyloxyfucoxanthin, gyroxanthin-diester, chlorophyll *a* and β-carotene. The pigments of this species are similar to those of chrysophytes and (or) prymnesiophytes. The prymnesiophyte reference culture, *Emiliania huxleyi,* provided by Jeffrey *et al.* (1997) contained chlorophyll *a*, c_2 and c_3, 19'-hexanoyloxyfucoxanthin, fucoxanthin, diadinoxanthin, diatoxanthin and β-carotene. The pelagophyte reference culture, *Pelagococcus subviridis*, provided by Jeffrey *et al.* (1997) contained chlorophyll *a*, c_2 and c_3, 19'-butanoyloxyfucoxanthin, fucoxanthin, diadinoxanthin, diatoxanthin and β-carotene.

Pigment profile 3 (Fig. 24).

T. helix and *G.* cf. *corsicum* contained chlorophyll c_3, chlorophyll c_2, fucoxanthin, hex-fucoxanthin, chlorophyll *a* and β-carotene which are typical of prymnesiophytes.

Pigment profile 4 (Fig. 25).

Lepidodinium viride contains chlorophylls *b* and *a*, lutein, violaxanthin and β-carotene. These pigments are typical of those of the chlorophytes and deviated very little from reference chlorophyte culture, *Duniella tertiolecta,* provided by Jeffrey *et al.* (1997).

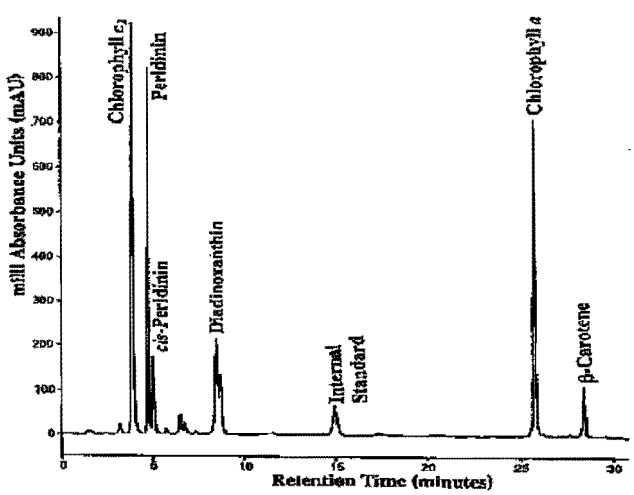

22

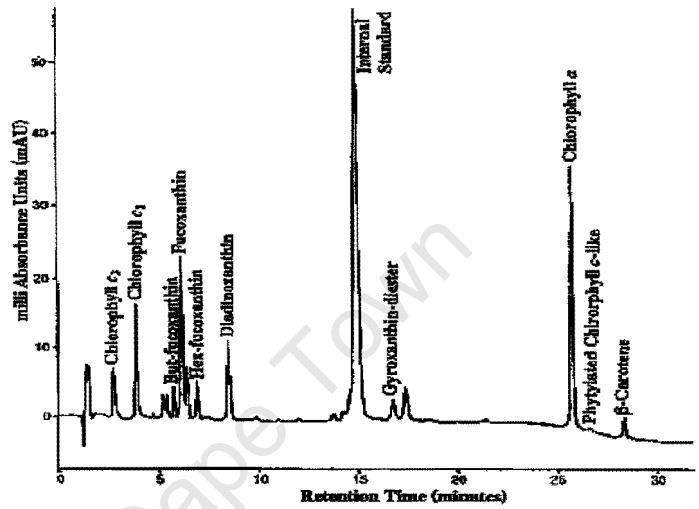

23

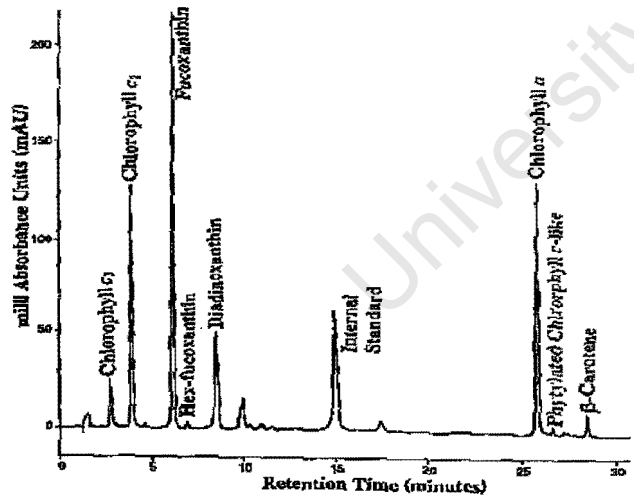

24

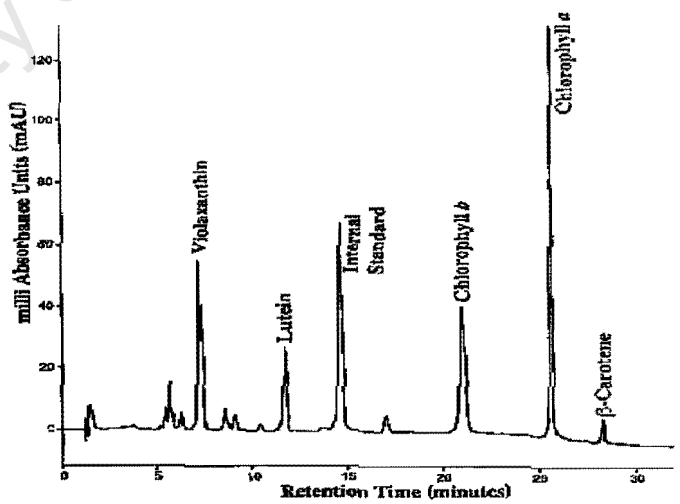

25

Figure 22 – 25. Pigment profiles of the South African isolates, generated by HPLC analysis.

Fig 22. Pigment content typical of *A. sanguinea, G. aureolum, H. orientalis* and *G.* cf. *zeta.*

Fig 23. Pigment content typical of *K. cristata.* Fig 24. Pigment content typical of *T. helix* and *G.* cf. *corsicum.* Fig 25. Pigment content typical for *L. viride.*

PHYLOGENETIC ANALYSES

Parsimony analyses

The total number of character included in the molecular data set were 700, of which 389 were parsimony informative. The morphological data set had 25 characters and 20 of these were parsimony informative. The combined data set included the 700 characters of the molecular data set and the 25 characters of the morphological data set, 381 of the 725 characters were parsimony informative.

Fifteen MPT's (trees not shown) were retained under unweighted analysis of the molecular data set. Under successive weights, one most parsimonious tree was retrieved (Fig. 26) (L = 9 420, CI = 0.653, RI = 0.839). All nodes were very well supported, with all jackknife values > 70%. For convenience, we delimit 11 major clades within the ingroup (indicated as 1 – 11 in Figs 26) and refer to species within these clades according to names appearing in Genbank. The outgroup consists of one ciliate and one apicomplexon species and the ingroup consists of delicate dinoflagellate species. A fully resolved, well supported (jackknife value =100) group (clade 10), comprising two *Akashiwo sanguinea* isolates, is sister to a group containing all other ingroup species (clades 2 – 11). Within this latter group are two sister groups, one of which contains clades 3 – 11, and the other clade 2. Clade 2 comprises ten *Karenia* isolates (Clade 2). Clade 11 comprises three *Karlodinium* isolates and clade 10 comprises two *Takayama* isolates, together these two clades are sister to a group containing clades 3 – 9. Clade 9, sister to a group consisting of clades 3 – 8, contains three *Heterocapsa* species and *Cachonina hallii*. Clade 8 contains *Gyrodinium* cf. *zeta*, *Gymnodinium corii* and *Gymnodinium simplex* and is sister to a group consisting of clades 3 – 7. *Gymnodinium pallustre* (Clade 7) is sister to a group consisting of clades 3 – 6. Clade 6, sister to clades 3 – 5, consists of *Gymnodinium fuscum* (the type species), *Gymnodinium*

catenatum and *Gymnodinium nolleri*. Clade 3 consists of three *Gymnodinium aureolum* strains and is sister and a group comprising clades 4 and 5, where clade 4 consists of *Gymnodinium chlorophorum* and *Lepidodinium viride* and, clade 5 of *Gymnodinium impudicum* and two *Gymnodinium* species.

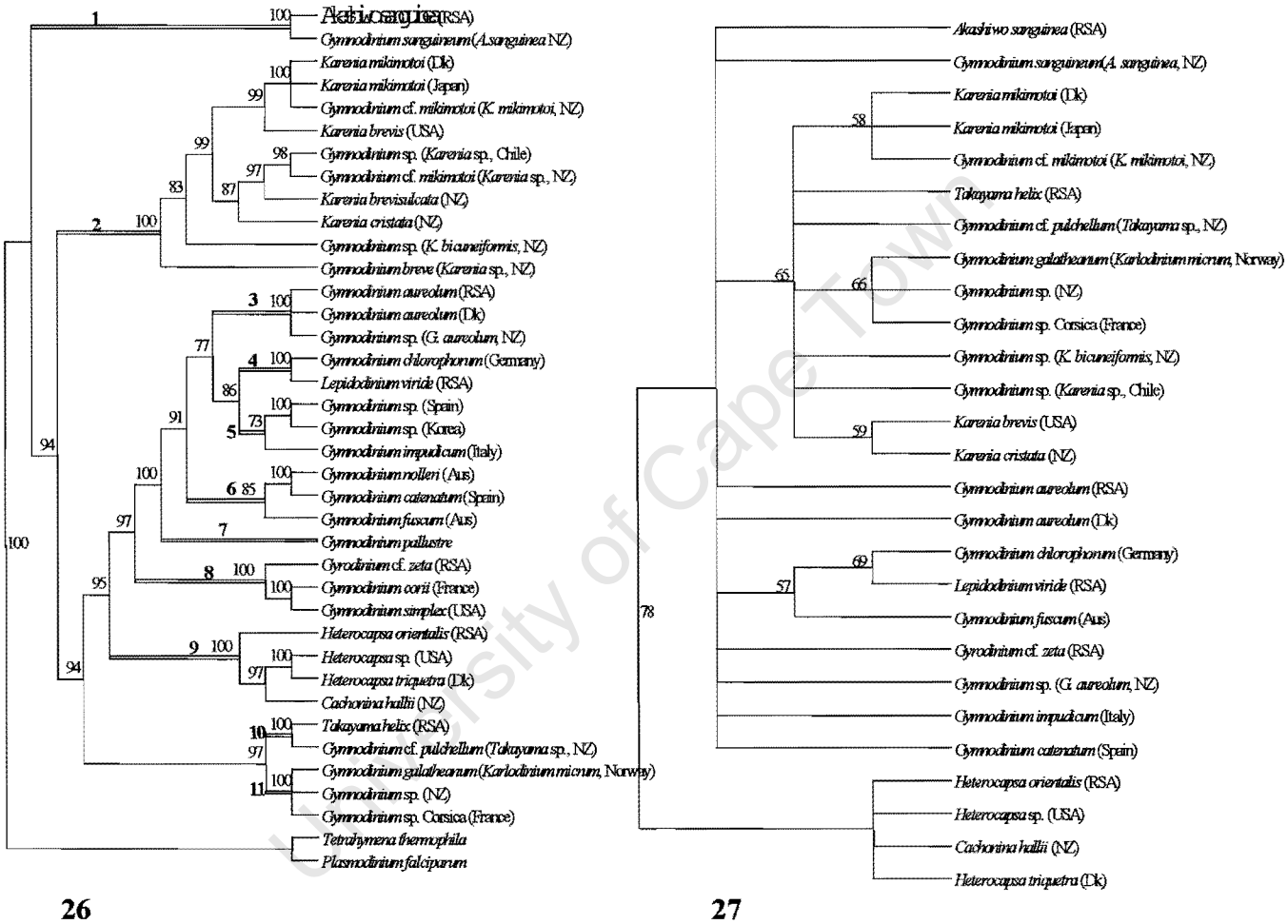

Figure 26. Single tree retrieved from parsimony analysis (L = 9420, CI = 0.653, RI = 0.838) of the molecular data set. Numbers above the branches indicate jackknife support values.

Figure 27. Strict consensus of 405 MPT's retrieved during parsimony analysis (L = 55, CI = 0.462, RI = 0.728) of the morphological data set.

For the morphological data, 405 MPT's trees (L = 55, CI = 0.462, RI = 0.728) were retained under the unweighted analysis. Where information was not available within the literature (Table 3), isolates were discarded in this data set. The outgroup species were discarded for the same reason and the tree was polarised using clade 9, which contains the lightly armoured *Heterocapsa* and *Cachonina* species. Although the strict consensus (Fig. 27) of the 405 MPT's retained are clearly less resolved and jackknife values lower than within the molecular data set (jakknife > 55%), this tree is congruent with the tree recovered from the molecular data and combined sets in that the main groupings are similar.

Similarly to the morphological data set, certain individuals in the combined data set were excluded as a result of a lack of information within the literature. For the combined data set, four trees (not shown) were retained under unweighted analysis. Under weighted analysis, one fully resolved dichotomous tree was retained (Fig. 28) (L = 910512, CI = 0.723, RI = 0.848) with similar groupings, although slightly differently placed within the overall topology, as the tree recovered from the molecular data set and with similar jackknife values.

Maximum likelihood analysis

One tree (Fig 29) (-ln L = 9785.626) was recovered from the molecular data set under the likelihood criterion. The tree has the same groupings to that of the combined data set but with less well resolved clades and lower jackknife values.

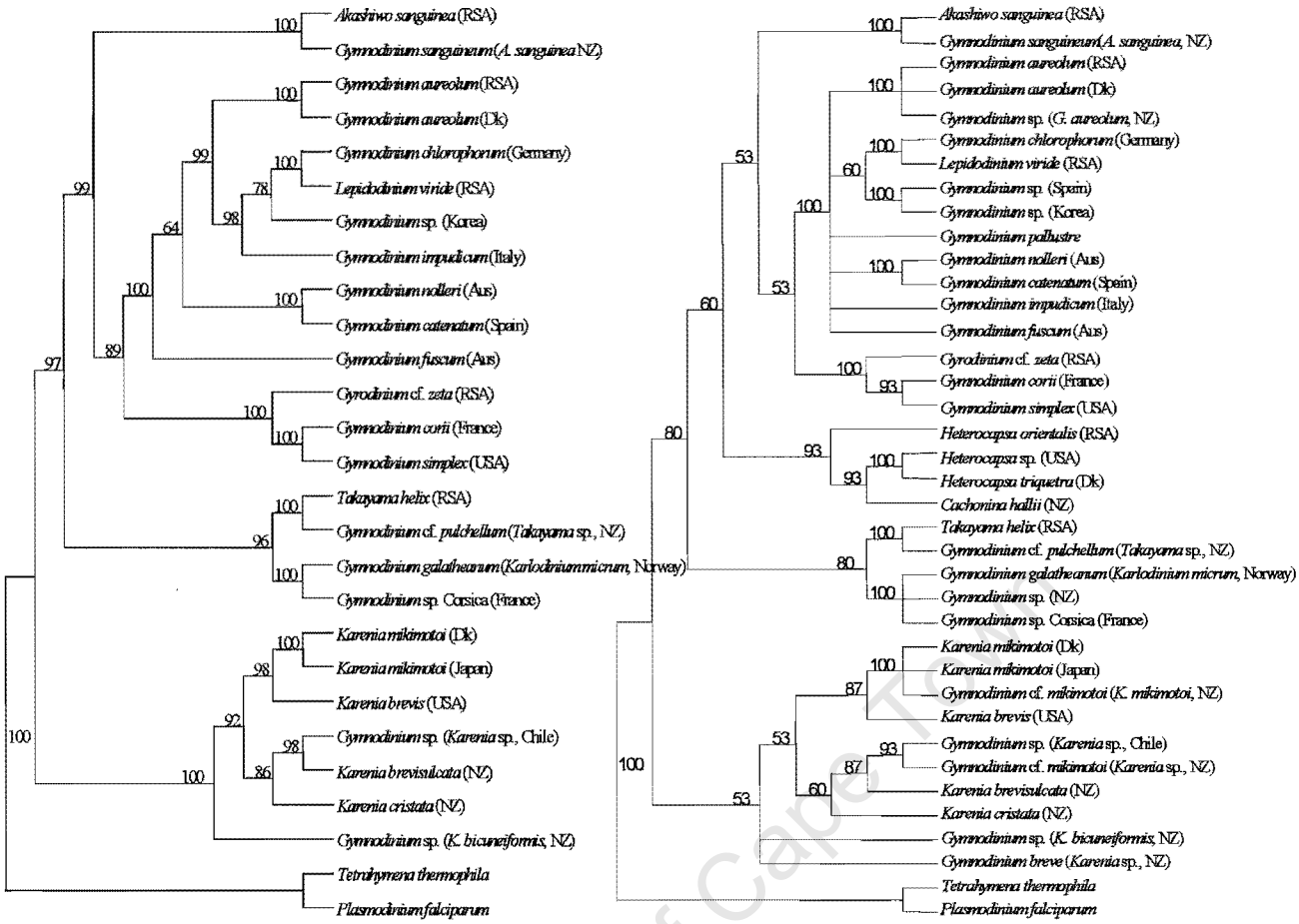

28 **29**

Figure 28. Single tree retrieved from parsimony analysis (L = 1403, CI = 0.612, RI = 0.7886) of the combined data set. Numbers above the branches indicate jackknife support values.

Figure 29. Single tree retrieved from maximum likelihood analysis of the molecular data set (-ln L = 9785.626). Numbers above the branches indicate jackknife support values.

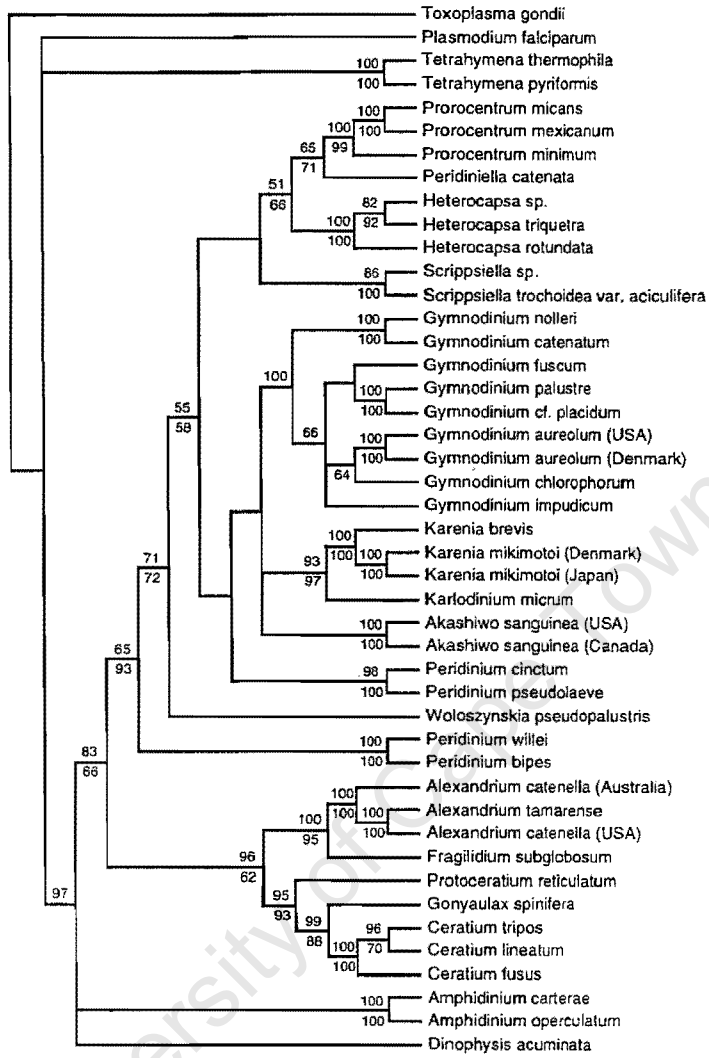

Figure 30. Strict consensus tree of 10 equally parsimonious trees obtained in PAUP* (From Daugbjerg et *al.* 2000). Bootstrap values above nodes are inferred from MP analysis and, below from NJ analysis, based on likelihood distances.ML analysis (L = 2842, CI = 0.427, RI = 0.601).

Morphology and pigment character scoring

The morphological features and pigment content of the South African isolates are summarised in Table 3.

Pairwise distances

Pairwise distance comparisons between selected individuals within the same species, species within the same genus and species within the different genera are summarised in Table 4. For this particular ingroup, the mean distance calculated for individuals within the same genus was 0.002 (range 0.000 – 0.008), species within the same genus was 0.041 (0.031 – 0.051) and species within different genera was 0.204 (range = 0.100 – 0.351).

Evolution of morphological (LM, SEM and pigment content) characters

In order to highlight some diagnostic characters for clades 1 – 11, results of character optimisations (Figs 31 – 41) were limited to selected characters depicting "true" similarity due to synapomorphies and symplesiomorphies.

Table 3. Morphological features and pigment content scored according to table 2.

	Species (As listed in Genbank)	Characters / character states 1 **Peridinin** absent = 0 present = 1	2 **Chl *c*2** absent = 0 present = 1	3 **Fucoxanthin** absent = 0 present = 1	4 **Chl *c*3** absent = 0 present = 1	5 **Gyroxanthin diester** absent = 0 present = 1	6 **Chl *b*** absent = 0 present = 1	7 **Violaxanthin** absent = 0 present = 1	8 **Lutein** absent = 0 present = 1	9 **Apical Groove** absent = 0 present = 1	10 **Apical groove Shape** encircling apex = 0 horseshoe = 1 straight = 2 sigmoid = 3	11 **Straight apical groove length** short front/short back = 0 long front/short back = 1 long front/long back = 2	12 **Aerosol toxin** absent = 0 present = 1
1	*Akashiwo sanguinea* (False Bay, RSA - AY518424) j, ad, ah	1	1	0	0	0	0	0	0	1	0	?	0
2	*Cachonina halliI* (NZ - AF033867) s	?	?	?	?	?	?	?	?	0	?	?	0
3	*Gymnodinium aureolum* (Table Bay, RSA) o, w, sh	1	1	0	0	0	0	0	0	1	1	?	0
4	*Gymnodinium aureolum* (Niva Bugt, DK - AF200671) o, w	1	1	0	0	0	0	0	0	1	1	?	0
5	*Gymnodinium breve* (Hawke's Bay, NZ - U92252) y	0	?	1	?	?	?	?	?	1	2	?	0
6	*Gymnodinium catenatum* (SPAIN - AF200672) a, b, h, j, m, o, v, w	1	1	0	0	0	0	0	0	1	1	?	0
7	*Gymnodinium chlorophorum* (Sylt, GERMANY - AF200669) k	0	0	0	0	0	1	1	?	1	1	?	0
8	*Gymnodinium corii* (FRANCE - AF318226)	?	?	?	?	?	?	?	?	?	?	?	?
9	*Gymnodinium* cf. *mikimotoi* (Waimangu Point, NZ - U92249) d, e, j, m, n, o, u, v	0	1	1	1	1	0	0	0	1	2	1	0
10	*Gymnodinium* cf. *mikimotoi* (Foveaux, NZ - U92250) y	?	?	?	?	?	?	?	?	1	2	?	?
11	*G.* cf. *pulchellum* (*T.* cf. *pulchella* - Kawau Island, NZ - U92254) r	0	?	1	?	?	?	?	?	1	3	?	?
12	*Gymnodinium fuscum* (La Trobe, AUS - AF 200676) i	?	?	?	?	?	?	?	?	1	1	?	0
13	*Gymnodinium galatheanum* (Oslo Fjord, NORWAY - AF200675) d, f, n, o, p, q, v, w, x	0	1	1	1	1	0	0	0	1	2	?	0
14	*Gymnodinium impudicum* (Naples, ITALY - AF 200674) a, h, I, o, w	1	1	0	0	0	0	0	0	1	1	?	0
15	*Gymnodinium nolleri* (AUS - AY036079) h, I, o, w	?	?	?	?	?	?	?	?	1	1	?	?
16	*Gymnodinium pallustre* (AF260382)	?	?	?	?	?	?	?	?	?	?	?	?
17	*Gymnodinium sanguineum* (Marlborough Sounds, NZ - U92253) d, i, j, o	1	1	0	0	0	0	0	0	1	0	?	0
18	*Gymnodinium simplex* (Gulf of Tehuantepec, USA - AF 060901) m, s	0	?	1	?	?	?	?	?	?	?	?	0
19	*Gymnodinium* sp. (Coromandel, NZ - U92257) o, w	1	1	0	0	0	0	0	0	1	1	?	0
20	*Gymnodinium* sp. (Whangakoko, NZ - U92257) d, f, m, o, p, q, v, w, x	0	1	1	1	1	0	0	0	1	2	?	0
21	*Gymnodinium* sp. (CHILE - AF318247) ac, ag	0	1	1	1	1	0	0	0	1	?	?	?
22	*Gymnodinium* sp. (SPAIN - L38640)	?	?	?	?	?	?	?	?	?	?	?	?
23	*Gymnodinium* sp. (KOREA - AF067862)	?	?	?	?	?	?	?	?	?	?	?	?
30	*Gymnodinium* sp. *(K. bicuneiformis* - False Bay, RSA ; Hawke's Bay, NZ - U92251) y,	?	?	?	?	?	?	?	?	1	2	1	0
24	*Gymnodinium* sp. Corsica (Corsica, FRANCE - AF318249) d, f, n, o, p, q, v, w, x	0	1	1	0	0	0	1	0	0	?	?	0
25	*Gyrodinium* cf. *corsicum* (False Bay, RSA) ah	0	1	1	1	0	0	0	0	1	2	1	0
26	*Gyrodinium* cf. *zeta* (Lambert's Bay, RSA) ae, ah	1	1	0	0	0	0	0	0	1	2	1	0
27	*Heterocapsa orientalis* (False Bay, RSA) z, ad, ah	1	1	0	0	0	0	0	0	0	?	?	0
28	*Heterocapsa* sp. (Woodshole, USA - AF260399)	?	?	?	?	?	?	?	?	0	?	?	0
29	*Heterocapsa triquetra* (DK - AF260401) s, z	?	?	?	?	?	?	?	?	0	?	?	0
31	*Karenia brevis* (Florida, USA - AF200677) b, d, j, q, v, o	0	1	1	1	1	0	0	0	1	2	1	1
32	*Karenia brevisuleata* (Wellington Harbour, NZ - AY243032) g, o	?	?	?	?	?	?	?	?	1	2	0	1
33	*Karenia cristata* (False Bay, RSA) l, aa, ab, sh	0	1	1	1	1	0	0	0	1	2	1	1
34	*Karenia mikimotoi* (Øresund, DK - AF200682) d, e, j, m, n, o, u, v	0	1	1	1	1	0	0	0	1	2	1	0
35	*Karenia mikimotoi* (Seto Island, JAPAN - AF200681) d, e, j, m, n, o, u, v	0	1	1	1	1	0	0	0	1	2	1	0
36	*Lepidodinium viride* (False Bay, RSA) ad, af, ah	0	0	0	0	0	1	1	1	1	1	?	0
37	*Takayama helix* (False Bay, RSA) r, ad, ah	0	1	1	1	0	0	0	0	1	3	?	0
38	*Tetrahymena thermophila* (X54512) - Outgroup	?	?	?	?	?	?	?	?	?	?	?	?
39	*Plasmodium falciparum* (U21939) - Otgroup	?	?	?	?	?	?	?	?	?	?	?	?

a Fraga *et al*. 1995a,b
b Zapata *et al*. 1998
c Garces *et al*. 1999
d Steidinger & Tangen 1996
e Partensky *et al*. 1988
f Johnson & Sakshoug 1993
g Chang 1995, 1999a,b
h Ellegaard & Oshima 1998
i Hansen *et al*. 2000
j Fukuyo *et al*. 1990
k Elbrachter & Schnepf 1996
l Botes *et al*. (in press)
m Rees & Hallegraeff 1991
n Tangen & Bjornland 1981
o Daugbjerg *et al*. 2001
p Braarud 1957
q Millie *et al*. 1995, 1997
r de Salas (in press)
s Dodge 1974, 1982, 1985
t Paulmier *et al*. 1995
u Takayama & Adachi 1984
v Taylor *et al*. 1995
w Hansen 2001
x Kempton *et al*. 2002
y Haywood *et al*. 1996
z Iwataki *et al*. (in press)
aa Mackenzie *et al*. 1995, 1966
ab Chang *et al*. 1995
ac Clement *et al*. 1999
ad Botes *et al*. 2002
ae Larsen 1996
af Watanabe *et al*. 1990
ag Carreto *et al*. 2001
ah Own observations

13	14	15	16	17	18	19	20	21	22	23	24	25
Scales	**Scale shape**	**Thecal plates**	**Amphiesmal vesicles with delicate material**	**Pedunkle-like structure**	**Nucleus shape**	**Oval - Hor/Ver**	**Nucleus position**	**Nucleus i.t.o. epicone**	**Apical crest/carina**	**Ventral pore**	**Hypocone W-shaped**	**Hypocone asymmetric**
absent = 0 present = 1	square = 0 triangular = 1	absent = 0 present = 1	absent = 0 present = 1	absent = 0 present = 1	Round = 0 Oval = 1 Round or Oval = 2	Horisontal = 0 Vertical = 1	central = 0 left = 1 right = 2	Epicone = 0 Hypocone = 1 Across epi & hypo = 2	absent = 0 present = 1	absent = 0 present = 1	absent = 0 present = 1	absent = 0 present = 1
0	?	0	0	0	1	1	0	2	0	0	0	0
1	1	1	0	?	0	?	0	1	0	0	0	0
0	?	0	0	0	1	0	1	2	0	0	0	0
0	?	0	0	0	1	0	1	2	0	0	0	0
0	0	0	?	?	0	?	1	1	1	0	0	0
0	?	0	0	0	0	?	0	2	0	0	0	0
0	?	0	1	0	1	1	0	2	0	0	0	0
?	?	?	?	?	?	?	?	?	?	?	?	?
0	?	0	0	1	2	1	1	2	0	0	0	0
0	?	0	?	0	0	?	1	1	0	0	0	0
0	?	0	?	?	?	?	0	1	0	?	0	0
0	?	0	1	0	?	?	0	0	0	0	0	0
0	?	0	?	1	0	?	0	2	0	1	0	0
0	?	0	?	0	0	?	0	2	0	0	0	0
0	?	0	?	0	?	?	?	?	0	?	0	0
?	?	?	?	?	?	?	?	?	?	?	?	?
0	?	0	0	0	1	1	0	2	0	0	0	0
0	?	?	?	?	0	?	0	2	0	?	0	0
0	?	0	0	0	1	0	1	2	0	0	0	0
0	?	0	?	1	0	?	0	2	0	1	0	0
0	?	0	?	?	?	?	0	1	0	?	0	0
?	?	?	?	?	?	?	?	?	?	?	?	?
?	?	?	?	?	?	?	?	?	?	?	?	?
0	?	0	0	?	1	1	1	1	0	0	1	0
0	?	0	0	0	0	?	1	?	0	0	0	0
0	?	0	0	1	2	?	0	0	0	1	0	0
0	?	0	0	0	1	0	0	2	0	0	0	0
1	1	1	0	0	1	0	0	1	0	0	0	0
1	1	1	0	?	1	0	0	0	0	0	0	0
1	1	1	0	?	0	?	0	2	0	0	0	0
0	?	0	0	1	0	?	1	1	1	0	0	0
0	?	0	0	?	2	0	0	1	0	0	0	0
0	?	0	0	1	1	0	0	1	1	0	0	1
0	?	0	0	1	2	1	1	2	0	0	0	0
0	?	0	0	1	2	1	1	2	0	0	0	0
1	0	0	1	0	1	1	0	2	0	0	0	0
0	?	0	0	1	1	0	1	2	0	0	0	0
?	?	?	?	?	?	?	?	?	?	?	?	?
?	?	?	?	?	?	?	?	?	?	?	?	?

Table 4. Pairwise distance comparisons between individuals within the same species and within the same genus, and between individuals of different genera (based on the Tamura-Nei Model).

Pairwise distance comparisons between individuals.	Individuals within the same species	Species within the same genus	Species within different genera
A. ***sanguinea*** **(RSA)** - *A. sanguinea* (NZ)	0.000	-	-
K. mikimotoi (Japan) - *K. mikimotoi* (Dk)	0.000	-	-
G. cf. *mikimotoi* (NZ) - *K. mikimotoi* (Japan)	0.000	-	-
G. aureolum (Dk) - ***G. aureolum*** **(RSA)**	0.003	-	-
Gymnodinium sp. (NZ) - *G. aureolum* (Dk)	0.001	-	-
Gymnodinium sp. Corsica (France) - *Gymnodinium* sp. (NZ)	0.002	-	-
Gymnodinium sp. Corsica (France) - *K. micrum* (*G. galatheanum*, Dk)	0.008		
K. cristata **(RSA)** - *K. brevis* (USA)	-	0.046	-
K. cristata **(RSA)** - *K. brevisulcata* (NZ)	-	0.040	-
K. brevisulcata (NZ) - *K. mikimotoi* (Dk)	-	0.051	-
K. cristata **(RSA)** - *K. bicuneiformis* (NZ)	-	0.046	-
L. viride **(RSA)** - *G. chlorophorum* (Germany)	-	0.031	-
G. catenatum (Spain) - *G. nolleri* (Dk)	-	0.031	-
K. brevis (USA) - ***A. sanguinea*** **(RSA)**	-	-	0.205
K. brevisulcata (NZ) - ***A. sanguinea*** **(RSA)**	-	-	0.208
K. cristata **(RSA)** - ***A. sanguinea*** **(RSA)**	-	-	0.207
G. chlorophorum (Germany) - ***G. aureolum*** **(RSA)**	-	-	0.142
L. viride **(RSA)** - ***G. aureolum*** **(RSA)**			0.160
L. viride **(RSA)** - *K. mikimotoi* (Dk)	-	-	0.290
G. fuscum (Aus) - ***L. viride*** **(RSA)**	-	-	0.235
G. fuscum (Aus) - ***G. aureolum*** **(RSA)**	-	-	0.211
G. fuscum (Aus) - *G. nolleri* (Dk)	-	-	0.239
G. fuscum (Aus) - *G. catenatum* (Aus)	-	-	0.243
G. fuscum (Aus) - *G. impudicum* (Dk)	-	-	0.215
G. impudicum (Dk) - *G. pallustre*			0.233
G. nolleri (Dk) - ***G. aureolum*** **(RSA)**	-	-	0.185
G. nolleri (Dk) - ***L. viride*** **(RSA)**	-	-	0.204
G. catenatum (Spain) - ***G. aureolum*** **(RSA)**	-	-	0.208
G. catenatum (Spain) - ***L. viride*** **(RSA)**	-	-	0.214
T. helix **(RSA)** - ***K. cristata*** **(RSA)**	-	-	0.100
T. helix **(RSA)** - *K. micrum (G. galatheanum*, Dk)	-	-	0.100
Gymnodinium sp. Corsica (France) - *G.* cf. *pulchellum* (NZ)	-	-	0.124
Gymnodinium simplex (USA) - ***Heterocapsa orientalis*** **(RSA)**	-	-	0.351
mean	0.002	0.041	0.204
range	0.000 - 0.008	0.031 - 0.051	0.100 - 0.351

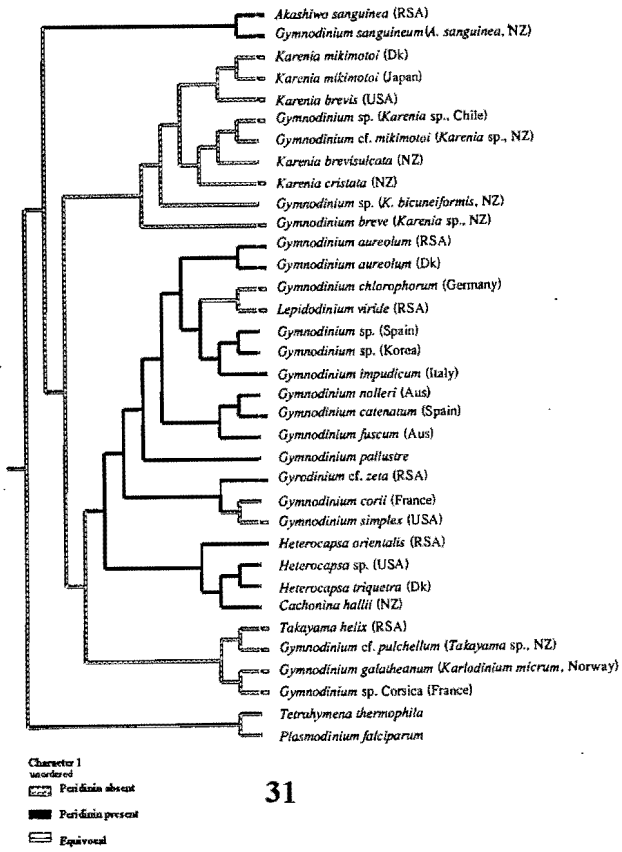

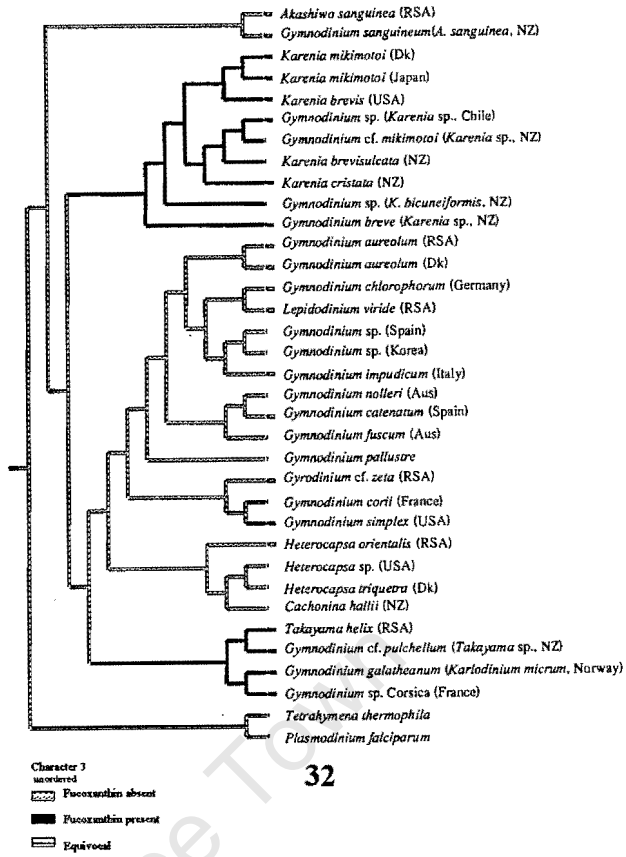

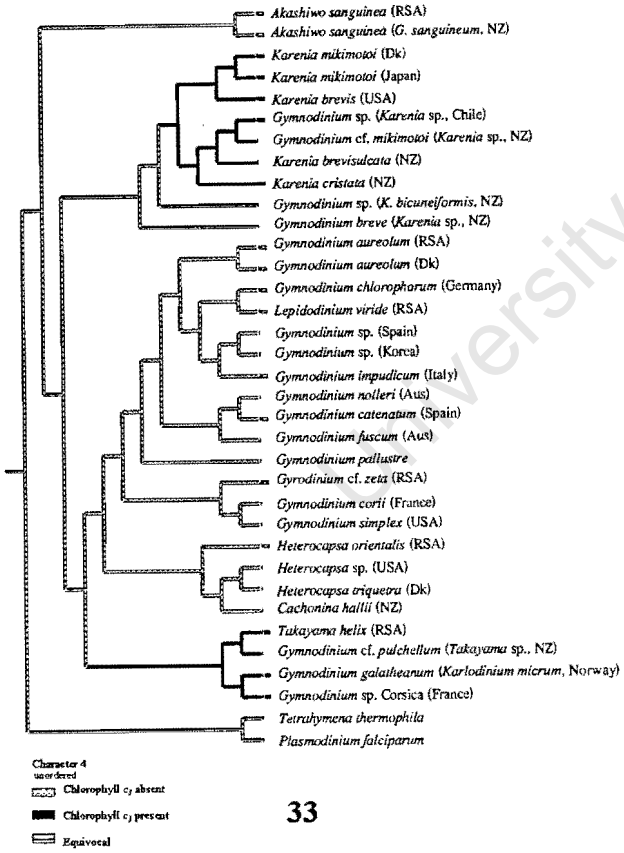

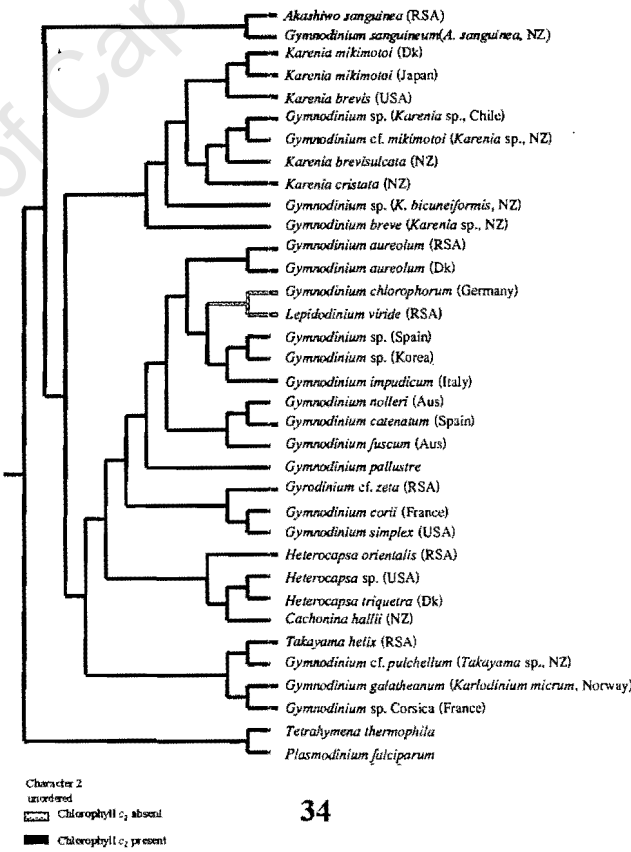

Figure 31 – 34. Optimisations of (31) Peridinin, (32) Fucoxanthin, (33) Chlorophyll c_3 and (34) Chlorophyll c_2 on the fully resolved tree based on the combined data set.

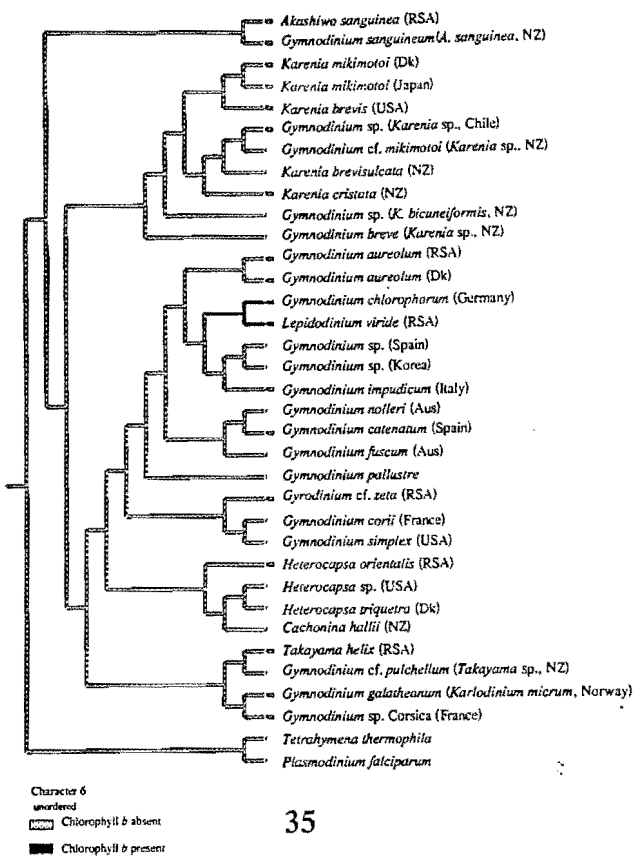

35

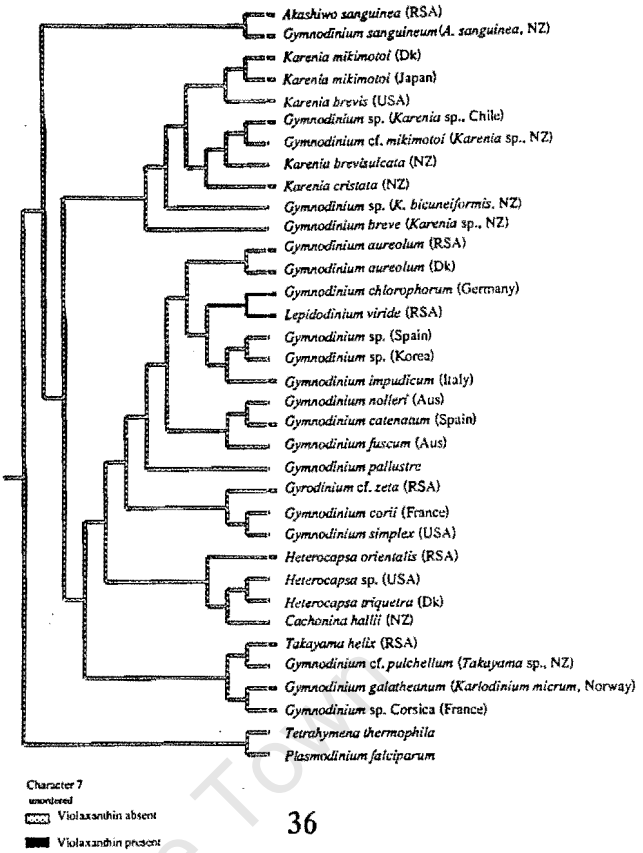

36

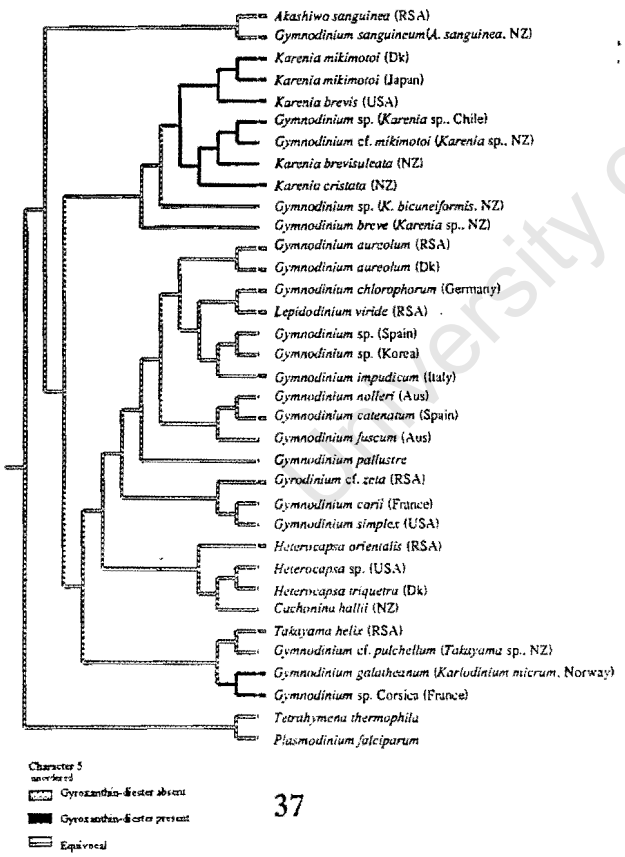

37

Figure 35 – 37. Optimisations of (35) Chlorophyll *b*, (36) Violaxanthin and (37) Gyroxanthin-diester on the fully resolved tree based on the combined data set.

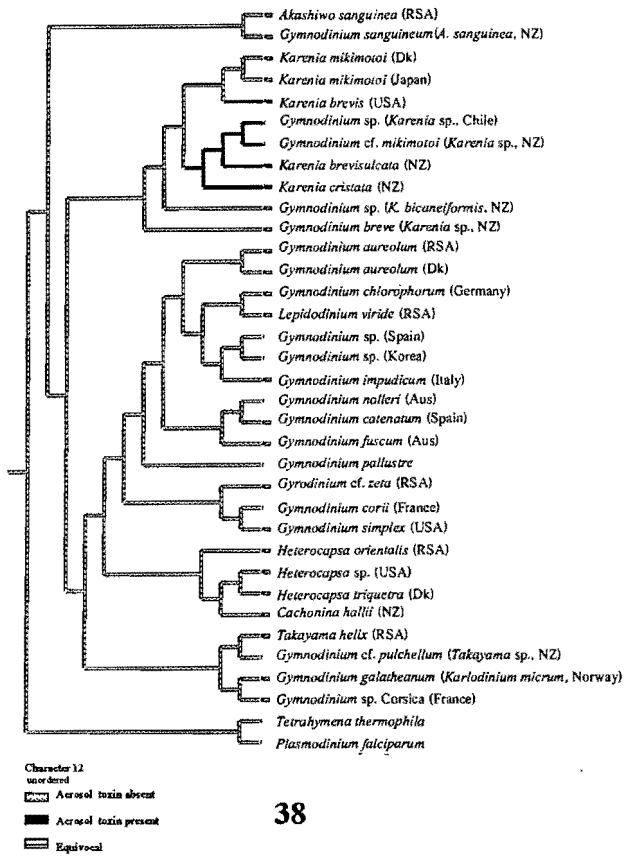

38

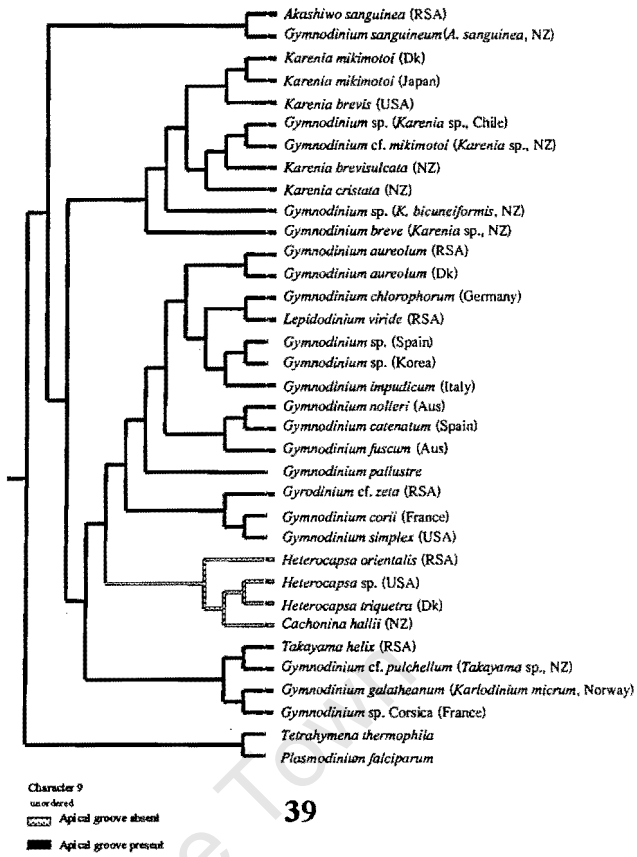

39

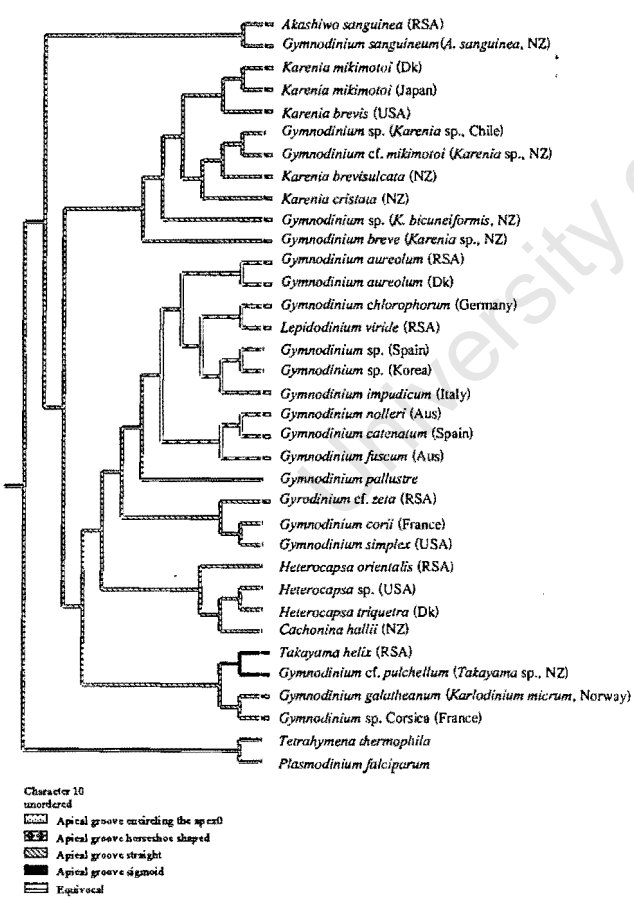

40

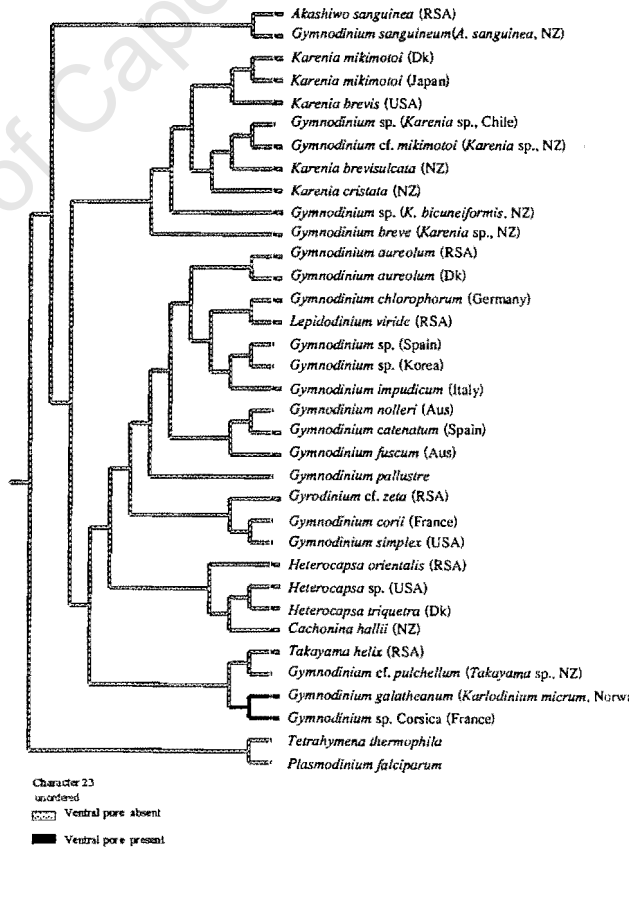

41

Figure 38 – 41. Optimisations of (38) an aerosol toxin, (39) apical groove, (40) apical groove shape and (41) ventral pore on the fully resolved tree based on the combined data set.

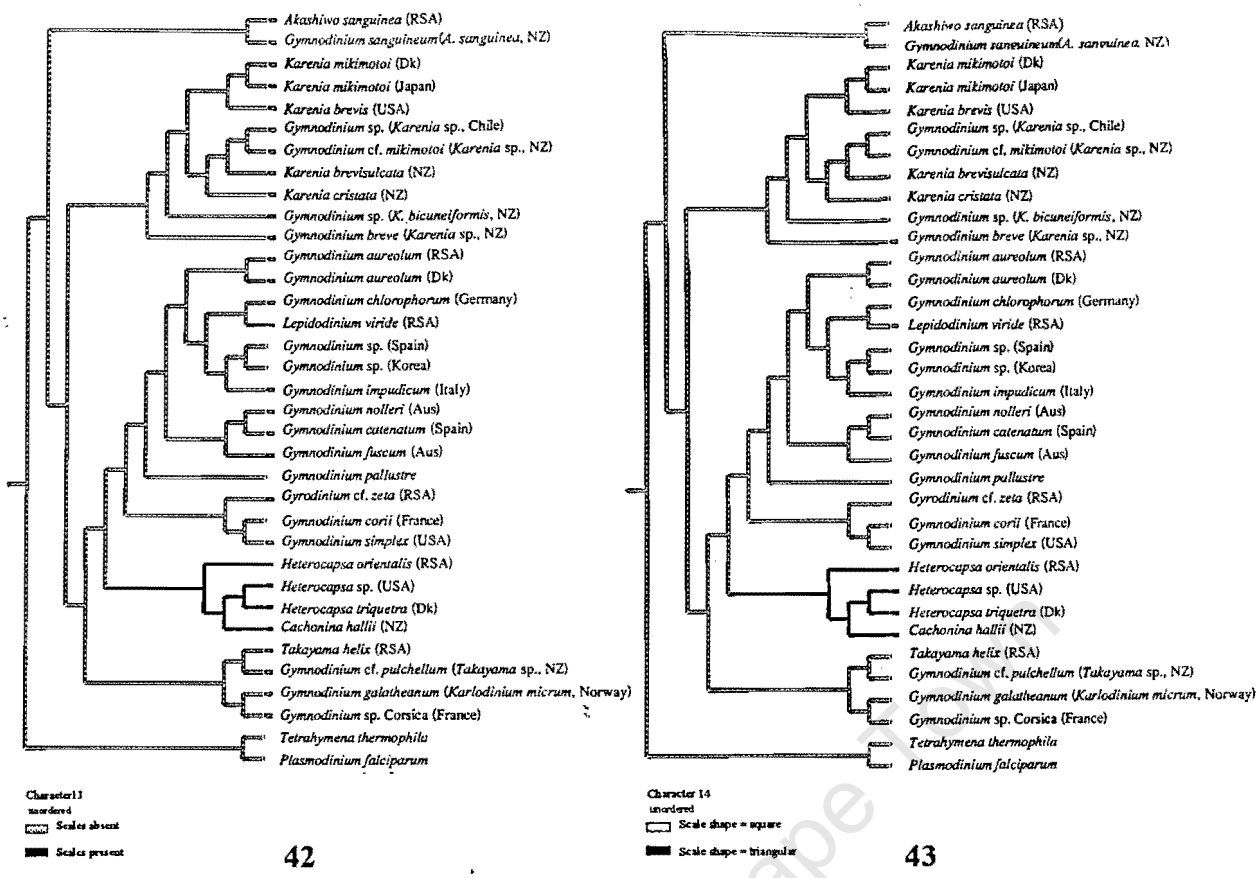

Figure 42 – 43. Optimisation of (42) scales and (43) scale shape on the fully resolved tree, based on the combined data set.

DISCUSSION

The considerable number of morphologically similar, yet diverse, species within Gymnodiniales has led to confusion world-wide (Steidinger *et al.* 1998b). Traditional methods such as light and electron microscopy revealed features of the flagellar apparatus, pusule, peduncle, nuclear chambers, chloroplasts etc. that were extremely useful in comparative cell ultrastructure but the resultant suite of morphological characters was not global (i.e. present in all of the taxa) and different researchers investigated different details over a wide range of taxa (Bolch *et al.* 1999, Chang 1999, Elbrächter & Schnepf 1996, Ellegaard & Moestrup 1999, Fraga *et al.* 1995, Hansen *et al.* 2000b, Hansen 2001, Haywood *et al.* 1996, Morril & Loeblich 1981, Palmer & Delwiche 1998, Paulmier *et al.* 1995, Rees &

Hallegraeff 1991, Watanabe *et al.* 1987). As a result, matrices of morphological and ultrastructural characters are incomplete (Chapman *et al.* 1998).

Molecular biological tools became available during the mid 1980s, offering the possibility of a great deal more global characters that would be more likely to lead to robust, well-resolved and consistent phylogenies. For example, molecular analyses have revealed phylogenetic relationships between some morpho-species in Gymnodiniales which resulted in the genus *Gymnodinium sensu lato* being split into four genera (Daugbjerg et *al.* 2000, Hansen et *al.* 2000a).

The LSU rDNA sequences of the South African isolates along with morphological and pigment data contributed greatly to a well-resolved and robust hypothesis of their relationships. Even though providing less resolution than the molecular data, morphological data do not contradict the molecular evidence and clearly provide support for some groups within the robust and well resolved tree topology which was obtained from the combined analyses. The tree obtained under maximum likelihood analysis of the molecular data set was highly congruent with that obtained with parsimony analysis. The tree topology obtained from the combined data set in turn was congruent with the strict consensus of 10 MPT's, provided by Daugbjerg and his colleugues (Daugbjerg et *al.* 2000) which was inferred from parsimony analysis (based on LSU rDNA, domain D1 – D3) (Fig. 30) and included the following unarmoured dinoflagellate species *Gymnodinium nolleri, G. catenatum, G. fuscum, G. pallustre, G.* cf. *placidum,* two *G. aureolum* isolates, *G. chlorophorum, G. impudicum, Karenia brevis, two K. mikimotoi* isolates, *Karlodinium micrum* and two *Akashiwo sanguinea* isolates. The clade containing the *Gymnodinium* species formed a trichotomy with the clade containing the two *A. sanguinea* isolates, and the clade containing the *Karenia* species and *K.*

micrum. Here *K. micrum* was sister to the clade containing *K. brevis* and the two *K. mikimotoi* isolates. Within the clade containing the *Gymnodinium* species, the group *G. nolleri* and *G. catenatum* was sister to the clade containing the rest of the *Gymnodinium* species. *G. fuscum* which was sister to *G. palustre* and *G.* cf. *placidum* formed a polytomy with *G. impudicum* and a clade containing two *G. aureolum* isolates and *G. chlorophorum*. *G. chlorophorum* however was sister to the two *G. aureolum* isolates.

The simultaneous parsimony analysis from our data sets however provides more resolution, the taxonomic implications of which are discussed below.

Clade 1 (Fig. 26):

One of the 9 South African isolates was placed within the clade containing *Akashiwo sanguinea* (Hirasaka) G. Hansen et Moestrup and is identical to the *A. sanguinea* isolates for this DNA region. The presence of an apical groove that curves around the apex in a clockwise direction is synapomorphic while the presence of peridinin is symplesiomorphic for both the terminal taxa within this monophyletic group.

Clade 2 (Fig. 26):

Two of the South African isolates were placed within a clade containing *Karenia* species such as *K. brevis, K. mikimotoi and K. brevisulcata* and have previously been described as new species, namely *Karenia cristata* Botes, Sym et Pitcher and *Karenia bicuneiformis* Botes, Sym et Pitcher (Botes *et al.,* 2003 b) based on autapomorphic characterstics.

Clade 3 (Fig. 26):

Another isolate was placed sister to an accession of *Gymnodinium aureolum* (Hulburt) G. Hansen. Both taxa possess a horseshoe-shaped apical groove, which is synapomorphic, and

peridinin which is symplesiomorphic for this monophyletic group. These two species are therefore considered as con-specific (pairwise distance value = 0.003).

Clade 4 (Fig. 26)

A third isolate was placed sister to the clade containing *Gymnodinium chlorophorum* Elbrächter et Schnepf. However, the pairwise distance between the two taxa (0.031) is within the range calculated among species within the same genus suggesting that these two taxa are not con-specific. As noted below, these also differ in some significant morphological features. Both have a horseshoe-shaped apical groove and the presence of chlorophyll *b* suggests that the common ancestor of these acquired an endosymbiont with plastids resembling those of prasinophyte green algae. In the case of the South African isolate, the cell surface is covered with square-shaped scales similar to those of prasinophytes. This acquisition would require transfer of the scale-forming genes from the endosymbiont nucleus to the host nucleus (and successful expression of these genes) prior to the loss of the endosymbiont nucleus (Palmer & Delwiche 1998). The South African isolate also had a peduncle-like structure as described by Watanabe et *al.* (1990). We therefore identified the species as *Lepidodinium viride* Watanabe, Suda, Inouye, Sawaguchi et Chihara. Nesting of these two taxa within *Gymnodinium senso stricto* (Daugbjerg *et al.* 2000) renders the latter paraphyletic.

Gymnodinium senso stricto is the only genus with a description that does not include reference to pigment content. The main diagnostic character for the genus is the horseshoe-shaped apical groove that runs in an anti-clockwise direction. Several authors (Hansen 2001, Hansen *et al.* 2000a, Daugbjerg *et al.* 2000) have pointed out that this genus is particularly complicated, with several puzzling discrepancies which indicate that this group eventually will need to be further subdivided.

The fact that the phylogenetic placement of the type species appears to be inconsistent within the tree is a major problem and requires attention. In the parsimony tree derived from LSU rDNA (D1 - D3) data (Hansen *et al.* 2000a) the type species is sister to a clade comprising *G. catenatum* and *G. nolleri* whilst under the maximum likelihood criterion (Hansen *et al.* 2000a) the type species is sister to a clade comprising *G. chlorophorum, G. aureolum* and *Gyrodinium impudicum*. In another tree topology (derived from LSU rDNA (D1 - D3) data) based on parsimony analysis and maximum likelihood (Daugbjerg *et al.* 2000), the type species was sister to *G. palustre* and *G. cf. placidum* and this clade was situated within a polytomy. When we included the type species in our analysis, it was sister to a clade comprising *G. catenatum* and *G. nolleri* based on parsimony analysis of the molecular data set (fig. 26), sister to *G. chlorophorum* and *L. viride* based on parsimony analysis of the morphological data set (fig. 27) and sister to a group comprising *G. aureolum, G. chlorophorum, L. viride, Gymnodinium* sp. from Korea, *G. impudicum, G. nolleri and G. catenatum* based on the parsimony analysis of the combined data set (fig. 28). It formed part of a polytomy (fig. 29) when based on maximum likelihood analysis of the molecular data set. In our opinion fig 28 is the best representation of the type species and suspect, however, that the type species might even represent a monotypic genus. It clearly warrants additional study and different DNA regions will be needed to clarify its phylogenetic position.

Ultrastructurally, the type species differs from the other species of *Gymnodinium senso stricto* with respect to the pusular type, the lack of a transverse striated flagellar root (the only dinoflagellate species known to lack this feature), the lack of striated collars around the flagellar canals, the lack of trichocysts and the lack of a peduncle (Hansen *et al.* 2000b, Hansen 2001). Discrepancies among the other taxa within *Gymnodinium senso stricto* also

exist and include aspects of the pusule (Hansen 2001), peduncle (Rees & Hallegraeff 1991, Elbrächter & Schnepf 1996, Ellegaard & Moestrup 1999), nuclear fiber connector and nuclear chambers (Hansen 2001) and chloroplasts (Ellegaard & Moestrup 1999, Rees & Hallegraeff 1991, Elbrächter & Schnepf 1996).

On the basis of this heterogeneity, and in the light of our phylogenetic results, we suggest that the genus *Gymnodinium senso stricto* be subdivided and that clade 4 (Botes & de Salas, unpublished data) *and G. catenatum* together with *G. nolleri* (Bolch & Hallegraeff, unpublished data) be described as new genera. Pairwise distance comparisons between taxa belonging to clades 3 - 7 are within the range calculated for among genus comparisons and therefore support the subdivision of the genus *Gymnodinium senso stricto* in order to maintain the monophyletic nature of genera.

Clade 8 (Figure 26):

The species within this clade namely *Gymnodinium simplex*, *Gymodinium corrii* and *Gyrodinium* cf. *zeta* were not included in the tree presented by Daugbjerg *et al.* (2000) and as it stands the taxonomic status of this well supported group remains unclear, indicating that much wider species sampling is necessary to contribute to a more complete Gymnodiniales taxonomic system.

Clade 9 (Fig. 26):

One of the South African isolates, at first mistaken for *Gymnodinium pyrenoidosum* Horiguchi et Chihara, but as no eyespot was present and with phylogenetic analysis, it was placed within a clade containing delicately armoured *Heterocapsa* species and identified as *Heterocapsa orientalis* (Iwataki *et al.* in press). Under both parsimony and maximum

likelihood criterion, this clade (containing armoured dinoflagellate species) was placed amongst the unarmoured gymnodinioid species. The strong affinity of this clade to the gymnodinioids has been noted previously (Daugbjerg *et al.* 2000, Lenaers *et al.* 1991). Daugbjerg *et al.* (2000) documented that peridinioid genera such as *Heterocapsa* and *Scrippsiella* Balech ex Loeblich III form strongly supported clades within the gymnodinioid, peridinioid and prorocentrioid (GPP) complex. Lenaers *et al.* (1991) commented on the placement of *Heterocapsa pygmaea* and *Cachonina niei* among the Gymnodiniales and said that "... these two species appear more closely related to Gymnodiniales than Peridiniales." Lenaers *et al.* (1991) and our tree have low taxon representaion and it is likely that extensive taxon sampling which includes other members of the thecate dinoflagellates will change the placement of this group. Currently the relationships of many groups within this complex are still unknown.

Clade 10 (Fig. 26):

One of the South African isolates, identified as *T. helix* (de Salas *et al.* 2003), was placed within a clade containing *Gymnodinium* cf. *pulchellum* (*Takayama* sp.) from New Zealand. Both these taxa are characterised by having sigmoid apical grooves and fucoxanthin as the major carotenoid. The pairwise distance between the two taxa suggests that these two species are very closely related. When compared to species within clades 2 and 11, the values calculated were within the range calculated for species between genera and support the recent recognition of this clade as a new genus (de Salas *et al.*, 2003).

Clade 11 (Figure 26):

One of the South African isolates is morphologically similar to *Gyrodinium corsicum* Paulmier, Berland, Billard et Nezan (E. Garcés pers. comm.) and was placed within a clade

together with *G. galatheanum* (*Karlodinium micrum* [Leadbeater et Dodge] J. Larsen) and a *Gymnodnium* sp. from New Zealand. Both *G. corsicum* and *K. mucrum* are characterised by having a straight apical groove, a ventral pore and fucoxanthin. Pairwise distance comparisons between *K. micrum* (*Gymnodinium galatheanum*, isolated in Denmark by Karl Tangen, AF 200675) and *Gymnodinium* sp. Corsica (isolated in France, AF 318249) indicated that these two species are identical. It is documented that *K. micrum* (≡ *Gymnodinium galateanum* Bruaard) contains gyroxanthin diester (Kempton *et al.* 2002). *G. corsicum* isolated from Alfacs Bay apparently also contain gyroxanthin diester (Hernández 2000). However, gyroxanthin-diester was not detected in our *G.* cf. *corsicum* culture. Gyroxanthin-diester was also not detected in the *Gyrodinium* sp. isolated from Oslofjord, Norway (Bjørnland & Tangen 1979), which was later identified as *G. galatheanum* (K. Tangen pers. comm.). Whether *K. micrum* (≡ *Gymnodinium galateanum* Braarud) and *G. corsicum* are identical needs to be further investigated.

Character evolution

Evolution of selected pigments (Figs 31 – 37):

There appears to be a degree of disagreement in the literature as to whether the presence of peridinin (Fig. 31) or fucoxanthin (Fig. 32) is the plesiomorphic state (Saldarriaga *et al.* 2001, Tengs *et al.* 2000, Yoon *et al.* 2002) within dinoflagellates. This uncertainty is also evident in our results with the plesiomorphic state of chlorophyll c_3 (Fig. 33) equally as unclear. The presence of fucoxanthin and chlorophyll c_3 within the clades *Karenia* and *Karlodinium* however, provides support to the theory that a Prymnesiophyte endosymbiont is present within these species (Tengs *et al.* 2000). It therefore seems likely that a Prymnesiophyte endosymbiont is also present within the newly erected *Takayama* clade.

The presence of chlorophyll c_2 (Fig. 34) is plesiomorphic and present in all species except in the clade containing *G. chlorophorum* and *L. viride*. Chlorophyll *b* (Fig. 35) and violaxanthin (Fig. 36) were acquired in these two species and this supports the theory that a Prasinophyte or Chlorophyte endosymbiont (Jeffrey *et al.* 1997, Watanabe *et al.* 1990) is present in these species.

It is not clear whether the presence of gyroxanthin-diester (Fig. 37) is plesiomorphic or apomorhic. It is however interesting to note that unlike the fucoxanthin and chlorophyll c_3, this pigment is only present in the *Karenia* and *Karlodinium* clades and not in the *Takayama* clade. In this case, it is not clear whether the presence of gyroxanthin-diester is due to the incorporation of an endosymbiont or not.

Evolution of selected morphological characters (Figs 38 – 43)

The equivocal status of the ancestor of the group containing the two *K. brevis* isolates, the two *K. mikimotoi* isolates, *K. brevisulcata*, *K. cristata* and the *Karenia* isolate from Chile makes it difficult to hypothesise whether the presence of an aerosol toxin within this group is homoplasious or homologous. Under accelerated transformation the feature would have originated once but was lost in the ancestor of the group comprising the two *K. mikimotoi* isolates . Under delayed transformation the two groups would have acquired the trait independently. Wider taxon sampling within this clade should clarify the situation.

The presence of apical grooves is plesiomorphic (Fig. 39) with the different apical groove shapes as synapomorphies (Fig. 40). Additional sampling could however still reveal that one preceded the other.

Taxa in the *Karlodinium* clade contain a straight apical groove, like the *Karenia* clade, but unlike the *Karenia* clade, it also contains a ventral pore as a synapomorphy (Fig. 41). It is noteworthy that, although not coded within the present chapter it was also found (see chapter 5) that a ventral pore was also present within the taxa belonging to the *Takayama* clade (de Salas *et al.* 2003).

The presence of scales (Fig. 42) indicates that scales are present in two clades, one of which is autapomorphic in the clade containing *G. chlorophorum* and *L. viride*, (with triangular shaped scales present on *L. viride* Fig. 43), and the other is synapomorphic in the *Heterocapsa* clade (with square shaped scales found on all *Heterocapsa* species Fig. 43) (Iwataki *et al.* 2003). It is therefore likely that the presence of scales within the ingroup is not homologous.

From the above discussion it is clear that most of the clades are defined by at least one synapomorphic character which supports the delineation of the monophyletic groups indicated. Morphological characters deemed diagnostic, for gymnodinioids, on genus level were characters 1 – 8 (pigment content), 10 (apical groove shape) and 23 (ventral pore). It is however possible that further research could with time reveal more phylogenetically informative characters such as the presence and nature of the nuclear fibre connector which was not included in our study. Morphological characters deemed diagnostic on species level were characters (and character states) 11 (length of the straight apical groove on the ventral and/or dorsal surface), 12 (presence of an aerosol toxin), 17 (presence of a peduncle like structure), 22 (presence of an apical crest), 24 – 25 (shapes of the hypocone) and 14 (shape of scales). These were often autapomorphic (newly derived character that defines only a single terminal taxon), at least with the extent of sampling performed here. It is worth noting that

character 14 or the acquisition of scales should be considered cautiously. All species of the genus *Heterocapsa* have triangular-shaped scales, a feature considered important on genus level, and the details of which are typical of particular species (Iwataki *et al.* in press). The acquisition of scales in *Lepidodinium viride* only, appear to result from the successful expression of scale-forming genes aquired from its endosymbiont prior to the loss of the endosymbiont nucleus (Palmer & Delwiche 1998) and is therefore diagnostic on species level. Although helpful in ultrastructural comparisons, characters 16 (amphiesmal vesicles containing delicate thecal material) and characters 18 – 21 (nucleus shape and position) were not considered taxonomically important, our results indicated that, within the framework of our study, these characters and other autapomorphic (newly derived character that defines only a single terminal taxon) characters were phylogenetically uninformative.

In conclusion, a total evidence approach involving the analysis of combined and multiple data sets, well-developed morphological characters and greater molecular sampling of taxa are likely to provide the most robust phylogenies. The mapping of organismal characters on a robust phylogenetic tree has been very helpful in assessing the usefulness of characters at various taxonomic levels.

CHAPTER 5

TAKAYAMA (GYMNODINIALES, DINOPHYCEAE) GEN. NOV., A NEW GENUS OF UNARMOURED DINOFLAGELLATES WITH SIGMOID APICAL GROOVES, INCLUDING THE DESCRIPTION OF TWO NEW SPECIES

ABSTRACT

A new, potentially ichthyotoxic genus, *Takayama* de Salas, Bolch, Botes et Hallegraeff *gen. nov.* is described from two new species: *T. tasmanica* de Salas, Bolch et Hallegraeff, *sp. nov.*, and *T. helix*, de Salas, Bolch, Botes et Hallegraeff, *sp. nov.*, isolated from Tasmanian (Australia) and South African coastal waters. The genus and two species are characterised by light and electron microscopy of field samples and laboratory cultures, as well as large subunit ribosomal DNA sequences and HPLC pigment analyses of several cultured strains. The new *Takayama* species have sigmoid apical grooves and contain fucoxanthin and its derivatives as the main accessory pigments. *T. tasmanica* is similar to the previously described species *Gymnodinium pulchellum* Larsen, *Gyrodinium acrotrochum* Larsen and *G. cladochroma* Larsen in its external morphology, but differs from these in having two ventral pores, a large, horseshoe-shaped nucleus and a central pyrenoid with radiating chloroplasts that puncture through the nucleus. It contains gyroxanthin-diester as an accessory pigment, which is missing in *T. helix*. *T. helix* has an apical groove that is nearly straight while still being clearly inflected. A ventral pore or slit is present. It has numerous peripheral, strap-shaped and spiralling chloroplasts with individual pyrenoids, and a solid nucleus. The genus *Takayama* has close affinities to the genera *Karenia* and *Karlodinium*, and may represent an intermediate step between the straight-grooved species and those with horseshoe-shaped grooves.

INTRODUCTION

Fish-killing, unarmoured, gymnodinioid dinoflagellates with sigmoid apical grooves have been reported since the 1980s (Onoue *et al.* 1985 as *Gymnodinium* type-'84 K, Takayama, 1985, as *Gymnodinium* sp. 1). The first species described with this character was *Gymnodinium pulchellum* Larsen, from a Port Phillip Bay field sample, which was considered to be most likely identical to Takayama's (1985), and Onoue's (1985) ichthyotoxic taxa. Fish mortalities have been attributed to *Gymnodinium pulchellum* –like species in Australia (Larsen 1994, Hallegraeff 2002), Japan (Onoue *et al.* 1985), and the U.S.A. (Steidinger *et al.* 1998). Two new species morphologically similar to G. *pulchellum* were also described by Larsen in 1996 from field samples collected in Port Phillip Bay as *Gyrodinium acrotrochum* Larsen and *Gyrodinium cladochroma* Larsen.

Until recently, unarmoured dinoflagellate taxonomy was based exclusively on morphological and cytological features (Kofoid & Swezy, 1921). However, a revision by Daugbjerg *et al.* (2000) combined large subunit ribosomal DNA (LSU-rDNA) sequences, ultrastructural characters and chloroplast pigment content to divide the large heterogeneous genus *Gymnodinium sensu lato* into four genera: *Gymnodinium sensu stricto,* with a horseshoe shaped apical groove and peridinin as the main carotenoid; *Akashiwo,* with a clockwise spiral apical groove and peridinin; *Karenia,* with a straight apical groove and fucoxanthin; and *Karlodinium,* with a short, straight apical groove, a ventral pore, and fucoxanthin. However, the status of *Gymnodinium pulchellum* was not resolved, as no cultures of *G. pulchellum* -like organisms were available at the time.

We have recently isolated *G. pulchellum*-like species from several locations in southern Australia and South Africa and established cultures of two sigmoid grooved species. Based on

morphological, ultrastructural and pigment analyses and LSU rDNA sequences we create a new genus: *Takayama* de Salas, Bolch, Botes et Hallegraeff *gen. nov.* for these two new species: *Takayama tasmanica* de Salas, Bolch et Hallegraeff *sp. nov.*, and *Takayama helix* de Salas, Bolch, Botes et Hallegraeff *sp. nov.* We also transfer *Gymnodinium pulchellum*, *Gyrodinium acrotrochum* and *G. cladochroma* to the genus *Takayama*.

MATERIALS AND METHODS

Culture conditions

Australian cells of *T. tasmanica* and *T. helix* were isolated from plankton net (20 µm mesh) samples collected in the Derwent estuary, and in North West Bay, in south eastern Tasmania (Fig. 1). Single cells were isolated with a micropipette into 28‰ GSe medium (Blackburn *et al.* 1989). Cultures were maintained in this medium, at 17°C, with a 12:12 L:D photoperiod of 100 µmol m^{-2} s^{-1}, supplied by cool white fluorescent lights. Cultures used in this study are detailed in Table 1. South African *T. helix* was isolated from False Bay at Gordon's Bay (Fig. 1) in the same manner as the Australian isolates but were maintained in F/2 medium (Guillard & Ryther 1962) at 18°C.

Light microscopy

Live cells of *T. tasmanica* and *T. helix* were examined and photographed with bright field and differential interference contrast using a Zeiss Axioskop 2 Plus microscope connected to a Canon Powershot G1 digital camera. Cell length, width, and degree of girdle displacement were measured on 50 individual cells in mid-logarithmic phase.

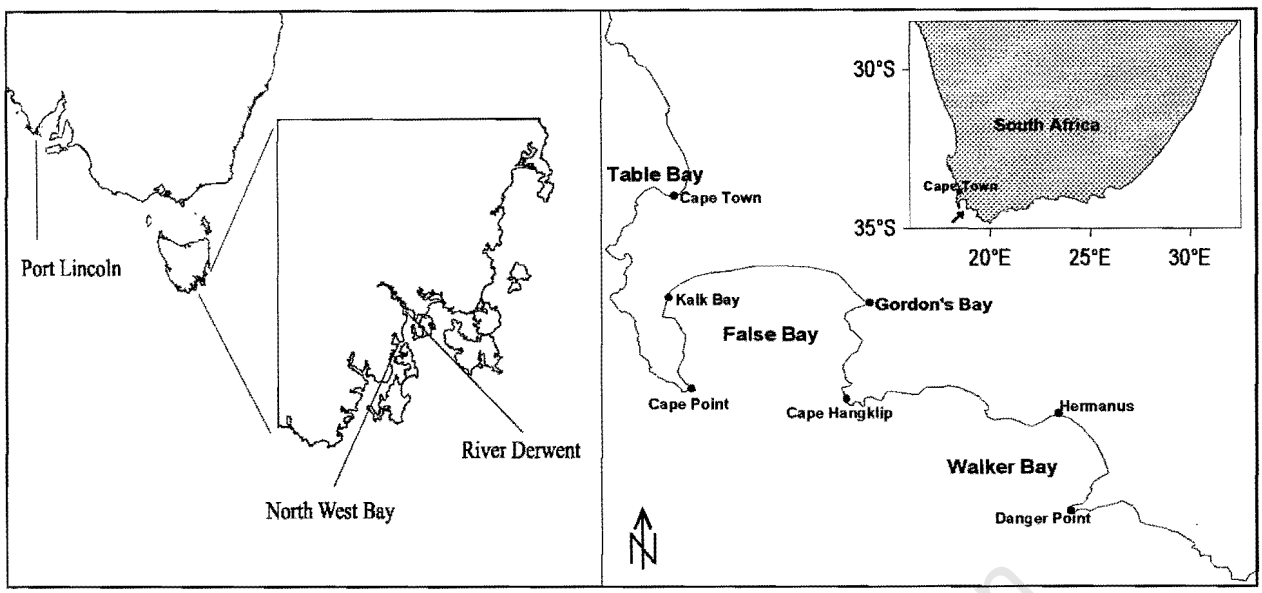

Fig. 1: Map of Australia and South Africa showing locations where *T. tasmanica* and *T. helix* have been isolated.

Scanning electron microscopy

Cells of the Australian isolates of *T. tasmanica* and *T. helix* were fixed by addition of equal volumes of 4% osmium tetroxide (OsO_4) solution prepared in culture medium. Samples were mounted, critical point dried and sputter-coated as described in de Salas *et al.* (2002). Cells were observed using a JEOL 35C and a JSM 840 scanning electron microscope. Scanning electron micrographs of the South African isolate of *T. helix* were obtained according to Botes *et al.* (2002).

Transmission electron microscopy

Cells of *T. tasmanica* and *T. helix* were fixed for 1 hour in a solution containing 2% OsO_4 and 2.5% glutaraldehyde made in GSe culture medium. After rinsing twice in culture medium and twice in distilled water, cells were dehydrated in an ethanol-acetone series and embedded in Spurr's resin. Sections of 60 nm thickness were taken using a Reichert Ultracut E microtome,

mounted on Formvar coated grids, stained with uranyl acetate (Hansen *et al.* 2000) and observed using an Phillips CM 100 transmission electron microscope.

Table 1: Cultures and field samples used in this study.

	Field Samples			
Species	Locality	Date		
T. tasmanica	Port Arthur	17.10.2001		
T. tasmanica	St. Helens	24.5.2002		
T. tasmanica	Tuggerah Lakes, N.S.W.	12.10.2002		
T. helix	River Derwent	19.3.2002		
T. helix	Port Arthur	17.10.2001		
T. helix	Port Lincoln (S.A.)	5.4.2002		
	Cultures			
Species	Locality	Date	Isolated by	Strain code
T. tasmanica	River Derwent	7.2.2001	M. de Salas	TTDW01
T. tasmanica	River Derwent	3.5.2001	M. de Salas	TTDW03
T. helix	North West Bay	14.5.2001	M. de Salas	THNWB01
T. helix	North West Bay	14.5.2001	M. de Salas	THNWB02
T. helix	False Bay, RSA	1998	L. Botes	CTCC19

Molecular data

Cultures were grown to mid-logarithmic phase and approximately 10 ml of culture were pelleted by gentle centrifugation. DNA extraction, PCR reaction, cycle-sequencing parameters, and sequence alignment and analysis were carried out as previously described in de Salas *et al.* (2002).

Pigment content

Approximately 10 ml of culture in mid-logarithmic phase were filtered gently onto 45-mm Gelman GF/F glass fibre filters and snap frozen in liquid nitrogen for storage. Pigments were extracted as described in de Salas *et al.* (2002), and analysed by the method of Zapata *et al.* (2000). Peaks were integrated using Waters Millennium software and identified by comparison of their retention times and spectra with those of mixed standards obtained from known cultures. A standard of gyroxanthin-diester (DHI Bioproducts, Denmark) was also compared, as this pigment is known from *Karenia* and *Karlodinium* species (Hansen *et al.* 2000).

RESULTS

Takayama de Salas, Bolch, Botes et Hallegraeff *gen. nov.*

Dinoflagellata inarmata cum fucoxanthin aut oriundis ex fucoxanthin pro pigmentis principalibus accessoriisque. Canalis apicalis sigmoides.

Unarmoured dinoflagellates with fucoxanthin or its derivatives as the major accessory pigments. Sigmoid apical groove.

ETYMOLOGY: Named after Dr. Haruyoshi Takayama, whose work first drew attention to the importance of apical grooves in unarmoured dinoflagellate taxonomy.

TYPE SPECIES: *Takayama tasmanica* de Salas, Bolch et Hallegraeff, *sp. nov.*

OTHER SPECIES IN GENUS: *Takayama helix* de Salas, Bolch et Hallegraeff *sp. nov.*

Takayama tasmanica de Salas, Bolch et Hallegraeff *sp. nov.*

Figs 2-12, 32, 33

Cellulae obovatae, leniter dorsiventraliter complanatae, 16-27 μm longae, 14-26 μm latae, 10-20 μm crassae. Epiconus hemisphaericus. Hypoconus truncatus incisus. Cingulum profunde incisum, latum, per 1/4 longitudinis cellulae totius dislocatum. Sulcus in hypocono latior quam in regione intercingulari, in epiconum breviter invasus. Canalis apicalis sigmoideus, e puncto infra dexteram extensionis sulcalis ascendens, epiconum transcendens, apicem cellulae circumiens, et per quasi 2/3 longitudinis epiconi dorsalis descendens. Partem tubiformem regio intercingularis sulci exhibens. Chloroplasti 7-10, e pyrenoide centrali per nucleum radiantes et in peripherio ramificantes. Nucleus sine capsula, maximam partem epiconi implens, latera dorsum apicemque pyrenoidis cingens.

Cells obovate in outline, slightly dorsoventrally flattened, 16 – 27 μm long, 14 – 26 μm wide, 10 – 20 μm thick. Epicone hemispherical. Hypocone truncated and incised. Cingulum deeply excavated and wide, displaced about 25 % of total cell length. Sulcus wider in the hypocone than the intercingular region, extending shortly into the epicone. Apical groove sigmoid, extending from below and to the right of the sulcal extension, across the epicone and around the cell apex, to approximately 2/3 of the way down the dorsal epicone. Tube like structure in the intercingular region of the sulcus. Chloroplasts 7 – 10, radiating from a central pyrenoid

and through the nucleus, branching peripherally. Nucleus without a capsule, filling most of the epicone, surrounding the pyrenoid laterally, dorsally and apically.

HOLOTYPE: Fig. 7, of culture TTDW01, isolated from the River Derwent, Tasmania, Australia (Fig. 1). Culture deposited into the University of Tasmania Harmful Algae Culture Collection.

ETYMOLOGY: named after the island of Tasmania, in south eastern Australia, where the species was first isolated.

DISTRIBUTION: North- and south-eastern Tasmania.

DESCRIPTION: *T. tasmanica* is a medium sized dinoflagellate. Measurements of 50 cells, compared with *T. helix, G. pulchellum, G. acrotrochum* and *G. cladochroma* are given in Table 2. Under the light microscope the cell outline appears obovate to almost spherical (Figs 2-4). The epicone is hemispherical, and comprises approximately 1/3 of the cell length. The hypocone is truncated and deeply incised by the sulcus. The sulcus itself is wide, but narrows in the intercingular region, and extends shortly into the epicone as a finger-like projection (Fig. 2). The cingulum is displaced approximately 1/4 of the total cell length. A sigmoid apical groove skirts around the apex of the cell (Fig. 3) and descends 2/3 of the length of the dorsal epicone, angled towards the right side of the cell. A spherical pusule is surrounded by sac or tear-drop shaped vesicles (Fig. 5). Chloroplasts radiate from a central pyrenoid, through the nucleus, branching irregularly underneath the cell surface (Figs 4, 6). In stressed cells the chloroplasts become rod shaped and their number is more obvious (Fig. 6). The nucleus is large and cup shaped (Fig. 4), and occupies most of the epicone. It is perforated by chloroplasts radiating out of the central pyrenoid, which it surrounds apically, dorsally and laterally.

Table 2: Comparison of measurements and morphological characteristics of *Takayama* species with *Gymnodinium pulchellum, Gyrodinium acrotrochum* and *G. cladochroma*.

Parameter	***Takayama tasmanica***	***Takayama helix***	***Takayama pulchella****	***Takayama acrotrocha****	*Takayama* ***cladochroma****
Cell length (µm)	16-27 (mean 22.8 ± 2.8 n = 50)	17-45 (mean 28.2 ± 4.6 n = 50)	16-25	22-27	18-22
Cell width (µm)	14-26 (mean 19.8 ± 2.7 n = 50)	11-31 (mean 22.3 ± 3.9 n = 50)	11-16	18-22	17-19
Length / width ratio	1.00-1.37 (1.15 ± 0.08 n = 50)	0.98 -1.74 (1.28 ± 0.15 n = 50)	1.45 – 1.56	1.22	1.06 – 1.16
Girdle displacement % total cell length	21-33 (mean 25.8 ± 2.4)	21-28 (mean 24.62 ± 2.75)	~23 % (from published figures)	25 - 80	25
Sulcal extension	finger-like, angled 45° to the rest of the sulcus	finger-like, angled 45° to the rest of the sulcus	short, finger-like	none	small- blunt
Apical groove	sigmoid, curving around the cell apex. Descending sideways 2/3 down dorsal	shallowly sigmoid, but passing through the cell apex. Descending 1/3 down the	sigmoid, counter-clockwise, encircling the cell apex	sigmoid, curves around the apex	sigmoid, curving around apex, and extending shortly on dorsal side

	down dorsal side	down the dorsal epicone			
Nucleus	large and multi-lobed, enveloping the central pyrenoid	ellipsoidal or round, centred in dorsal epicone or slightly to the left	large, located on the left part of the cell	Large, fills up most of the epicone	on left side of the cell
Chloroplasts	7-10, radiating though the nucleus and branching under the surface. Pyrenoids centrally located inside the nucleus	numerous, peripheral, arranged in spiralling bands	several, irregularly shaped, with pyrenoids	mostly in hypocone, disc shaped, with pyrenoids	few, large and branched, with conspicuous pyrenoids

* from Larsen 1994, 1996

Using SEM, the sigmoid apical groove can be seen to skirt around the cell apex, but does not pass directly over it (Figs 7, 8). The ventral termination of the apical groove becomes shallower (Fig. 7) and has no clearly defined starting point. The area that lies between the apical groove and the sulcus is swollen and rod-like (Fig. 8). Often a slit, also visible as a pore, is present in the lower part of the apical groove (Figs. 7-11). Another pore, situated in the left ventral epicone just above the sulcus (Fig. 9), is visible in some (but not all) cells. In well preserved samples, the apical groove appears as a cleft shaped incision into the cell surface (Figs 7-10). The cell surface itself is composed of amphiesmal vesicles that are

rectangular in the sulcus and adjacent to the apical groove, but polygonal elsewhere (Figs 7, 8). The sulcus can be seen to intrude into the epicone at an angle (Figs. 7 and 11), but this is not obvious in all cells, as the intrusion is short and shallow. A tube-like appendage that occupies the intercingular region is visible in Figs 7 - 11.

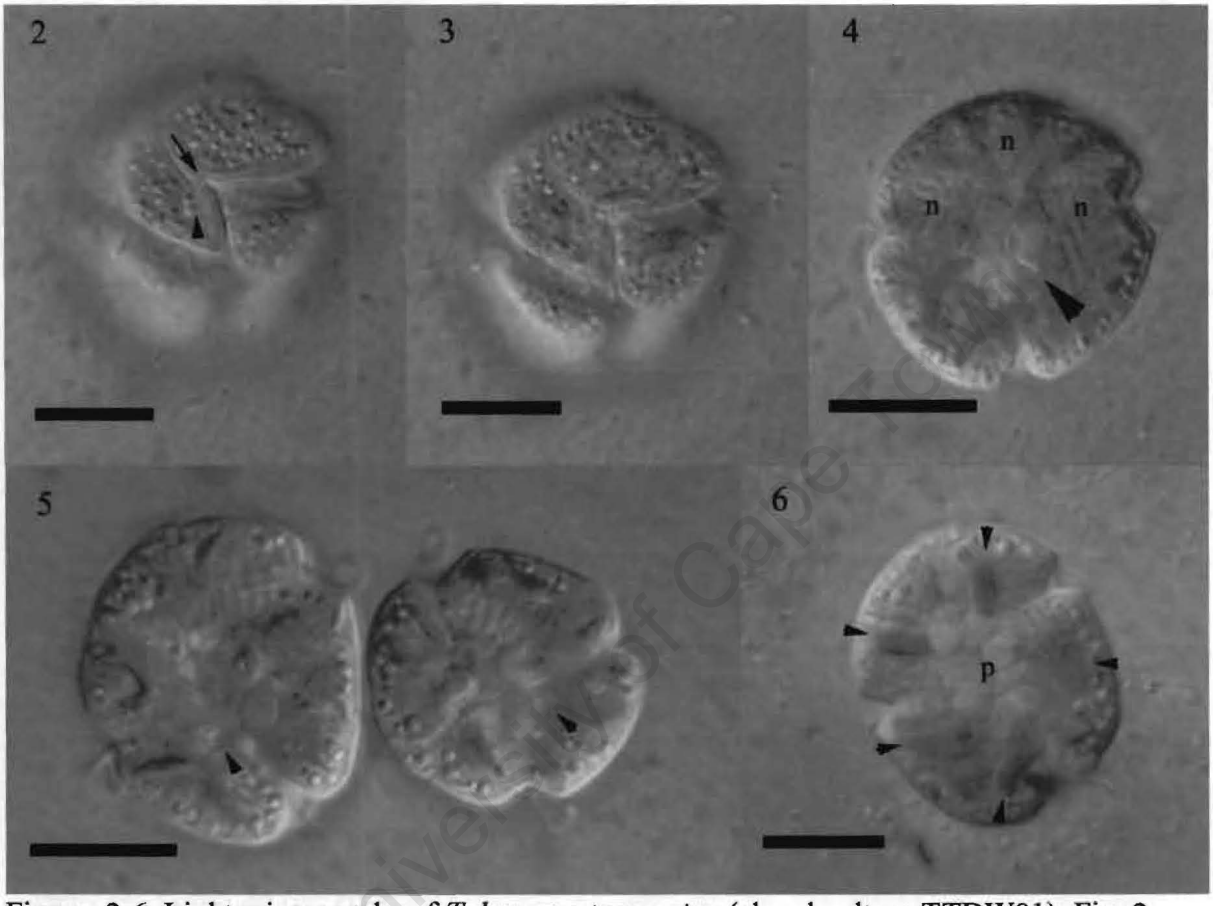

Figure. 2-6. Light micrographs of *Takayama tasmanica* (clonal culture TTDW01). Fig. 2 Ventral view of cell in surface focus, showing the indistinct origin of the apical groove (arrowhead) and sulcal intrusion into epicone (arrow). Fig. 3 Ventral view of same cell on slightly deeper focus showing sigmoid shape of apical groove skirting around cell apex. Fig. 4 Central focus of same cell showing central pyrenoid (arrowhead), enveloping nucleus (n) and irregular, radiating chloroplasts. Fig. 5 Pair of cells showing size variation in clonal cultures. Note the spherical pusules (arrowheads). Fig. 6 Central focus of stressed cell showing the central pyrenoid (p) and radiating, rod shaped chloroplasts (arrowheads). Scale bars all 10 μm long.

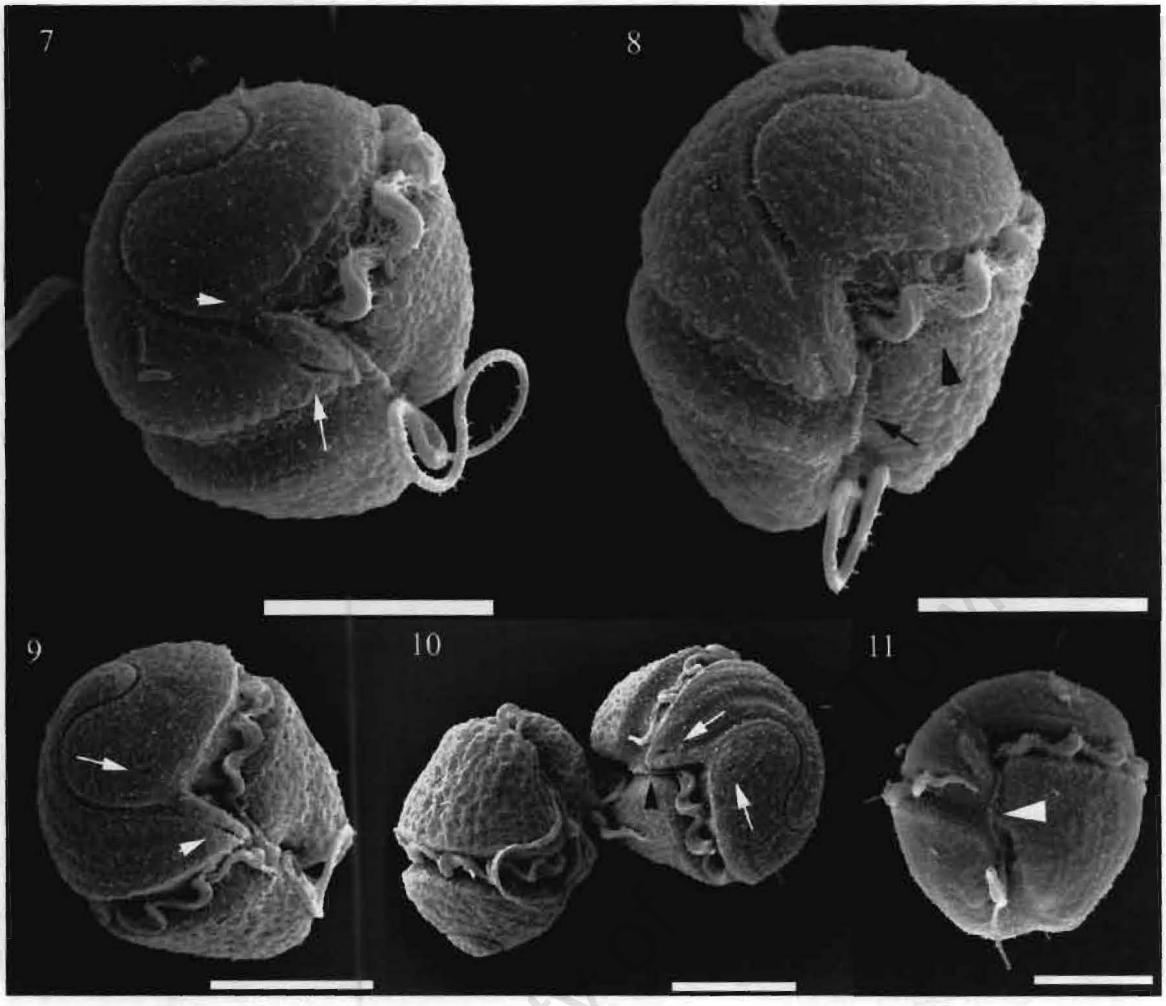

Figure. 7 – 11. Scanning electron micrographs of *Takayama tasmanica* (clonal culture TTDW01). Fig. 7 Ventral view of cell showing sigmoid apical groove, sulcal intrusion into epicone (arrowhead), and pore or slit on cingular end of apical groove (arrow). Fig. 8 Ventral view of another cell showing transverse flagellum with mucus strands (arrowhead), tube like structure in sulcus (arrow), and arrangement of amphiesmal vesicles in parallel rows to apical groove (a). Fig. 9 Ventral view of cell showing slit in cingular end of apical groove (arrowhead) and ventral pore in epicone (arrow). Fig. 10 View of pair of cells showing tube like structure in sulcus (arrowhead) and pair of ventral pores in same position as Fig. 9 (arrows). Fig. 11 Ventral view of hypocone showing swollen flap between apical groove and sulcus, pore in cingular end of apical groove, and tube-like structure located between the two flagellar insertion points (arrowhead). Scale bars: 10 μm long.

Using TEM of thin sections, the central pyrenoid is revealed to be surrounded by a starch cap (Fig. 12). The shape of the nucleus, which lacks a nuclear capsule or envelope chambers, is illustrated in Fig. 12. It surrounds the central pyrenoid anteriorly and laterally. The chloroplasts appear to be engulfed by the nucleus as they radiate to the cell surface.

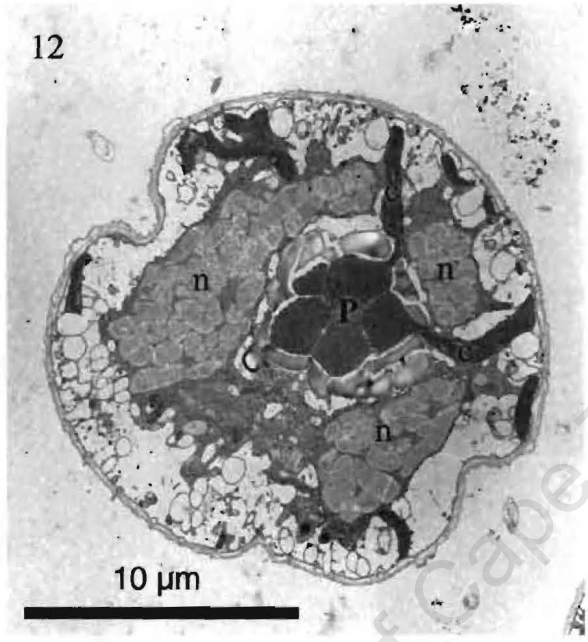

Figure 12. TEM cross section of *Takayama tasmanica* (clonal culture TTDW01), showing central pyrenoid (p), enveloping nucleus (n), and chloroplasts passing through openings in the nucleus on their way to the cell periphery (C). Scale bar 10 µm long.

PIGMENT CONTENT: The photosynthetic and accessory pigments of *T. tasmanica* include chlorophyll *a* and chlorophylls c_2 and c_3. No chlorophyll c_1 was detected. The following carotenoids were identified, quantified as a percentage of chlorophyll *a*: 19'-butanoyloxyfucoxanthin (5.7%), fucoxanthin (75.8%), a trans-neoxanthin-like pigment (1.8%), a 19'-hexanoyloxyfucoxanthin-like pigment (trace), diadinoxanthin (20.9%), diatoxanthin (4.5%), a gyroxanthin –like pigment (11.5%), and gyroxanthin-diester (0.5%).

MOLECULAR DATA: The large subunit ribosomal DNA (LSU rDNA) sequence of *T. tasmanica* diverges approximately 3.79%. from *T. helix* (Aus and RSA), 3.4% from *Gymnodinium cf. pulchellum* from Kawau Is., New Zealand (Genebank Accession No. U92254), and also diverges from other close relatives such as *Karlodinium micrum* and *Karenia umbella* by 11.5% and 14.9%, respectively. A phylogenetic reconstruction of *Takayama, Karenia* and *Karlodinium* (Fig. 13) shows that the genus *Takayama* forms a distinct lineage related to *Karenia* and *Karlodinium*. These genera are, in turn, a clearly defined group within the Gymnodiniales, with *Takayama* positioned closer to *Karlodinium* than *Karenia*.

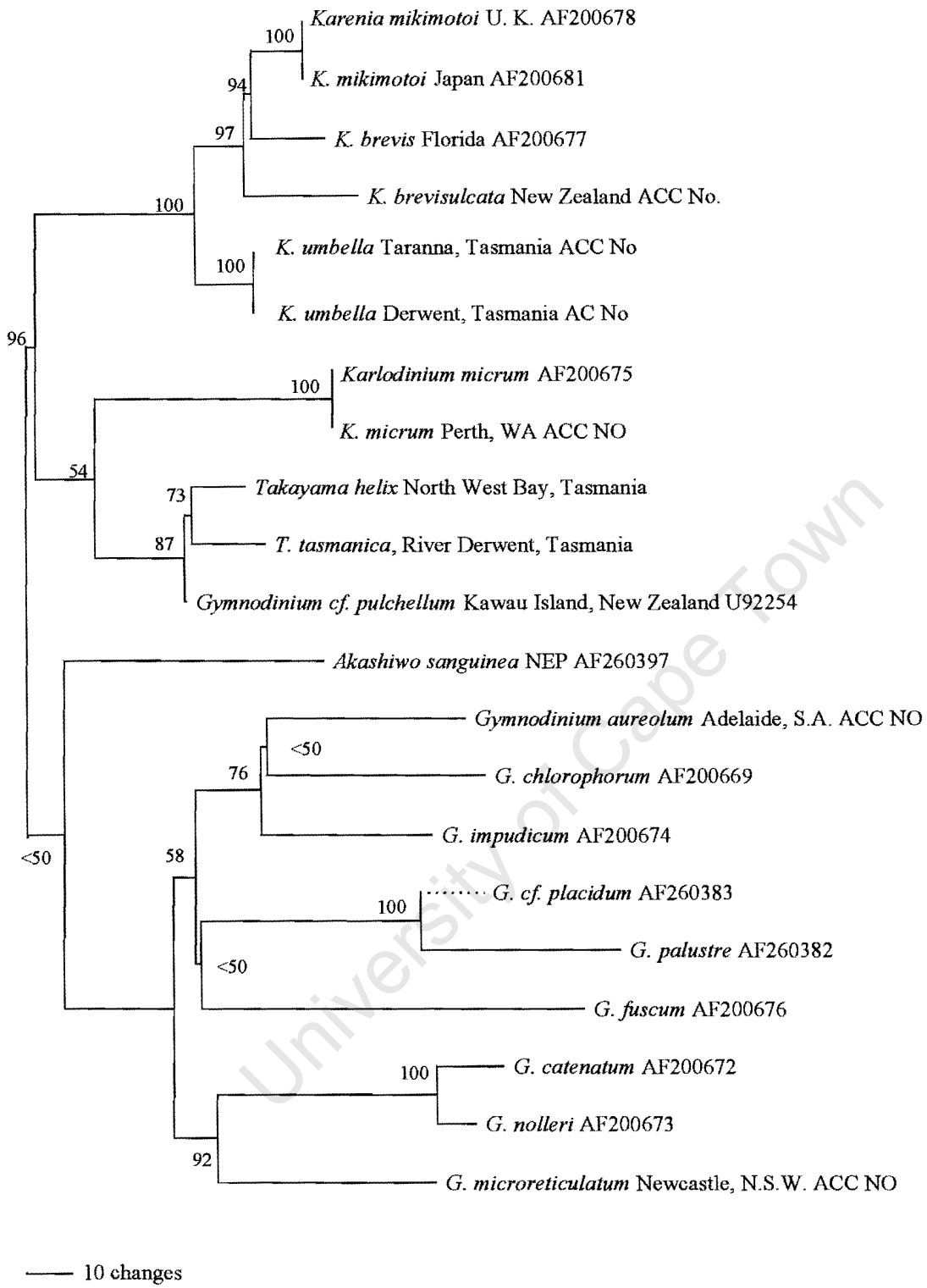

Figure 13. Neighbour-joining tree showing phylogenetic analysis of three species of *Takayama*, compared with *Karenia* and *Karlodinium*, with other gymnodinioid species. Numbers next to branching points indicate bootstrap support (1000 replicates, full heuristic search) for groups.

Takayama helix de Salas, Bolch, Botes et Hallegraeff *sp. nov.*

Figs 14-28, 34, 35

Cellulae rhomboideae ad fere circulares, 17-45 µm longae, 11-31 µm latae, 9-25 µm crassae. Epiconus late conicus ad hemisphaericus. Hypoconus truncatus incisus. Cingulum profunde incisum, latum, per quasi 1/4 longitudinis cellulae totius dislocatum. Sulcus latus sed in regione intercingulari latior quam in hypocono, in hypoconum breviter invasus. Canalis apicalis leniter sigmoideus, e puncto infra sinistram extensionis sulcalis ascendens, apicem cellulae transcendens, et per quasi 1/3-1/2 longitudinis epiconi dorsalis descendens. Partem tubiformem regio intercingularis sulci exhibens. Chloroplasti multi, peripherales, elongati, in zonis spiralibus dispositi, pyrenoides discretas continentes. Nucleus grandis solidusque, plerumque ellipsoideus sed forma locoque varius.

Cells rhomboidal to almost circular in outline, 17 – 45 µm long, 11 – 31 µm wide, 9 – 25 µm thick. Epicone broadly conical to hemispherical. Hypocone truncated and incised. Cingulum deeply excavated and wide, displaced about 25 % of total cell length. Sulcus wide, but narrower in the intercingular region than in the hypocone, extending shortly into the epicone. Apical groove shallowly sigmoidal, extending from below and to the left of the sulcal extension, over the cell apex, to approximately 1/3 to 1/2 of the way down the dorsal epicone. Tube- like structure present in the intercingular region of the sulcus. Chloroplasts numerous, peripheral, elongated and shallow, arranged in spiralling bands and containing individual pyrenoids. Nucleus large and solid, normally ellipsoidal, but with variable shape and position.

HOLOTYPE: Fig. 21, of culture THNWB01, isolated from North West Bay, Tasmania, Australia (Fig. 1). Culture deposited into the University of Tasmania Harmful Algae Culture Collection.

SYNONYMS: *Gymnodinium* sp. 6; Takayama, H. 1998. Morphological and Taxonomical Studies on the Free-living Unarmoured Dinoflagellates Occurring in the Seto Inland Sea and Adjacent Waters. PhD Thesis. University of Tokyo. Plate 6, Figs 8, 9.

ETYMOLOGY: named after the Greek *helix*, after the spiralling arrangement of chloroplasts and surface furrows in the epicone.

DISTRIBUTION: East coast of Tasmania from the North East to the far south, Port Lincoln (S.A. – Fig. 1 a), South Africa (Fig. 1b), and Japan.

DESCRIPTION: *Takayama helix* is a small to medium sized dinoflagellate known from field samples and laboratory cultures. Average cell measurements in comparison with close relatives *T. tasmanica*, *G. pulchellum*, *G. acrotrochum* and *G. cladochroma* are provided in Table 2.

Cells of *T. helix* have a distinctive appearance under the light microscope. The cell outline is elliptical or rhomboidal, with the epicone conical or hemispherical and the hypocone truncated and incised (Figs 14, 15). The cingulum and sulcus are deeply excavated. The sulcus is broad posteriorly but narrow between the two terminal ends of the cingulum, and extends into the epicone as a finger-like protrusion at a variable angle (Figs 14, 16). The apical groove extends from below and to the right of the sulcus, and passes near and to the left of the apex, and extends approximately 1/3 to 1/2 way down the dorsal side (Fig. 15). The groove is sigmoid, shaped like a shallow, open 'S' (Figs 14, 17), but clearly inflected and never straight. Chloroplasts are thin, shallow and elongated, and are arranged in spiralling bands, especially in the epicone (Fig. 15). Numerous light refractive lipid bodies are apparent

(Fig. 18), spread through the cell but more common near the periphery. The nucleus is variable, but usually large and elongated, located in the epicone or almost centrally, being sometimes wider in the left part of the cell (Fig. 19). A spherical pusule (Fig. 20), surrounded by sac-shaped vesicles is present below the sulcal surface on the right central hypocone. Scanning electron microscopy of the apical groove show clearly its sigmoid shape from the ventral side across the apex to the dorsal side (Figs 21-25). Spiralling surface impressions are often visible that match the spiralling chloroplasts (Figs 21, 23, 25). The apical groove almost connects with the cingulum, and the epicone surface between it and the sulcus is swollen (Figs 21, 22, 25). A slit, at times also appearing as a pore, is found in the shallow ventral end of the groove (Figs 21, 25). This feature is also visible in light micrographs of live material (Figs 14, 16). The region of epicone between this pore and the sulcus is swollen (Figs 21, 25).

Transmission electron microscope images provide the best detail of the location and shape of the peripherally located chloroplasts (Fig. 26). Chloroplasts are arranged in bands and located peripherally, with individual pyrenoids (Figs 26, 27). The pusule, damaged due to fixation, is located adjacent to the sulcus (Fig. 28). Cultures of this species form a mucus matrix within which they spend most of their time.

PIGMENT CONTENT: The photosynthetic and accessory pigments of *T. helix* include chlorophyll *a* and chlorophylls c_2 and c_3. No chlorophyll c_1 was detected. The following carotenoids were identified, quantified as a percentage of chlorophyll a: 19'-butanoyloxyfucoxanthin (13.7%), fucoxanthin (109.1%), 9'-cis-neoxanthin (1.3%), 4-keto-19'-hexanoyloxyfucoxanthin (trace), trans-neoxanthin-like (1.5%), a 19'-hexanoyloxyfucoxanthin-like pigment (5.7%), an alloxanthin-like pigment (4.6%), diadinoxanthin (42.8%), and diatoxanthin (28.6%).

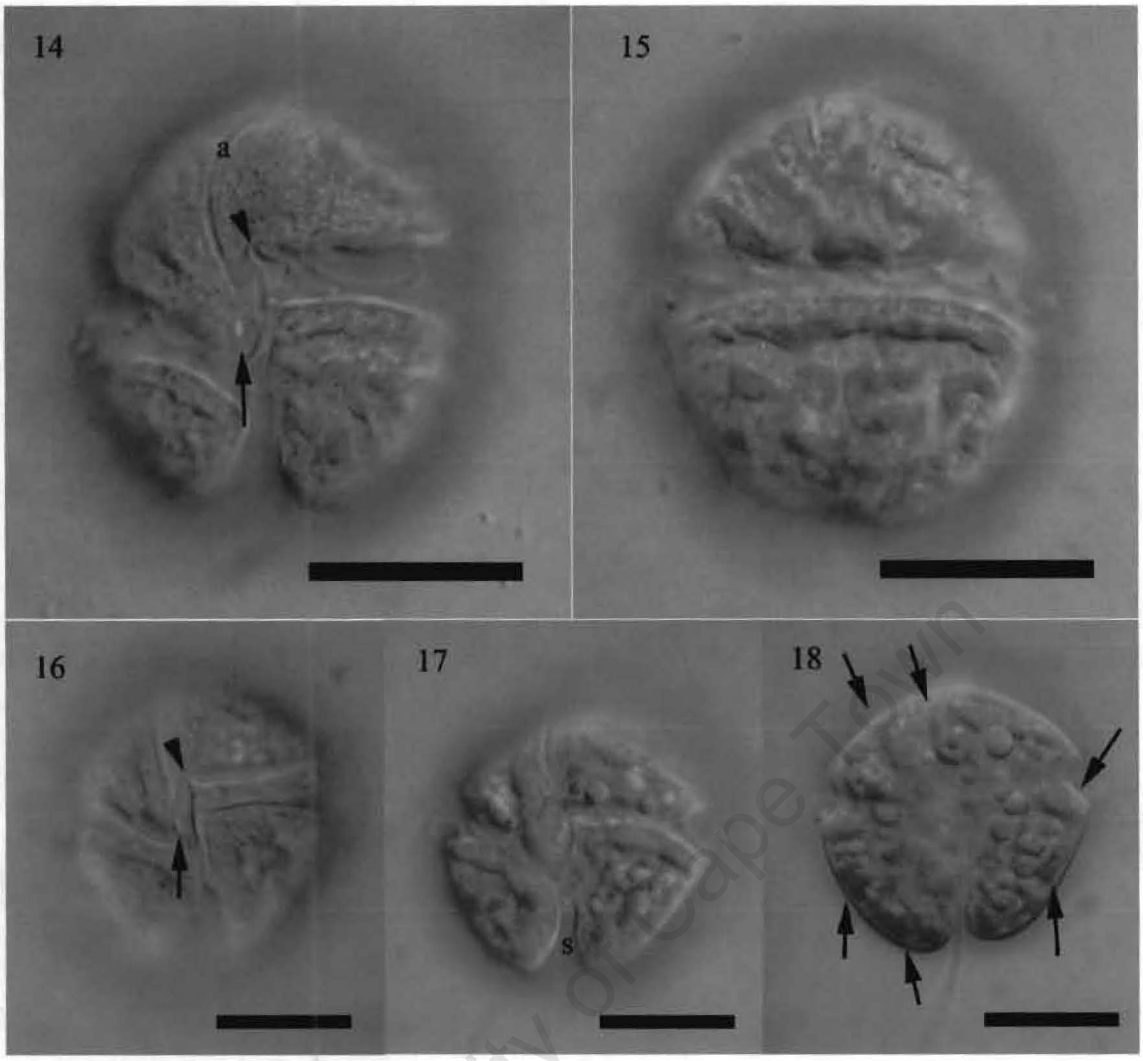

Figure 14-18. Light micrographs of *Takayama helix* (clonal culture TTNWB01). Fig. 14 Ventral view of cell in surface focus showing sulcal intrusion into epicone (arrowhead), apical groove (a), and pore in cingular end of apical groove (arrow). Fig. 15 Dorsal view in surface focus showing spiralling arrangement of chloroplasts that give the species its name, and apical groove extending approximately 1/3 down dorsal surface. Fig. 16 Ventral view of another cell showing pore in cingular end of apical groove (arrow) and narrow sulcus in intercingular region (arrowhead). Fig. 17 Ventral view of same cell in slightly deeper focus showing widening of sulcus (s) below the cingulum and apical groove. Fig. 18 Central focus of same cell showing cell outline, irregularly shaped, elongated chloroplasts (arrows), and lipid globules in cytoplasm. Scale bars: 10 μm.

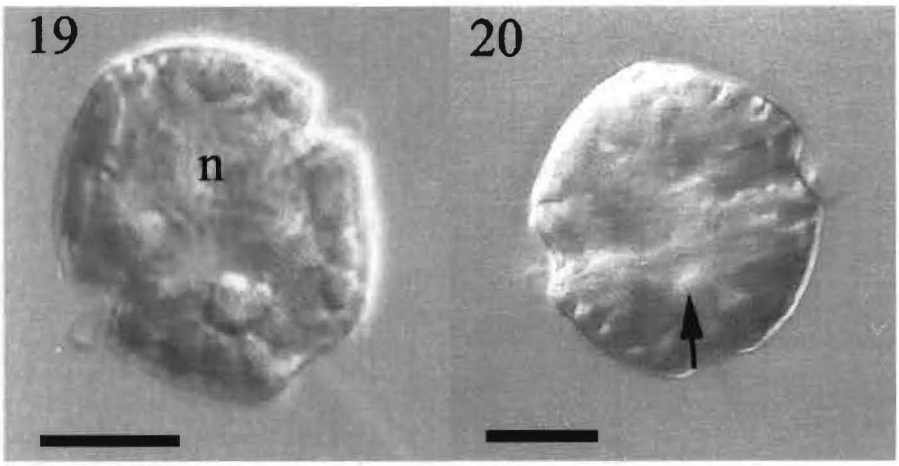

Figure 19-20. Light micrographs of South African T. helix. Fig. 19 Ventral view of cell showing a triangular nucleus (n), positioned across the epicone, but only invading the epicone in the left side of the cell. Fig. 20 Ventral subsurface view of cell showing shape and position of the pusule (arrow). Scale bars 10 μm.

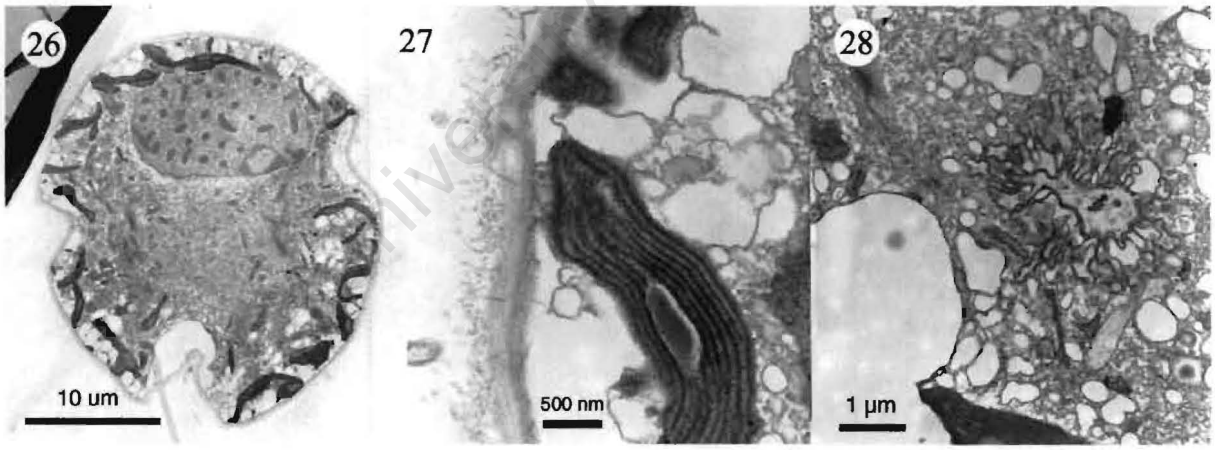

Figure 26-28. Transmission electron micrographs of *Takayama helix* (clonal culture TTNWB01). Fig. 26 Cross section through cell showing ellipsoidal, anteriorly located nucleus (n) with nucleolus, and peripheral chloroplasts. Fig. 27 Chloroplast detail showing individual lenticular pyrenoid. Fig. 28 Detail of pusule adjacent to sulcus.

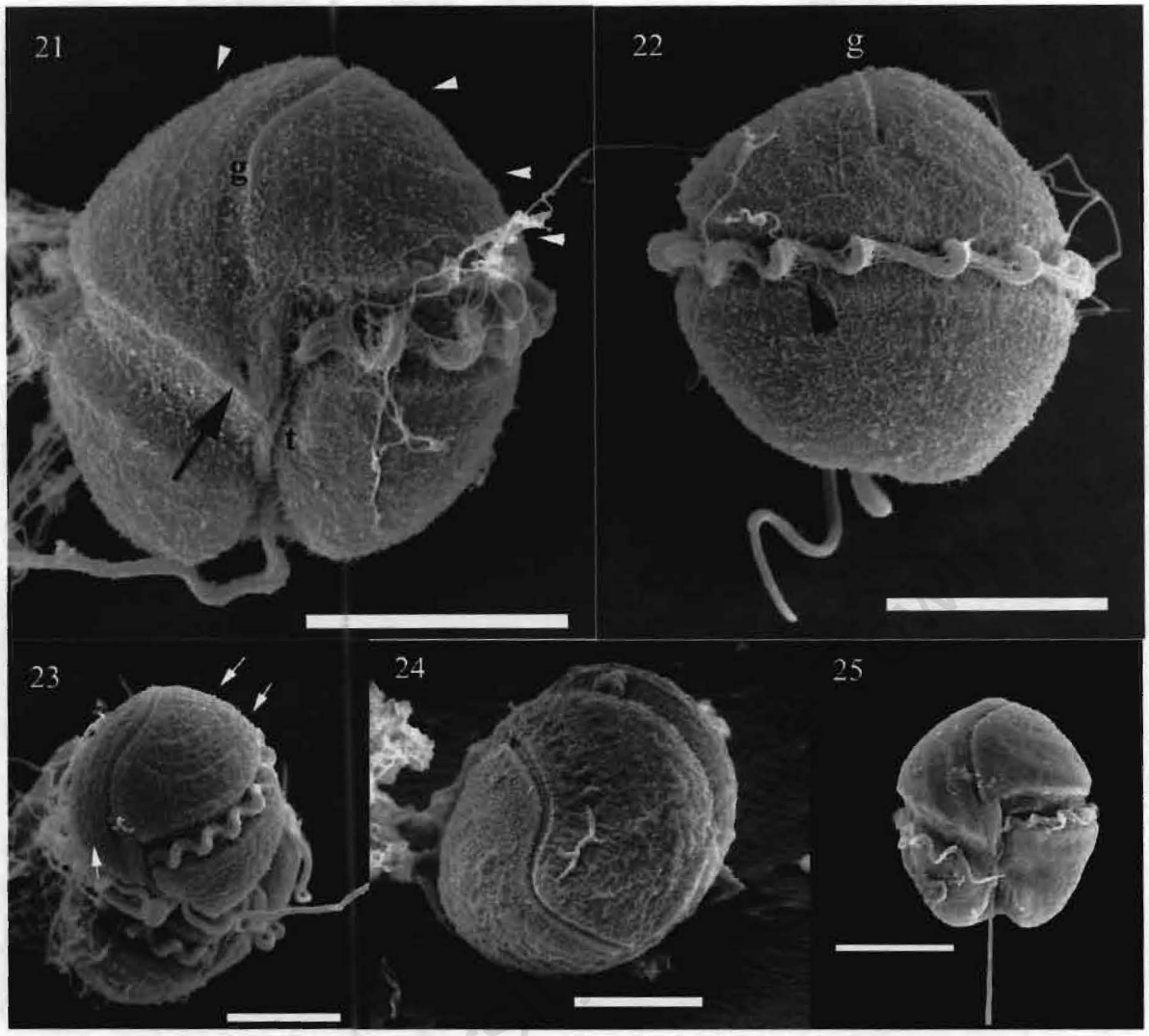

Figure 21 – 25. Scanning electron micrographs of *Takayama helix*. Fig. 21 Ventral view of cell (clonal culture TTNWB01) showing apical groove (g), spiralling surface grooves surrounding it (arrowheads), slit in cingular end of apical groove (arrow), and tube-like structure in sulcus (t). Fig. 22 Dorsal view of cell (clonal culture TTNWB01) showing apical groove (a) extending approximately 1/2 of the way down dorsal epicone, and transverse flagellum (arrowhead). Fig. 23 Apical view of cell (clonal culture TTNWB01) showing shape of apical groove and spiralling bands overlying chloroplast bands (arrows). Fig. 24 Apical view of cell from a field sample from Port Philip Bay (Vic), showing inflected shape of apical groove. Fig. 25 Ventral view of cell from South Africa. Scale bars: 10 μm.

MOLECULAR DATA: LSU rDNA sequences of Tasmanian and South African *T. helix* were identical. Sequences of *T. helix* (Aus and RSA) diverge approximately 3.79%. from *T. tasmanica*, 2.14% from *Gymnodinium cf. pulchellum* from Kawau Is., New Zealand (Genebank Accession No. U92254), and 11.34% and 12.99% from *Karlodinium micrum* and *Karenia umbella*, respectively. The phylogenetic reconstruction (using the LSU rDNA sequences) of *Takayama, Karenia, Karlodinium* and other gymnodinioids displayed in Fig. 13 shows that *T. helix* is closely related to *T. tasmanica*, and forms part of a well defined group within the *Karenia – Karlodinium* generic complex. However, the group formed by *T. helix* and *T. tasmanica* is clearly separated from *Karenia* and *Karlodinium*.

DISCUSSION

The taxonomic affinities of the three sigmoid grooved species described by Larsen (1994, Larsen 1996): *Gymnodinium pulchellum, Gyrodinium acrotrochum* and *Gyrodinium cladochroma* were left unresolved in Daugbjerg *et al.*'s (2000) revision of gymnodinioid dinoflagellates. The other fucoxanthin containing gymnodinioids were designated separate generic status (*Karenia, Karlodinium*); however, determination of the genetic affinities of *G. pulchellum* was not attempted in the absence of ultrastructure and LSU rDNA sequences. From the new data presented here, comprising cell morphology, chloroplast pigment content and LSU rDNA sequences, the creation of a new genus for sigmoid grooved species with fucoxanthin (and its derivatives) as its main carotenoids is justified. Pigment analysis confirms that the genus *Takayama* is closely related to the fucoxanthin-containing genera *Karenia* and *Karlodinium*. This is corroborated by LSU rDNA sequences, which show that sigmoid grooved dinoflagellates, including *Takayama tasmanica, T. helix* (from Australia and South Africa), and a GeneBank sequence (Accession number U92254) referred to as

Gymnodinium cf. pulchellum, from Kawau Island, New Zealand, form a clearly defined clade that clusters close to *Karlodinium* while remaining distinct.

Two species of *Takayama* examined in detail in this study, *T. tasmanica* and *T. helix*, exhibit morphological features that indicate their close taxonomic relationship: a sigmoid or clearly inflected apical groove intermediate between the straight grooved genera (*Karenia*, *Karlodinium*), and the loop shaped species in *Gymnodinium sensu stricto* (Daugbjerg *et al.* 2000). A tube shaped structure which lies along the sulcus in the intercingular region, and is also documented by Steidinger *et al.* (1998), which may be homologous with the putative peduncle of *Karlodinium* (Taylor 1992) or a vetral ridge. A swollen structure occurs between the proximal extreme of the apical groove and the sulcus, and a pore or slit exists in the proximal extreme of the apical groove.

Despite the range of similarities between *T. tasmanica* and *T. helix*, the following differences justify their discrimination as separate species: *T. tasmanica* has a clear 'S' shaped apical groove, like that previously described in *Gymnodinium pulchellum*, *Gyrodinium acrotrochum* and *Gyrodinium cladochroma* (Onoue *et al.* 1985, Takayama 1985, Larsen 1994, Larsen 1996, Steidinger *et al.* 1998a), while *T. helix* has a shallowly sigmoid groove, unlike any previously described species. However, apical grooves like the one present in *T. helix* have been illustrated before from samples in Japan (Takayama 1998, Plate 6, Figs 8, 9). *T. tasmanica* has a central pyrenoid surrounded by starch, whereas *T. helix* has individual pyrenoids inside peripherally located chloroplasts. The chloroplasts of *T. tasmanica* radiate out from the central pyrenoid and penetrate through the nucleus, which occupies much of the cell and surrounds the pyrenoid laterally and anteriorly. The nucleus of *T. helix* is also large, ellipsoidal in shape in some cells, longitudinally elongated and displaced towards the left side

of the cell in others, but always solid rather than cup-shaped. LSU rDNA sequences of *T. tasmanica* and *T. helix* differ by a larger amount (3.79%) to widely accepted separate species within other genera, such as *Karenia brevis – K. mikimotoi* (2.81%), and *Gymnodinium catenatum – G. nolleri* (2.46%). Additionally, *T. tasmanica* produces gyroxanthin -diester, a pigment typical of *Karenia* and *Karlodinium* species, which is not produced by either Tasmanian or South African *T. helix*.

Takayama tasmanica is morphologically similar to *Gymnodinium pulchellum* (Larsen 1994), *Gyrodinium acrotrochum* and *G. cladochroma* (Larsen 1996), three Port Phillip Bay (Victoria, Australia) species illustrated for comparison in Figs 29 – 31. The sulcal intrusion into the epicone of *T. tasmanica* (Figs 2, 7, 10) is similar to *G. pulchellum* and *G. cladochroma* (Figs 29, 31), however, both these species have a solid nucleus in the left side of the cell, unlike the centrally located, cup-shaped nucleus of *T. tasmanica* (Figs 4 – 6, 12). Like *T. tasmanica*, *G. acrotrochum* (Fig. 30) has a nucleus that occupies most of the epicone (Larsen 1994), but the chloroplasts are disc-shaped and possess individual pyrenoids, and there is no sulcal intrusion into the epicone like that of *T. tasmanica*.

Previously published accounts of sigmoid grooved species include Takayama's (Takayama 1985) '*Gymnodinium* sp. 1', which appears to have a sulcal intrusion, and as such is probably either *G. pulchellum* or *G. cladochroma*, and Onoue's (Onoue *et al.* 1985, Fig. 1) '*Gymnodinium* type-'84 K', which is not described in sufficient detail to assess its precise identity. However, Fukuyo's (Fukuyo *et al.* 1990) description of this organism does not include a sulcal intrusion and illustrates a centrally located nucleus, which makes it closest to *G. acrotrochum*. Carrada *et al.* (1991) illustrate a sigmoid grooved organism with a short sulcal intrusion, likely to be either *G. pulchellum* or *G. cladochroma*. Since many of the

features that identify species in the genus relate to nucleus and chloroplast details, scanning electron micrographs alone are not sufficient to distinguish between species of *Takayama*. For example Steidinger *et al.* (1998a) report of fish kills in Florida (U.S.A) caused by *G. pulchellum* could instead refer to *G. cladochroma*, as both species have a left-sided nucleus, which is reported (but not illustrated) in their paper. Steidinger's (Steidinger *et al.* 1998a) SEMs show cells that have a distinct inflection of the sulcus at the point of origin of the longitudinal flagellum (p. 434, Figs 2, 6), and a truncated sulcal intrusion (Figs 5, 6), characters which are represented in *G. cladochroma* (Larsen 1996 p. 348, Fig. 37), but not *G. pulchellum* (Larsen 1994 p. 32, Fig. 58). A common feature of these illustrations is the presence of a small, tight apical groove that occupies less of the epicone surface than *T. tasmanica*. The presence of a tube-like structure lying along the intercingular region of the sulcus has also been mentioned by Steidinger *et al.* (1998a) for US material. Such a structure is present both in *T. tasmanica* and *T. helix* (Figs 8, 21), and may be a feature of all species in the genus. While easily visible by SEM, its recognition can be difficult under a light microscope, and as such we prefer not to include this feature in the generic diagnosis. The presence of a ventral pore above and to the left of the sulcal intrusion in *T. tasmanica* (Figs. 9, 10), though difficult to preserve for electron microscopy, has also been shown by Carrada *et al.* (1991). This character has not been seen in *T. helix*, but appears to be easily obscured or overgrown, and *T. helix* produces copious amounts of mucus. As its presence is difficult to verify, and almost impossible to see under the light microscope, we have not included it in the species or genus diagnoses. However, it should be noted that its position is almost identical to the ventral pore that is a diagnostic character of *Karlodinium micrum* (Daugbjerg *et al.* 2000). Features such as the tube- like structure present in *T. tasmanica*, *T. helix*, and documented by Steidinger *et al.* (1998a), and the *Karlodinium*-like ventral pore (Figs 9, 10), support the

findings of the sequencing work (Fig. 13) that show *Takayama* to be the closest genus to *Karlodinium*.

In conclusion, the exact identity of the species described by Larsen (1994, Larsen 1996), *G. cladochroma* and *G. pulchellum*, will remain unresolved until new material or cultures of all morphotypes from the type locality (Port Phillip Bay) are available. Re-description of these species is essential, as the level of detail present in the latin (and english) diagnoses is insufficient. For example, features essential for the discrimination between species in the genus, such as sulcal intrusions into the epicone, and relative shape, size and position of chloroplasts and pyrenoids are excluded from the diagnosis, and only mentioned in the discussion. The only major difference between *G. cladochroma* and *G. pulchellum* is the presence of branched chloroplasts in the former species, which are described simply as 'irregular' in the latter. This character can be misleading, since cells placed under a microscope can change the shape of their chloroplasts, which tend to shrink and assume a globular or disc-shaped form.

Morphological examination and sequencing of the LSU rDNA from cultures isolated from Port Phillip Bay should provide a clear understanding of the genetic affinities of all formally described species with sigmoid apical grooves.

The close affinity between Larsen's (Larsen 1994, Larsen 1996) species and *T. helix* and *T. tasmanica* justify the transfer of the former to the genus *Takayama*:

Takayama pulchella (Larsen) de Salas, Bolch et Hallegraeff *comb. nov.*, (Basionym: *Gymnodinium pulchellum* (Larsen 1994 Fig 58, page 32))

Takayama acrotrocha (Larsen) de Salas, Bolch et Hallegraeff *comb. nov.*,

(Basionym: *Gyrodinium acrotrochum* (Larsen 1996 Fig. 35, page 342))

Takayama cladochroma (Larsen) de Salas, Bolch et Hallegraeff *comb. nov.*

(Basionym: *Gyrodinium cladochroma* (Larsen 1996 Fig. 37, page 343))

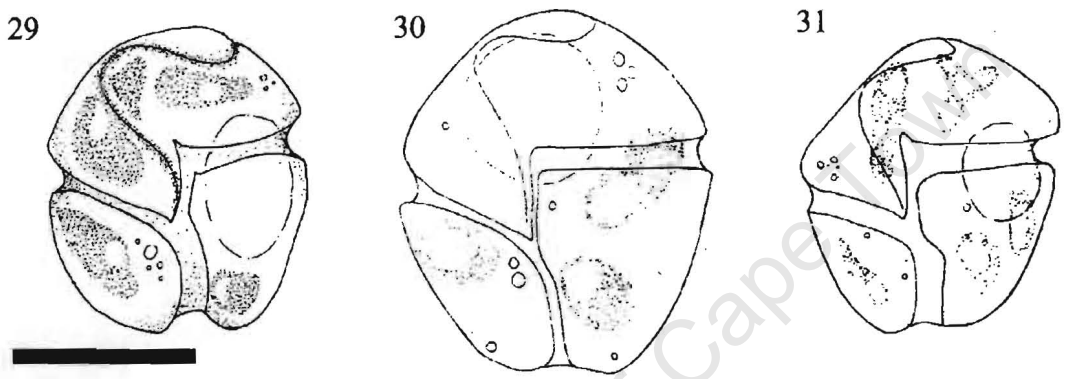

Figure 29-31. Previously described sigmoid-grooved gymnodinioid species (after Larsen 1994, Larsen1996). Fig. 29. Holotype of *Gymnodinium pulchellum*. Note sharp sulcal intrusion into epicone, chloroplasts with individual pyrenoids and left sided nucleus. Fig. 30. Holotype of *Gyrodinium acrotrochum*. Note lack of sulcal intrusion, anterior nucleus, and disc-shaped chloroplasts with individual pyrenoids. Fig. 31. Holotype of *Gyrodinium cladochroma*. Note truncated sulcal intrusion into epicone, peripheral chloroplasts with individual pyrenoids, and left sided nucleus. Scale bar 10 µm.

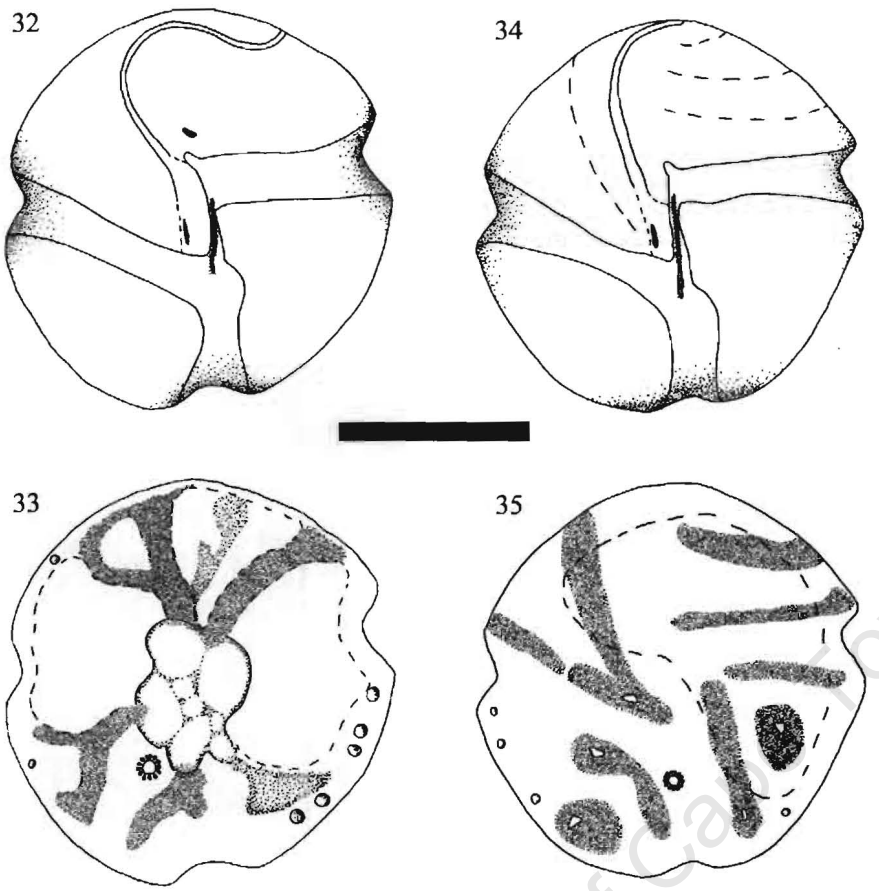

Figure 32-35. Schematic representations of *Takayama*. Fig. 32. Surface view of *T. tasmanica*. Fig. 33. Arrangement of nucleus, pyrenoid and chloroplasts in *T. tasmanica*. Fig. 34. Surface view of *T. helix*. Fig. 35. Chloroplast arrangement and nucleus position in *T. helix*. Scale bar 10 μm.

SECTION 2

Distribution of bloom-forming dinoflagellate species in False Bay and Walker Bay

CHAPTER 6

BLOOM FORMING DINOFLAGELLATE SPECIES IN FALSE BAY AND WALKER BAY, SOUTH AFRICA.

ABSTRACT

The southern Benguela upwelling system is regularly subjected to harmful algal blooms that often affect inshore marine ecosystems and coastal marine organisms. Although not all are toxic, most are perceived as noxious owing to secondary effects following bloom decay. A monitoring programme was therefore initiated in 1989 and was extended, for the period from 1997 – 2000, to include more sampling sites and transect sampling. Ten of the 26 dinoflagellate species that were observed in False Bay and Walker Bay during this time are unarmoured and sixteen are armoured. Seven are bloom forming species whereas nine species have never been recorded in the area before. Eight of the 26 species have previously been recorded as potentially harmful or toxic. The daily abundance and magnitude of bloom events from 1992 - 2000 were highest during 1995-96. The timing of the dinoflagellate blooms, from mid October to mid July, coincided well with the wind-induced upwelling season and even though the SST in False Bay was more often 15 °C, the averaged dinoflagellate cell concentration was highest between 17 – 20 °C. It was further found that the species composition of the dinoflagellate assemblages within False Bay and Walker Bay were consistent for any given upwelling season irrespective of the actual cell count at the various sampling sites. Sampling of a transect on the other hand provided information on the spatial variation in the dinoflagellate species composition within the bay which is determined by the vertical stability of the water column and the availability of nutrients and light. Information such as generated in this study is in turn essential for managing marine resources and ecosystems, contributing to policy decisions, protect public health and support aquaculture development.

INTRODUCTION

Water discolorations, referred to as 'red tides', are a common feature of the southern Benguela upwelling system and are more often caused by dinoflagllates which occur in response to seasonal upwelling (Brown et al. 1979, Horstman 1981, Horstman *et al.* 1991, Pitcher & Calder 2000). Although not all are toxic, most are perceived as noxious owing to secondary effects following bloom decay (Brown *et al.* 1979, Grindley & Taylor 1964, Horstman 1981). These blooms often affect the ecological balance of inshore marine ecosystems, and coastal marine organisms. They can further have a major impact on human health if contaminated shellfish is consumed. After massive abalone mortalities due to the toxic species *Karenia cristata* (Botes *et al.*, 2003 b) that bloomed in False Bay and Walker Bay in 1988 and 1989 (Horstman *et al.* 1991) and to a lesser extend in 1995-96 (Pitcher & Matthews 1996), the awareness of the impacts of HAB's on the abalone industry was greatly increased. A monitoring programme was therefore required and in 1989, a harmful algal bloom (HAB) monitoring programme was implemented in the southern Benguela to provide a warning and information system to the public and the aquaculture and fishing industries of South Africa (Pitcher & Calder 2000). The monitoring programme has remained simple and included the daily collection of water samples at Elands Bay, situated approximately 180 km north of Cape Point on the West Coast, and Gordon's Bay, situated approximately 45 km east of Cape Point on the South Coast.

Few phytoplankton studies, mostly describing red tide events (Grindley & Taylor 1964, Grindley & Taylor 1970, Brown *et al.* 1979, Horstman 1981, Horstman *et al.* 1991, Pitcher & Matthews 1996, Pitcher & Calder 2000) have taken place between Cape Point and Danger Point (Figure 1). Daily sampling at Gordon's Bay was therefore, for the period 1997 – 2000, extended to include Kalk Bay. It was further extended to include Hermanus and Danger Point where abalone mariculture facilities are based. An 18 nautical mile transect from Gordon's Bay (Fig. 1), consisting of 12 stations, was sampled monthly from December 1996 – December 1999.

The aim of this paper is therefore to report on the dinoflagellate species composition within False Bay and Walker Bay, the interannual and seasonal variation of dinoflagellates in Gordon's Bay and their longshore variation within the two bays.

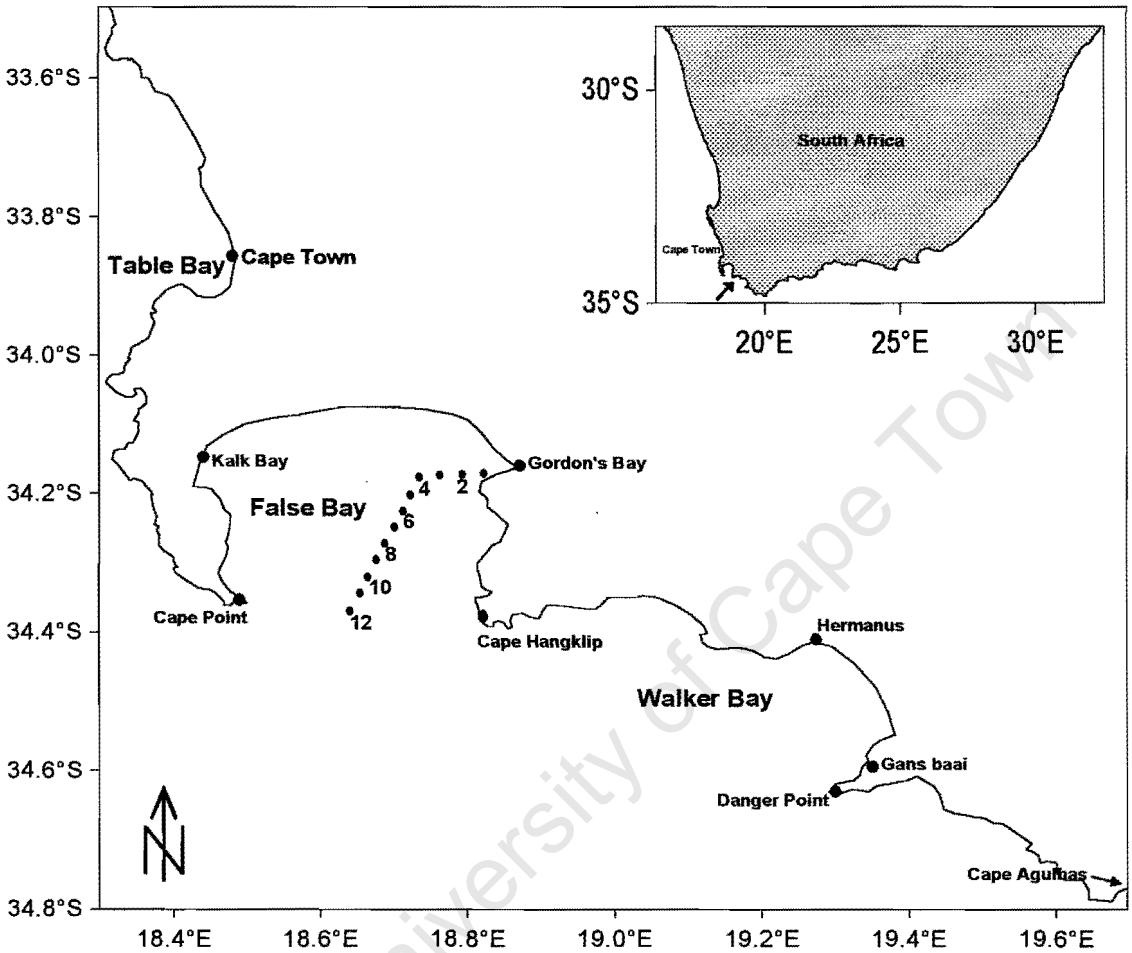

Figure 1. The study area, False Bay and Walker Bay, is situated between Cape Point and Danger Point. A transect with 12 stations from Gordon's Bay harbour extends into False Bay, covering a distance of 18 nautical miles.

MATERIALS AND METHODS

Shore-based sampling

Water samples were collected daily at Gordon's Bay from 1992 to 2000, and at Kalk Bay, Hermanus and Danger Point from 1997 to 1999 (Fig. 1).

Transect sampling

An 18 nautical mile transect from Gordon's Bay (Fig. 1), consisting of 12 stations was sampled monthly from December 1996 – December 1999. Two dinoflagellate blooms were sampled during this time. On 21 December 1997, 6 of the twelve stations were sampled whereas on 14 December 1998, 4 of the 12 stations were sampled. A Chelsea Instruments Aquapack was used to profile the water column, at each station, for temperature and *in situ* fluorescence. Samples for nutrients and phytoplankton analysis were collected at every even numbered station by means of 1*l* National Institute for Oceanography (N.I.O.) bottles at depths 0, 5, 10 and 20m. Phytoplankton samples were preserved with 5% formaldehyde (buffered with $CaCO_3$ AR grade, pH ≥ 7) and enumerated by the Ütermohl method (Hasle 1978), using an inverted microscope. Nutrients samples were analysed, as described by Mostert (1983), using an auto-analyser. Sea surface temperature was measured daily at Gordon's Bay and hourly wind data were obtained from Cape Point. NOAA AVHRR satellite images were obtained one day prior to the two bloom events that was sampled on 21 December 1997 and 14 December 1998.

RESULTS

Dinoflagellate species composition

Of the 26 dinoflagellate species (Table 1) encountered during this study, 10 were unarmoured (†) and 16 were armoured (‡), while 7 are potentially harmful or toxic (* Botes *et al.* in 2003 a, Cockraft *et al.* 2000, Grindley & Taylor 1964, Horstman *et al.* 1991, Matthews & Pitcher 1996, Pitcher *et al.* 2001).

Transect and shore based sampling

A time series of daily dinoflagellate abundance and sea surface temperature (STT) over the 8 year period, 1992 – 2000, provides information on the daily dinoflagellate abundance and SST at Gordon's Bay (Fig. 2). Each year SST was highest during mid summer (as high as 23 °C) and

lowest during mid winter (as low as 10°C). The averaged cell concentration (Fig. 3), which is indicative of the frequency and magnitude of bloom events (Fig. 2), was highest during 1995-96 whereas it was lowest during 1997 – 98.

Over the 8 year period, the bloom forming species *Karenia cristata, Akashiwo sanguinea, Prorocentrum rostratum, Prorocentrum triestinu*m and *Scrippsiella trochoidea* formed major components of the dinoflagellate assemblages in False Bay and Walker Bay whereas *Karenia bicuneiformis* was only observed in these two bays since 1996 (Fig. 4). Most of the years were dominated by unarmoured bloom forming species except in 1994 –5 when *K. cristata* and *P. rostratum* were the dominant within False Bay. It is noteworthy that there was an increase in the average cell concentration of *K. cristata* and *A. sanguinea* during 1994-95, while a decrease in the average cell concentration of the *P. rostratum, P. triestinum, S. trochoidea* and *Dinophysis acuminata*. Although *P. rostratum* was the dominant species during 1997 – 98, the average cell concentration of all species decreased dramatically.

Table 1. Dinoflagellate species encountered in False Bay (1992-2000) and Walker Bay (1997-2000).

Dinoflagellate species
Alexandrium catenella (Whedon & Kofoid) Balech * ‡
Akashiwo sanguinea (Hirasaka) G. Hansen & Moestrup * †
Ceratium furca (Ehrenberg) Claparede & Lachmann * ‡
Ceratium lineatum (Ehrenberg) Cleve ‡
Dinophysis acuminata (Claparede & Lachmann) * ‡
Dinophysis fortii Pavillard * ‡
Gonyaulax polygramma Stein * ‡
Gymnodinium aureolum (Hulburt) G. Hansen †
Gyrodinium spirale (Bergh) Kofoid & Swezy †
Heterocapsa orientalis Iwataki, Botes, Sawaguchi, Sekiguchi & Fukuyo (in press) ‡
Karenia bicuneiformis Botes, Sym & Pitcher (2003 b) †
Karenia cristata Botes, Sym & Pitcher (2003 b) * †
Lepidodinium viride Watanabe, Suda, Inouye, Sawaguchi & Chihara †
Noctiluca scintillans (Macartney) Kofoid & Swezy †
Protoperidinium depressum (Bailey) Balech ‡
Protoperidinium pentagonum (Gran) Balech ‡
Protoperidinium steinii (Jorgensen) Balech ‡
Polykrikos schwartzii Butschli †
Prorocentrum micans Ehrenberg * ‡
Prorocentrum rostratum Stein ‡
Prorocentrum triestinum Schiller ‡
Scrippsiella trochoidea (Stein) Loeblich III ‡
Takayama helix de Salas, Bolch, Botes & Hallegraeff (2003) †
Zygabikodinium lenticulatum (Mangin) Loeblich & Loeblich ‡
Gymnodinioid sp.1 †
Gymnodinioid sp.2 †

* Potentially harmful or toxic

† unarmoured

‡ armoured

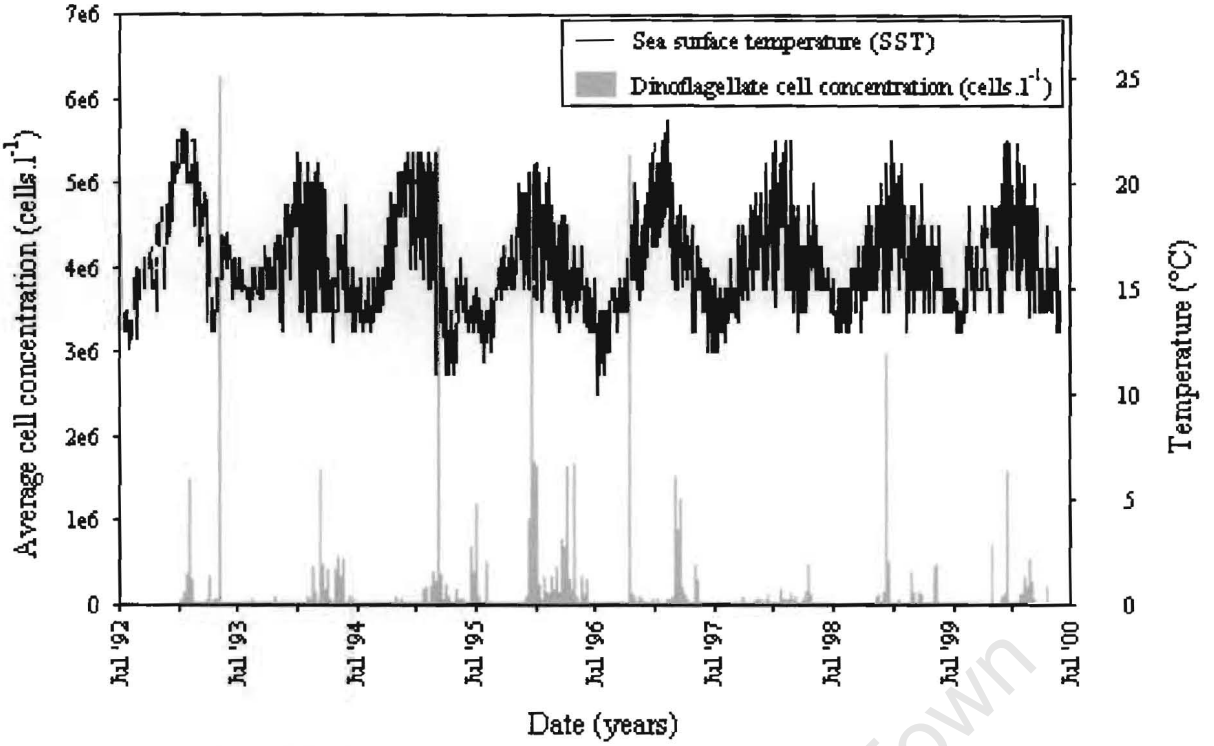

Figure 2. A daily time series of dinoflagellate abundance and sea surface temperature (SST) at Gordon's Bay (1 July1992 – 1 July 2000).

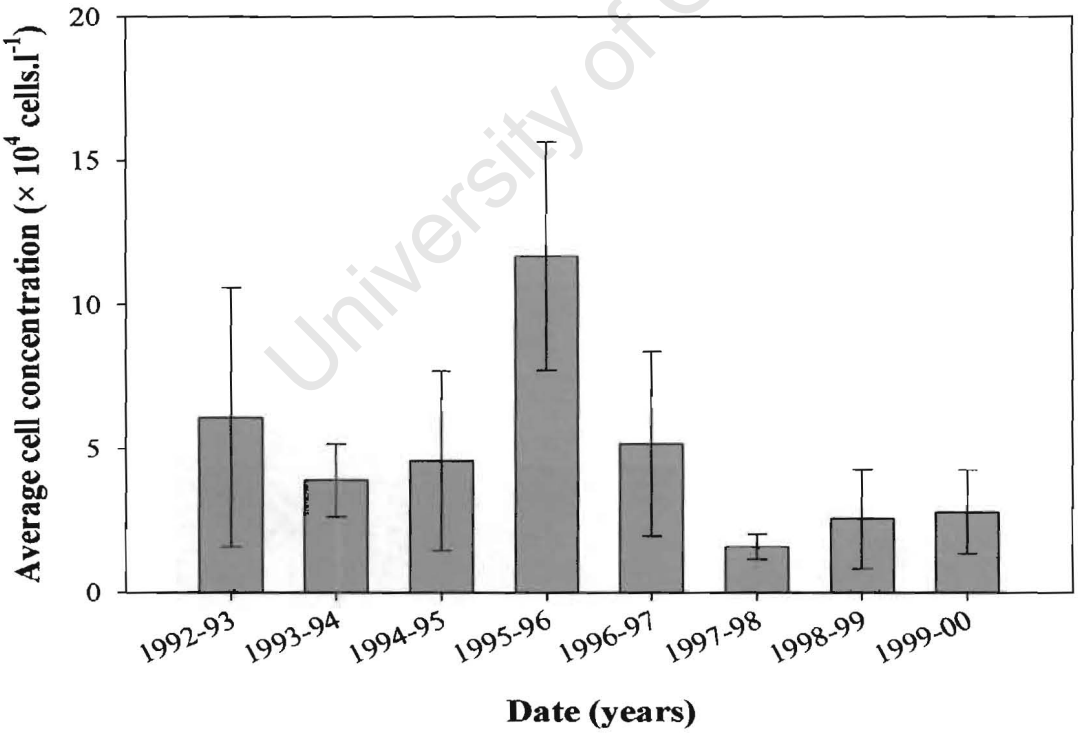

Figure 3. Average yearly dinoflagellate cell concentration at Gordon's Bay (1992 – 2000), whiskers = 95% Confidence levels.

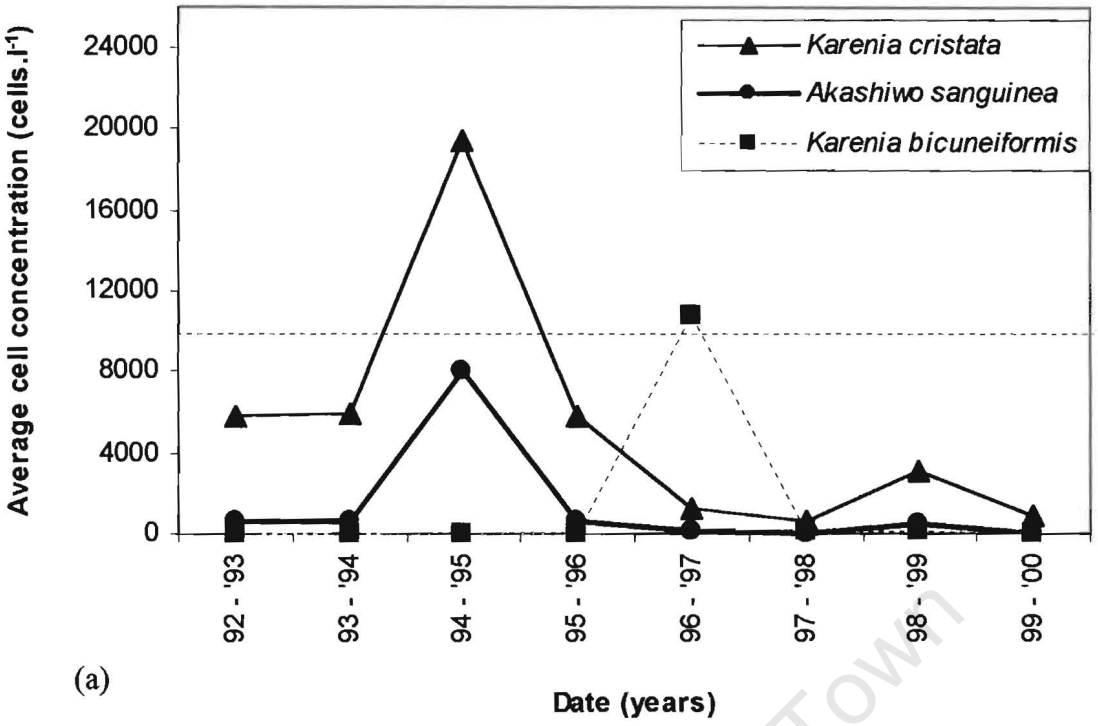

(a)

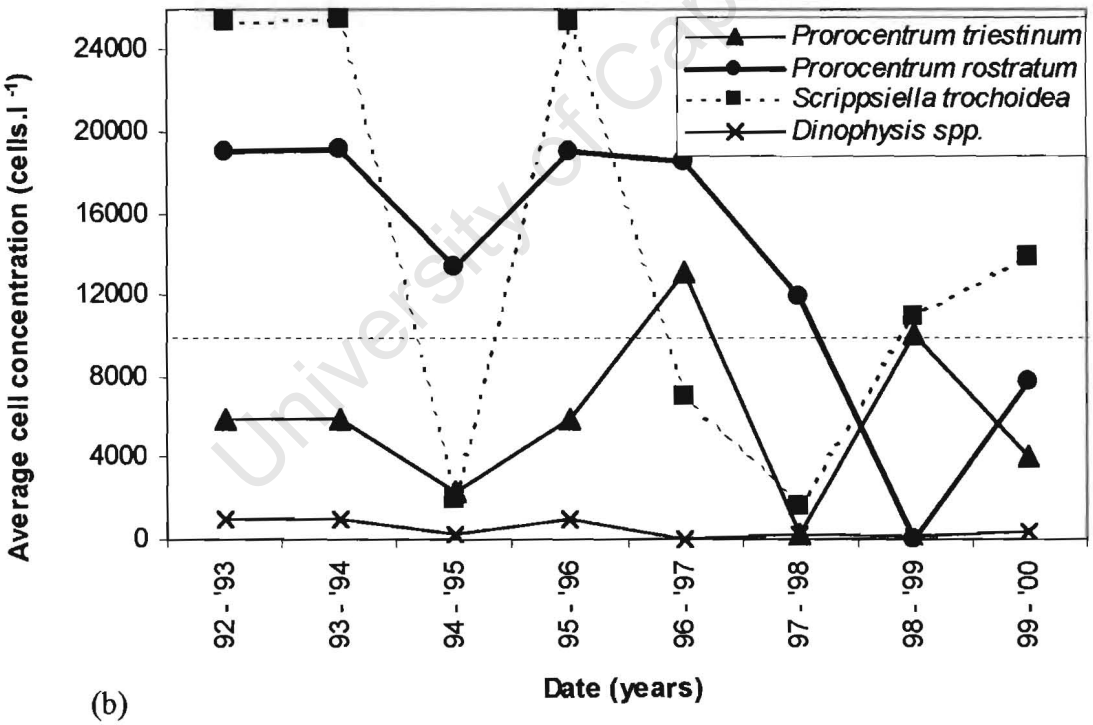

(b)

Figure 4. Yearly (Jun – July) averaged cell concentrations of (a) unarmoured and (b) armoured dinoflagellate species in False Bay. Species above the dashed line were considered dominant.

The time series of the averaged dinoflagellate abundance and sea surface temperarture (SST) (from 1992 – 2000) provides information on the seasonal trends of dinoflaglellates and SST at Gordon's Bay (Fig. 5). Dinoflagellate bloom events did not coincide well with the SST trend which reached a maximum over January - February. Instead, the events coincide well with wind-induced upwelling season (Fig. 7). Dinoflagellates were essentially absent from mid July to mid October (Figs 5, 6) when deep mixing takes place, resulting in an isothermal water column (Fig. 7 f). From mid October onwards the water column warmed inshore and became weakly stratified (Fig. 7 a) and was accompanied by an increase in bloom events. In December, a weak thermocline was established at ~ 40m (Fig. 7 b), while in February there was an uptilt of isotherms due to upwelling with thermocline established at ~ 20m (Fig. 7 c), whereas in April the thermocline was uplifted ~10m (Fig. 7 d). The average dinoflagellate cell concentration (Fig. 6) which is indicative of the frequency and magnitude of bloom events (Fig. 5) was highest during this time (December to May). In June deep mixing (Fig. 7 e) resulted in an upper mixed layer of 40 metres. A sharp decrease in bloom events (Fig. 5) and averaged dinoflagellate cell concentration (Fig. 6) was evident during time but with blooms events still persisting into July. It was found that, even though the SST in False Bay was more often 15 °C, the averaged dinoflagellate cell concentration was highest between 17 – 20 °C (Fig. 8).

It was clear, from figures 9 and 10, that although the average cell concentration at each of the four collection sites (Gordon's Bay, Kalk Bay, Hermanus and Danger Point) within False Bay and Walker Bay varied, the species composition for any given upwelling season was consistent (at all 4 collection sites). During July 1997 – June 1998, the average dinoflagellate cell concentration in False Bay was less at Gordon's Bay, whereas in Walker Bay it was less at Danger Point. During July 1998 – June 1999, the averaged dinoflagellate cell concentration in False bay was less at Kalk Bay, whereas in Walker it was once again less at Danger Point.

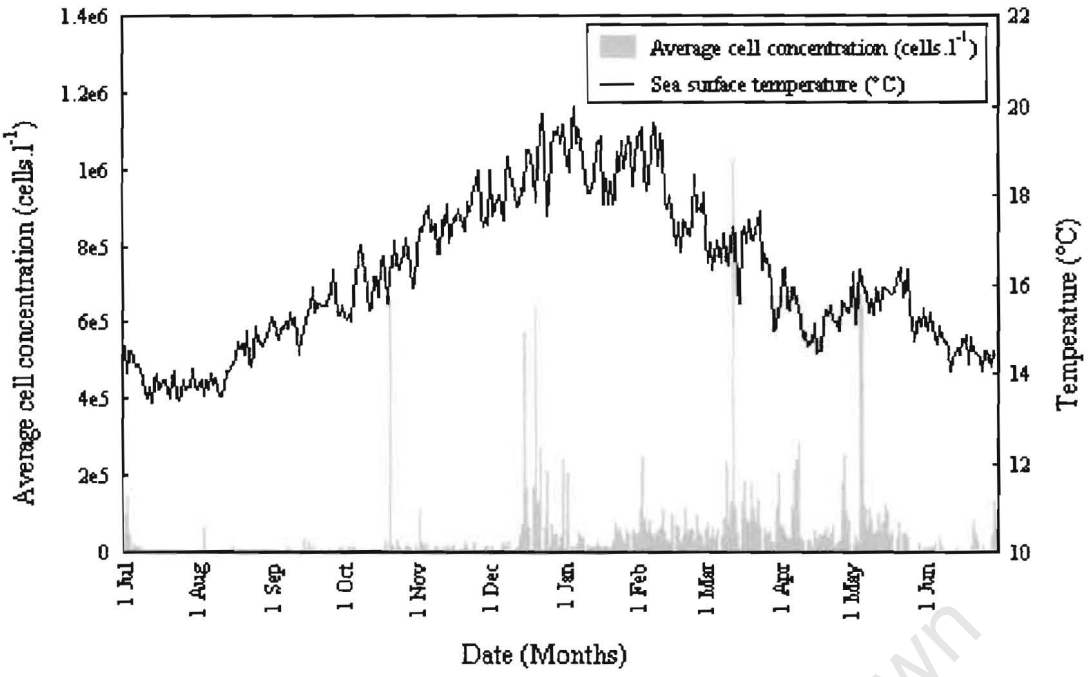

Figure 5. Seasonal variation as depicted by the daily average dinoflagellate cell concentration and sea surface temperature (SST) at Gordon's Bay for the period 1992 – 2000.

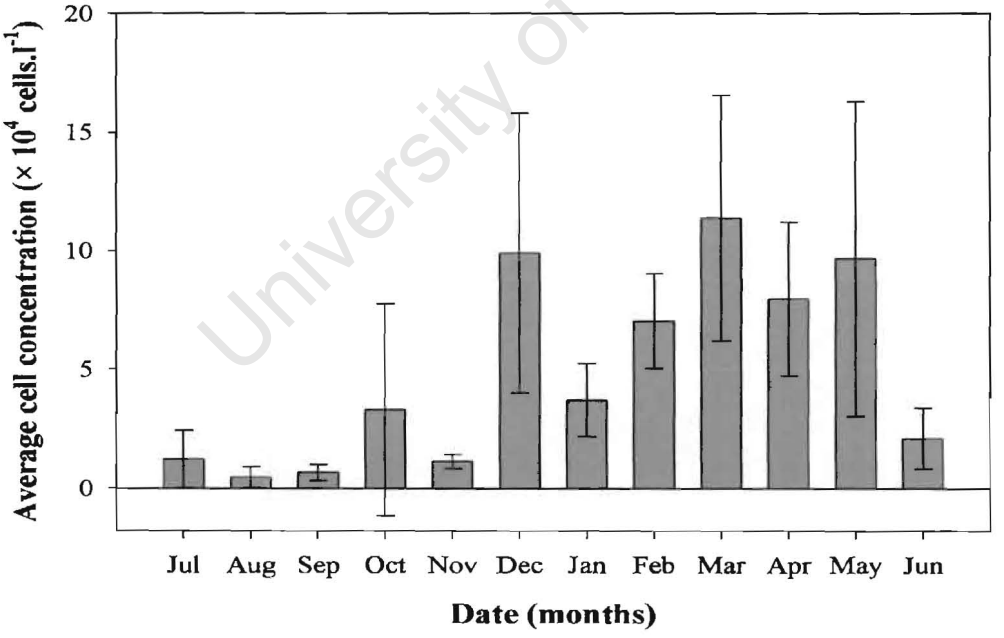

Figure 6. Monthly averaged dinoflagellate cell concentrations at Gordon's Bay for the period 1992 – 2000, whiskers = 95% confidence levels.

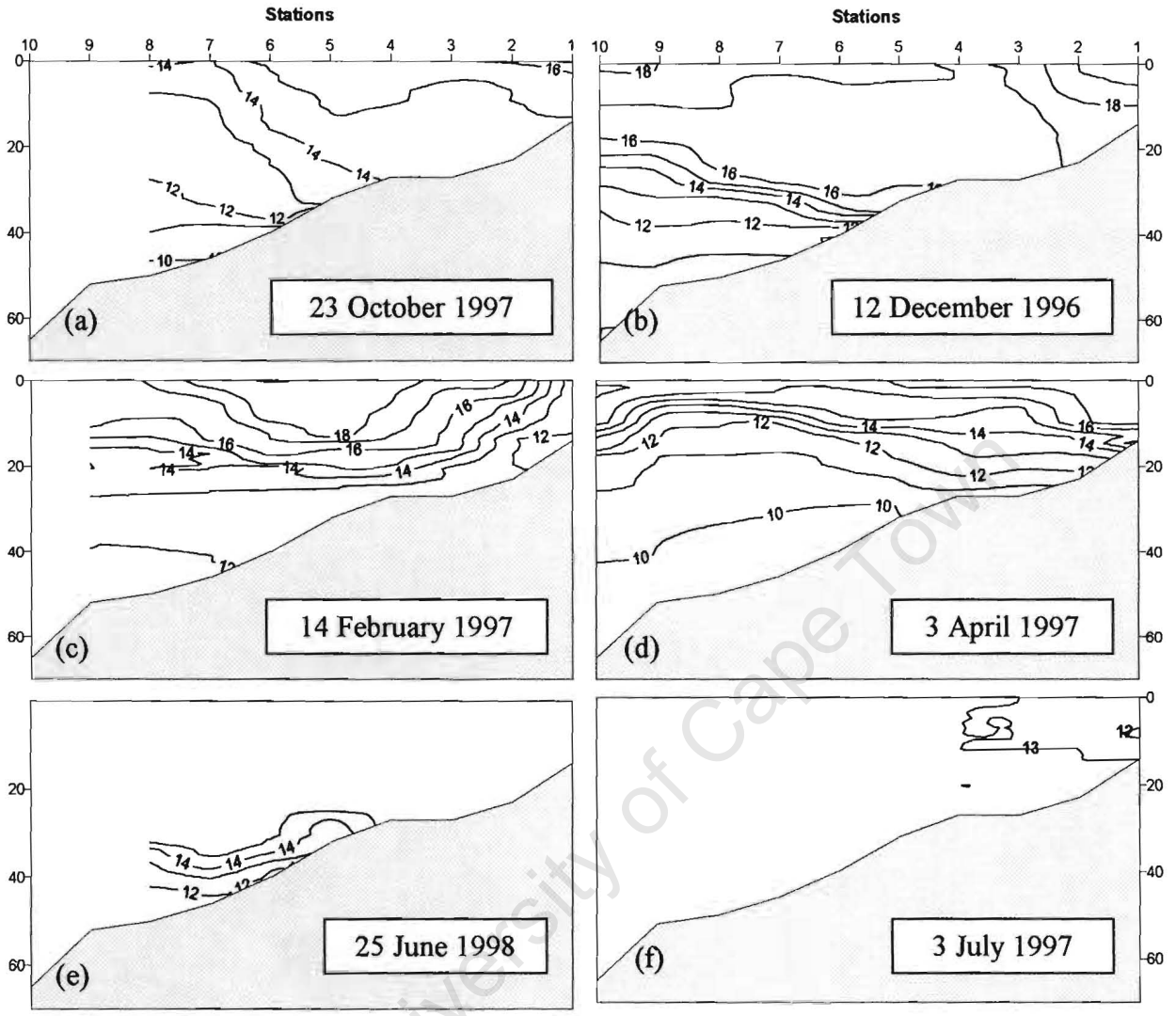

Figure 7. Vertical cross sections of temperature, indicative of upwelling, along the transect which is at Gordon's Bay.

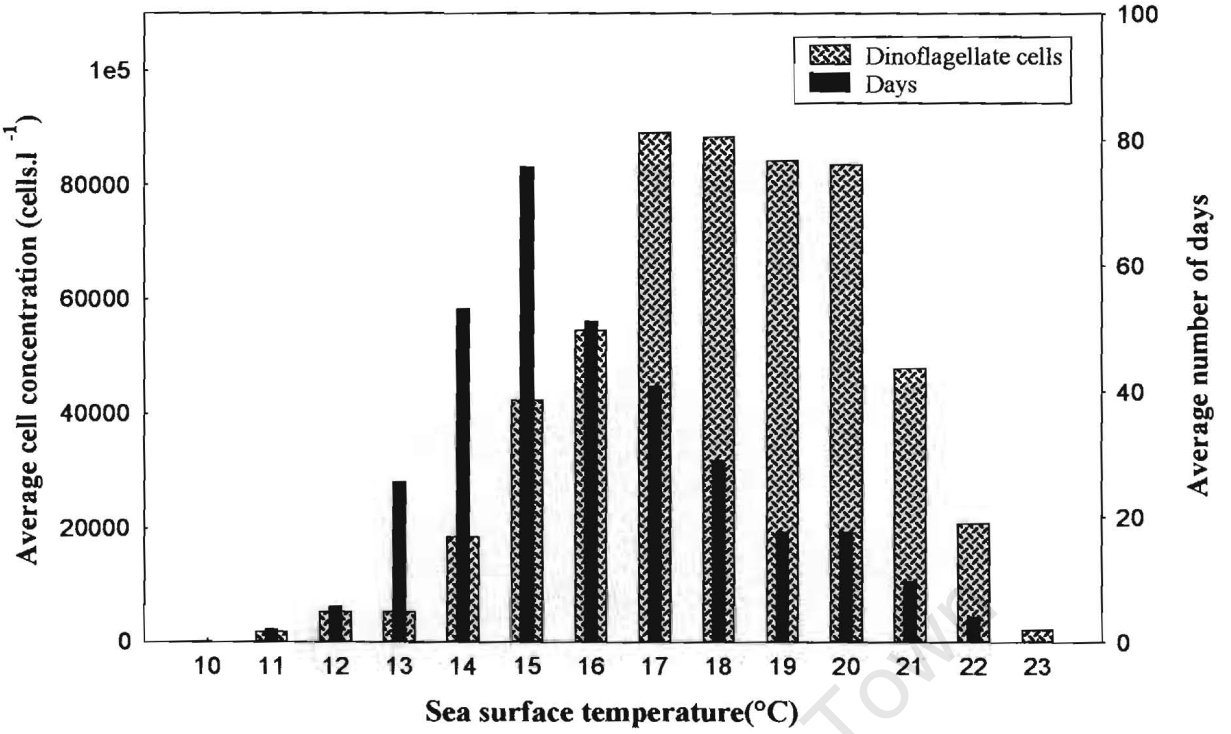

Figure 8. Average dinoflagellate cell concentration and frequency of SST observations at Gordon's Bay (1992 – 2000).

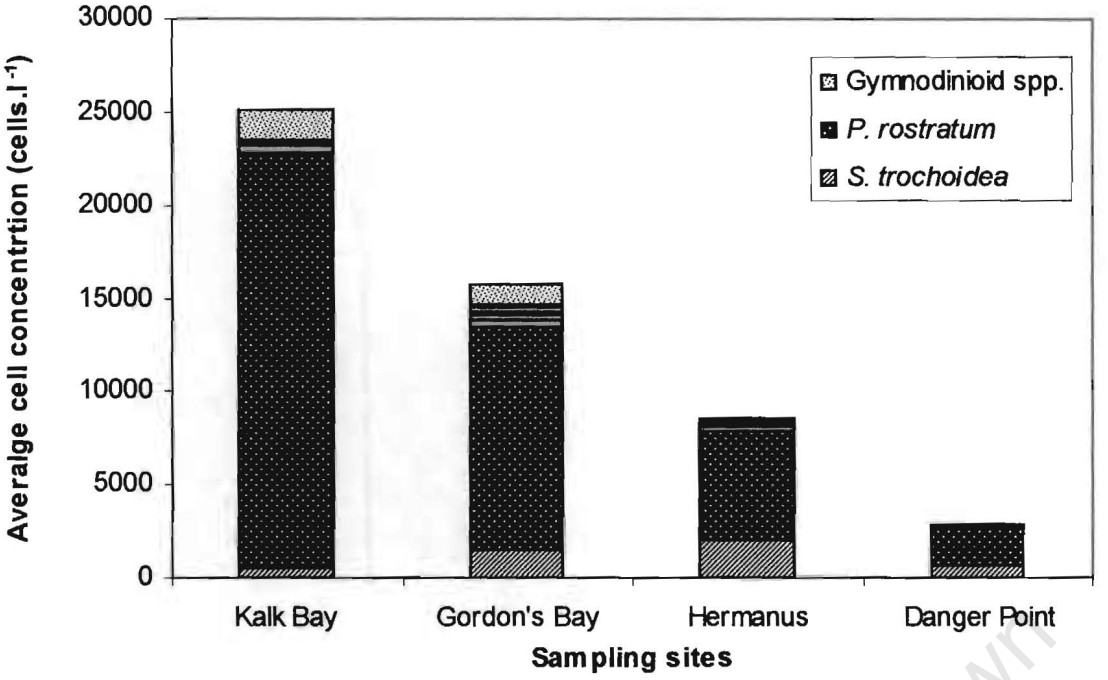

Figure 9. Averaged daily dinoflagellate cell concentration at four sampling sites for the period July 1997- June 1998.

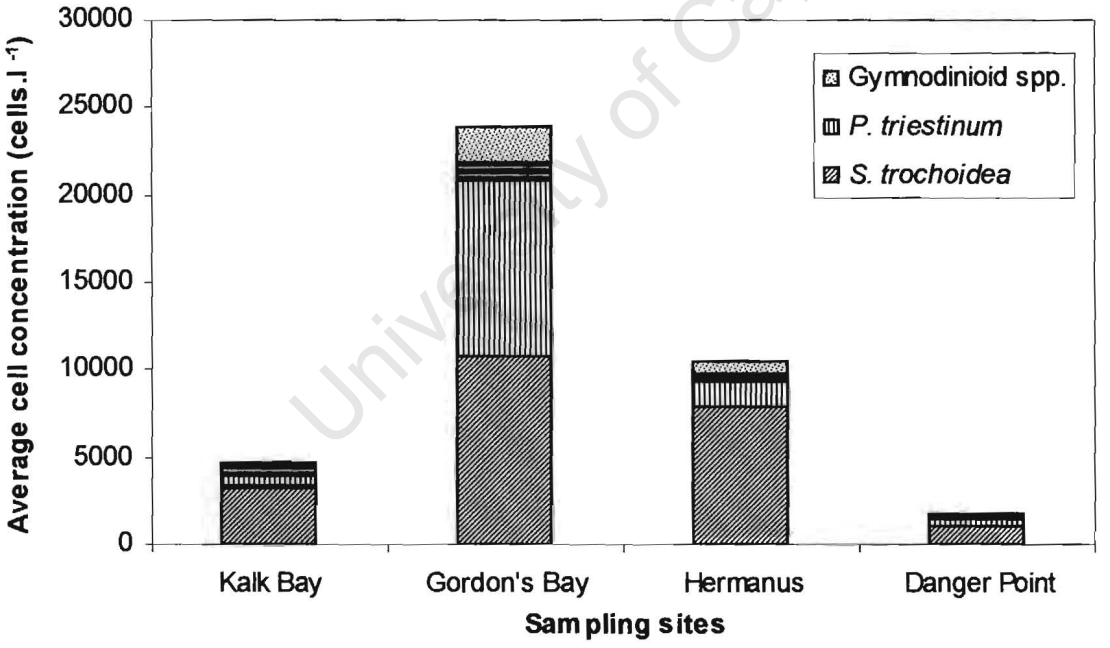

Figure 10. Average dinoflagellate cell concentration at four sampling sites for the period July 1998- June 1999.

Two dinoflagellate bloom events were encountered when monthly transect sampling was conducted, the first was on 21 December 1997 (Figs 11 a, b Figs 12 a – c) and the second on 14 December 1998 (Figs 13 a, b Figs 14 a – c). The bloom event that was sampled on 21 December 1997 was preceded by weak onshore N –NW's and S - SW's which, dominated on 19 and 21 December 1997 (Fig. 11 a). Stronger SE's dominated on 22 and 23 December, while 24 December were dominated by weak S – SE's. On 20 December 1997, SST in the northern and middle part of the bay was ~ 18 °C, while in the southern part of the bay declined to ~ 16°C (Fig. 11 b). Relative *in situ* fluorescence values (Fig. 12 b) indicated a subsurface phytoplankton maximum between 5 and 15m situated above the 16 °C isotherm (Fig.12 a) where nutrient concentrations were low (at 10m, station2; nitrate concentration = 1.98 μm l^{-1}, phosphate concentration = 0.94 μml^{-1} and silicate concentration = 5.86 μm l^{-1}). Cell counts revealed subsurface bloom concentrations of *P. rostratum* > 3 million cells l^{-1} at station 2 and 6. Cell concentrations of surface samples were > 200 000 cells l^{-1} (Fig. 12 c). This offshore bloom was detected in the shore based samples of 19, 21 and 24 December during wind relaxation periods (Fig. 11 a).

The second bloom event was sampled on 14 December 1998 when southerly winds generally persisted (Fig. 13 a), although it weakened during the latter part of 12 December and 14 – 15 December. Here, the SST on the eastern part of the bay was ~18 °C while SST on the western part of the bay was ~ 16 °C (Fig. 13 b). Relative *in situ* fluorescence values indicated a phytoplankton surface maximum at station 1 where the SST was ~ 18 °C (Figs 14 a, b). Cell counts revealed the presence of a *S. trochoidea* surface bloom

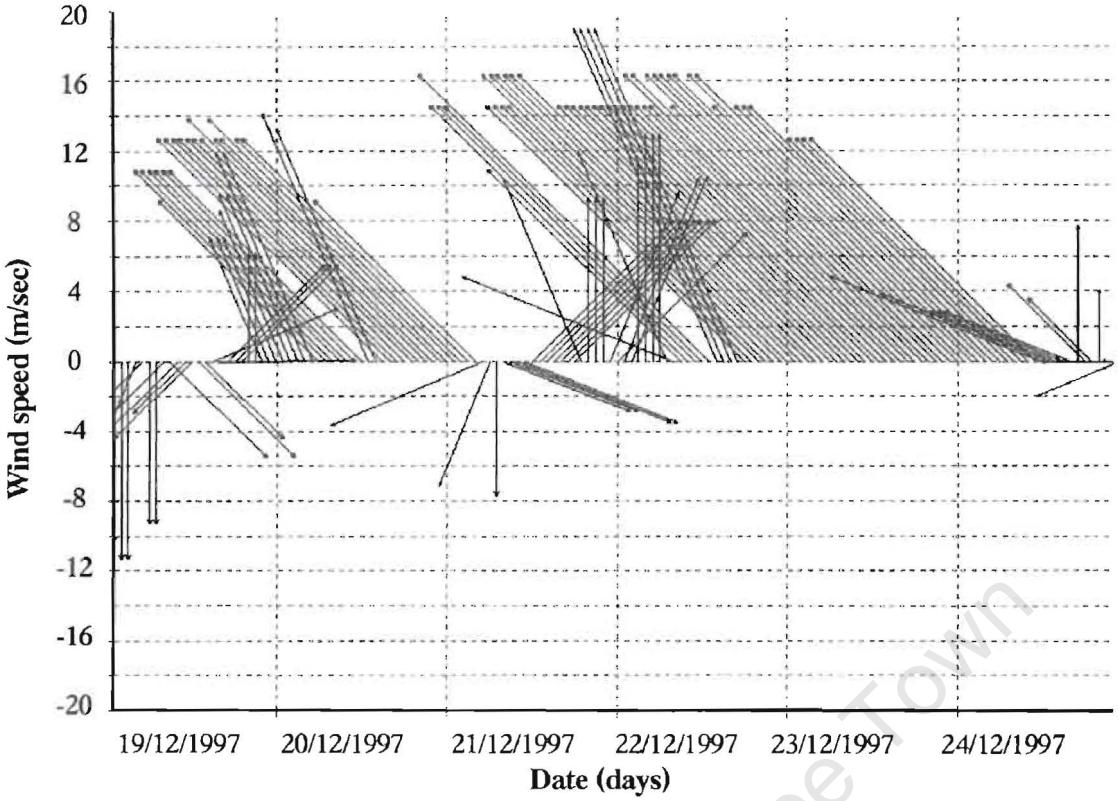

(a)

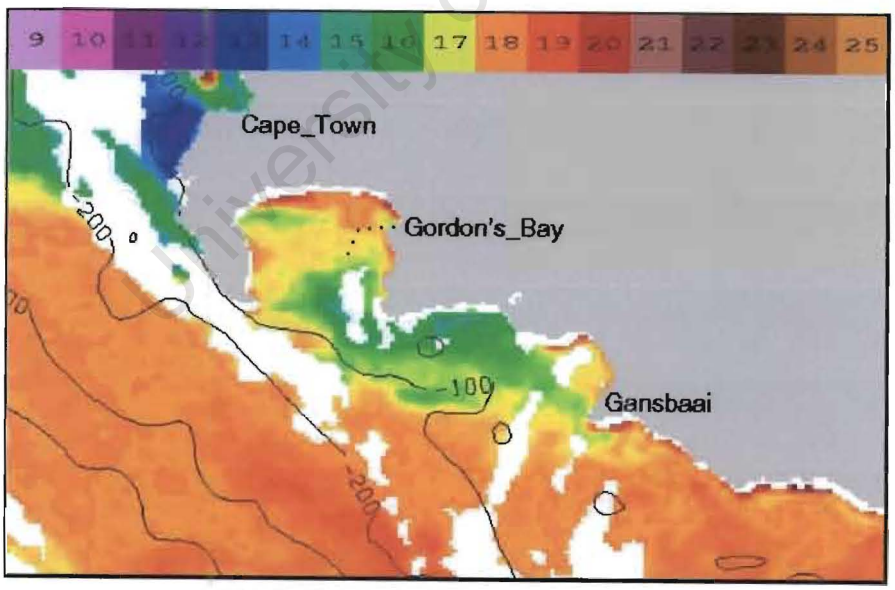

(b)

Figure 11. (a) Wind speed and direction recorded at Cape Point from 19 – 24 December 1997. (b) Satellite image of the Western Agulhas Bank showing SST on 20 December 1997.

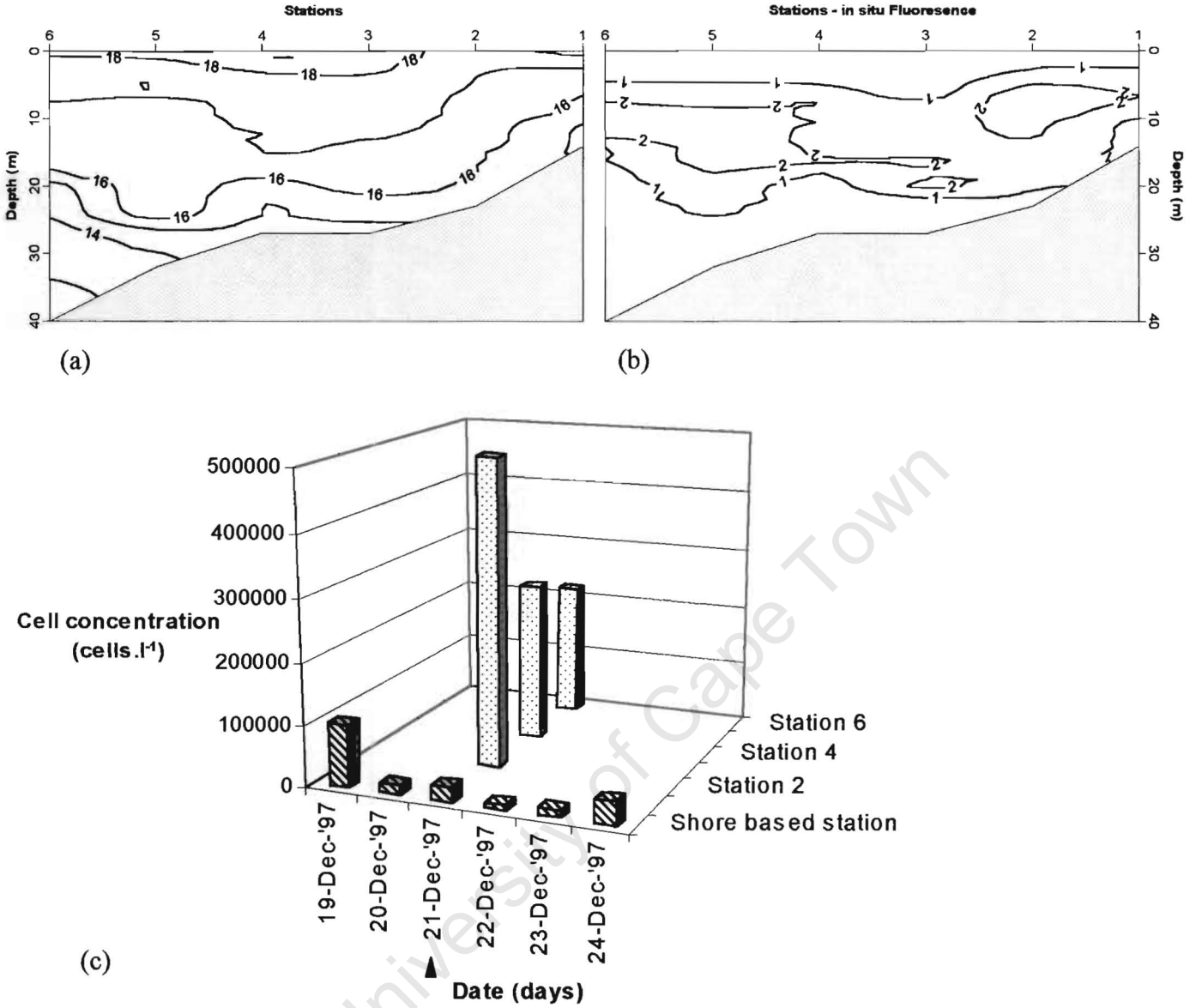

Figure 12. (a) Vertical cross sections of temperature and (b) *in situ* fluorescence on 21 December 1997. (c) Dinoflagellate cell concentration of shore based samples from 19 – 24 December 1997 and transect surface samples at station 2, 4 and 6 on 21 December 1997.

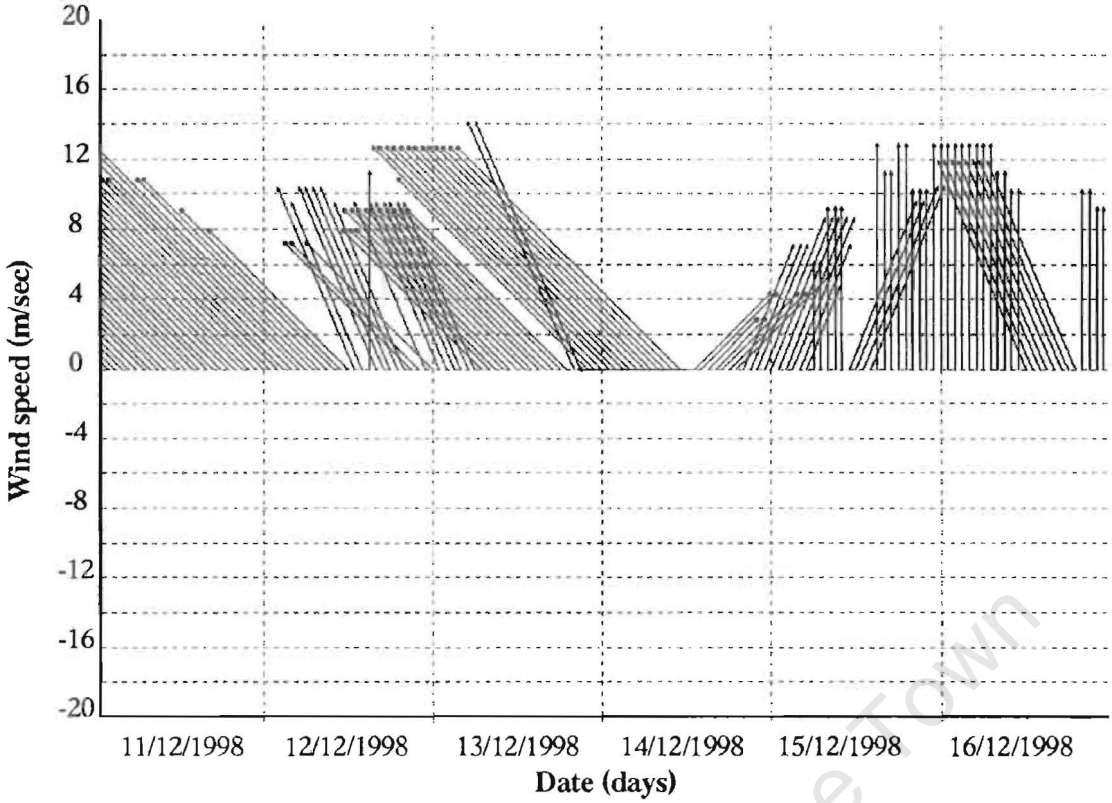

(a)

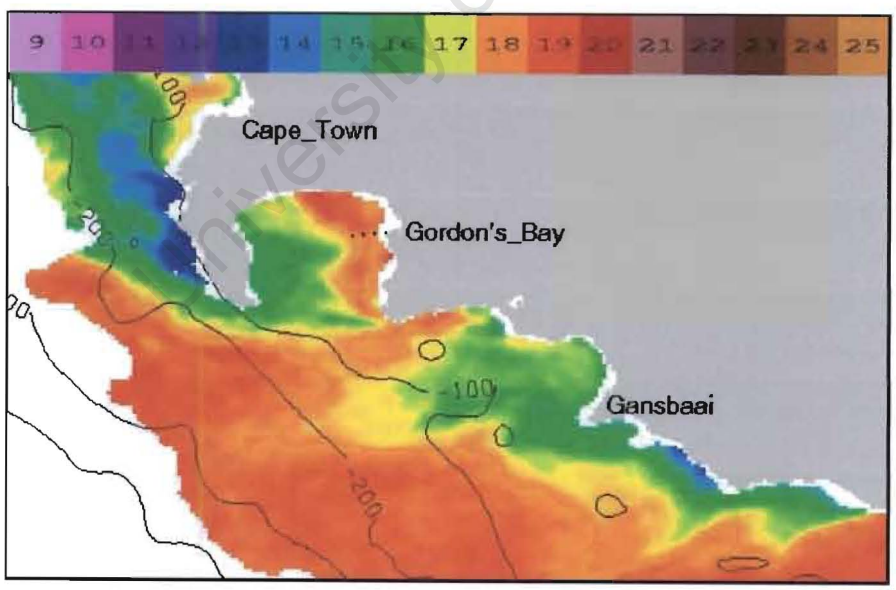

(b)

Figure 13. (a) Wind speed and direction recorded at Cape Point from 11 – 16 December 1998. (b) Satellite image of the Western Agulhas Bank showing SST on 13 December 1998.

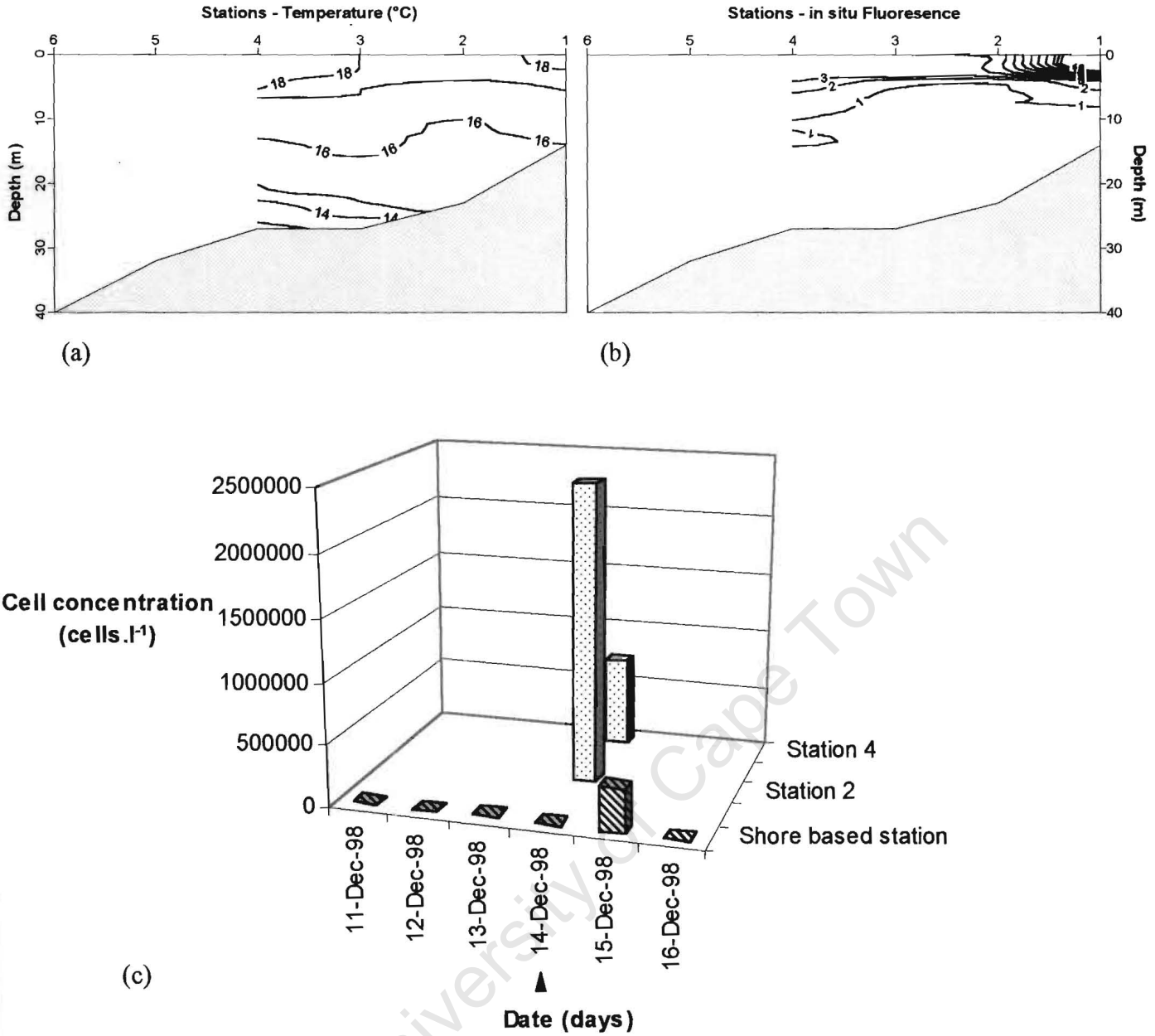

Figure 14. (a) Vertical cross sections of temperature and (b) *in situ* fluorescence on 14 December 1998. (c) Dinoflagellate cell concentration of shore based samples from 11 – 16 December 1998 and transect surface samples at station 2 and 4 on 21 December 1998.

with cell concentrations of ~ 2.5 million cells l^{-1} at station 2 and was detected in the shore based samples on 15 December when very weak southerly winds prevailed.

The *S. trochoidea* surface maximum was accompanied by other dinoflagellate species such as *P. triestinum*, *A. sanguinea* and *Gyrodinium spirale*, when nutrient concentrations were low (at 0m; nitrate concentration = 2.59 μm l^{-1}, phosphate concentration = 2.32 μm l^{-1} and an silicate concentration = 3.83 μm l^{-1}).

DISCUSSION

Reports of algal blooms are receiving increased attention in the media and it is believed by some that there is a global increase in algal blooms (Hallegraeff 1995). The reality of this 'increase' should however be viewed with caution as it could be attributed to an increase in awareness and improved surveillance. For example, more intense monitoring of False Bay and Walker Bay during the coarse of this study has revealed the presence of several (*Gymnodinium aureolum, Gyrodinium spirale, Heterocapsa orientalis* (Iwataki *et al.* in press), *Karenia bicuneiformis* (Botes *et al.* 2003 b), *Lepidodinium viride, Protoperidinium depressum, Protoperidinium pentagonum, Protoperidinium steinii* and *Takayama helix* (de Salas *et al.* 2003) dinoflagellate species not previously recorded (Table 1) in the area. Although no adverse effects were attributed to any of the blooms observed during the coarse of this study, 8 species (*A. sanguinea, K. cristata, G. polygramma, C. furca, P. micans, A. catenella, D. acuminata* and *D. fortii*) have previously been recorded as harmful (Botes *et al.* in press a, Horstman *et al.* 1991, Grindley & Taylor 1964, Matthews & Pitcher 1996, Cocroft *et al.* 2000, Horstman 1981, Pitcher *et al.* 2001, Pitcher *et al.* 1993, Pitcher & Calder 2000).

Some species, such as *Alexandrium catenella, A. sanguinea, Ceratium furca, Ceratium lineatum, Dinophysis acuminata, Dinophysis fortii, Gonyaulax polygramma, Noctiluca scintillans, S. trochoidea, Prorocentrum micans, P. rostratum, Protoperidinum depressum, Protoperidinium*

pentagonum and Zygabikodinium lenticulatum, were not confined to the south coast (False Bay and Walker Bay) of South Africa, but occurred on the west coast (Botes 2003, Horstman 1981, Pitcher & Calder 2000) as well. Blooms of *A. sanguinea, K. cristata, K. bicuneiformis, P. rostratum, P. triestinum, S. trochoidea* and to a lesser extend *D. acuminata,* were however common in False Bay and Walker Bay whereas blooms of *C. furca, C. lineatum, D. acuminata, P. micans* and *A. catenella* are common on the West Coast (Pitcher & Calder 2000). Although cell concentrations of *D. acuminata* never reached concentrations sufficiently high to contaminate shellfish (Pitcher & Calder 2001), it was recorded on several occasions in 1992 – 94 and 1995 – 96. Blooms of *Noctiluca scintillans,* which have previously been recorded in False Bay (Horstman 1981, Pitcher & Calder 2000), were not detected in the shore based monitoring samples in False Bay from 1992 –2000 and neither in Walker Bay from 1997 – 2000. It was also found that even though patchy bloom concentrations might be found within the bays (as sampled during the transect on 21 Dec 1997 and 14 Dec 1998), the species composition within the two bays for any given upwelling season was consistent.

Red tide activity between July 1992 and June 2000 was very variable with the magnitude of blooms markedly higher during 1995 - 96 than during the El Niño event in 1997-98, possibly due in part to large scale meteorological patterns not investigated in this study. The incidence of blooms in Gordon's Bay, unlike that on the West Coast, persisted into July. The low average cell concentration from July to October, when the water column is isothermal as a result of vertical mixing, could possibly serve as a seed population for the next red tide season. It has previously been documented (Pitcher *et al.* 1995, Shannon 1985) that there is a decrease in the average monthly winds in December and it is noteworthy that this lull coincides with an increase in the averaged dinoflagellate cell concentration. The higher average dinoflagellate cell concentration in March, April and May is associated with increased wind relaxation periods whereas increased NWs

during winter (Boyd *et al.* 1985) causes deep mixing and decreased dinoflagellate cell concentrations.

The study area is subjected to the influence of south easterlies (SE's) during summer and, north-westerlies (NW's) during winter (Boyd *et al.* 1985). Typical flow patterns resulting from strong S – SE's, lead to a westward movement of water from Walker Bay to False Bay (Boyd *et al.* 1985) which enters the bay at Cape Point resulting in a clockwise circulation within False Bay (van Ballegooyen 1991, Atkins 1970, Gründling & Largier 1991 Jury 1991, van Ballegooyen 1991). Eddies or gyres are known to occur under weak SE's at Gordon's Bay, as a result of the bottom topography and coastline, and at Kalk Bay, due to the orographic effect of the Kalk Bay mountain range (Atkins 1970, Gründling & Largier 1991, Jury 1991, C. Waiman pers. comm.). The reduced wind effect on the sea surface at Kalk Bay, as a result of the mountain range, may cause isolated cells or eddies. Anti-clockwise movement within False Bay (van Ballegooyen 1991, Atkins 1970, Gründling & Largier 1991, Jury 1991, van Ballegooyen 1991) and eastward movement from False Bay to Walker Bay results from strong NW's (Boyd *et al.* 1985). These circulation patterns could possibly contribute to the similarity in the species composition of dinoflagellate assemblages within False Bay and Walker Bay.

The higher averaged cell concentrations at Kalk Bay during 1997 –98 and at Gordon's Bay during 1998-98 could be as a result of the eddies or gyres that break away in an anticlockwise fashion from the clockwise circulation within False Bay (Atkins 1970, H. Waldron pers. comm.). It is further evident that in 1997-98 and 1998-99, the averaged cell concentration at Danger Point was considerably lower than that at Hermanus, or any other collection site. This could be due to the fact that Danger Point is fairly exposed with considerable wave action and is not as sheltered as for example Gordon's Bay.

By comparing shore based samples with those taken during transect sampling, it was clear that shore based samples are not necessarily a very good reflection of dinoflagellate cell concentrations within False Bay. This is because wind relaxation periods followed by onshore winds (winds with a easterly component at Kalk Bay, winds with a westerly component at Gordon's Bay and Walker Bay) are necessary to permit the concentration of organisms inshore (Stumpf *et al.* 1998). Shore based monitoring however, still provides very valuable information on species composition and dominance. It also provides insight into the frequency and seasonality of dinoflagellates within the study area. Transect sampling on the other hand provides information on the spatial variation in the phytoplankton species composition which is determined by the vertical stability of the water column and the availability of nutrients and light (Gentien 1998) and here *P. rostratum and S. trochoidea* were typically associated with a warm (16 °C and 18°C respectively) stratified water column, low in nutrients.

In conclusion, information generated in monitoring programmes which are accompanied by scientific research, such as described here, is essential in providing information that can be used to effectively manage marine resources, protect public and ecosystem health, support aquaculture development, and contribute to policy decisions and coastal zone issues (Pitcher 1998).

SECTION 3

Potential threat of bloom forming dinoflagellates species to the developing abalone mariculture industry

CHAPTER 7

THE POTENTIAL THREAT OF ALGAL BLOOMS TO THE ABALONE (*HALIOTIS MIDAE*) MARICULTURE INDUSTRY SITUATED AROUND THE SOUTH AFRICAN COAST.

ABSTRACT

Toxic algal blooms are common world-wide and pose a serious problem to the aquaculture and fishing industries. Dinoflagellate species such as *Karenia brevis*, *K. mikimotoi*, *Heterosigma akashiwo* and *Chatonella* cf. *antiqua* are recognised toxic species implicated in various faunal mortalities. Toxic blooms of *K. cristata* were observed on the south coast of South Africa for the first time in 1988 and were responsible for mortalities of wild and farmed abalone. *Karenia cristata* and various other dinoflagellate species common along the South African coast, as well as *K. mikimotoi* (Isolation site: Norway) and *K. brevis* (Isolation site: Florida) were tested for toxicity by means of a bioassay involving *Artemia* larvae as well as abalone larvae and spat. *K. cristata*, like *K. brevis*, contains an aerosol toxin; however the toxin present in *K. cristata* has not yet been isolated and remains unknown. *Karenia brevis* was therefore used to determine which developmental phase of the bloom would affect abalone farms most, and whether ozone could be used as an effective mitigating agent. Of the seventeen phytoplankton species tested, *K. cristata, Akashiwo sanguinea, K. mikimotoi* and *K. brevis* pose the greatest threat to the abalone mariculture industry. *Karenia brevis* was most toxic during its exponential and stationary phases. Results suggest that ozone is an effective mitigation agent but its economic viability for use on abalone farms must still be investigated.

INTRODUCTION

The global increase of harmful algal blooms (HABs) and their effects on shellfish such as oysters, mussels, surfclams and scallops are well documented (Matsuyama *et al.* 1998b, Matsuyama 1999, Nagai *et al.* 1996, Shumway *et al.*1990, Shumway & Cembella 1993, Shumway 1995, Shumway *et al.* 1994, Smolowitz & Shumway 1997). The consequences of these blooms have developed into a world-wide concern over the past several decades. Not all HABs are directly or even indirectly toxic, but some like the 'brown tide' species *Aureococcus anophagefferens* Hargraves et Sieburth, can interfere with the ability of bivalves to ingest algae, and thus reduce growth rates (Bricelj & Lonsdale 1997, Probyn *et al.* 2001). Other than the reported toxic effect of *Heterocapsa circularisquama* Horiguchi and *Karenia mikimotoi* (Miyake et Kominami ex Oda) G. Hansen *et* Moestrup on the abalone, *Haliotis discus* Reeve (Matsuyama *et al.* 1998a), and the two cases of paralytic shellfish poisoning (PSP) toxicity in *Haliotis tuberculata* Linnaeus from north-west Spain (Bravo *et al.* 1996, Bravo *et al.* 1999, Martinez *et al.* 1993, Nagashima *et al.* 1995) and *Haliotis midae* Linnaeus from South Africa (Pitcher *et al.* 2001), no published information is available on the effect of HABs on the abalone mariculture industry.

The first aim of this study was to investigate the effect of various microalgal species on abalone larvae and abalone spat (3 mm individuals), and to assess whether these microalgae might pose a threat to the mariculture industry, particularly on the south coast of South Africa. The second aim was to determine the developmental phase of algal cultures most toxic to abalone. Finally, the application of ozone as a potential mitigation agent was investigated. Although the primary objective of this study was to examine the toxicity of various algal species to abalone larvae and juveniles, the bioassay used is that which was originally designed for bioassays with *Artemia* (ARTOXKIT M). The ARTOXKIT M standardised

bioassay is routinely used internationally in marine research and aquatic toxicology (Chang & Redfearn 1999, Demaret *et al.* 1995, Lush & Hallegraeff 1996, Medlyn 1980, Persoone & Wells 1987) because of the commercial availability of dried *Artemia* cysts, and the simplicity and cost-effectiveness of the kit. We incorporated this bioassay into our study so that our results can be compared to those of other studies using the ARTOXKIT M assay. Because of the difficulty of maintaining *Karenia cristata* Botes, Sym et Pitcher (Botes *et al.* 2003 b) in culture, *Karenia brevis* (Davis) G. Hansen et Moestrup (which, like *K. cristata* contains an aerosol toxin (Hemmert 1975)) was used for the second and third experiments described in this paper.

MATERIALS AND METHODS

Establishment of unialgal cultures

Dinoflagellate species commonly found along the South African coast (Table 1) were isolated into culture vessels containing F/2 (Guillard & Ryther 1962) and Keller (Keller & Guillard 1985) growth media. The culture vessels were maintained in incubators at 18°C under a photon flux density of ca. 200 $\mu Em^{-2}s^{-1}$ (14:10 h LD photoperiod). Cultures were subsequently sub-cultured into larger containers.

Artemia *and abalone bioassay*

Hatching of *Artemia* cysts was performed as outlined in the ARTOXKIT M standard operational procedure. The test design of the ARTOXKIT M is based on a disposable multi-well test plate (four rows and six columns) using a control (column 1) and five increasing toxicant concentrations (columns 2 – 6), each with four replicates (rows). The control contained 2 ml of seawater (20 µm-filtered and UV-treated), while the five treatment concentrations contained 2 ml of dinoflagellate cultures arranged in increasing concentrations

Table 1. List of algal species, and their origin, tested for toxicity

Species	Origin
Akashiwo sanguinea (Hirasaka) G. Hansen et Moestrup	False Bay, RSA
Chatonella cf. *antiqua* (Hada) Ono	False Bay, RSA
Gonyaulax polygramma Stein	False Bay, RSA
Gymnodinium aureolum (Hulburt) G. Hansen et Moestrup	Table Bay, RSA
Karenia cristata Botes, Sym et Pitcher	False Bay, RSA
Gymnodinium cf. *pulchellum* Larsen	False Bay, RSA
Gyrodinium cf. *zeta* Larsen	Lamberts Bay, RSA
Gyrodinium cf. *corsicum* Paulmier, Berland, Billard et Nezan	False Bay, RSA
Heterosigma akashiwo (Hada) Hada ex. Y. Hara et Chihara	False Bay, RSA
Heterocapsa orientalis Iwataki, Botes et Fukuyo	False Bay, RSA
Lepidodinium viride Watanabe, Suda, Sawaguchi et Chihara	False Bay, RSA
Prorocentrum micans Ehrenberg	False Bay, RSA
Prorocentrum rostratum Stein	False Bay, RSA
Prorocentrum triestinum Schiller	False Bay, RSA
Scrippsiella trochoidea (Stein) Balech	False Bay, RSA
Takayama helix de Sala, Bolch, Botes *et* Hallegraeff	False Bay, RSA
Karenia brevis (Davis) G. Hansen et Moestrup	Florida, USA
Karenia mikimotoi (Miyake et Komani ex Oda) G. Hansen et Moestrup	Norway, EUR

from columns 2 to 6. Subsequently, 10 two-day old *Artemia* larvae (2nd instar stage) were transferred into each of the four replicate wells of each column. After 24 hours the dead larvae (larvae were considered dead if they did not exhibit any internal or external movement over 30 seconds of observation) in each well were counted. The abalone larvae bioassay was similar to the *Artemia* bioassay except that 10 abalone larvae (two-day old) were placed into each replicate well in place of the *Artemia* larvae. After 24 hours the abalone larvae were considered dead if the larvae inside the shell appeared to have ruptured (Fig. 1). For the

abalone spat bioassay, five individuals (3 mm animals) were transferred into each replicate well and were deemed dead after 24 hours if they were detached from the sides of the container, were unable to right themselves after dropping off the sides, and failed to show tentacle movement after 30 seconds of observation.

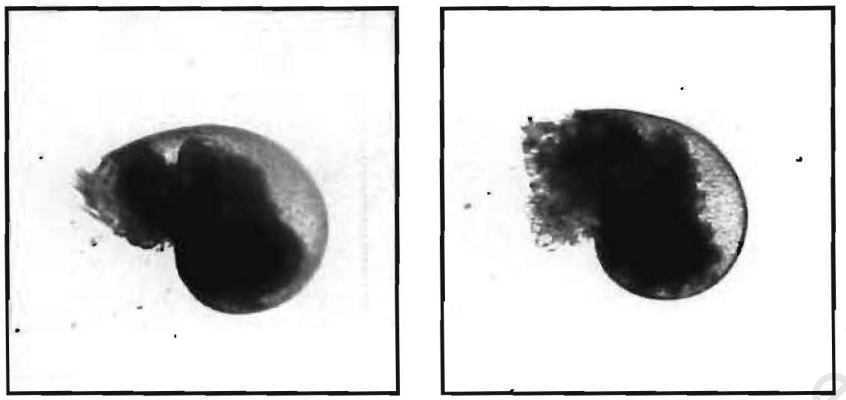

(a) (b)

Figure 1. Two-day-old abalone larvae (a) before, with intact velum and body, and (b) after, with a flocculated appearance of the velum and body, exposure to toxic dinoflagellate cultures.

Assessment of 17 potentially toxic phytoplankton species

This experiment was included to investigate the potential threat that phytoplankton species might pose to the developing South African abalone mariculture industry. Cultures of the various microalgal species were isolated and maintained as previously described, with the exception of *Karenia cristata* which was collected in the field and concentrated by filtration through a 15 µm mesh to increase cell concentration. The toxicity of each species (in exponential phase) to *Artemia* larvae, abalone larvae and abalone spat was investigated in three ways: (a) cultures with intact cells (whole cells), (b) cultures that were sonicated (broken cells) and (c) cultures with cells removed by filtration on Whatman GF/F filter paper (filtrate).

Mortality associated with different phases of the bloom event

This experiment was designed to determine whether the four developmental phases (lag, exponential, stationary and death phases) of the 'red tide' exhibited different toxicity effects on abalone larvae and spat. Four culture flasks were inoculated with *K. brevis* at the start of the experiment. A Turner Designs fluorometer was used to determine the growth phase of the culture within each culture flask (Parsons *et al.* 1984). Toxicity of *K. brevis* (whole cells, broken cells and the filtrate) to *Artemia* larvae, abalone larvae and spat was tested for each of the four phases.

Evaluation of ozone as a mitigation possibility

Preliminary experiment revealed that using an Aquazone Purifiers ozonizer (output = 250 mgh^{-1}), cells of *K. mikimotoi*, *K. brevis*, *Akashiwo sanguinea* (Hirasaka) G. Hansen et Moestrup, *Heterosigma akashiwo* (Hada) Hada ex. Y. Hara et Chihara and *Chatonella* cf. *antiqua* (Hada) Ono were killed after 10 minutes (41.67 mg/10 minutes) of ozonation. This ozonation regime was then used in subsequent experiments

Karenia brevis (7.8×10^6 cell l^{-1}) was used to establish whether ozone could be used as a mitigation agent. Column 1 (control) of the ARTOXKIT M contained 20 µm filtered and UV-treated seawater, column 2 (ozonated control) contained ozonated 20 µm filtered and UV-treated seawater, column 3 (toxicity test) contained *K. brevis* culture with intact cells (exponential phase), columns 4-6 (tests for mitigation effect of ozone) contained ozonated culture with intact cells (whole cells), ozonated culture with broken cells (broken cells) and ozonated culture where cells have been filtered out (filtrate) respectively. In order to minimise free radicals present during the experiments, the flasks were left to stand for one hour before proceeding with the experiments.

Statistical analyses

When assessing the toxicity of the 17 potentially toxic phytoplankton species, the mortality rate of *Artemia* larvae, abalone larvae and spat as affected by dinoflagellate cell concentration was modelled using a binomial (with probit link) general linear model (GLM). To determine whether larval or spat death at any of the cell concentrations (i.e. treatment concentrations) was significantly greater with respect to that of the control, animal mortality at each cell concentration was compared with that of the control by treating cell concentration as a factor in the GLM analysis. The result is a table of *p*-values that indicate the probability of mortality being significantly greater ($p > 0.05$) with respect to the control. To derive 10 and 50% lethal concentrations (LC_{10} and LC_{50}, respectively) and associated standard errors, the '`dose.p`' procedure in the 'MASS' package of Venables & Ripley (1999) was used subsequent to fitting the GLM model. Even though it is standard procedure to calculate LC_{50} values, LC_{10} values were also calculated. With cell concentration as a continuous variable rather than a factor (as in the preceding contrast analysis), LC_{10} or LC_{50} values could not be calculated in situations where the observed proportion of larval or spat mortalities failed to exceed 10 or 50% mortality. As probit analysis requires a consistent trend of mortality with increasing cell concentration, LD-values could not be estimated when mortalities were high (above 10 or 50%) at intermediate cell concentrations but low at low and high cell concentrations, as was sometimes the case with abalone spat. In the few cases where LC-values could not be determined using probit analysis (despite consistent trends in mortality), we used loess smoothing to derive estimates. In such cases standard errors of the estimates are not reported. When assessing the mortality associated with different phases of the bloom event, student's *t*-tests were used to statistically compare estimates of LC_{50} between growth phases. Statistical analysis of results obtained from the experiment investigating ozone as a possible mitigation agent was similar to that of experiment A where *Artemia* larvae, abalone larvae and spat

mortalities in each treatment were compared with that of the control using GLM. All statistical procedures were performed using version 1.6.1 of the statistical package, *R*, an implementation of the *S*-language (Ihaka & Gentleman, 1996).

RESULTS

Assessment of 17 potentially toxic phytoplankton species

The toxicity assays (Table 2) suggest that toxicity differed for *Artemia* larvae, abalone larvae and abalone spat. Toxicity also differed when whole or broken cells, or the filtrate of the algal cultures was used, and when the animals were exposed to differing dinoflagellate cell concentrations. As it is unlikely that abalone farmers could afford to lose 50% of the animals, both LC_{50} and LC_{10} values are presented as these could be used to indicate when mitigation actions should be taken. Of the 17 phytoplankton species tested, *Akashiwo sanguinea* (Fig. 2), *Karenia cristata* (Fig. 3), *K. brevis* (Fig. 4) and *K. mikimotoi* (Fig. 5) (Table 2) could pose a significant threat to abalone mariculture. It is of interest to note, however, that none of these four dinoflagellates species caused *Artemia* larval mortalities >10%, and in most cases mortalities of *Artemia* were not significant.

A. sanguinea (Fig. 2) caused significant mortality in abalone larvae, resulting in LC_{50} and LC_{10} values of $3.1 \times 10^5 \pm 6.8 \times 10^3$ and $6.2 \times 10^4 \pm 9.7 \times 10^3$ cells l^{-1}, respectively, for whole cells and LC_{50} and LC_{10} values of ca. 3.6×10^5 (no SE available) and 5.5×10^4 (no SE available) cells l^{-1}, respectively, for broken cells. No LC_{50} or LC_{10} values could be determined for the filtrate because of the inconsistent trend of abalone larval mortalities with

Table 2. Results of toxicity assays on 17 phytoplankton species ('whole cells', 'broken cells' and 'filtrate') on *Artemia* larvae (ArtL) and abalone larvae (AL) and spat (AS). Significance levels (ns – not significant; $*p < 0.05$; $**p < 0.01$; $***p < 0.0001$) indicate whether assays resulted in higher mortality rates of larvae or spat when exposed to any of the five cell concentrations tested with respect to mortality rates in controls (in the absence of phytoplankton cells). LC_{50} values (mean number of cells.l^{-1} ± SE of estimate) could only be calculated for certain species, and LC_{10} values are thus given for the sake of convenience for some of the 'less toxic' species. Note that statistically significant mortality effects (with respect to the controls) could still be detected even when very low mortality rates eliminated the possibility of calculating LC_{10} values. † - mortality always below 10%; ‡ - mortality below 50%; § - mortality above 10 or 50%, but inconsistent trend of mortality with increasing concentration prevented determination of LC-values; [a] LC-values predicted from loess curves.

		whole cells			broken cells			filtrate		
Species	tested on	*p*	LC_{10}	LC_{50}	*p*	LC_{10}	LC_{50}	*p*	LC_{10}	LC_{50}
C. cf. *antiqua*	ArtL	ns	†	†	***	$3.6 \times 10^6 \pm 2.2 \times 10^5$	‡	*	†	†
	AL	ns	†	†	ns	†	†	ns	†	†
	AS	***	†	†	***	†	†	***	$5.5 \times 10^6 \pm 2.8 \times 10^5$	†
G. aureolum	ArtL	*	†	†	*	†	†	ns	†	†
	AL	ns	†	†	ns	†	†	ns	†	†
	AS	***	†	†	***	†	†	ns	†	†
K. brevis	ArtL	ns	†	†	ns	†	†	ns	†	†
	AL	ns	†	†	ns	†	†	ns	†	†
	AS	***	$7.5 \times 10^5 \pm 5.6 \times 10^4$	$2.4 \times 10^6 \pm 4.6 \times 10^4$	***	$1.5 \times 10^6 \pm 9.2 \times 10^4$	$4.7 \times 10^6 \pm 2.3 \times 10^5$	***	$8.9 \times 10^5 \pm 6.2 \times 10^4$	$2.7 \times 10^6 \pm 5.9 \times 10^4$
G. cf. *corsicum*	ArtL	*	†	†	ns	†	†	*	†	†
	AL	ns	†	†	ns	†	†	ns	†	†
	AS	ns	†	†	ns	†	†	***	†	†
G. polygramma	ArtL	ns	†	†	*	†	†	ns	†	†
	AL	*	†	†	ns	†	†	ns	†	†
	AS	ns	†	†	***	†	†	***	†	†
T. helix	ArtL	ns	†	†	ns	†	†	ns	†	†
	AL	***	$8.4 \times 10^5 \pm 6.5 \times 10^4$	†	***	$1.1 \times 10^6 \pm 8.3 \times 10^4$	†	***	†	†
	AS	***	†	†	ns	†	†	***	†	†
K. mikimotoi	ArtL	ns	†	†	*	†	†	ns	†	†
	AL	***	$3.3 \times 10^5 \pm 4.1 \times 10^4$	$1.1 \times 10^6 \pm 2.6 \times 10^5$	***	*ca.* 2.6×10^{5a}	*ca.* 1.4×10^{6a}	***	*ca.* 3.4×10^{5a}	*ca.* 3.2×10^{6a}
	AS	***	§	§	***	§	§	***	§	§
A. sanguinea	ArtL	ns	†	†	*	†	†	ns	†	†

	AL	***	$6.2 \times 10^4 \pm 9.7 \times 10^3$	$3.1 \times 10^5 \pm 6.8 \times 10^3$	***	*ca.* 5.5×10^{4a}	*ca.* 3.6×10^{5a}	***	§	§
	AS	***	§	‡	***	†	†	ns	†	†
G. cf. *zeta*	ArtL	*	†	†	ns	†	†	*	†	†
	AL	*	†	†	ns	†	†	*	†	†
	AS	***	†	†	***	†	†	ns	†	†
H. akashiwo	ArtL	*	†	†	*	†	†	ns	†	†
	AL	ns	†	†	ns	†	†	ns	†	†
	AS	ns	†	†	***	$6.3 \times 10^6 \pm 3.3 \times 10^5$	†	ns	†	†
H. orientalis	ArtL	ns	†	†	ns	†	†	ns	†	†
	AL	ns	†	†	***	†	†	ns	†	†
	AS	ns	†	†	***	†	†	ns	†	†
K. cristata	ArtL	*	†	†	ns	†	†	*	†	†
	AL	***	$1.1 \times 10^6 \pm 5.8 \times 10^4$	$2.7 \times 10^6 \pm 4.6 \times 10^4$	***	†	†	ns	†	†
	AS	***	$2.5 \times 10^6 \pm 7.4 \times 10^4$	†	ns	†	†	***	†	†
L. viride	ArtL	ns	†	†	ns	†	†	ns	†	†
	AL	ns	†	†	***	†	†	ns	†	†
	AS	ns	†	†	***	†	†	ns	†	†
P. micans	ArtL	ns	†	†	*	†	†	ns	†	†
	AL	*	†	†	ns	†	†	***	†	†
	AS	ns	†	†	***	§	†	**	†	†
P. rostratum	ArtL	*	†	†	ns	†	†	ns	†	†
	AL	*	†	†	ns	†	†	*	†	†
	AS	***	†	†	***	†	†	ns	†	†
P. triestinum	ArtL	*	†	†	*	†	†	***	†	†
	AL	*	†	†	***	†	†	ns	†	†
	AS	ns	†	†	***	†	†	ns	†	†
S. trochoidea	ArtL	*	†	†	*	†	†	*	†	†
	AL	***	†	†	ns	†	†	*	†	†
	AS	ns	†	†	***	†	†	***	§	†

increasing cell concentrations. Toxicity of *A. sanguinea* to the abalone spat was not as severe as for the larvae, with median mortality rates of above 40% only attained at one concentration of whole cells.

The *K. cristata* (Fig. 3) assay involving whole cells resulted in abalone larval mortalities with an estimated LC_{50} value of $2.7 \times 10^6 \pm 4.7 \times 10^4$ cells l^{-1} and LC_{10} value of $1.1 \times 10^6 \pm 5.8 \times 10^4$ cells l^{-1}. Abalone spat mortality rates of around 30% were observed at the highest cell density tested with a LC_{10} of $2.5 \times 10^6 \pm 7.3 \times 10^4$ cells l^{-1}.

The toxic effect of *K. brevis* was restricted to abalone spat (Fig. 4) with a LC_{50} value of $2.4 \times 10^6 \pm 4.6 \times 10^4$ cells l^{-1} and a LC_{10} value of $7.5 \times 10^5 \pm 5.6 \times 10^4$ cells l^{-1} for whole cells. LC_{50} and LC_{10} values of $4.7 \times 10^6 \pm 2.3 \times 10^5$ and $1.5 \times 10^6 \pm 9.3 \times 10^4$ cells l^{-1}, respectively, were determined for broken cells, while LC_{50} and LC_{10} values for the filtrate were $2.7 \times 10^6 \pm 6.2 \times 10^4$ and $8.9 \times 10^5 \pm 6.2 \times 10^4$ cells l^{-1}, respectively.

K. mikimotoi caused significant abalone larval and spat mortalities (Fig. 5). The LC_{50} for whole cells was estimated at $1.1 \times 10^6 \pm 2.6 \times 10^4$ cells l^{-1} with LC_{10} at $3.3 \times 10^5 \pm 4.1 \times 10^4$ cells l^{-1}. For broken cells LC_{50} was ca. 1.4×10^6 cells l^{-1} with the lower LC_{10} value at ca. 2.6×10^5 cells l^{-1}. LC_{50} and LC_{10} for the filtrate were *ca.* 3.2×10^6 and 3.4×10^5 cells l^{-1}, respectively (estimates were obtained from fitting loess curves, and SE values could not be estimated). Toxicity effects of this species on abalone spat were also significant, with mortalities of greater than 50% even at the lowest cell concentration tested. However, no clear relationship between *K. mikimotoi* concentration and mortality was evident, with median mortality rates increasing then decreasing with increasing cell density.

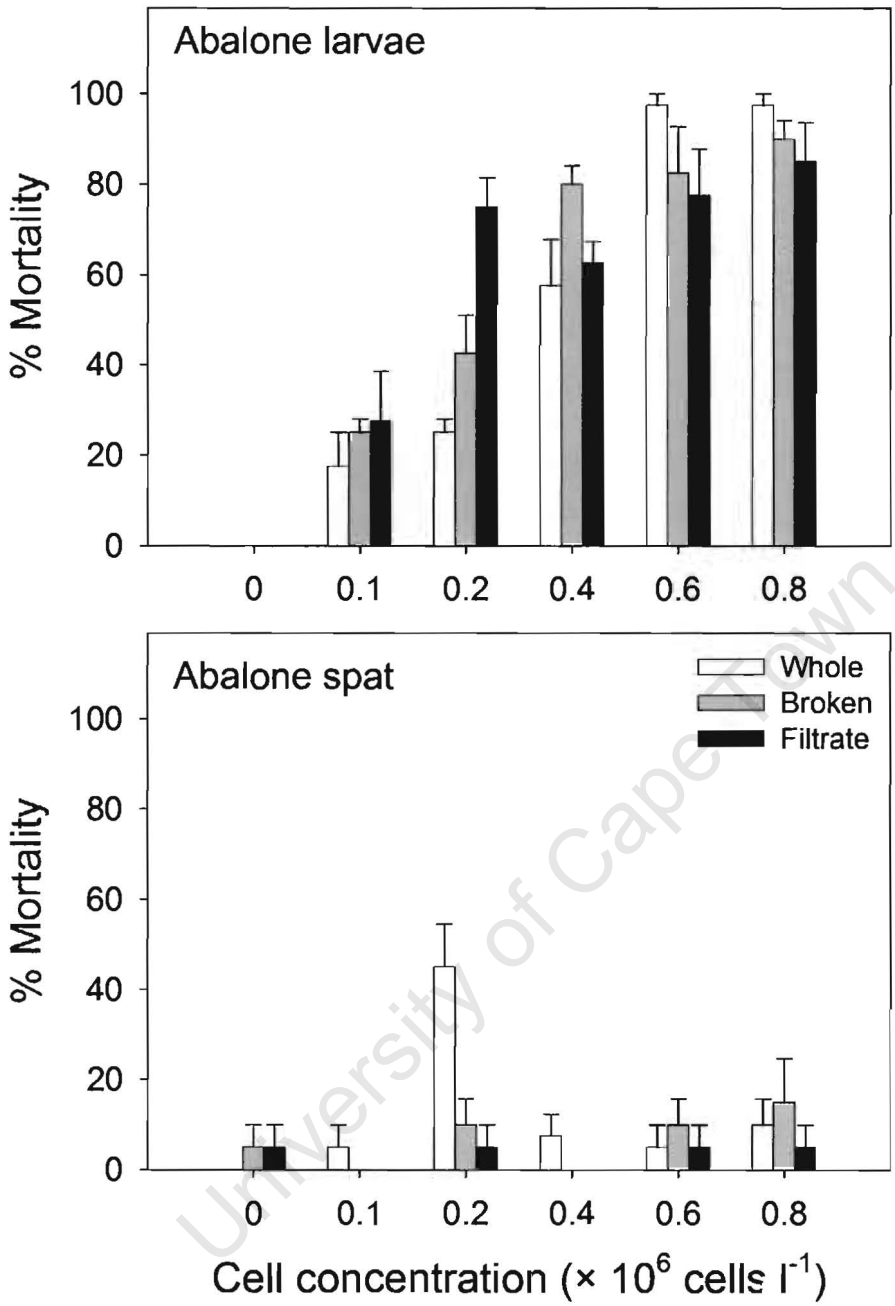

Figure 2. Graph of % mortality of abalone larvae and abalone spat after 24 hrs of exposure to *Akashiwo sanguinea* (Whiskers = mean + SE).

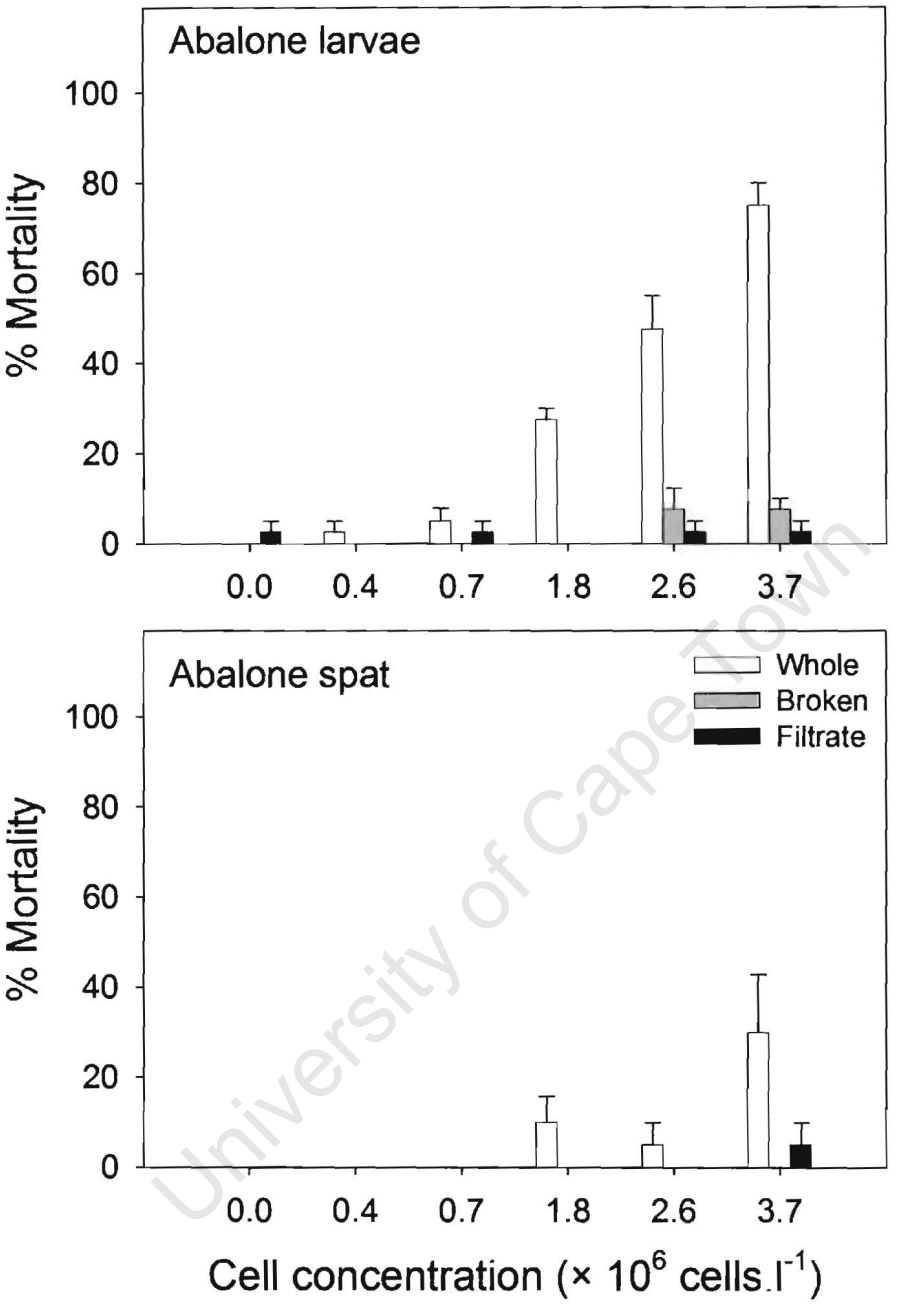

Figure 3. Graph of % mortality of abalone larvae and abalone spat after 24 hrs of exposure to *K. cristata* (Whiskers = mean + SE).

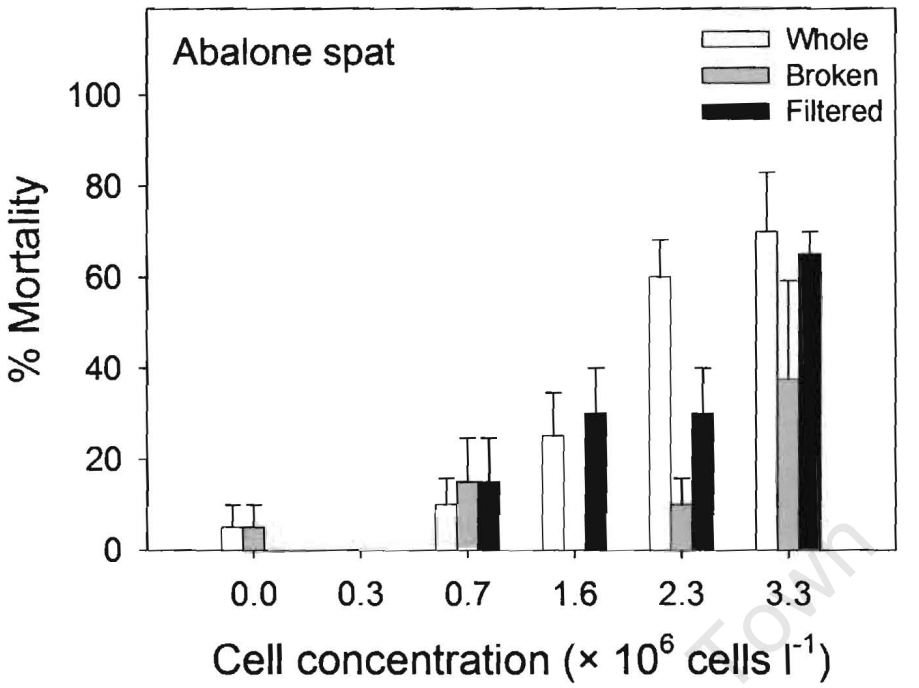

Figure 4. Graph of % mortality of abalone spat after 24 hrs of exposure to *Karenia brevis* (Whiskers = mean + SE).

Chatonella cf. *antiqua, Heterosigma akashiwo, T. helix* de Salas, Bolch, Botes *et* Hallegraeff, *Prorocentrum micans* Ehrenberg and *Scrippsiella trochoidea* (Stein) Balech resulted in *Artemia* larvae or abalone larvae or spat mortalities of > 10% (Table 2). The LC_{10} value for the effect of *C.* cf. *antiqua* (filtrate) on abalone spat is $5.5 \times 10^6 \pm 2.8 \times 10^5$ cells l^{-1} and $3.6 \times 10^6 \pm 2.2 \times 10^5$ cells l^{-1} for *C.* cf. *antiqua* (broken cells); the LC_{10} for *H. akashiwo* (broken cells) on abalone spat is $6.3 \times 10^6 \pm 3.3 \times 10^5$ cells l^{-1} and $8.4 \times 10^6 \pm 6.5 \times 10^4$ cells l^{-1} for *T. helix* (whole cells) on abalone larvae; and the LC_{10} for *T. helix* (broken cells) on abalone larvae is $1.1 \times 10^6 \pm 8.3 \times 10^4$ cells l^{-1}. No LC_{10} values could be obtained for *S. trochoidea*.

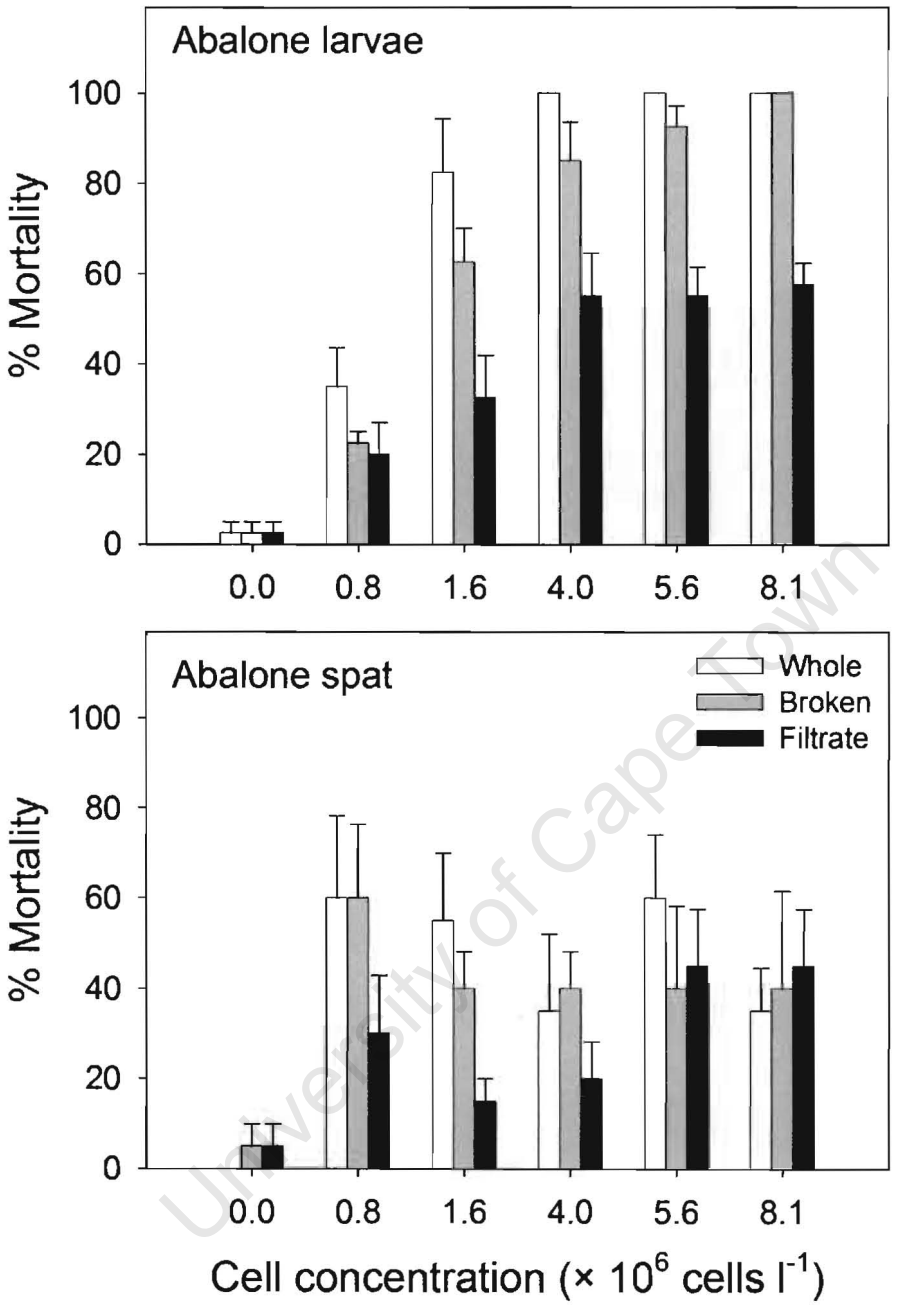

Figure 5. Graph of % mortality of abalone larvae and abalone spat after 24 hrs of exposure to *Karenia mikimotoi* (Whiskers = mean + SE).

Although death rates of *Artemia* larvae, abalone larvae and abalone spat when exposed to *Gymnodinium aureolum* (Hulburt) G. Hansen et Moestrup, *Gyrodinium* cf. *corsicum* Paulmier, Berland, Billard et Nezan, *Gonyaulax polygramma* Stein, *Gyrodinium* cf. *zeta* Larsen, *Heterocapsa orientalis* Iwataki, Botes et Fukuyo (Iwataki *et al.* in press), *Lepidodinium viride* Watanabe, Suda, Sawaguchi et Chihara, *Prorocentrum rostratum* Stein and *Prorocentrum triestinum* Schiller were in some circumstances greater than that of their respective controls, in no case did mortalities exceed 10% (Table 2) and therefore, in the context of the current study, mortalities were considered to be relatively insignificant.

Mortality effects associated with different phases of the bloom event

Results of toxicity assays of *K. brevis* (during lag, exponential, stationary and death phase) on abalone spat are presented in Fig. 6 and Table 3. Neither whole cells, broken cells nor filtrate resulted in significant mortality effects on abalone spat at any concentration tested during the lag phase. Significant mortalities were, however, obtained during the exponential and stationary phases with mortalities during the exponential phase occurring at lower cell densities than in the stationary phase. In the death phase, mortalities occurred at much higher cell densities than in the stationary phase (LC_{50} values and student's *t*-test, $p < 0.005$ in Table 3). *Karenia brevis*, in the exponential phase, is therefore significantly more toxic than in stationary phase. Toxicity diminishes once the cultures reach the death phase, and LC_{50} values would most likely be at concentration in excess of those tested in this experiment.

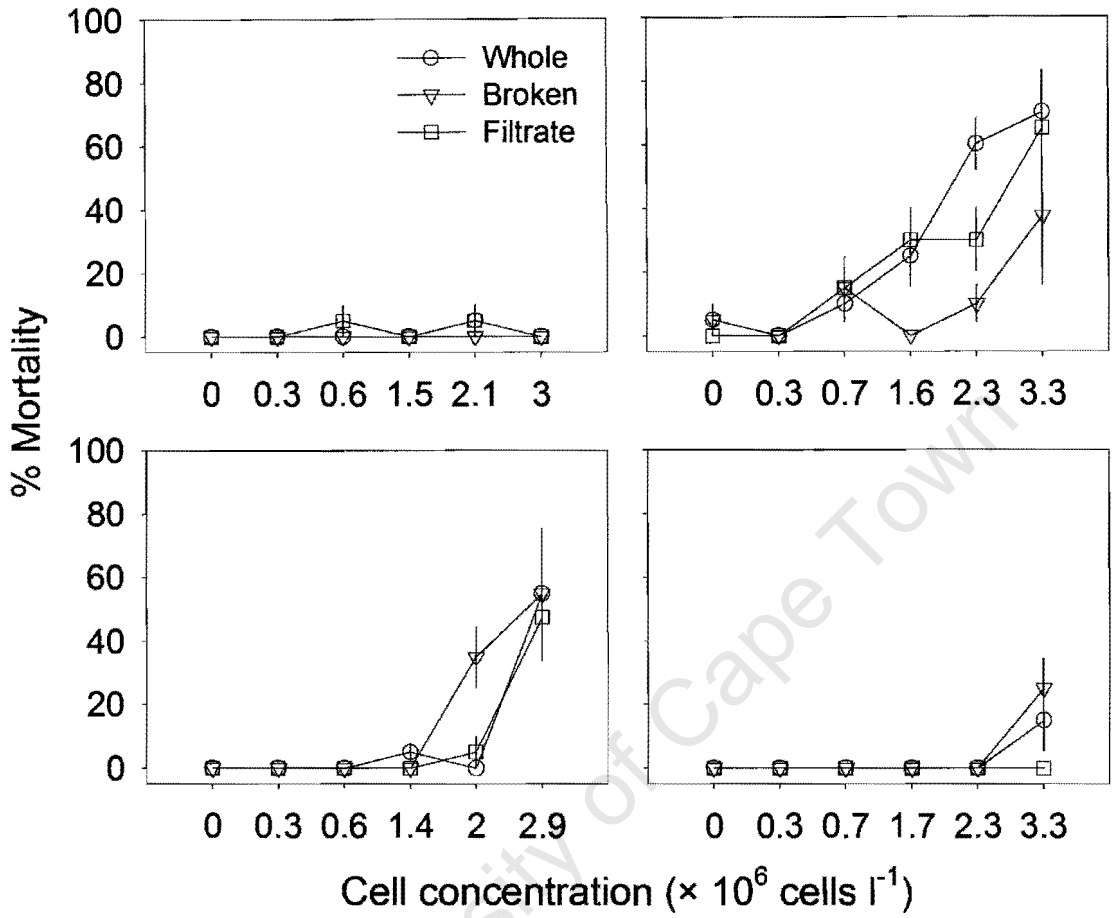

Figure 6. Graph of % abalone spat mortalities during the four growth phases of *Karenia brevis* and various cell concentrations (top left – lag phase; top right – exponential phase; bottom left – stationary phase; bottom right – death phase). Estimated LC_{50} values are presented in Table 3 (symbols represent mean mortalities and vertical bars represent ± SE).

Table 3. LC_{50} values (mean number of cells $l^{-1} \pm$ SE of estimate) showing the effect of *Karenia brevis*, obtained from the exponential and stationary cell growth phases, on abalone spat. LC_{50} values could not be estimated for the lag and death phases because at no stage did more than half the animals die within the range of cell concentrations tested (see Figure 12). The Student's *t*-tests determine whether LC_{50} values of cells obtained from the exponential phase differ from that of the stationary phase for each of the treatment groups.

treatment	exponential phase	stationary phase	*t*-value	*P*
whole cells	$2.4 \times 10^6 \pm 4.6 \times 10^4$	$2.8 \times 10^6 \pm 3.7 \times 10^4$	-16.56	<0.0001
broken cells	$4.7 \times 10^6 \pm 2.3 \times 10^5$	$2.6 \times 10^6 \pm 3.8 \times 10^4$	17.25	<0.0001
filtrate	$2.7 \times 10^6 \pm 5.8 \times 10^4$	$2.9 \times 10^6 \pm 3.3 \times 10^4$	-5.17	<0.005

Evaluation of ozone as a mitigation possibility

Karenia brevis had no effect on *Artemia* larvae or abalone larvae, but the culture with whole cells (7.8×10^6 cell l^{-1}) resulted in 100% mortality of abalone spat. The culture (whole and broken cells, as well as the filtrate) after ozonation for 10 minutes, had no adverse effect on the assay animals and neither did the control that was ozonated (Fig. 7).

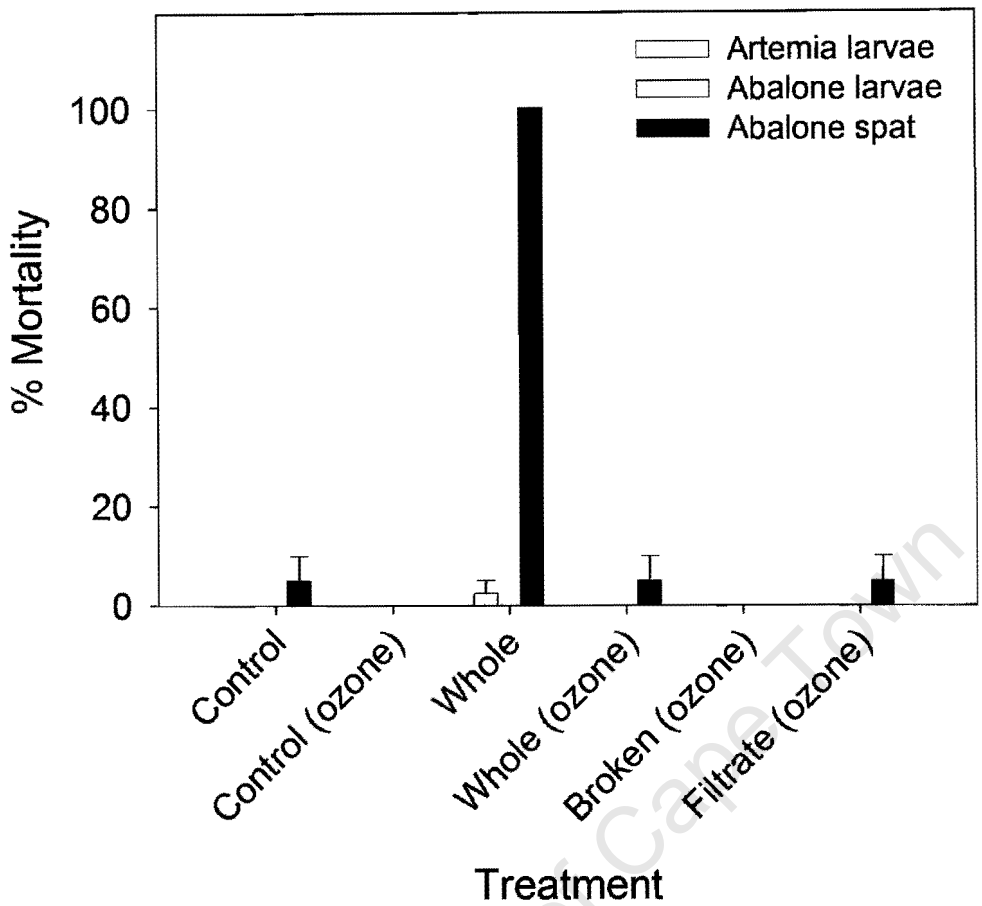

Figure 7. Graph of % mortality of *Artemia* larvae, abalone larvae and abalone spat when exposed to *Karenia brevis* (7.8×10^6 cells l^{-1}) and using various ozonation treatments and controls (Whiskers = mean + SE).

DISCUSSION

Assessment of 17 potentially toxic phytoplankton species

Although none of the 17 species tested (at cell concentrations $<10 \times 10^6$ cells l^{-1}) resulted in high mortalities on the two-day old *Artemia* larvae used in our assays, several other studies have found evidence to the contrary. For example, death among four-day old *Artemia* larvae resulted from exposure to *Alexandrium minutum* Halim and *Heterosigma carterae* (syn. *Heterosigma akashiwo*) (Lush & Hallegraeff, 1996) and the *Gymnodinium* sp. which

bloomed in Wellington Harbour in 1998 (Chang & Redfearn, 1999). Similarly, Medlyn (1980) found that *Karenia brevis* was toxic to adult *Artemia.* We incorporated this bioassay into our study for comparative purposes and because the ARTOXKIT M is a standardised bioassay that is routinely used internationally in marine research and aquatic toxicology.

The ARTOXKIT M documentation recommends using instar II larvae, but it is known that different *Artemia* instar stages and adults vary in their susceptibility to toxins. Sorgeloos *et al.* (1978) demonstrated that instar II larvae are more sensitive than instar I and that instar II and III are equally sensitive. Medlyn (1980), on the other hand, indicated that adults are most sensitive to *K. brevis* toxins. Using adult *Artemia,* however, is often not practical as this requires additional laboratory space, maintenance of the food source and extended time to grow to adult stage. The most likely reason for the low *Artemia* mortalities recorded in our study is that most other studies used much higher dinoflagellate cell concentrations (> 10×10^6 cells l^{-1}). What is clear from our studies, however, is that abalone larvae and spat are much more susceptible to dinoflagellate toxins than *Artemia* larvae.

Of the 17 species tested in the present study, *Akashiwo sanguinea, K. cristata, K. brevis* and *K. mikimotoi* were found to cause the largest mortalities among abalone larvae or spat, and thus may pose a significant threat to the abalone mariculture industry if blooms were to enter farms at concentrations tested in our study. Under certain conditions, these species resulted in mortality rates of more than 50%, with LC_{50} values ranging from 3.1×10^5 cells l^{-1} for *A. sanguinea* to 4.7×10^6 cells l^{-1} for *K. brevis.*

Initially, it was surprising that *A. sanguinea* was found to be toxic to abalone larvae as it is generally considered a non-toxic species. Other studies, however, have found it to be

acutely toxic to oyster larvae (*Crassostrea gigas* Thunberg) (Cardwell *et al.* 1979) and juvenile and adult oysters (*Ostrea lurida* Carpenter) (Nightingale 1936, Woelke 1961). Whilst our study did not provide evidence that exposure of abalone spat to *A. sanguinea* resulted in direct mortality, observations suggested that it did affect the strength of attachment of the spat to the sides and bottom of the container, and their ability to right themselves after they became dislodged.

The LC_{50} value of *K. cristata* for abalone larvae was estimated at ca. 2.7×10^6 cells l^{-1}, whereas for abalone spat an estimate would most likely result in a LC_{50} value at cell densities greater than those tested in our study. The spat that were still alive after exposure to *K. cristata,* were very weak suggesting that this dinoflagellate species contains a very mild toxin and needs cell concentrations in excess of 10×10^6 cells l^{-1} to kill adult abalone (Horstman *et al.* 1991).

Karenia brevis (whole cells, broken cells and filtrate) resulted in mortality of abalone spat only. In all cases, the spat that were alive after 24 hours were weak and when dislodged, were unable to right themselves. As with *K. cristata, K. mikimotoi* had an adverse effect on both abalone larvae and spat but, whereas only whole cells of *K. cristata* had a toxic effect, broken cells and the filtrate of *K. mikimotoi* cultures also exhibited a toxicity effect. Abalone larvae that were exposed to *K. cristata* and *K. mikimotoi* and which were alive after the 24 hour treatment either displayed velum movement with no vertical movement, or shed their shells. It is interesting to note, in comparison, that Matsuyama *et al.* (1998a) and Sawada & Wada (1983) concluded that *K. mikimotoi* was highly toxic to juvenile *Haliotis discus* and that *K. mikimotoi* significantly affected adults of this species.

Although no significant mortalities were evident in abalone larvae and spat when exposed to the two highest cell concentrations of *Chatonella* cf. *antiqua* and *Heterosigma akashiwo* (whole and broken cells), the abalone larvae displayed velum movement but no vertical migration. Similarly, Nagai *et al.* (1996) found that *H. akashiwo* had no effect on juvenile pearl oysters (*Pinctada fucata* Dunker) and Nielsen & Strøngrem (1991) showed that *H. akashiwo* had no effect on the mussel, *Mytilus edulis* Linnaeus. Matsuyama *et al.* (1998a), however, found that *H. akashiwo* (at 10^5 cells ml^{-1}) was responsible for mortalities of juveniles of the abalone, *Haliotis discus* and also juveniles of *Sulculus diversicolor* Reeve. In their assay, however, only one individual at a time was exposed to three different cell concentrations and the statistical validity of their result must, therefore, be seen within this limitation.

Mortality associated with different phases of the bloom event

Significant abalone spat mortalities were observed during the exponential and stationary growth phases of *K. brevis*. Mortalities during the exponential phase occurred at lower cell densities than during the stationary phase. This was true for whole cell cultures, suspensions of broken cells, and for the filtrate after removal of dinoflagellate cells. *Karenia brevis*, in the exponential phase, is therefore significantly more toxic than in stationary phase. Toxicity diminishes once the cultures reach the death phase, then occurring only at very high cell concentrations. Animals that were still alive after exposure to cultures during this phase appeared disorientated and were unable to right themselves when dropped off the sides of the culture container. For the abalone farmer these results provide an indication of which phase or stage during an algal bloom would pose the greatest risk and may also suggest when mitigating actions, such as recirculation, should be initiated.

Evaluation of ozone as a mitigation technique

Ozonating (250mg O_3 hr^{-1}) suspensions of *K. mikimotoi, A. sanguinea, K. brevis, H. akashiwo* and *C.* cf. *antiqua* for 10 minutes killed algal cells and inactivated the toxic effect of *K. brevis* on abalone spat. Similarly, Ho & Wong (2001) found that cells of *Prorocentrum triestinum, Scrippsiella trochoidea* and *K. digitata* Yang, Takayama, Matsuoka et Hodgkiss were broken within 15 minutes by indirect diffusion of ozone (1 gm O_3 m^{-3} seawater hr^{-1}). These results suggest that ozone can effectively be used as a mitigation agent to minimize the loss of abalone larvae in the hatchery and early settled spat in the nursery during a red tide event. The economic viability for its use on abalone farms, however, must still be investigated.

An important conclusion of this study is that dinoflagellate species such as *K. mikimotoi, K. brevis, T. helix, G.* cf. *corsicum, H. akashiwo, C.* cf. *antiqua,* listed in the IOC Taxonomic Reference list of Toxic Plankton Algae (Intergovernmental oceanographic Commission of UNESCO 2003), are not necessarily toxic to abalone. For the species that this study has shown to be potentially toxic to abalone larvae or spat, it may be appropriate for abalone farmers to undertake mitigating actions following algal blooms. Whether it would be best for farmers to recirculate 'in-house' water during a red tide event, or to utilize mitigation techniques such as ultra-filtration or ozonation, would depend on a range of local circumstances and upon farm design.

SYNTHESIS

Algal blooms are a natural phenomenon that have occurred throughout recorded history. On a global scale, there is evidence of changes in large scale meteorological patterns that together with various other human-induced factors, result in changes in the distribution of algal species, and in the emergence of formerly unrecorded or rare species in previously unaffected areas (Hallegraeff 1995).

Skills in algal taxonomy and improvement on standard techniques are essential for not only discriminating algal species but for assessing phylogenetic relationships, species diversity and genetic and morphological character diversity. Such diversity plays an integral role in the adaptation of some species to their environment or otherwise preference to certain environments and ultimately their distribution. Chapters 1 to 5 contribute significantly to the field of dinoflagellate taxonomy. The development of a technique that overcomes cell distortion and collapsing in species that are unarmoured or that possess delicate thecal plates makes SEM examination possible for a wider range of taxa. Not only does the technique overcome cell distortion but it also requires limited expertise and equipment, is inexpensive and less time consuming than standard SEM techniques. Besides contributing to a more resolved gymnodinioid taxonomic system by describing new species and genera, these chapters include the first attempt in South Africa to investigate the genetic relatedness and diversity among dinoflagellate species in the southern Benguela upwelling current. It also constitutes the first attempt to utilise optimisation on well resolved phylogenetic trees to assess the diagnostic value of dinoflagellate morphological characters at species and genus level.

In the absence of comprehensive inventories, the diversity of phytoplankton in the southern Benguela upwelling system is poorly established. Though several new species have been recorded in chapter 6, it is likely that they merely escaped detection in the past owing to inadequate sampling and insufficient taxonomic skills that would allow discrimination among species. The frequency and magnitude of bloom events between 1992 and 2000 were highest during 1995-96. The timing of the dinoflagellate blooms, from mid October to mid July, correlated well with the wind-induced upwelling season and even though the SST in False Bay was more often than not 15 °C, the averaged dinoflagellate cell concentration was highest between 17 – 20 °C. It was further found that the species composition of the dinoflagellate assemblages within False Bay and Walker Bay were consistent for any given year irrespective of the actual cell count at the various sampling sites. Sampling of a transect on the other hand provided information on the spatial variation in the dinoflagellate species composition within False Bay which is determined by the vertical stability of the water column and the availability of nutrients and light. This information is essential for managing marine resources and ecosystems, contributing to policy decisions, protecting public health and supporting aquaculture development.

The consequences of harmful algal blooms have developed into a world-wide concern over the past several decades and these are known to affect various bivalve shellfish, crabs and fish. Chapter 7 presents results of a first attempt to assess the potential threat of 17 dinoflagellate species, common between Cape Point and Danger Point, to the growing abalone mariculture industry. Four species proved to be a significant threat to abalone larvae and spat with *K. brevis,* although not found in South Africa, the most toxic in its exponential growth phase. Mortalities during its exponential phase occurred at lower cell densities than during the stationary phase. This was true for whole cell cultures, suspensions of broken cells,

and for the filtrate after removal of *K. brevis* cells. It is worth emphasizing that it was clear from the results that dinoflagellate species such as *K. mikimotoi, K. brevis, G.* cf. *pulchellum, G.* cf. *corsicum, H. akashiwo, C.* cf. *antiqua,* listed in the IOC Taxonomic Reference list of Toxic Plankton Algae, are not necessarily toxic to abalone. It was further found that ozonating (250mg O_3 hr^{-1}) suspensions of *K. mikimotoi, A. sanguinea, K. brevis, H. akashiwo* and *C.* cf. *antiqua* for 10 minutes killed algal cells and inactivated the toxic effect of *K. brevis* on abalone spat. These results suggest that ozone can effectively be used as a mitigation agent to minimize the loss of abalone larvae in the hatchery and early settled spat in the nursery during a red tide event. Whether it would be best for farmers to recirculate 'in-house' water during a red tide event, or to utilize mitigation techniques such as ultra-filtration or ozonation, would depend on a range of local circumstances and upon farm design. The economic viability for its use on abalone farms, however, must still be investigated.

Future directions

Although this thesis contributed significantly to our knowledge of the taxonomy, distribution and toxicity of dinoflagellate species in the southern Benguela current, a number of issues of importance to further our understanding of Southern Benguela dinoflagellates remain unresolved. To conclude this thesis, the following recommendations for future research are made:

- The type species, *G. fuscum*, is clearly problematic and warrants additional study with different DNA regions to clarify its phylogenetic position.
- On the basis of the heterogeneity of the genus *Gymnodinium senso stricto*, and in the light of our phylogenetic results, we suggest that the genus be subdivided and that clade 3 (Botes & de Salas, unpublished data) and 5 (Bolch & Hallegraeff, unpublished data) be described as new genera.

- Whether *K. micrum* (≡ *Gymnodinium galateanum* Braarud) and *G. corsicum* are identical needs to be further investigated.
- The taxonomic status of one well supported group containing *Gymnodinium simplex*, *Gyrodinium* cf. *zeta* and *Gymnodinium corii* still remains uncertain, indicating that much wider species sampling is necessary to contribute to a all-inclusive Gymnodiniales taxonomic system.
- As things stand the diversity of phytoplankton in the southern Benguela upwelling system, between Cape Point and Danger Point, is poorly established. Chapter 6 was limited to reporting on the dinoflagellate species diversity and their distribution within the southern Benguella system. A more intensive study investigating the diversity and distribution of diatom, dinoflagellates, flagellate and ciliate species, (Botes, Pitcher & Pienaar, unpublished data) in the Walker Bay area would contribute to more complete understanding of the phytoplankton diversity and distribution in the southern Benguela current.
- With the increase in utilization of coastal waters for aquaculture in South Africa, *K. cristata* is likely to have and even greater impact on the industry. At present, the toxin of *K. cristata* has not yet been isolated and remains unknown. A study investigating the toxin structure, the mode of action of the toxin and possible methods of detection is therefore essential especially in terms of regulations for food safety.
- The viability of using ozone as a mitigation agent needs to be investigated to ensure the practical use of ozone on land based abalone farms.

LITERATURE CITED

ANDERSON D.M. 1989. Toxic algal blooms and red tides: A global perspective. In: *Red Tides: Biology, Environmental Science and Toxicology*. (Eds. Okaichi T., Anderson D.M. & Nemoto T.), Elsevier Science, pp 11 – 16.

ATKINS G.R. 1970. Wind and current patterns in False Bay. *Trans. Roy. Soc. S. Afr.* **39**: 139 – 148.

BARLOW R.G., CUMMINGS D.G. & GIBBS S.W. 1997. Improved resolution of mono- and divinyl chlorophylls a and b and zeaxanthin and lutein in phytoplankton extracts using reverse phase C-8 HPLC. *Mar.Ec. Prog. Ser.* **161**: 303-307.

BJØRNLAND T. & TANGEN K. 1979. Pigmentation and morphology of a marine *Gyrodinium* (Dinophyceae) with w major carotenoid different from peridinin and Fucoxanthin. *J. Phycol.* **15**: 457 – 463.

BLACKBURN S. I., HALLEGRAEFF G. M. & BOLCH C. J. 1989. Vegetative reproduction and sexual life cycle of the toxic dinoflagellate *Gymnodinium catenatum* from Tasmania, Australia. *J. of Phycol.* **25**: 577-590.

BOLCH C.J.S. 2001. PCR protocols for genetic identification of dinoflagellates directly from single cysts and plankton cells. *Phycologia* **40**: 162-167.

BOLCH C. J. S., NEGRI A. P. & HALLEGRAEFF G. M. 1999. *Gymnodinium microreticulatum* sp nov (Dinophyceae): a naked, microreticulate cyst-producing dinoflagellate, distinct from *Gymnodinium catenatum* and *Gymnodinium nolleri*. *Phycologia* **38**: 301-313.

BOTES L. 2003. Phytoplankton identification catalogue – Saldanha Bay, April 2001. *GLOBALLAST Monograph Series* **7**.

BOTES L., PRICE B., WALDRON M. & PITCHER G.C. 2002. A simple and rapid scanning electron preparative technique for delicate "gymnodinioid" dinoflagellates. *Micrs. Res. and Tech.* **59**: 128 – 130.

BOTES L., SMIT A.J. & COOK P.A. (2003a). The potential threat of algal blooms to the abalone (*Haliotis midae*) mariculture industry situated around the South African coast. *Harmful Algae* **2**(4): 247-259.

BOTES L., SYM S.D. & PITCHER G.C. (2003b). *Karenia cristata* sp. nov. and *Karenia bicuneiformis* sp. nov. (Gymnodiniales, Dinophyceae): two new *Karenia* species from the South African coast. *Phycologia* **42** (6): 32-40.

BOYD A.J., TROMP B.S. & HORSTMAN D.A. 1985 The hydrology of the South African South-Western Coast between Cape Point and Danger Point in 1975. *S. Afr. Mar. Sci.* **3**: 145 – 168.

BRAARUD T. 1957 A red water organism from Walvis Bay. *Galathea Rep.* **1**: 137-138.

BRAET F., DE SANGER R. & WISSE, E. 1997. Drying cells for cells for SEM, AFM and TEM by hexamethyldisilazane: a study on hepatic endothelial cells. *J. of Micr.* **186**: 84-87.

BRAVO I., CACHO E., FRANCO J.M., MIGUEZ A., REYERO M.I. & MARTINEZ A. 1996. Study of PSP toxicity in *Haliotis tuberculata* from the Galician coast. In: *Harmful and Toxic Algal Blooms*, (Eds. Yasumoto, T., Oshima, Y., Fukuyo, Y), Intergovernmental Oceanographic Commision of UNESCO, pp. 421 –424.

BRAVO I., REYERO M.I., CACHO E. & FRANCO J.M. 1999. Paralytic shellfish poisoning in *Haliotis tuberculata* from the Galacian coast: geographical distribution, toxicity by lenghts and parts of the mollusc. *Aquat. Toxic.* **46:** 79-85.

BRAY D.R., BAGO J. & KOEGLER, P. 1993. Comparison of HMDS and CPD methods for SEM of biological specimens. *Micrs. Res. and Tech.* **26**: 489-495.

BRICELJ V.M. & LONSDALE D.J. 1997. *Aureococcus anophagefferens*: Causes and ecological consequences of brown tides in U.S. mid Atlantic coastal waters. *Limn. and Oceanogr.* **42**: 1023 – 1038.

BROWIN P.C., HUTCHINGS L. & HORSTMAN D.A. 1979. A red water outbreak and associated fish mortality at Gordon's Bay near Cape Town. *Fish. Bull. S. Afr.* **11**: 46 – 52.

CAMPBELL P.H. 1973. The phytoplankton of Gales Creek with emphasis on the taxonomy and ecology of estuarine phytoflagellates. Ph.D thesis, University of North Carolina, Chapel Hill. 359 pp.

CEMBELLA A.D., SHUMWAY S.E. & LAROCQUE R. 1994. Sequestering and putative biotransformation of paralytic shellfish toxins by the sea scallop Placopecten magellanicus: seasonal and spatial scales in natural populations. *J. Exp. Mar. Biol. and Ec.* **180**: 1 - 22.

CARDWELL R.D., OSLEN S., CARR M.I. & SANBORN E.W. 1979. Causes of oyster mortality in South Puget Sound. NOAA Tech. Mem. ERL MESA-39. Washington Department of Fisheries, Salmon Research and Development. Brinnan, Washington, USA.

CARRADA G. C., CASOTTI,R., MODIGH,M. & SAGGIOMO, V. 1991. Presence of *Gymnodinium catenatum* (Dinophyceae) in a coastal Mediterranean lagoon. *J. Plank. Res.* **13**: 229-238.

CHANG F.H. 1999a. A new species of *Gymnodinium* that caused the 1998 summer human respiratory syndrome and decimation of marine life in Wellington Harbour, New Zealand, In: *Harmful Algae News* (Ed. Wyatt T.) Intergovernmental Commission of UNESCO **19**:1 - 3.

CHANG F.H. 1999b. *Gymnodinium brevisulcatum* sp. nov. (Gymnodiniales, Dinophyceae), a new species isolated from the 1998 summer toxic bloom in Wellington Harbour, New Zealand. *Phycologia* **38**:377-385.

CHANG F.H. & REDFEARN P. 1999. Algal toxins in Wellington Harbour. In: *Aquaculture Update* (Ed. Hickman B.) Science Communication NIWA, Wellington **21**: 9.

CHAPMAN R.L, BUCHHEIM M.A., DELWICHE C.F., FRIEDL T., HUSS V.A.R., KAROL D.G., LEWIS L.A., MANHART J., MCCOURT R., OLSEN J.L. & WATERS D.A. 1998. Molecular

Systematics of the Green Algae. In: *Molecular Systematics of Plants II: DNA Sequencing* (Eds. D.E. Soltis, P.S. Soltis & J.J. Doyle.) Kluwer Academics Publishers, Massachusetts, USA. pp 508-540.

COCKCROFT A.C., SCHOEMAN D.A., PITCHER G.C., BAILEY G.W. & VAN ZYL D.L. 2000. A mass stranding, or "walkout", of West Coast rock lobster *Jasus lalandii* in Elands Bay, South Africa: causes results and implications. In: *The Biodiversity Crises and Crustacea.* (Eds. Von Kaupel Klein J.C. & Schram F.R.), *Crustacean Iss.* **11**: 673 - 688.

DAMARET A., SOHET K. & HOUVENAGHEL G., 1995. Effects of toxic dinoflagellates on the feeding and mortality of *Artemia franciscana* and larvae. In: *Harmful Marine Algal Blooms. Technique et Documentation* (Eds. Lassus P., Arzul G., Erard E., Gentien P., Marcaillou C.), Lavoisier, Intercept Ltd. pp. 427-432.

DAUGBJERG N., HANSEN G., LARSEN J. & MOESTRUP O. 2000. Phylogeny of some of the major genera of dinoflagellates based on ultrastructure and partial LSU rDNA sequence data, including the erection of three new genera of unarmoured dinoflagellates. *Phycologia* **39**: 302-317.

DE SALAS M. F., BOLCH, C. J. S. & HALLEGRAEFF G. M. (2003). *Karenia umbella* sp. nov. (Gymnodiniales, Dinophyceae), associated with an aquaculture fish mortality event in Tasmania, Australia. *Journal of Phycology* **39**: 1-14.

DODGE J.D. & CRAWFORD R.M. 1971. A fine-structural survey of dinoflagellate pyrenoids and food-reserves. *Bot. J. of the Linn. Soc* **64**: 105-115.

DODGE J.D. 1974. A redescription of the dinoflagellate *Gymnodinium simplex* with the aid of electron microscopy. *J. mar. bio. Ass. U.K.* **54**: 171 - 177.

DODGE J.D. 1982. Marine dinoflagellates of the British Isles. Her Majesty's Stationery Office, LONDON, PP 144- 146.

DODGE J.D. 1985. Atlas of dinoflagellates, Ferramd Press, London. pp 32.

ELBRÄCHTER M. & SCNEPF E. 1996. *Gymnodinium chlorophorum*, a new green bloom forming dinoflagellate (Gymnodiniales, Dinophyceae) with a vestigial prasinophyte endosymbiont. *Phycologia* **35**: 381-393.

ELLEGAARD M. & OSHIMA Y. 1998. *Gymnodinium nolleri* Ellegaard et Moestrup sp. ined. (Dinophyceae) from Danish waters, a new species producing *Gymnodinium catenatum*-like cysts: molecular and toxicological comparisons with Australian and Spanish strains of *Gymndonium catenatum*. *Phycologia* 37: 369 - 378.

ELLEGAARD M. & MOESTRUP Ø. 1999. Fine structure of the flagellar apparatus and morphological details of *Gymnodinium nolleri* sp. nov. (Dinophyceae), an unarmoured dinoflagellate producing a microreticulate cyst. *Phycologia* **38**: 289-300.

FRAGA S., BRAVO I., DELGADO M., FANCO J.M. & ZAPATA M. 1995a. *Gyrodinium imudicum* sp. nov. (Dinophyceae), a non-toxic, chain forming, red tide dinoflagellate. *Phycologia* **34**: 514- 521.

FRAGA S., BRAVO I., DELGADO M., FANCO J.M. & ZAPATA M. 1995b. Differences between two chain forming, athecate, red tide dinoflagellates; *Gymnodinium catenatum* Graham and *Gyrodinium* sp. In: *Harmful Marine Algal Blooms*. (Eds. P. Lassus, G. Arzul, E. Erard, P. Gentien, C. Marcaillou), Lavoisier, Intercept Ltd. pp 39-44.

FRITZ L. & TRIEMER R.E. 1985. A rapid simple technique utilizing calcofluor white M2R for the visualization of dinoflagellate thecal plates. *J. Phycol.* **21**: 662-664.

FUKUYO, Y., TAKANO, H., CHIHARA, M. & MATSUOKA, K. 1990. Red Tide Organisms in Japan: an Illustrated Taxonomic Guide. Uchida Rokakuho. Tokyo

GARCÉS E., DELGADO M., MASÓ M. & CAMP J. 1995. *In situ* growth rate and distribution of the ichthyotoxic dinoflagellate *Gyrodinium corsicum* Paulmier in an estuarine embayment (Alfacs Bay, NW Mediterranean Sea*). J. Plankton Res.* **21**: 77-94.

GENTIEN P. 1998. Bloom dynamics and ecophysiology of the *Gymnodinium mikimotoi* species complex. In: *Physiological Ecology of Harmful Algal Blooms.* (Eds. Anderson, D.M., Cambella, A.D. and Hallegraeff), G.M. Springer-Verlag, Berlin, Heidelberg, pp 155 – 173.

GRINDLEY J.R. & TAYLOR F.J.R. 1964. Red water and marine fauna mortality near Cape Town. *Trans. Roy. Soc. S. Afr.* **37**: 111 - .130.

GRINDLEY J.R. & TAYLOR F.J.R. 1970. Factors affecting plankton blooms in False Bay. *Trans. Roy. Soc. S. Afr.* **39**: 201 – 210.

GRÜNDLING M.L. & LARGIER J.L. 1991. Physical oceanography of False Bay: a review. *Trans. Roy. Soc. S. Afr.* **47**: 387 – 400.

GUILLARD R.R.L. & RYTHER J.H. 1962. Studies of marine planktonic diatom. I. *Cyclotella nana* Hustedt and *Detonula confervadea* (Cleve) Gran. *Can. J. Microbiol.* **8**: 229-239.

HALLEGRAEFF G.M. 1993. A review of harmful algal blooms and their apparent global increase. *Phycologia* **32**: 79 - 99

HALLEGRAEFF G.M. 1995. Harmful algal blooms: A global overview. In. *Manual on Harmful Marine Microalgae.* (Eds. Hallegraeff G.M., Anderson D.M. Cembella A.D.), IOC Manuals and guides No 33. UNESCO, France pp 1 - 22.

HALLEGRAEFF, G. M. 2002. Aquaculturists' guide to harmful Australian microalgae. Print Centre, Hobart.

HANSEN G. 1989. Ultrastructure and morphogenesis of scales in *Katodinium rotundatum* (Lohmann) Loeblich (Dinophyceae). *Phycologia* **28**: 385-394.

HANSEN G. 1995. Analysis of the thecal plate pattern in the dinoflagellate *Heterocapsa rotundata* (Lohmann) comb. nov. (=*Katodinium rotundatum* (Lohmann) Loeblich). *Phycologia* **34**: 166-170.

HANSEN G. 2001. Ultrastructure of *Gymnodinium aureolum* (Dinophyceae): Toward a further redefinition of *Gymnodinium sensu stricto*. *J. Phycol.* **37**: 612 - 623.

HANSEN G., DAUGBJERG N. & HENDRIKSEN P. 2000a. Comparative study of *Gymnodinium mikimotoi* and *Gymnodinium aureolum* comb. nov. (= *Gyrodinium aureolum*) based on morphology, pigment composition and molecular data. *J. Phycol.* **36**: 394-410.

HANSEN G., MOESTRUP Ø & ROBERTS K.R. 2000b. Light and electron microscopical observations on the type species of *Gymnodinium, G. fuscum* (Dinophyceae). *Phycologia* **39**: 365-376.

HASLE G.R. 1987. The inverted microscope method. In. Sournina, A. *Phytoplankton Manual*, UNESCO, Paris, pp 88 – 96.

HAYWOOD A., MACKENZIE L., GARTHWAITE I. & TOWERS N. 1996. *Gymnodinium breve* 'look alikes': Three *Gymnodinium* isolates from New Zealand In: *Harmful and Toxic Algal Blooms* (Eds. T. Yasumoto, Y. Oshima and Y. Fukuyo), Intergovernmental Oceanographic Commission of Unesco, pp. 227-230.

HEMMERT W.H. 1975. The public health implications of *Gymnodinium breve* red tides, a review of the literature and recent events. In: *Proceedings of the First International Conference on Toxic Dinoflagellate Blooms.* (Ed. LoCicero, V.R.), The Massachusetts Science and Technology Foundation: Massachusetts, pp 489-497.

HERMAN E.M. & SWEENEY B.M. 1976. *Cachonina illdefina* sp. nov. (Dinophyceae): Chloroplast tubules and degeneration of the pyrenoid. *J. Phycol.* **12**: 198-205.

HERNÁNDEZ F.J R. 2002 Aplicación del análisis de pigmentos por cromatografía líquida de alta eficacia (HPLC) al estudio de la composición y distribución del fitoplancton marino. Universidad de Vigo. February 2002. 264p.

HO K. C. & WONG Y. K. 2001. A study on the cost-effectiveness of using ozone in mitigating dinoflagellate blooms. Abstract – Harmful Algae Management and Mitigation Conference, Chingdao, China.

HORSTMAN D.A. 1981. Reported red-water outbreaks and their effects on fauna of the West and South Coasts of South Africa, 1959 – 1980. *Fish. Bull. S. Afr.* **15**: 71 –88.

HORSTMAN D.A., MCGIBBON S., PITCHER G.C., CALDER D., HUTCHINGS L. & WILLIAMS P. 1991. Red tides in False Bay, 1959-1989, with particular reference to recent blooms of *Gymnodinium* sp. *Trans. Roy. Soc. S. Afr.* **47**: 611 – 628.

HORIGUCHI T. 1995. *Heterocapsa circularisquama* sp. nov. (Peridiniales, Dinophyceae): A new marine dinoflagellate causing mass mortality of bivalves in Japan. *Phycol. Res.* **43**: 129-136.

HORIGUCHI T. 1997. *Heterocapsa arctica* sp. nov. (Peridiniales, Dinophyceae), a new marine dinoflagellate from the arctic. *Phycologia* **36**: 488-491.

IHAKA R. & GENTLEMAN R. 1996. R: A language for data analysis and graphics. *J. Comp. Graph. Stat.* **5**: 299-314.

IOC TAXONOMIC REFERENCE LIST OF TOXIC ALGAE. 2003. Intergovernmental Oceanographic Commission of UNESCO, http://ioc.unesco.org/hab/data4taxlist.htm

IWATAKI M., TAKAYAMA H., MATSUOKA K. & FUKUYO Y. 2002a *Heterocapsa lanceolata* sp. nov. and *Heterocapsa horiguchii* sp. nov. (Peridiniales, Dinophyceae), two new marine dinoflagellates from coastal Japan. *Phycologia* **41**: 470-479.

IWATAKI M., WONG M.W. & FUKUYO Y. 2002b. New record of *Heterocapsa circularisquama* (Dinophyceae) from Hong Kong. *Fish. Sc.* **68**: 1161-1163.

IWATAKI, M., BOTES, L., SAWAGUCHI, T., SEKIGUCHI, K. & Y. FUKUYO (in press) Cellular and body scale structure of *Heterocapsa ovata* sp. nov. and *Heterocapsa orientalis* sp. nov. (Peridiniales, Dinophyceae). *Phycologia.*

JEFFREY S.W., MANTOURA R.F.C. & WRIGHT S.W. 1997. Phytoplankton pigments in oceanography. United Nations Educational, Scientific and Cultural Organisation (SCOR), Paris, pp 37-84.

JOHNSEN G. & SAKSHQUGE E. 1993. Bio-optical characteristics and photoadaptive responses in the toxic and bloom-forming dinoflagellates *Gyrodinium aureolum*, *Gymnodinium galatheanum* and two strains of *Prorocentrum minimum J. Phycol.* **29**: 627-642.

JURY M.R. 1991. The weather of False Bay. *Trans. Roy. Soc. S. Afr.* **47**: 401 - 417.

KELLER M.D. & GUILLARD R.R.L. 1985. Factors significant to marine dinoflagellate culture, In. *Toxic Dinoflagellates* (Eds. D.M. Anderson, A.W. White, D.G. Baden), New York, pp. 113-116.

KEMPTON J.W., LEWITUS A.J., DEEDS J.R., LAW M.J. & PLACE A.R. 2002. Toxicity of *Karlodinium micrum* (Dinophyceae) associated with a fish kill in a South Carolina brackish retention pond. *Harmful Algae* **1**: 233 - 241.

KOFOID C.A. 1907. Dinoflagellata of the San Diego region, III. Descriptions of new species. *University of California Publications Zoology* **3**: 299-340.

KOFOID, C. A. & SWEZY, O. 1921. The Free-Living Unarmoured Dinoflagellata. University of California Press. Berkeley

LARSEN J. 1994. Unarmoured dinoflagellates from Australian waters .1. The genus *Gymnodinium* (Gymnodiniales, Dinophyceae). *Phycologia* **33**: 24-33.

LARSEN J. 1996. Unarmoured dinoflagellates from Australian waters II. Genus *Gyrodinium* (Gymnodiniales, Dinophyceae). *Phycologia* **35**: 342-349.

LENAERS G., MAROTEAUX L., MICHOT B. & HERZOG M. 1989. Dinoflagellates in evolution. A molecular phylogenetic analysis of large subunit ribosomal RNA. *J. of Evol.* **32**:53-63.

LENAERS G., SCHOLIN C. BHAUD Y., SAINT-HILAIRE D. & HERZOG M. 1991. A molecular phylogeny of dinoflagellate protists (Pyrrhophyta) inferred from the sequence of 24S rRNA devergent domains D1 and D8. *J. Mol. Evol.* **32**: 53 – 63.

LEWIS J., HIGMAN W. & KUENSTNER S. 1995. Occurrence of *Alexandrium* sp. cysts in sediments from the North East coast of Britain. In: *Harmful Marine Algal Blooms*. (Eds. Lassus P., Arzul G. Erard E., Gentien P. & Marcaillou-LeBaut C.), Lavoisier Science Publishers, Paris, pp. 175 - 180.

LOEBLICH A.R. III. 1968. A new marine dinoflagellate genus, *Cachonina*, in axenic culture from the Salton Sea, California with remarks on the genus *Peridinium*. *Proc. Biol. Soc. Washington* **81**: 91-96

LOEBLICH A.R. III. 1977. Studies on synchronously dividing populations of *Cachonina niei*, a marine dinoflagellate. *Bull. Jap. Soc. Phycol.* **25**: 119-128.

LOEBLICH A.R. III, SCHMIDT R.J. & SHERLEY J.L. 1981. Scanning electron microscopy of *Heterocapsa pygmaea* sp. nov., and evidence for polyploidy as a speciation mechanism in dinoflagellates. *J. Plankton Res.* **3**: 67-79.

LUSH G.J. & HALLEGRAEFF G.M. 1996. High toxicity of the red tide dinoflagellate *Alexandrium minutium* to the brine shrimp *Artemia salina*. In: Harmful and Toxic Algal Blooms (Eds. Yasumoto, T., Oshima, Y., Fukuyo, Y.),. Intergovernmental Oceanographic Commission of UNESCO, pp. 389-392.

MADISON D.R. & MADISON W.P. 2000. MaClade 4. Sinquer Association Inc., Sunderland, Massachusetts, USA.

MARTINEZ A., FRANCO J.M., BRAVO I., MAZOY M. & CACHO E., 1993. PSP toxicity in *Haliotis tuberculata* from NW Spain. In: Smayda,T.J., and Shimizu, Y., (Eds.), Toxic Phytoplankton Blooms in the Sea. Amsterdam, Elsevier, pp.419-423

MASSART J. 1920. Recherches sur les organismes inférieurs. VIII. Sur la motilité des Flagellates. In: *Bulletins de la Classe des Sciences.* (Eds. M. Lamertin & M. Hayez), pp. 116-141.

MATSUYAMA Y., 1999. Harmful effect of Dinoflagellate *Heterocapsa circularisquama* on shellfish aquaculture in Japan. *JARQ* **33**: 283-293.

MATSUYAMA, Y., KOISUMI Y. & UCHIDA T. 1998a. Effect of harmful phytoplankton on the survival of the abalones, *Haliotis discus* and *Sulculus diversicolor*. *Bull. Nansei Natl. Fish. Res. Inst.* **31**: 19-24.

MATSUYAMA Y., UCHIDA T. & HONJO T., 1998b. The effects of *Heterocapsa circularisquama* and *Gymnodinium mikimotoi* on the clearance rate and survival of blue mussels, *Mytilus galloprovincialis*. In: *Harmful Algae.* (Eds. Reguera, B., Blanco, J., Fernandez M., Wyatt, T.), Xunta de Galicia and Intergovernmental Oceanographic Commission of UNESCO 1998. GRAFISANT. Spain, pp. 422-424.

MATSUOKA K., IIZUKA S., TAKAYAMA H., HONJO T., FUKUYO Y. & ISHIMARU T. 1989. Geographic distribution of *Gymnodinium nagasakiense* Takayama *et* Adashi around west Japan. In: *Red tides: biology, environmental science and toxicology* (Eds. T. Okaichi, D.M. Anderson & T. Nemoto), pp. 101-104. Elsevier, New York.

MATTHEWS S.G. & PITCHER G.C. 1996. Worst recorded marine mortality on the South African coast. In: *Harmful and Toxic Algal Blooms.* (Eds. T. Yasumoto, Y. Oshima & Y. Fukuyo), pp. 89-92. Intergovernmental Oceanographic Commission of UNESCO.

MEDLYN R.A. 1980. Susceptibility of four geographical strains of adult *Artemia* to *Ptychodiscus brevis* toxin(s). In: *The Brine Shrimp Artemia Vol I. Morphology, Genetics, Radiobiology, Toxicology.* (Eds. Persoone, G., Sorgeloos, P., Roels O., Jaspers, E.), Universal Press. Belgium, pp. 225-231.

MILLIE D. F., KIRKPATRICK G.J. & VINYARD B.T. 1995. Relating photosynthetic pigments and *in vivo* optical density spectra to irradiance for the Florida red-tide dinoflagellate *Gymnodinium breve*. *Mar. Ecol. Prog. Ser.* **120**: 65-75.

MILLIE D.F., SCHOFIELD O.M., KIRKPATRICK G.J., JOHNSEN G., TESTER P.A. & VINYARD B.T. 1997. Detection of harmful algal blooms using photopigments and absorption signatures: A case study of the Florida red tide dinoflagellate, *Gymnodinium breve*. *Limnol. Oceanogr.* **42**: 1240 - 1251.

MORRILL L.C. & LOEBLICH A.R. III. 1981. A survey for body scales in dinoflagellates and a revision of *Cachonina* and *Heterocapsa* (Pyrrhophyta). *J. Plankton Res.* **3**: 53-65.

MORRILL L.C. & LOEBLICH A.R. III. 1983. Formation and release of body scales in the dinoflagellate genus *Heterocapsa*. *J. Mar. Biol. Assoc. U.K.* **63**: 905-913.

MOSTERT, S. A. 1983 Procedures used in South Africa for the automatic photometric determination of micronutrients in seawater. *S. Afr. J. Mar. Sci.* **1**: 189 – 198.

NAGAI K., MATSUYAMA Y., UCHIDA T., YAMAGUCHI M., ISHIMURA M., NISHIMURA A., AKAMATSU S. & HONJO, T. 1996. Toxicity and LD50 levels of the red tide dinoflagellate *Heterocapsa circularisquama* on juvenile pearl oysters. *Aquaculture* **144**, 149-154.

NAGASHIMA Y., ARAKAWA O., SHIOM, K. & NOGUCHI T. 1995. Paralytic shellfish poisons of ormer, *Haliotis tuberculata*, from Spain. *J. Food Hyg. Soc. Japan* **36**: 627-631.

NATION J.L. 1983 A new method using hexamethyldisilazane for preparation of soft insect tissues for SEM. *Stain Technol.* **58**: 347-351.

NIELSEN M.V. & STRØNGREM T. 1991. Shell growth response of mussels (*Mytilis edulis*) exposed to toxic microalgae. *Mar. Biol.* **108**: 263-267.

NIGHTLINGALE W.H. 1936. Red tide organisms – Their occurrence and influence upon marine aquatic animals with special reference to shellfish in the waters of the Pacific coast. The Argus Press, Seatle, Washington, USA.

ONOUE Y., NOZAWA K., KUMANDA K., TAKEDA K. & ARAMAKI T. 1985. Occurence of a toxic dinoflagellate "*Gymnodinium*-Type '84 K" in Kagoshima Bay. *Bull. of the Jap. Soc. of Scientific Fish.* **51**: 1567.

PALMER J.D. & DELWICHE C.F. 1998. The origin and evolution of plastids and their genomes. In. *Molecular Systematics of Plants II: DNA Sequencing,* (Eds. D.E. Soltis, P.S. Soltis & J.J. Doyle.Kluwer), Academics Publishers, Massachusetts, USA. pp 375-409.

PARSONS T.R., MAITA Y. & LALLI C.H., 1984. *A Manual of Chemical and Biological Methods for Seawater Analysis.* New York, Pergamon: [xiv] + pp 173.

PARTENSKY, F., VAULOT D., COUTÉ A. & SOURINIA A. 1988. Morphological and nuclear analysis of the bloom-forming dinoflagellates *Gyrodinium* cf. *aureolum* and *Gymnodinium nagasakiense*. *J. Phycol.* **24**: 408-415.

PAULMIER G., BERLAND B., BILLARD C. & NEZAN E. 1995. *Gyrodinium corsicum* nov. sp. (Gymnodiniales, Dinophycées), organisme responsible D'une, eauverte, dans L'etang marin de Diana (Corse), en Avril 1994. *Cryptogamie. Algol.* **16**: 77-94.

PENNICK N.C. & CLARKE K.J. 1977. The occurrence of scales in the peridinian dinoflagellate *Heterocapsa triquetra* (Ehrenb.) Stein. *British Phycol. J.* **12**: 63-66.

PERSOONE G. & WELLS P.G. 1987. *Artemia* in aquatic toxicology: a review. In: Artemia *Research and its Applications. Vol I. Morphology, Genetics, Strain characterisation, Toxicology* (Eds.) Sorgeloos, P., Bengtson, D.A., Decleir, W., Jaspers, E.,. Universa Press, Belgium. pp 259-275.

PITCHER G.C. 1998. Harmful algal blooms of the Benguela Current, National Book Printers, South Africa. pp 18.

PITCHER G.C. & CALDER D. 2000. Harmful algal blooms of the Southern Benguela Current: A review and appraisal of monitoring from 1989 to 1997. *S. Afr. J. of Mar Sci.* **22**:219-253.

PITCHER G.C., FRANCO J.M., DOUCETTE G.J., POWELL C. L. & MOUTON A. 2001. Paralytic shellfish poisoning in the abalone *Haliotis midae* on the west coast of South Africa. *J. Shellfish Res.* **2**: 895-904.

PITCHER G.C., HORSTMAN D.A. & CALDER D. 1993. Formation and decay of red tide blooms in the southern Benguela upwelling system during the summer of 1990/91. In: *Toxic Phytoplankton Blooms in the Sea*, (Eds. Smayda T.J. & Shimizu Y.), Elsevier Science Publishers, pp. 317 – 322.

PITCHER G.C. & MATHEUWS S. 1996. Noxious *Gymnodinium* species in South African waters. In. *Harmful Algae News*. (Ed. Wyatt T.) Intergovernmental Oceanographic Commission of UNESCO, **15**: 1 – 3.

POMROY A.J. 1989. Scanning electron microscopy of *Heterocapsa minima* sp. nov. (Dinophyceae) and its seasonal distribution in the Celtic Sea. *British Phycol. J.* **24**: 131-135.

PROBYN T., PITCHER G., PIENAAR R. & NUZZI R. 2001. Brown tides and mariculture in Saldanha Bay, South Africa. *Mar. Poll.* **42**: 405-408.

REES A.J.J. & HALLEGRAEFF G.M. 1991. Ultrastructure of the toxic, chain-forming dinoflagellate *Gymnodinium catenatum* (Dinophyceae). *Phycologia* **30**:90-105.

SAKO Y., ROKUSHIMA M., YAMAGUCHI M., ISHIDA Y. & UCHIDA A. 1998. Phylogenetic analysis and molecular identification of red tide dinoflagellate Gymnodinium mikimotoi using ribosomal RNA genes. In: *Harmful Algae* (Eds. Reguera B., Blanco J., Fernandez M.L. & Wyatt T.), Xunta de Galicia and Intergovernmental Oceanographic Commission of UNESCO, pp 295 - 298.

SALDARRIAGA J.F., TAYLOR F.J.R., KEELING P.J. & CAVALIER-SMITH T. 2001. Dinoflagellate nuclear SSU rRNA phylogeny suggests multiple plastid losses and replacements. *J. Mol. Evol.* **53**: 204 - 213.

SAUNDERS G.W., HILL D.R.A., SEXTON J.P. & ANDERSEN R.A. 1997. Small-subunit ribosomal RNA sequences from selected dinoflagellates: testing classical evolutionary hypothesis with molecular systematic methods. *Plant Syst. and Evol.* **11**: 237-259.

SAWADA S. & WADA Y. 1983. Several examination of a *Gymnodinium* sp. type '65 red tide occurred in Uwa Sea on resistibility of fish and shellfish. Reports on the Assessments of Red Tide Prediction, Fishery Agency of Japan. pp. 131-140. (in Japanese).

SCHOLIN C.A. HERZOG M. SOGIN M. & ANDERSON D.M. 1994. Identification of group- and strain-specific genetic markers for globally distributed *Alexandrium* (Dinophyceae). II. Sequence analysis of a fragment of the LSU rRNA Gene. *J. Phycol.* **30**: 999-1011.

SHANNON L.V. 1985. The Benguela ecosystem. 1. Evolution of the Benguela, physical features and processes. In: *Oceanography and Maine Biology. An Annual Review* 23. (Ed. Barnes M. Aberdeen), University Press, pp 105 - 182.

SHUMWAY S.E. 1995. Phycotoxin-related shellfish poisoning: bivalve molluscs are not the only vectors. *Rev. Fish. Sci.* **3**: 1-31.

SHUMWAY S.E., BARTER J. & SHERMAN-CASWELL S. 1990. Auditing the impact of toxic algal blooms on oysters. *Environmental Auditor* **2**: 41-56.

SHUMWAY S.E. & CEMBELLA A. 1993. The impact of toxic algae on scallop culture and fisheries. *Rev. Fish. Sci.* **1**: 121-150.

SHUMWAY S.E., SHERMAN S.A., CAMBELLA A.D. & SELVIN R. 1994. Accumulation of paralytic shellfish toxins by surfclams, *Spisula solidissima* (Dillwyn, 1897) in the Gulf of Maine: Seasonal changes, distribution between tissues, and notes on feeding habits. *Natural Toxins* **2**: 236-251

SHUMWAY S.E., EGMOND H.P.V., HURST J.W. & BEAN L.L. 1995. Management of shellfish resources. In: *Manual on Harmful Marine Microalgae*, (Eds. Hallegraeff G.M., Anderson D.M. & Cembella A.M.), UNESCO, Paris, pp. 433 - 474.

SMAYDA T.J. 1990. Novel and nuisance phytoplankton blooms in the sea: Evidence for a global epidemic. In: *Toxic Marine Phytoplankton*, (Eds. Granéli E., Sundström B., Edler L. & Anderson D.M.), Elsevier Science Publishing, New York, pp. 29 - 40.

SMOLOWITZ R. & SHUMWAY S.E. 1997. Possible cytotoxic effects of the dinoflagellate, *Gyrodinium aureolum*, on juvenile bivalve molluscs. *Aquaculture International* **5**: 291-300.

SORGELOOS P., REMICHE-VAN DER WIELEN C. & PERSOONE G. 1978. The use of *Artemia* nauplii for toxicity tests – a critical analysis. *Ecotoxicology Environ. Safety*. **2**: 249-255.

STEIDINGER K.A. & BADEN D.G. 1984. Toxic marine dinoflagellates. In. *Dinoflagellates* (Ed. D.K. Spector), pp 285-288. Academis Press, New York.

STEIDINGER K.A. & TANGEN K. 1996. Dinoflagellates. In: Identifying marine phytoplankton. (Eds. C.R. Thomas). Academic press, London. pp. 387-584.

STEIDINGER K.A., LANDSBERG J.H., TRUBY E.W. & BLAKESLEY B.A. 1996. The use of SEM in identifying small "gymnodinioid" dinoflagellates. *Nova Hedwigia* **112**: 415-422.

STEIDINGER K. A., LANDSBERG J. H., TRUBY E. W. & ROBERTS B. S. 1998a. First report of *Gymnodinium pulchellum* (Dinophyceae) in North America and associated fish kills in the Indian River, Florida. *J. Phycol.* **34**: 431-437.

STEIDINGER K.A., VARGO G.A., TESTER P.A. & TOMAS C.R. 1998b. Bloom dynamics and physiology of *Gymnodinium breve* with emphasis on the Gulf of Mexico. In. *Physiological Ecology of Harmful Algal Blooms.* (Eds. D.A. Anderson, A.D. Cembella and G.M. Hallegraeff), pp 133-154. Springer-Verlag, Germany.

STEIN F.R.VON 1883. Der organismus der Arthrodelen Flagellaten nach eigenen Forschungen in systematischer Reihenfolge bearbeitet. W. Engelmann, Leipzig. 30pp.

STUMPF R.P., RANSIBRAHMANAKUL V., STEIDINGER K.A. & TESTER P.A. 1998. Observations of sea surface temperature and winds associated with Florida, USA, red tides

(*Gymnodinium breve* blooms). In. *Harmful Algae*. (Eds. Reguera, B., Fernández, M.L. and Wyatt, T.), Xantu de Galicia and Intergovernmental Oceanographic Commission of UNESCO, pp. 145 – 148.

SWIFT M.J. & MCLAUGHLIN J.J.A. 1970. Some nutritional, physiological, and morphological studies on *Melosira juergensii* and *Heterocapsa kollmeriana*. *Annals of New York Academy of Sciences* **175**: 577-600.

SWOFFORD D.L. 2003. PAUP* - Phylogenetic Analysis Using Parsimony (*and other methods), version 4. Sinauer Associates, Sunderland, Massachusetts, USA.

SYM S.D. 1992 A survey of the genus *Pyramimonas Scmarda* (Prasinophyceae) from Southern African inshore waters. PhD thesis, University of the Witwatersrand, Johannesburg. Vol. I and II, 332 pp. + 81 plates.

TAKAYAMA H. 1985. Apical grooves of unarmoured dinoflagellates. *Bull. Plankton. Soc. Jpn.* **32**: 129-140.

TAKAYAMA H. 1998. Morphological and taxonomical studies on the free-living unarmoured dinoflagellates occurring in the Seto Inland Sea and adjacent waters. PhD Thesis. University of Tokyo. 211 pp.

TAKAYAMA H. 1990. Dinophyceae. In: *Red tide organisms in Japan – an illustrated taxonomic guide*. (Eds. Y. Fukuyo, H. Takano, M. Chihara and K. Matsuoka). pp 430. Uchida Rokakuho, Co. Ltd., Ohtsuka 3-34-3, Bunkyo-ku, Tokyo, Japan.

TAKAYAMA H. & ADACHI R. 1984. *Gymnodinium nagasakiense* sp. nov., a red tide forming dinophyte in the adjacent waters of Japan. *Bull. Plankton Soc. Jpn* **31**:7-14.

TAMURA K. & NEI M. 1993. Estimation of the number of nucleotide substitutions in the control region of mitochondrial DNA in humans and chimpanzees. *Mol. Biol. Evol.* **10**: 512-526.

TANGEN K. & BJÖRNLAND T. 1981. Observations on pigments and morphology of *Gyrodinium aureolum* Hulburt, a marine dinoflagellate containing 19'-hexanoyloxyfucoxanthin as the main carotenoid. *J. Plankton Res.* **3**: 389 - 401

TAYLOR F.J. R., FUKUYO Y. & LARSEN J. 1995. Taxonomy of Harmful Dinoflagellates. In: *IOC Manuals and Guides No.33- Manual on Harmful Marine Microalgae,* (Ed. by Hallegraeff G., Anderson D.M., Cembella A.D.), pp 283-318. *UNESCO.* Paris.

TENGS T., DAHLBERG O.J., SHALCHIAN-TABRIZI K., KLAVENESS D., RUDI K., DELWICHE C.F. & JAKOBSEN K.S. 2000. Phylogenetic analyses indicate that the 19'-Hexanoyloxy-fucoxanthin-containing dinoflagellates have tertiary plastids of haptophyte origin. *Mol. Biol. Evol.* **17**: 718-729.

TYRRELL J.V., CONNELL L.B. & SCHOLIN C.A. 2002. Monitoring for *Heterosigma akashiwo* using a sandwich hybridisation assay. *Harmful Algae* **1**: 205 - 214.

TRUBY E.W. 1997. Preparation of single-celled marine dinoflagellates for electron microscopy. *Micrs. Res. Tech.* **36**: 337-340.

TSUTSUI K. & KUMON H. 1976. Preparative method for suspended biological materials for SEM by using of polycationic substance layer. *J. Electron. Microsc.* **25**: 163-168.

UCHIDA T. 1975. Nutrition of *Glenodinium* sp. isolated from Nagasaki Harbor. *Bull. Plankton Soc. Jpn* **22**: 11-16.

VAN BALLEGOOYEN R.C. 1991. The dynamics relevant to the modelling of synoptic scale circulations within False Bay. *Trans. Roy. Soc. S. Afr.* **47**: 419 – 431.

VENABLES W.N. & RIPLEY B.D. 1999. *Modern Applied Statistics with S-Plus,* 3rd ed. Springer-Verlag, New York. pp. 501.

WATANABE M.M., SUDA S., INOUYE I., SAWAGUCHI T. & CHIHARA M. 1990. *Lepidodinium viride* gen. et sp. nov. (Gymnodiniales, Dinophyta), a green dinoflagellate with a chlorophyll *a*- and *b* containing endosymbiont. *J. Phycol.* **26**: 741- 751.

WATANABE M.M., TAKEDA Y., SASA T., INOUYE I., SUDA S., SAWAGUCHI T. & CHIHARA M. 1987. A green dinoflagellate with chlorophyll *a* & *b*: Morphology, fine structure of the chloroplasts and chlorophyll composition. *J. Phycol.* **23**: 382-389.

WATANABE M.M., HIROKI M., SHIMIZU A., ERATA M., MORI F. & SAKURAI Y. 1997. NIES-collection. List of strains Fifth edition Microalgae and Protozoa. pp. 140.

WOELKE C.E. 1961. Pacific oyster *Crassostrea gigas* mortalities with notes on common oyster predators in Washington waters. *Proc. Nat. Shellf. Assoc.* **50**: 53-66.

YANG Z. 1993. Maximum likelihood estimation of phylogeny from DNA sequences when substitution rates vary over sites: approximate methods. *Mol. Biol. and Evol.* **39**: 306 – 314.

YANG Z. 1994. Maximum likelihood estimation of phylogeny from DNA sequences when substitution rates vary over sites. *Mol. Biol. and Evol.* **10**: 1369 – 1304.

YANG Z.B., TAKAYAMA H., MATSUOKA K. & HODGKISS I.J. 2000. *Karenia digitata* sp. nov. (Gymnodiniales, Dionphycea), a new harmful algal bloom species from the coastal water of west Japan and Hong Kong. *Phycologia* **39**: 463 - 470.

YANG Z.B., HODGKISS I.J. & HANSEN G. 2001. *Karenia longicanalis* sp. nov. (Dinophyceae): a new bloom-forming species isolated from Hong Kong, May 1998. *Botanica Marina* **44**: 67 - 74.

YOON H.S., HACKETT J.D. & SHATTACHARYA D. 2002. A single origin of the peridinin- and fucoxanthin-containing plastids in dinoflagellates through tertiary endosymbiosis. PNAS 99: 11724 - 11729.

ZAPATA M., FREIRE J. & GARRIDO J.L. 1988. Pigment composition of several harmful algae as determined by HPLC using Pyridine-containing mobile phases and ad polymeric octadecylsilica column. In: *Harmful Algae*. (Eds. B. Reguera, J. Blanco, M.L. Fernández

and T. Wyatt). Xunta de Galicia and Intergovernmental Oceanographic Commission of UNESCO, Grafisont, Santiago de Copostela, spain. pp304-307.

ZAPATA M., RODRIGUEZ F. & GARRIDO J. L. 2000. Separation of chlorophylls and carotenoids from marine phytoplankton: a new method using reversed-phase C8 column and pyridine-containing mobile phases. *Mar. Ecol. Prog. Ser.* **195**: 29-45.

APPENDIX 1

Please find CD, containing the PAUP files, in the back of the thesis.

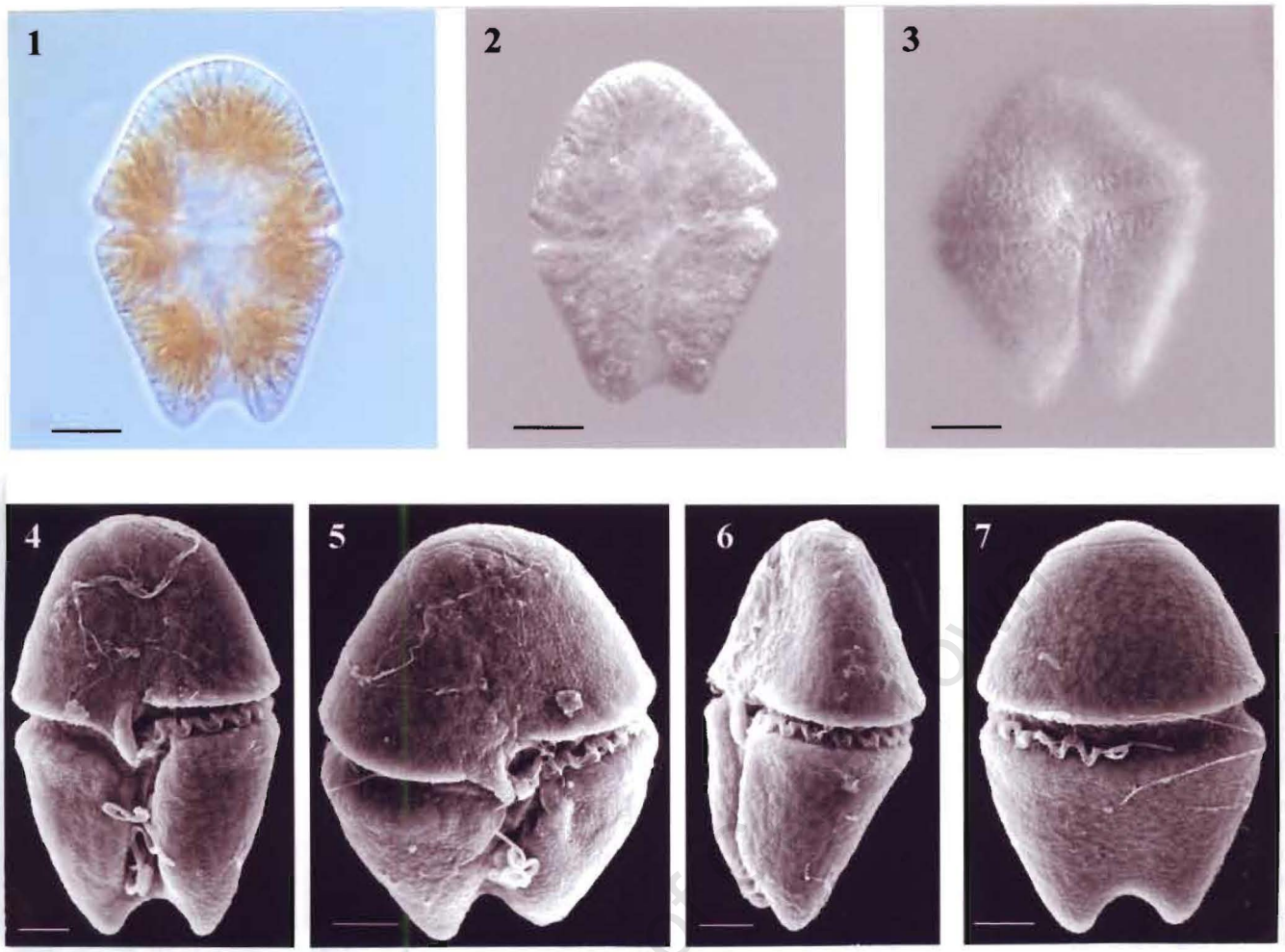

Figure 1 – 7. Light and electron micrographs of *A. sanguinea*. Fig. 1 Reddish-brown (due to the presence of peridinin) chloroplasts radiating outwards from the center of the cell. Fig. 2 Large nucleus situated in the center of the cell. Fig. 3 Cingulum-sulcus region indicating very little displacement between the cingulum and sulcus. Figs 4 – 7. Apical groove encircling the apex. Scale bars = 10μm.

Figure 1 – 6. Light and electron micrographs of *G. aureolum*. Fig. 1 Cell has numerous reddish-brown (due to the presence of peridinin) chloroplasts. Fig. 2 Chloroplasts are narrow and elongated. Fig. 3 Cingulum-sulcus region showing the sulcus extension onto the epicone. Fig. 4 The nucleus is horizontally ellipsoidal and situated in the center of the cell. Figs 5 – 6 Horseshoe shaped apical groove clearly visible. Scale bars = 10μm.

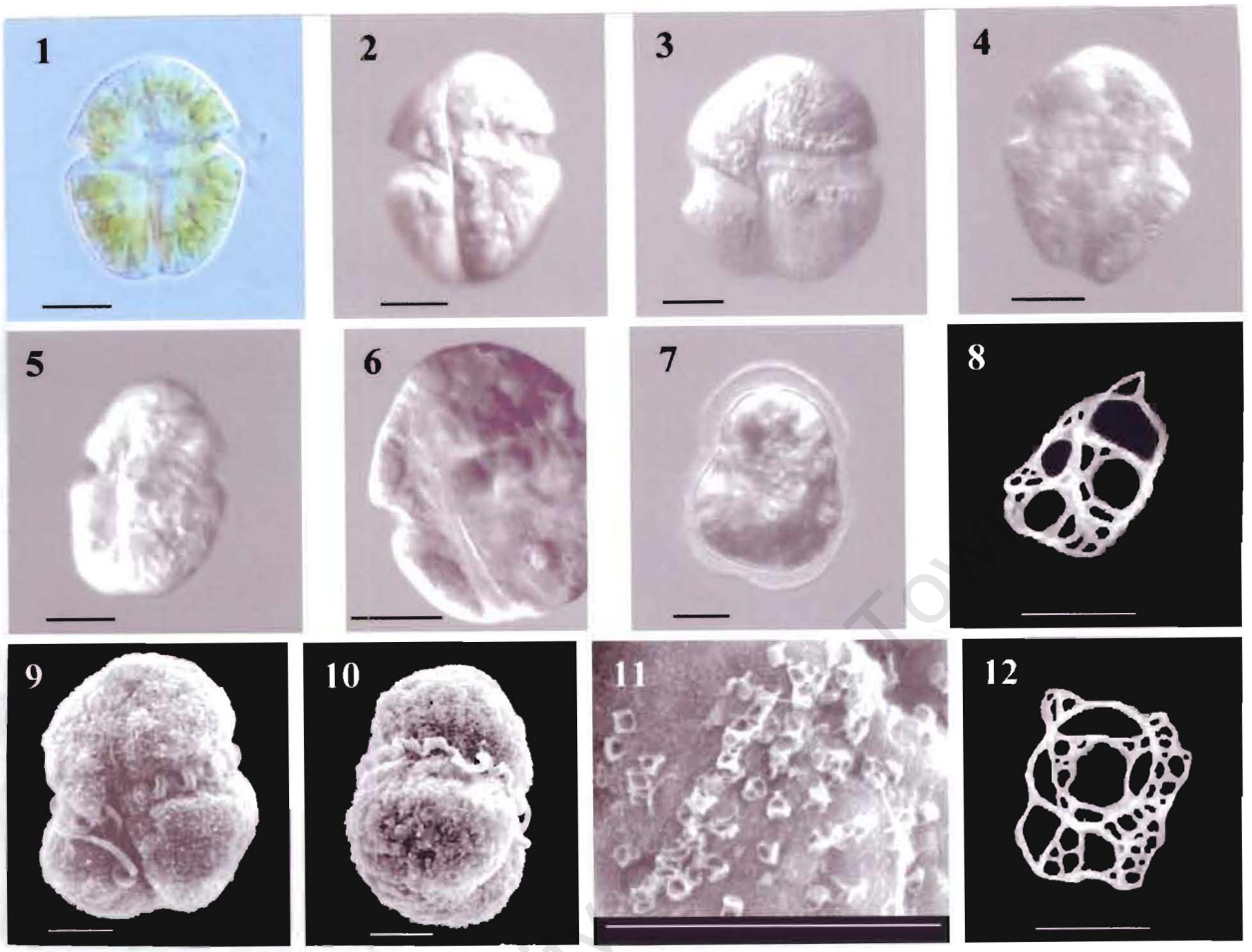

Figure 1 – 12. Light and electron micrographs of *L. viride*. Fig. 1 Green chloroplasts (due to the presence of chlorophyll *b*) are interconnected and closely associated with the periphery of the cell. Fig. 2 Cingulum-sulcus region showing the extension of the sulcus onto the epione. Fig. 3 Horseshoe shaped apical groove. Fig. 4 Nucleus is vertically ellipsoidal in the middle of the cell. Figs 5, 6 and 10 show the peduncle-like structure. Fig. 7 Dead cell surrounded by mucous and scales. Fig. 9 Cell surface covered with scales. The apical groove is clearly visible. Figs 8, 11 and 12 show the basket shaped scales. All scale bars = 10μm except in figs 8 and 12 where is = 0.5μm.

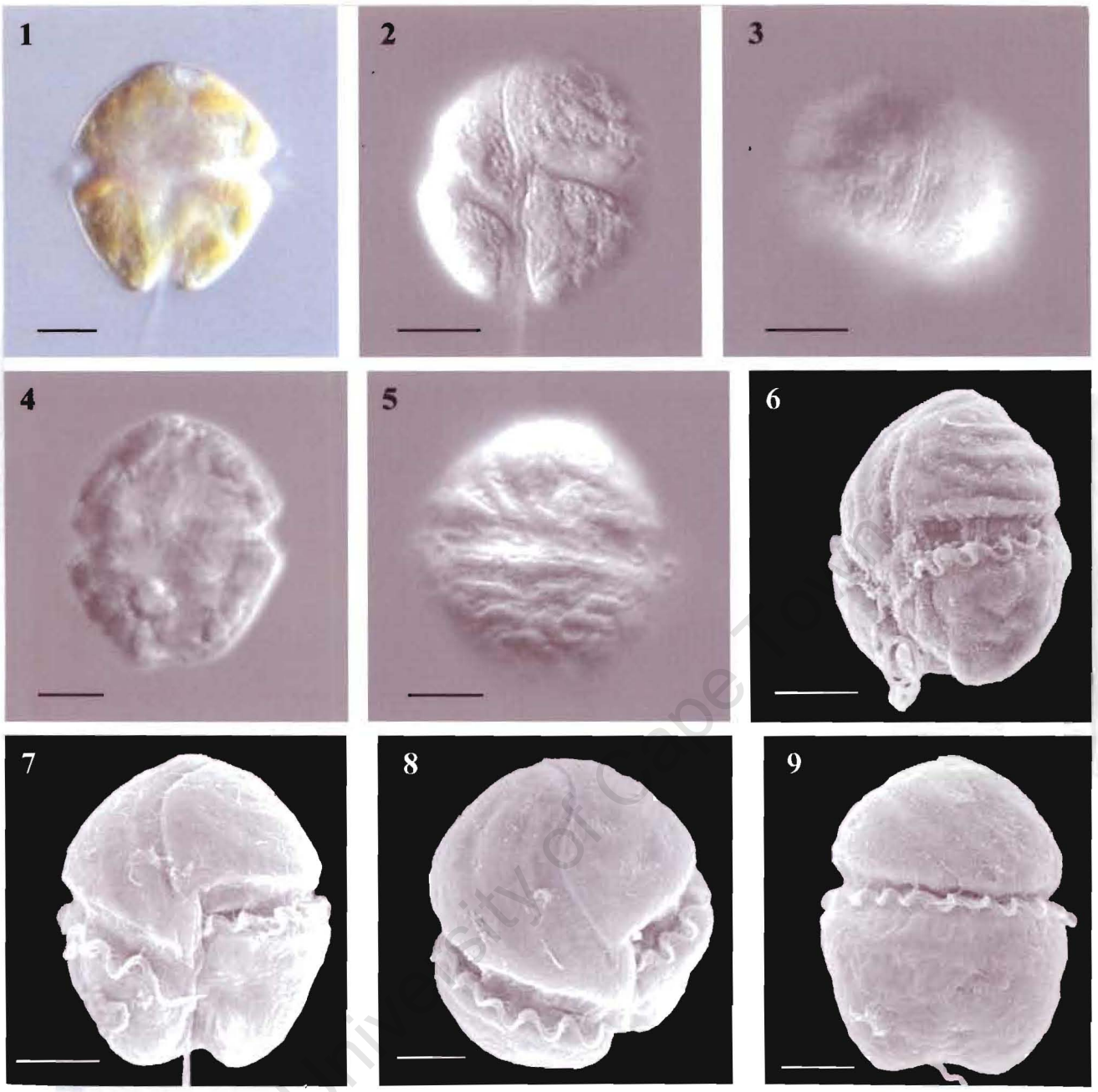

Figure 1 – 9. Light and electron micrographs of *T. helix*. Fig. 1 The yellow-brown ribbon shaped chloroplasts (due to the presence of fucoxanthin) are often orientated in a horizontal manner. Figs 2, 3, 7 – 9 show the sigmoid apical groove. Fig. 4 Nucleus is vertically ellipsoidal on the left side of the cell. Figs 5 and 6 Chloroplasts running in a horizontal orientation. Figs 7 – 9 Sigmoid apical groove in ventral, apical and dorsal view. Fig. 7 Ventral slit present immediately below the apical groove. Scale bars = 10μm.

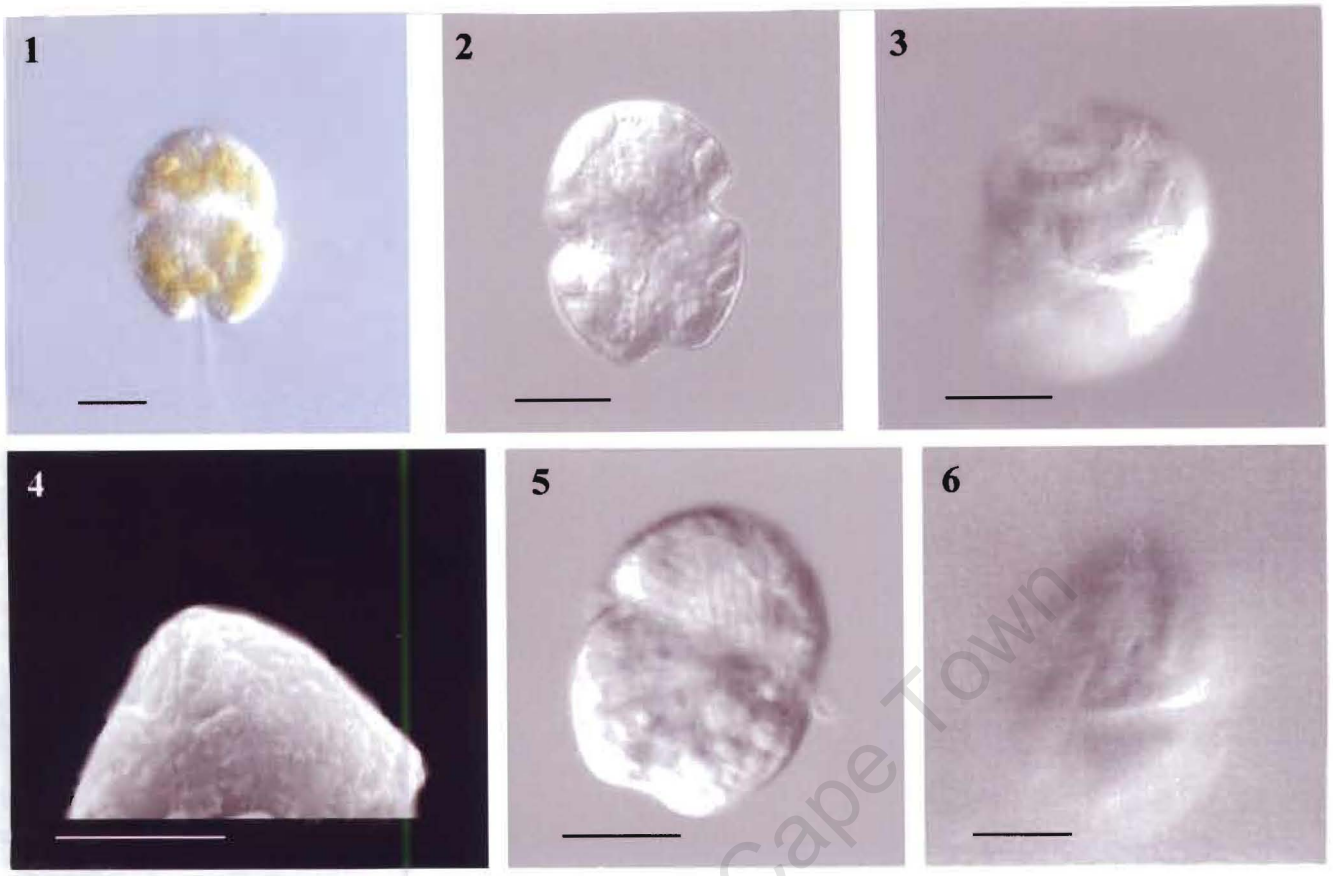

Figure 1 – 6. Light and electron micrographs of *G.* cf. *corsicum*. Fig. 1. Yellow-brown chloroplasts (due to the presence of fucoxanthin) are irregular in shape. Fig. 2 The nucleus occupies most of the epicone. Short apical groove is visible at the apex. Fig. 3 Irregularly shaped chloroplasts are present. Fig. 4 Straight apical groove with the ventral pore to its left. Fig. 5 Nucleus clearly visible in the epicone. Fig. 6 Ventral pore visible to the left of the apical groove. Scale bars = 10μm.

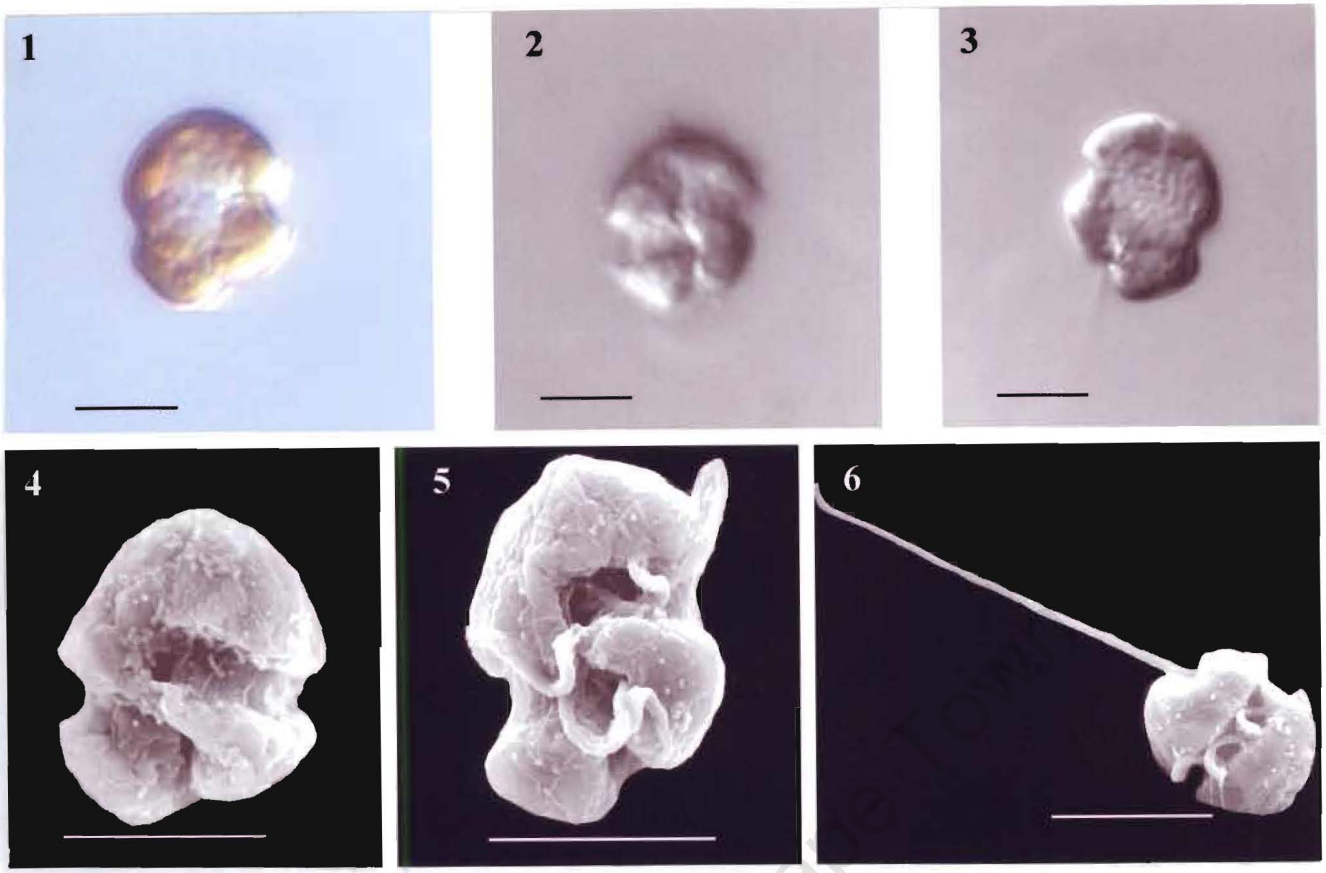

Figure 1 – 6. Light and electron micrographs of *G.* cf. *zeta*. Fig. 1 Cell has a reddish-brown appearance (due to the presence of peridinin). Fig. 2 The cingulum and sulcus are wide, deeply incised and has a 'z' shaped appearance. Figs 3 and 4 Nucleus is centrally situated and occupies most of the cell. Figs 4 and 5 The straight apical groove is visible on the epicone. The right lobe is larger and more displaced. The left lobe extends into a thumb-like structure in the intercingular region. Figs 5 and 6 the dimensions of both flagella are large in comparison to the rest of the cell. Scale bars = 5µm.

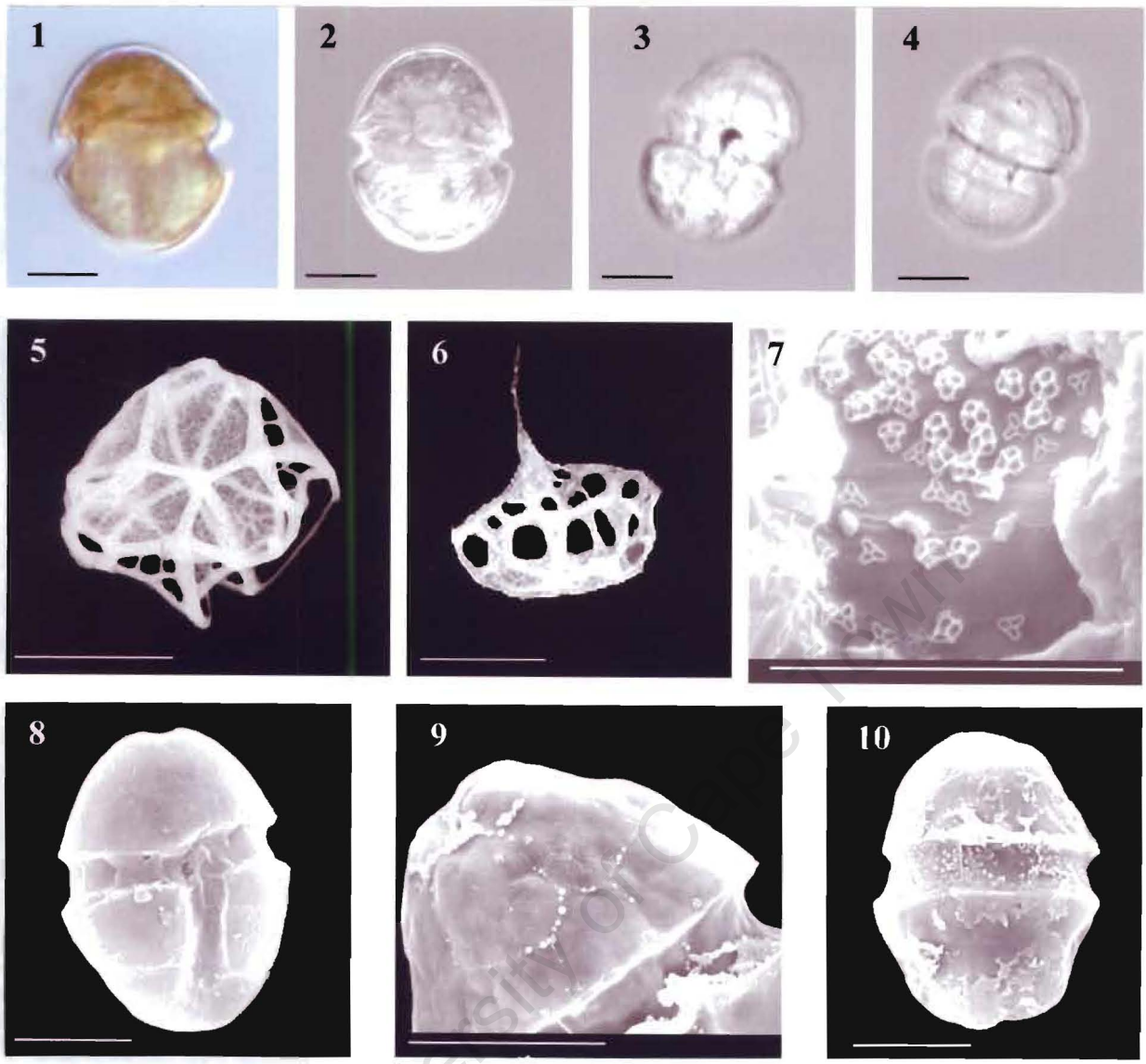

Figure 1 – 10. Light and electron micrographs of *H. orientalis*. Fig. 1 Reddish-brown appearance (due to the presence of peridinin). Fig. 2 The pyrenoid is situated in the epicone and the nucleus is situated in the hypocone. Figs 3 and 4 The delicate plates are visible on the theca. Figs 5 – 7 Triangular shaped scales with a central spine and no short spines. Fig. 8 Apical groove is absent. Delicate thecal plates visible on the epicone. Fig. 9 Thecal plates clearly visible. Fig. 10 Triangular shaped scales present on the cell's surface. Scale bars = 10μm, except in figs 5 and 6 where it = 0.5μm, and in fig. 7 where it = 5μm.